GDL/GMF-98-01

SECONDARY BREAKUP AND TURBULENCE INTERACTIONS OF DROPS

J.-H. Chen, W.-H. Chou, Z. Dai, J.-S. Wu and G.M. Faeth
Department of Aerospace Engineering
The University of Michigan
Ann Arbor, Michigan 48109-2140, U.S.A.

Final Report

15 July 1995 - 14 July 1998

AFOSR Grant No. F49620-95-1-0364
Air Force Office of Scientific Research, Bolling AFB, D.C. 20332-0001
J. M. Tishkoff, Technical Manager

REPORT DOCUMENTATION PAGE

AFRL-SR-BL-TR-98-

0677

1. AGENCY USE ONLY (Leave blank)	2. REPORT DATE	3. REPORT TYPE AND DATES COVERED
	14/9/98	Final Tech. Rept. 15/7/95-14/7/98

4. TITLE AND SUBTITLE

(U) Secondary Breakup and Turbulence Interactions of Drops

5. FUNDING NUMBERS

PE - 61102F
PR - 2308
SA - BS
G - F49620-95-1-0364

6. AUTHOR(S)

J.-H. Chen, W.-H. Chou, Z. Dai, J.-S. Wu and G.M. Faeth

7. PERFORMING ORGANIZATION NAME(S) AND ADDRESS(ES)

The University of Michigan
Ann Arbor, MI 48109

8. PERFORMING ORGANIZATION REPORT NUMBER

GDL/GMF-98-01

9. SPONSORING/MONITORING AGENCY NAME(S) AND ADDRESS(ES)

AFOSR/NA
110 Duncan Avenue, Suite B115
Bolling AFB DC 20332-0001

10. SPONSORING/MONITORING AGENCY REPORT NUMBER

11. SUPPLEMENTARY NOTES

12a. DISTRIBUTION/AVAILABILITY STATEMENT

Approved for public release; distribution is unlimited

12b. DISTRIBUTION CODE

13. ABSTRACT *(Maximum 200 words)*

Experimental studies of two types of drop/gas interactions that are important in the near-injector, dense region of sprays were carried out, as follows: (1) secondary drop breakup, which tends to control interphase transport processes in dense sprays; and (2) turbulence generation by rapidly moving drops in gas environments, which tends to control turbulence production in dense sprays. The drop breakup measurements showed that breakup should be treated as a rate process rather than by jump conditions in some instances and provided data about the temporal properties of breakup in the important bag and shear breakup regimes. The turbulence generation measurements showed that homogeneous dispersed flows of drops (particles) in gases consist of particle wake disturbances embedded in relatively large interwake turbulence fields and provided data about the particle wake properties and the overall turbulence properties of these flows for various particle sizes and fluxes.

14. SUBJECT TERMS	15. NUMBER OF PAGES
Multiphase Flow, Homogeneous Turbulence, Drop Breakup, Turbulence Modification	214
	16. PRICE CODE

17. SECURITY CLASSIFICATION OF REPORT	18. SECURITY CLASSIFICATION OF THIS PAGE	19. SECURITY CLASSIFICATION OF ABSTRACT	20. LIMITATION OF ABSTRACT
Unclassified	Unclassified	Unclassified	UL

ACKNOWLEDGMENTS

The authors wish to acknowledge the contributions of D. R. Glass, W. C. Eaton, G. L. Gould, T. G. Griffin, T. Larrow, D. McLean and W. Nowicki for assisting with apparatus development; and S.C. Bauerle and D. L. Laird for assisting with financial management and publications preparation.

This research was sponsored by the Air Force Office of Scientific Research, Air Force Systems Command, under AFOSR Grant No. F49620-95-1-0364.

Table of Contents

List of Tables

List of Figures

Nomenclature

Symbol	Description
C_D	drag coefficient
d, d_o	initial drop diameter
d_p	particle diameter
D	dissipation factor, $\varepsilon d_p C_D^{1/3}/(2 U_p^3)$
$E_u(k)$	streamwise energy spectrum
f	frequency
k	wave number, $2\pi f/\bar{u}$
L_u	streamwise integral length scale
MMD	mass median drop diameter
Oh	Ohnesorge number
PDF(ϕ)	probability density function of ϕ
Re	particle Reynolds number, $d_p U_p/\nu_G$
SMD	Sauter mean diameter
t	time
t^*	characteristic breakup time, $d_o(\rho_G/\rho_F)^{1/2}/u_o$
u	streamwise velocity
U_p	relative streamwise particle velocity
v	crosstream velocity
We	Weber number, $\rho_G d_o u_o^2/\sigma$
x	streamwise distance
ε	rate of dissipation of turbulence kinetic energy
ν	kinematic viscosity
ρ	density

σ		surface tension
Subscripts		
G		gas property
F		liquid property
Superscripts		
$\bar{(\,)}$	=	mean value
$\bar{(\,)}'$	=	r.m.s. fluctuating value

1. Introduction

Sprays and spray processes have been studied extensively due to their many applications; see Faeth (1996) and Faeth et al. (1995) and references cited therein. Unfortunately, sprays are complex multiphase turbulent flows and fundamental understanding of their properties is not well developed — particularly those processes relating to the near-injector dense portion of the flow. This is a serious deficiency because the dense-spray region involves the breakup of the liquid to form a dispersed phase, which is crucial to the mixing properties of sprays, and also generates the initial conditions required to analyze the structure of the better understood dilute portion of sprays. Thus, the objective of the present investigation was to study two aspects of dense sprays that involve drop/gas interactions, namely: (1) secondary drop breakup, which is an intrinsic outcome of primary breakup of the liquid, and is the most significant rate process of dense sprays; and (2) turbulence generation by dispersed phases, which is the most significant source of turbulence production within dense sprays. The research has relevance to air-breathing propulsion systems, liquid rocket engines and internal combustion engines, among others.

The following description of the research is brief. Additional details may be found in the articles, papers and theses resulting from the investigation that are summarized in Table 1. The table also provides a summary of the participants in the investigation, oral presentations of research results and a summary of honors/awards obtained during the grant period. Finally, for convenience, several articles resulting from the research are reproduced in appendices, as follows: Chou et al. (1997), Chou and Faeth (1998), Chen et al. (1998), Wu et al. (1995), Faeth et al. (1995), and Faeth (1996).

The following report considers secondary breakup and turbulence generation, in turn. Each part is written to stand alone so that readers can skip to portions of the report of interest to them.

Table 1. Summary of Investigation

Articles, Papers, Theses and Reports:

Chen, J.-H. (1998) Turbulence Generation in Homogeneous Dispersed Particle-Laden Flows. Ph.D. Thesis, The University of Michigan, Ann Arbor, Michigan, in preparation.

Chen, J.-H., Wu, J.-S. and Faeth, G.M. (1998) Turbulence Generation in Homogeneous Particle-Laden Flows. AIAA J., submitted.

Chen, J.-H., Wu, J.-S. and Faeth, G.M. (1998) Turbulence Generation in Homogeneous Particle-Laden Flows. AIAA Paper No. 98-0240.

Chen, J.-H., Faeth, G.M. and Wu, J.-S. (1998) Particle-Generated Turbulence in Dispersed Homogeneous Flows. Bull. Amer. Phys. Soc., in press (abstract only).

Chou, W.-H. (1997) Temporal Variation of Drop Properties and Formation Rates During Secondary Breakup. Ph.D. Thesis, The University of Michigan, Ann Arbor, MI.

Chou, W.-H. and Faeth, G.M (1998) Temporal Properties of Secondary Drop Breakup in the Bag Breakup Regime. Int. J. Multiphase Flow, in press.

Chou, W.-H., Hsiang, L.-P. and Faeth, G.M. (1997) Temporal Properties of Drop Breakup in the Shear Breakup Regime. Int. J. Multiphase Flow, 23, 651-669.

Chou, W.-H., Hsiang, L.-P. and Faeth, G.M. (1997) Dynamics of Drop Deformation and Formation during Secondary Breakup in the Bag Breakup Regime. AIAA Paper No. 97-0709.

Dai, Z. and Faeth, G.M. (1997) Turbulent Primary Drop Breakup from Free Bow Sheets. Bull. Amer. Phys. Soc. 42, 2195 (abstract only).

Dai, Z. and Faeth, G.M. (1998) Secondary Drop Breakup from Shock-Wave Disturbances in the Multimode Breakup Regime. Bull. Amer. Phys. Soc., in press (abstract only).

Dai, Z. and Faeth, G.M. (1998) Temporal Properties of Multimode Secondary Breakup. AIAA Paper No. 99-0333.

Dai, Z., Hsiang, L.-P. and Faeth, G.M. (1997) Spray Formation at the Free Surface of Turbulent Bow Sheets. Proc. 21st Symp. on Naval Hydrodynamics, National Academy Press, Washington, D.C., 490-505.

Dai, Z., Chou, W.-H. and Faeth, G.M. (1998) Drop Formation due to Turbulent Primary Breakup at the Free Surface of Plane Liquid Wall Jets. Phys. Fluids 10, 1147-1157

Dai, Z., Sallam, K.A. and Faeth, G.M. (1998) Turbulent Primary Breakup of Plane Free Bow Sheets. Proc. 22nd Symp. on Naval Hydrodynamics, National Academy Press, Washington, D.C., in press.

Faeth, G.M. (1997) Spray Combustion: A Review. Proc. 2nd Intl. Conf. Multiphase Flow (A. Serizawa, T. Fukami and T. Bataille, ed.), Kyoto University, Kyoto, Vol. 1, CO-1 to CO-16.

Faeth, G.M. (1996) Spray Combustion Phenomena. 26th Symposium (International) on Combustion, The Combustion Institute, Pittsburgh, 1593-1612.

Faeth, G. M. (1997) Combustion Fluid Dynamics (Tools and Methods). Proc. Workshop on Fuels with Improved Fire Safety, National Academy Press, Washington, D.C., 81-96.

Faeth, G.M. Hsiang, L.-P. and Wu, P.-K. (1995) Structure and Breakup Properties of Sprays. Int. J. Multiphase Flow 21 (Suppl.),99-127.

Faeth, G.M., Dai, Z. and Hsiang, L.-P. (1995) Turbulent Primary Drop Breakup in Bow Sprays. Bull. Amer. Phys. Soc. 41, 1766 (abstract only).

Hsiang, L.-P., and Faeth, G.M. (1995) Drop Deformation and Breakup Due to Shock Wave and Steady Disturbances. Int. J. Multiphase Flow 21, 545-560.

Hsiang, L.-P. Wu, J.-S., Chou, W.-H. and Faeth, G.M. (1995) Breakup and Turbulence Generation in Dense Sprays. Report No. GDL/GMF-95-01, The University of Michigan, Ann Arbor, MI,

Ruff, G.A. and Faeth, G.M. (1995) Non-Intrusive Measurements of the Structure of Dense Sprays. Prog. Astro. Aero. 166, 263-296.

Sallam, K.A., Dai, Z. and Faeth, G.M. (1998) Drop Formation at the Surface of Plane Turbulent Liquid Jets in Still Gases. Int. J. Multiphase Flow, invited.

Tseng, L.-K., Ruff, G.A., Wu, P.-K. and Faeth, G.M. (1996) Continuous- and Dispersed-Phase Structure of Pressure Atomized Sprays. Prog. Astro. Aero. 171, 3-30.

Wu, J.-S. and Faeth, G.M. (1995) Effect of Ambient Turbulence Intensity on Sphere Wakes at Intermediate Reynolds Numbers. AIAA J., 33, 171-173.

Wu, J.-S. and Faeth, G.M. (1995) Turbulence Generation in Homogeneous Particle-Laden Flows. Bull. Amer. Phys. Soc. 40, 1993 (abstract only).

Wu, P.-K., and Faeth, G.M. (1995) Onset and End of Drop Formation Along the Surface of Turbulent Liquid Jets in Still Gases. Phys. Fluids A 7, 2915-2917.

Wu, P.-K., Miranda, R.F. and Faeth, G.M. (1995) Effects of Initial Flow Conditions on Primary Breakup of Nonturbulent and Turbulent Round Liquid Jets. Atom. Spray 5, 175-196,

Wu, P.-K., Hsiang, L.-P. and Faeth, G.M. (1995) Aerodynamic Effects on Primary and Secondary Breakup. Prog. Astro. Aero. 169, 247-279.

Participants:

Chen, J.-H., Graduate Student Research Assistant and Doctoral Candidate, The University of Michigan

Chou, W.-H., Graduate Student Research Assistant and Doctoral Candidate, The University of Michigan

Dai, Z., Postdoctoral Research Fellow, The University of Michigan

Faeth, G.M., Principal Investigator and Professor, The University of Michigan

Hsiang, L.-P., Postdoctoral Research Fellow, The University of Michigan

Wu, J.-S., Postdoctoral Research Fellow, The University of Michigan

Oral Presentations:

Faeth, G.M. (1995) Dense-Spray Structure and Liquid Breakup. General Motors Research Laboratories, Warren, MI, invited.

Faeth, G.M. (1995) Sprays and Liquid Breakup. Engineering Seminar Series, University of Michigan, Dearborn, MI, invited.

Faeth, G.M. (1995) Primary Breakup of the Surface of Turbulent Liquids. ONR Workshop on Free Surface Flows, Pasadena, CA.

Faeth, G.M. (1995) Temporal Variation of Drop Properties and Formation Rates During Secondary Breakup. 31st Joint Propulsion Conference and Exhibit, San Diego, CA.

Faeth, G.M. (1995) Turbulence Generation in Homogeneous Particle-Laden Flows. 48th Annual Meeting, APS Division of Fluid Dynamics, Irvine, CA,

Faeth, G.M. (1996) Secondary and Atomization and Turbulence Interactions of Drops. AFOSR Contractors Meeting on Propulsion, Virginia Beach, VA.

Faeth, G.M. (1996) Spray Combustion Phenomena. 26th Symposium (International) on Combustion, Naples, invited.

Faeth, G.M. (1996) Transitions from Liquid to Supercritical Fuel Injection. IPTEC Workshop, Wright Laboratory, Wright-Patterson AFB, OH, invited.

Faeth, G.M. (1996) Combustion Fluid Dynamics (Tools and Methods). Workshop on Fuels with Improved Fire Safety, National Academy of Sciences, Washington, DC, invited.

Faeth, G.M. (1996) Spray Structure and Liquid Breakup Properties. Foster Lecture, University of Oklahoma, Norman, OK, invited.

Faeth, G.M. (1996) Distortion and Drop Formation at the Surface of Turbulent Liquids. ONR Workshop on Free-Surface and Wall-Bounded Turbulence and Turbulent Flow, Pasadena, CA.

Faeth, G.M. (1996) Spray Formation at the Free Surface of Turbulent Bow Sheets. 21st Symposium on Naval Hydrodynamics, Trondheim, Norway.

Faeth, G.M. (1997) Spray Combustion: A Review. 35th AIAA Aerospace Sciences Meeting, Reno, NV, invited.

Faeth, G.M. (1997) Primary and Secondary Breakup in Sprays. Research Seminar, United Technologies Research Center, East Hartford, CT, invited.

Faeth, G.M. (1997) Structure and Liquid Breakup Properties of Natural and Technological Sprays. Graduate Colloquium Lecture, Purdue University, W. Lafayette, IN, invited.

Faeth, G.M. (1997) Dynamics of Ligament and Drop Formation during Shear Breakup. 35th Aerospace Sciences Meeting, Reno, NV.

Faeth, G.M. (1997) Surface Distortion and Primary Spray Breakup in Turbulent Bow Sheets. ONR Workshop on Free-Surface and Wall-Bounded Turbulence and Turbulent Flows, Pasadena, CA.

Faeth, G.M. (1998) Atomization Physical Phenomena: Primary and Secondary Liquid Breakup in Sprays. Workshop on Rocket Combustion Modeling, ONERA-CERT, Toulouse, France, invited.

Faeth, G.M. (1998) Drop/Turbulence Interactions in Dense Sprays. ARO/AFOSR Contractors' Meeting on Chemical Propulsion, Long Beach, CA, invited.

Faeth, G.M. (1998) Turbulence Generation in Homogeneous Particle-Laden Flows. 36th AIAA Aerospace Sciences Meeting, Reno, NV.

Faeth, G.M. (1998) Aerodynamic Primary Breakup at the Surface of Round Nonturbulent Liquid Jets in Crossflow. 36th AIAA Aerospace Sciences Meeting, Reno, NV.

Faeth, G.M. (1998) Turbulent Primary Drop Breakup in Bow-Sprays. ONR Workshop on Free-Surface and Wall-Bounded Turbulence and Turbulent Flows, Pasadena, CA.

Faeth, G.M. (1998) Observations of Deformation and Breakup of Nonturbulent Round Liquid Jets in Gaseous Crossflows. 11th Annual Conference on Liquid Atomization and Spray Systems, Sacramento, CA.

Honors/Awards

Faeth, G.M. (1996) Invited Plenary Lecture, Twenty-Sixth Symposium (International) on Combustion, Naples, August 1996.

Faeth, G.M. (1996) Foster Lecturer, School of Aerospace and Mechanical Engineering, The University of Oklahoma, Norman, OK, November 1996.

Faeth, G.M. (1996) Best Paper Presented at the Spring Technical Meeting of the Central States Section of the Combustion Institute.

Faeth, G.M. (1997) Invited Graduate Colloquium Lecture, School of Mechanical Engineering, Purdue University, West Lafayette, IN.

---

2. Secondary Breakup

2.1 Introduction

Secondary breakup of drops is an important fundamental process of multi-phase flows with applications to liquid atomization, dispersed multiphase flow, spray drying, combustion instability, heterogeneous detonations, the properties of rain and interactions between high-speed vehicles and rain, among others. In particular, recent studies of the structure of dense sprays confirm the conventional view of liquid atomization that primary breakup of the liquid surface yields drops that intrinsically are unstable to secondary breakup and that secondary breakup tends to control mixing rates in dense sprays in much the same way that drop vaporization tends to control mixing rates in dilute sprays, see Faeth (1996), Faeth et al. (1995) and references cited therein. Motivated by these observations, the objectives of the present investigation were to study drop deformation and breakup for well-defined shock-wave and steady disturbances.

Reviews of past work on secondary breakup are reported by Faeth (1996), Faeth et al. (1995), Hinze (1995), Hsiang and Faeth (1992, 1993, 1995) and references cited therein. These reviews indicate that regimes of drop deformation and breakup, and that the outcomes of breakup (i.e., drop size and velocity drop size and velocity distributions after breakup) when effects of liquid viscosity are small (small Ohnesorge number conditions), are known reasonably well. On the other hand, earlier work has shown the drop breakup processes can extend over significant distances and times compared to characteristic distances and times of the dense spray region, and that very little is known about the temporal properties of secondary drop breakup. Thus, the objective of the present investigation was to resolve the temporal properties of secondary breakup, i.e., the drop size and velocity distributions, and the rate of liquid removal from the parent drop, as a function of time during secondary breakup. The methodology involved experiments in shock tubes in order to simulate effects of drop conditions similar to drop processes at the end of primary breakup in practical sprays. Attention was limited to the important shear and bag breakup regimes, observed at small Ohnesorge numbers where effects of liquid viscosity are small. Phenomenological theories were used to help interpret and correlate the

measurements. The present description of the research is brief, see Hsiang and Faeth (1995), Chou and Faeth (1998) and Chou et al. (1997) for more details.

2.2 Experimental Methods

Apparatus. A shock tube with the driven section open to the atmosphere was used to generate shock-wave disturbances. The driven section was rectangular (38 × 64 mm) with a length of 6.7 m to provide 17-24 ms of uniform flow behind the shock wave. Shock strengths were weak (shock Mach numbers of 1.01-1.15); therefore, gas properties behind the shock waves approximated air at normal temperature and pressure. A vibrating capillary drop generator, with electrostatic selection to control the drop spacing, was used to provide a continuous drop stream to interact with the shock wave at the test location.

Instrumentation. Drops were observed in two ways: pulsed shadowgraph photographs to visualize the breakup process, and single- and double-pulsed holography to observe the outcome of breakup. See Hsiang and Faeth (1992, 1993, 1995) for the details and experimental uncertainties of these measurements.

Test Conditions. Test conditions can be summarized most easily using the drop deformation and breakup regime map of Fig. 1. This map shows the various deformation and breakup regimes as a function of Weber and Ohnesorge numbers, as suggested by Hinze (1955). Two regions were considered during the present study: (1) the shear breakup regime with We of 125-370 and Oh of 0.003-0.039; and (2) the bag breakup regime with We of 13-20 and Oh of 0.004-0.043.

2.3 Results and Discussion

Shear Breakup Regime. Except where noted otherwise, drop size distributions satisfy the universal root normal distribution of Simmons (1977). This distribution has two parameters while MMD/SMD = 1.2 for the universal root normal form. Thus, drop sizes are a fully defined by a single parameter which will be taken to be the SMD in the following.

Shear breakup involved two temporal regimes: (1) the transient breakup regime, and (2) the quasi-steady breakup regime. The variation of SMD as a function of time, showing the two regimes, is illustrated in Fig. 2. The transient breakup regime is observed at short times after the start of breakup, particularly for liquids that have a small liquid viscosity so that the temporal rate of growth of the thickness of the boundary layer due to gas motion over the windward side of the drop is slow. At the end of this period, the boundary layer stabilizes in the quasi-steady period with a thickness that is more or less a fixed fraction of the drop diameter. The SMD of drops produced by secondary breakup can be correlated reasonably well by the boundary layer thickness in both regimes to yield:

$$SMD(t)/d_o = 2.0(\nu_L t/d_o^2)^{1/2}, \text{ transient period} \quad (1)$$

$$SMD(t)/d_o = 0.09, \text{ quasi-steady period} \quad (2)$$

where the smaller of these two estimates should be used. As discussed by Chou et al. (1997), Eqs. (1) and (2) are consistent with the findings of Hsiang and Faeth (1992) for the jump conditions for secondary breakup upon noticing that these jump conditions emphasized breakup in the transient regime. The corresponding drop velocity distributions were found to be uniform at each instant of time with velocities approximating the velocity

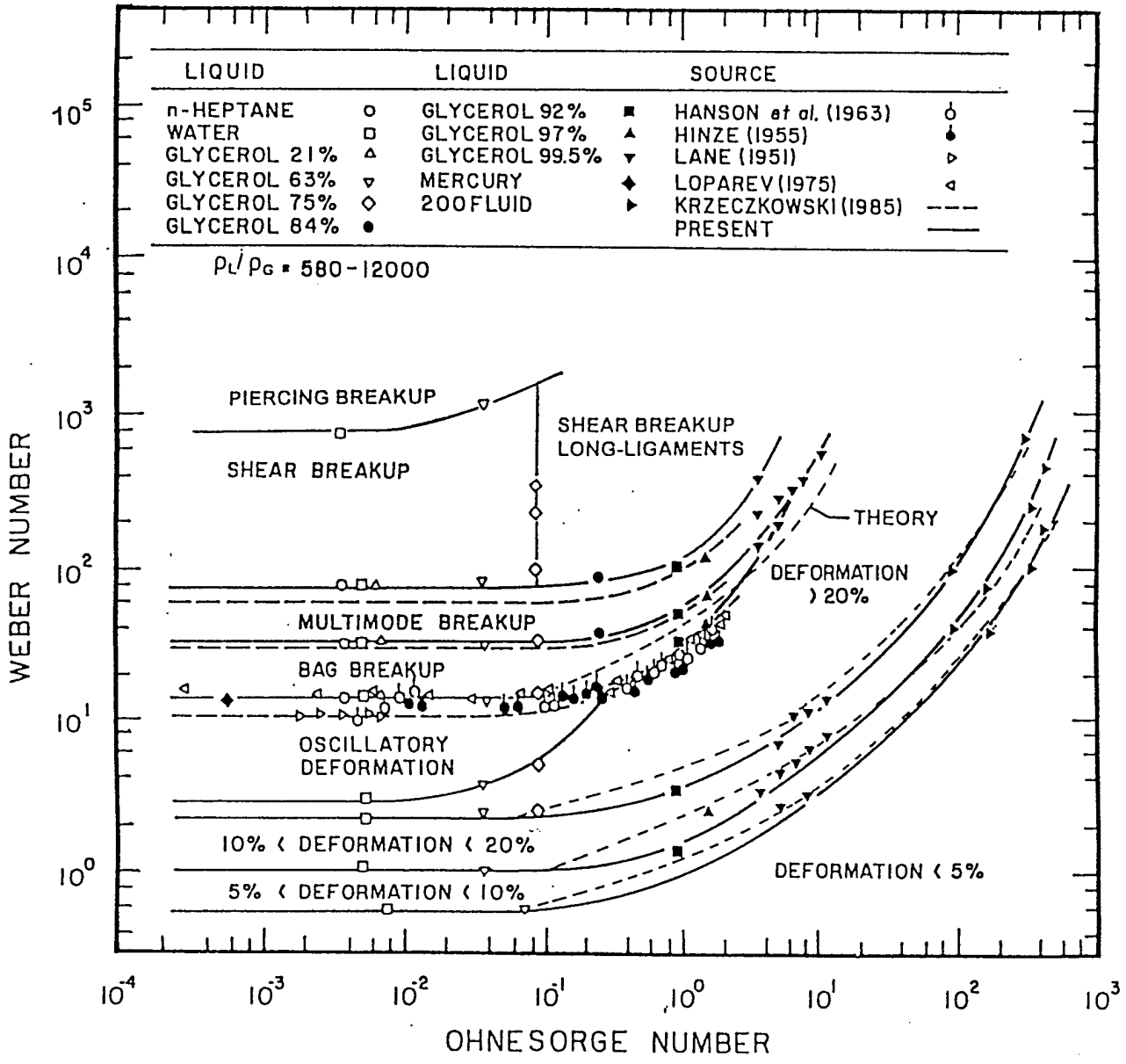

Fig. 1 Drop deformation and breakup regime map for shock-wave disturbances. From Chou et al. (1997).

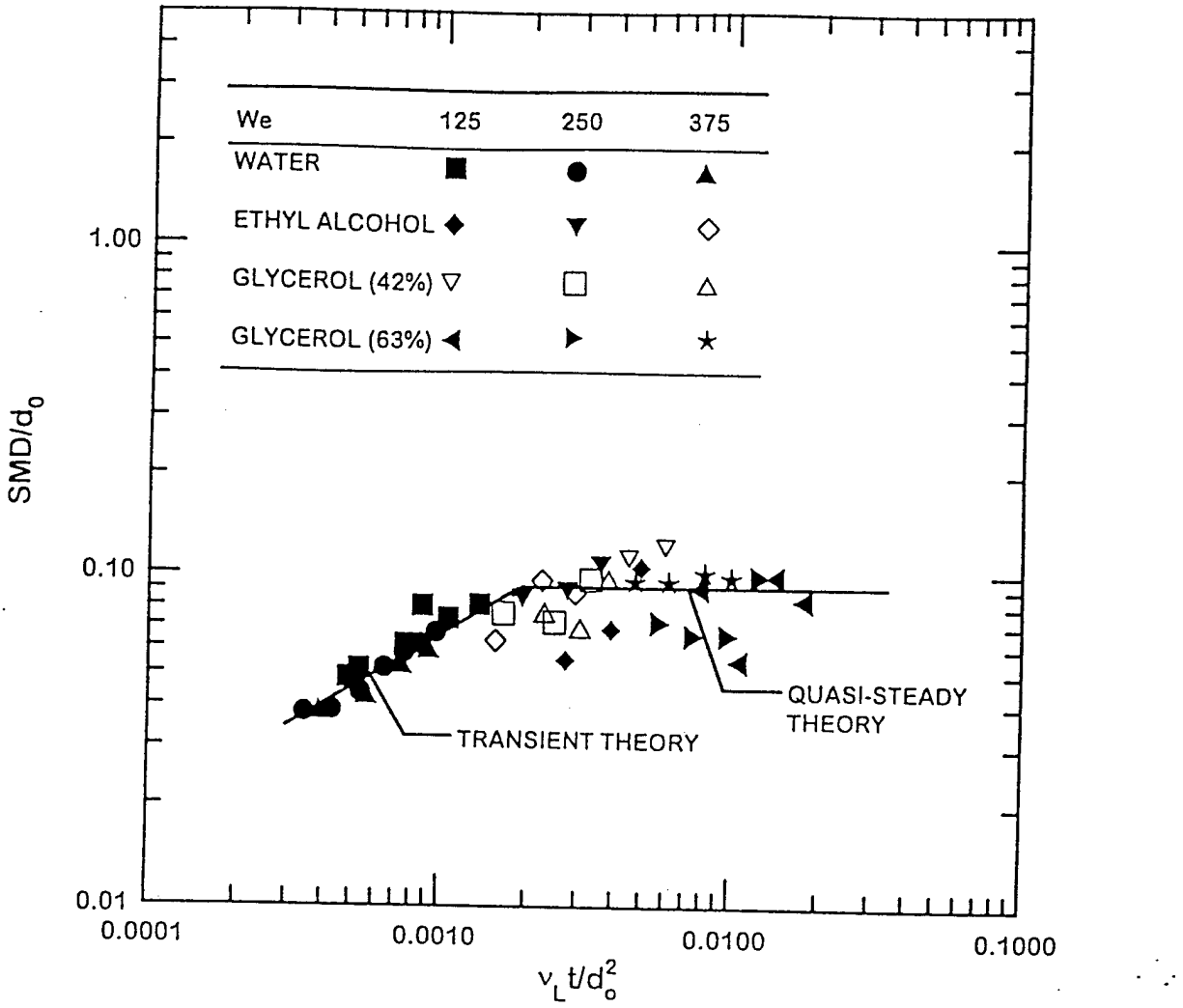

Fig. 2 Temporal variation of the SMD of drops produced by shear breakup. From Chou et al. (1997).

of the parent drop, see Hsiang and Faeth (1993) for a correlation of the parent drop velocity based on phenomenological theory.

Drop deformation rates were estimated based on a simplified analysis as described by Chou et al. (1997) . The resulting formulation was rather complex but it was found that the results could be expressed in a relatively simple correlation as illustrated in Fig. 3. This expression properly accounts for the fact that the drop only deforms with no breakup for $t/t^* \leq 1.5$, and that drop breakup ends at $t/t^* = 5.5$.

The extent of the drop-containing region was also resolved as a function of time as illustrated in Fig. 4. The boundaries of the drop-containing region are given by the motion of the parent drop, and the motion of the smallest drop formed at the onset of breakup. The span of the drop-containing region depends on the liquid/gas density ratio and comprises $x/d = 40\text{-}120$ at the end of breakup for $\rho_L/\rho_G = 1000$ and requires a time period of $t = 5.5$ t^*. As noted earlier, these distances and times can be large compared to distances and times associated with the dense spray region in some instances. Thus, present results are needed to properly treat secondary drop breakup.

Bag Breakup Regime. The bag breakup regime involves the formation of a thin bag with a basal ring at its base. The basal ring contains roughly 56% of the initial drop mass and eventually yields drops that are nearly monodisperse due to Rayleigh type breakup and have mean diameters of roughly 31% of the original drop diameter. The bag contains roughly 44% of the initial drop mass and eventually yields nearly monodisperse drops having mean diameters of roughly 4% of the initial drop diameter. Drop velocities in each case are nearly uniform and can be associated with parent drop velocities based on phenomenological theory.

The bag breakup process involves two periods of liquid removal as illustrated in Fig. 5. The bag breaks up in the first period which occurs where $t/t^* = 3.2\text{-}3.5$. The basal ring breaks up in the second period which occurs almost simultaneously at $t/t^* = 5.0$.

The spatial and temporal properties of bag breakup are illustrated in Fig. 6. The positions of the parent drop and the most remote drop are illustrated similar to behavior in the shear breakup regime in Fig. 4. Similar to shear breakup, bag breakup is seen to require significant times and distances and should be treated as a rate processes for many applications.

2.4 Conclusions

Shear Breakup. Major conclusions for shear breakup are as follows:

(1) Values of $Oh > 0.1$ involve long ligaments from the periphery of the drops so that present results are limited to conventional shear breakup with $Oh < 0.1$.

(2) Drops produced by shear breakup satisfy the universal root normal distribution with MMD/SMD = 1.2, at each instant of time.

(3) The SMD of drops produced by shear breakup at small Oh exhibit transient and quasisteady regimes as given by Eqs. (1) and (2).

(4) The parent drop accelerates rapidly due to its large drag coefficient which is caused by deformation.

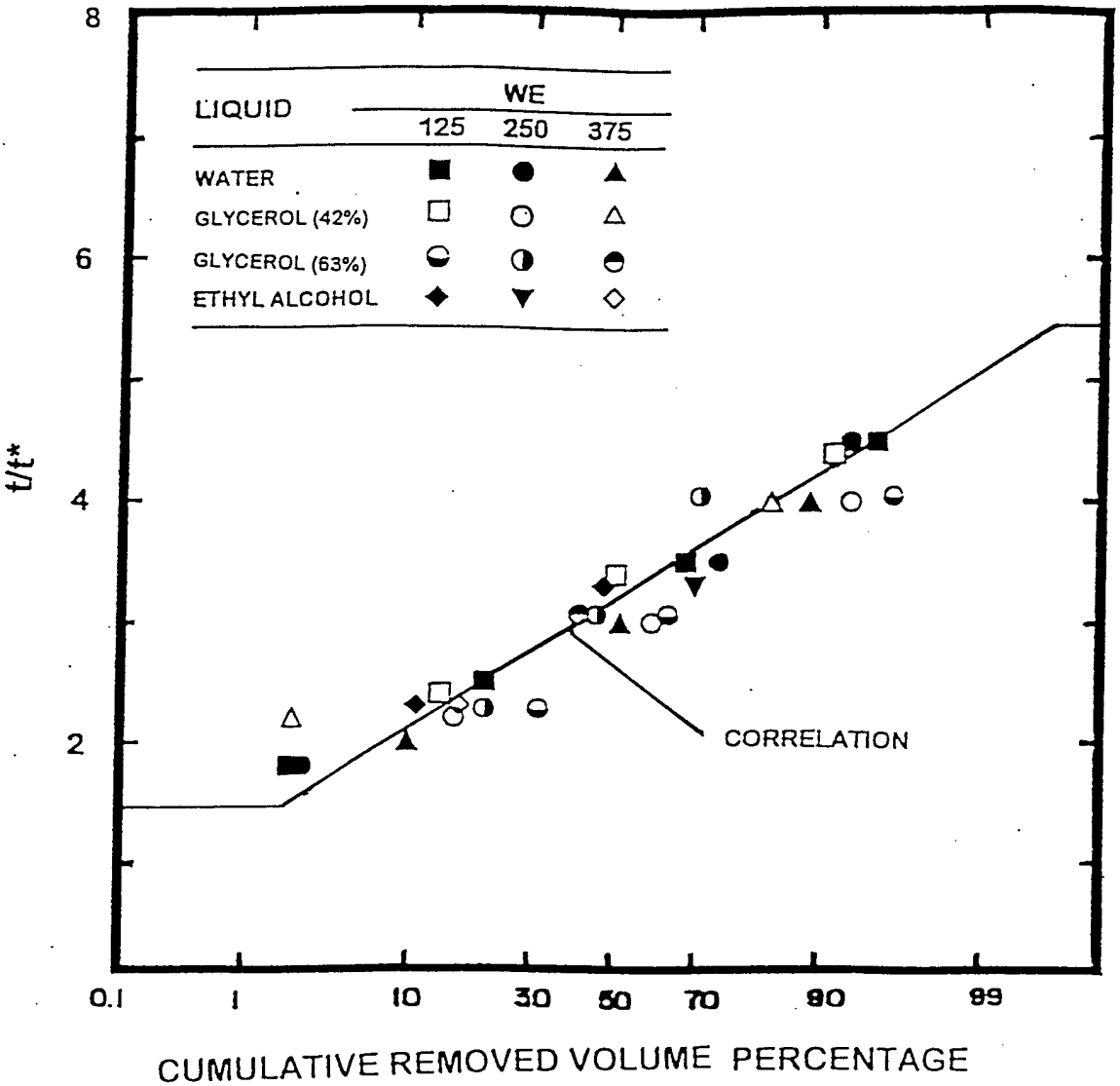

Fig. 3 Degree of mass removal from the parent drop as a function of time during shear breakup. From Chou et al. (1997).

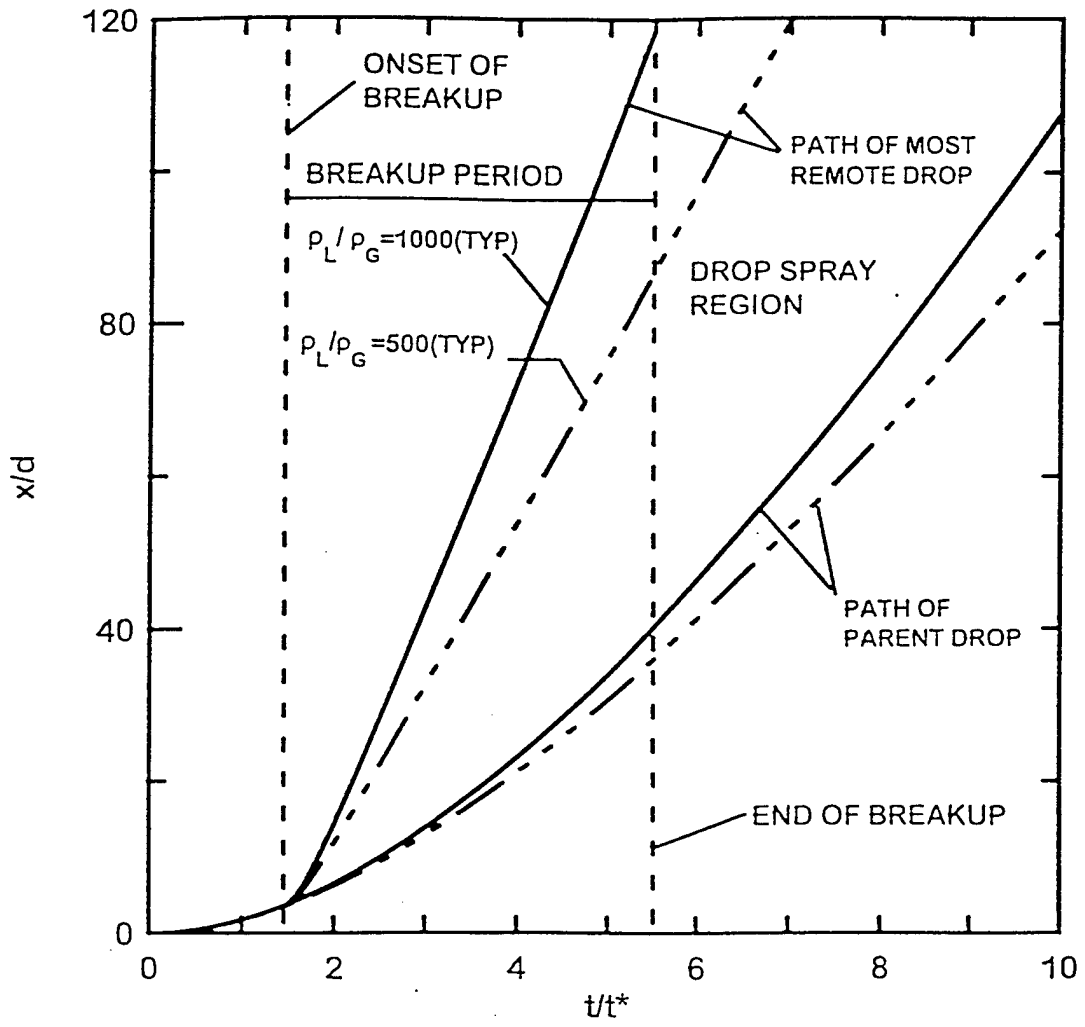

Fig. 4 Growth of the spray-containing region during shear breakup. From Chou et al. (1997).

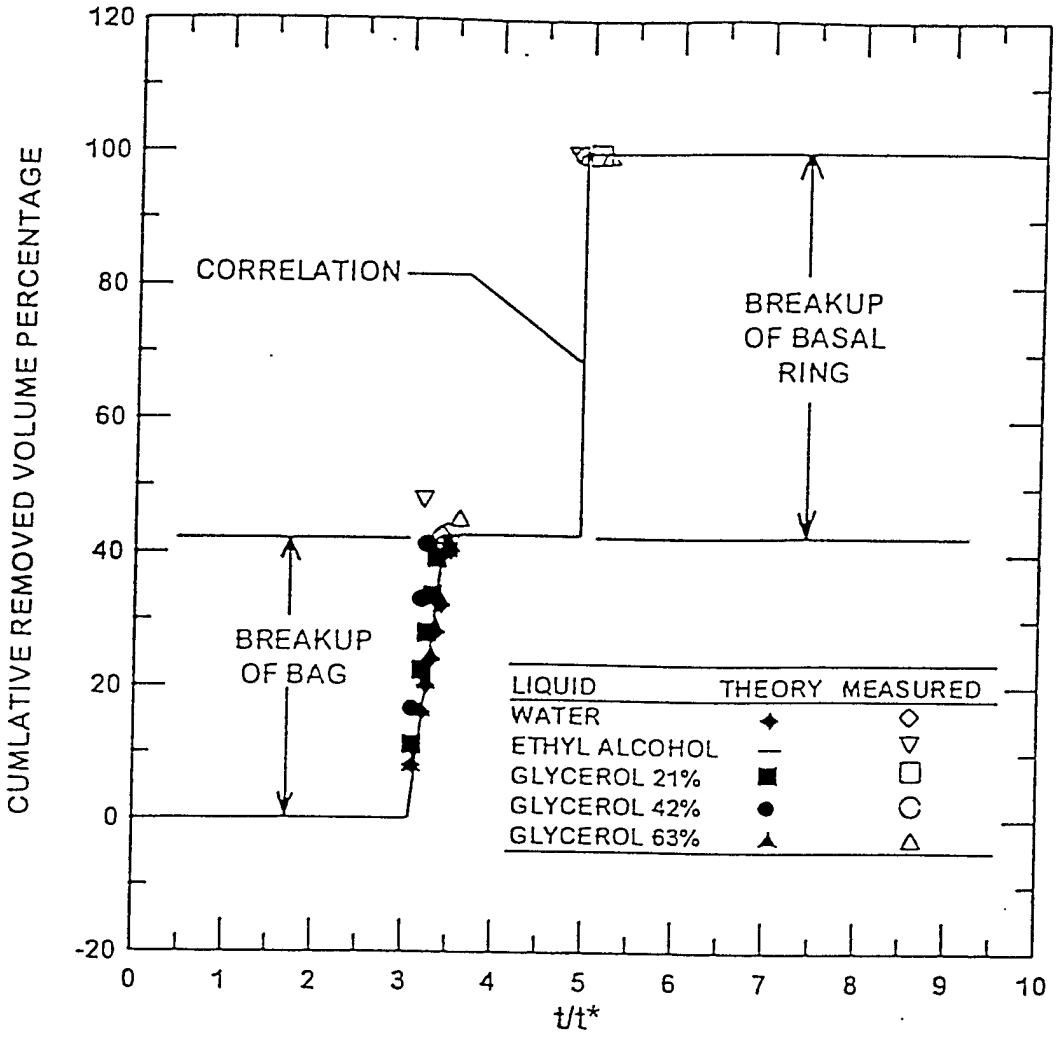

Fig. 5 Cumulative removed volume percentage of liquid from the parent drop as a function of time during bag breakup. From Chou and Faeth (1998).

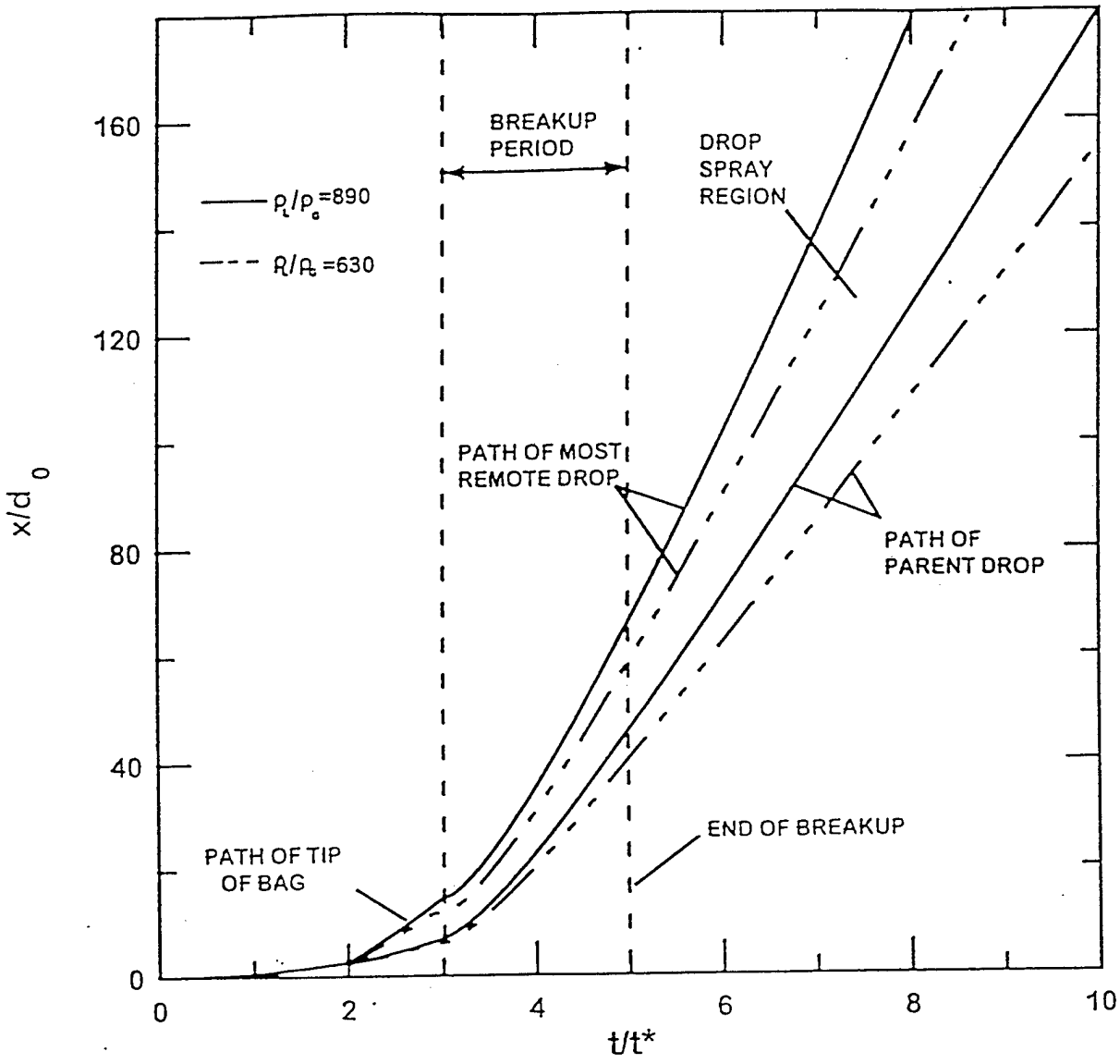

Fig. 6 Streamwise positions of the parent and the most remote drops as a function of time during bag breakup. From Chou and Faeth (1998).

(5) Mean velocities of drops produced by shear breakup are relatively independent of size at each instant.

(6) Mean and fluctuating velocities at each instant are associated with the parent drop velocity at that instant.

(7) The rate of liquid removal from the parent drop can be correlated quite simply as illustrated in Fig. 3.

(8) Shear breakup requires significant times and distances and should be treated as a rate process rather than by jump conditions in some instances.

Bag Breakup. Major conclusions for bag breakup are as follows:

(1) The basal ring contains 56% of the drop mass and yields nearly monodisperse drops having mean diameters of roughly 30% d_o.

(2) The bag contains the rest of the drop liquid and yields monodisperse drops having diameters of roughly 4% d_o.

(3) The bag and basal ring drops should be treated as separate populations formed at $t/t^* = 3.2$-3.5 and 5.0, respectively.

(4) The parent drop exhibits large acceleration rates due to its large drag coefficient. Bag and ring drops have nearly uniform velocities associated with the velocity of the parent drop when they are formed.

(5) Bag breakup required significant times and distances and should be treated as a rate process in some instances.

Current Work. In view of these findings current work is emphasizing the temporal properties of multimode breakup, which is bounded by the bag and shear breakup regimes, see Fig. 1.

3. Turbulence Generation

3.1 Introduction

Turbulence generation by drops controls the turbulence properties, and thus the mixing properties, within dense sprays (Faeth et al. 1996; Faeth et al. (1996). This behavior follows because velocities are relatively uniform, inhibiting the conventional production of turbulence, while the relative velocities of drops are large, which implies significant flow disturbances from drop wakes within dense sprays.

Drop-generated turbulence differs from grid-generated turbulence because drops are present throughout the flow, and their arrival at any point is random, yielding a truly stationary turbulent field. In contrast, grids generate turbulence at a plane of the flow yielding an unsteady flow field that subsequently decays. Thus, drop-generated turbulence is unique compared to conventional turbulence and has been studied very little in spite of its importance to practical spray processes. Motivated by these observations, turbulence generation was studied during this phase of the present investigation.

Past studies of turbulence generation have mainly considered homogeneous dilute dispersed flows (Lance and Bataille 1982; Parthasarathy and Faeth 1990; Mizukami et al.

1992). Lance and Bataille (1982) studied homogeneous air/water bubbly flows downstream of a turbulence-generating grid. Effects of turbulence generation were observed as progressive increases of turbulence levels with increasing void fractions. Unfortunately, these results are difficult to interpret due to combined effects of turbulence generation and grid-generated turbulence.

Initial work in this laboratory on turbulence generation is described by Parthasarathy and Faeth (1987, 1990) and Mizukami et al. (1992). Aside from qualitative observations of turbulence generation in bubbly jets (Parthasarathy and Faeth 1987) experimental conditions consisted of uniform fluxes of nearly monodisperse spherical glass beads falling at roughly constant speeds in stagnant (in the mean) air and water. Measurements included phase velocities and turbulence properties of the continuous phase. Turbulence properties were analyzed using a stochastic method based on Campbell's theorem (Rice 1954) that involved synthesis of randomly-arriving particle wakes. The measurements showed that particle-generated turbulence had rather different properties from conventional turbulence. The theory helped explain this behavior as a result of the random arrival of particle wakes so that *mean* wake properties contribute to the apparent turbulence field. However, while the stochastic theory assisted data interpretation, quantitative predictions were not very satisfactory because particle wake properties at intermediate Reynolds numbers (typical of drops in sprays) in turbulent environments were unknown and had to be extrapolated from results at large Reynolds number turbulent wakes in nonturbulent environments. These studies were also problematical because the nearly stagnant (in the mean) continuous phases caused significant experimental uncertainties due to the resulting large turbulence intensities (up to 1000%) along with problems of buoyant disturbances.

Subsequent work sought to resolve the properties of wakes at intermediate Reynolds numbers in turbulent (roughly isotopic) environments (Wu and Faeth 1994, 1995). It was found that these wakes scaled in the same manner as self-preserving laminar wakes (Schlichting 1975) but with enhanced viscosities due to the presence of turbulence. Thus, the wakes were termed "laminar-like turbulent wakes." Naturally, the properties of laminar-like turbulent wakes differed considerably from the wake properties assumed by Parthasarathy and Faeth (1990) and Mizukami et al. (1992). These results also suggested that turbulence generation dominated flows are likely to consist of laminar-like turbulent wakes embedded in relatively large inter-wake turbulent regions. Nevertheless, differences between the ambient turbulence properties of the wake studies and actual flows dominated by turbulence generation are a concern.

Based on this status, the specific objectives of the present study were as follows: (1) to complete new measurements of flow properties resulting from turbulence generation with reduced experimental uncertainties, (2) to use the measurements to determine the nature of the wake disturbances and the potential for wake-to-wake interactions during turbulence generation, and (3) to use the measurements to highlight differences between turbulence fields associated with turbulence generation and more conventional turbulence. The present discussion of the study is brief, see Chen et al. (1998) for more details.

3.2 Experimental Methods

Apparatus. A sketch of the test apparatus appears in Fig. 7. The arrangement consists of a vertical counterflow wind tunnel with upflowing air and freely-falling particles. The air flow system consisted of a rounded inlet, a flow straightener and a contraction with air flow supplied by a variable-speed blower at the top of the tunnel. The particle flow was provided by a variable-speed screw feeder with the particles dispersed by an array of screens and finally aligned to the vertical direction using a flow straightener.

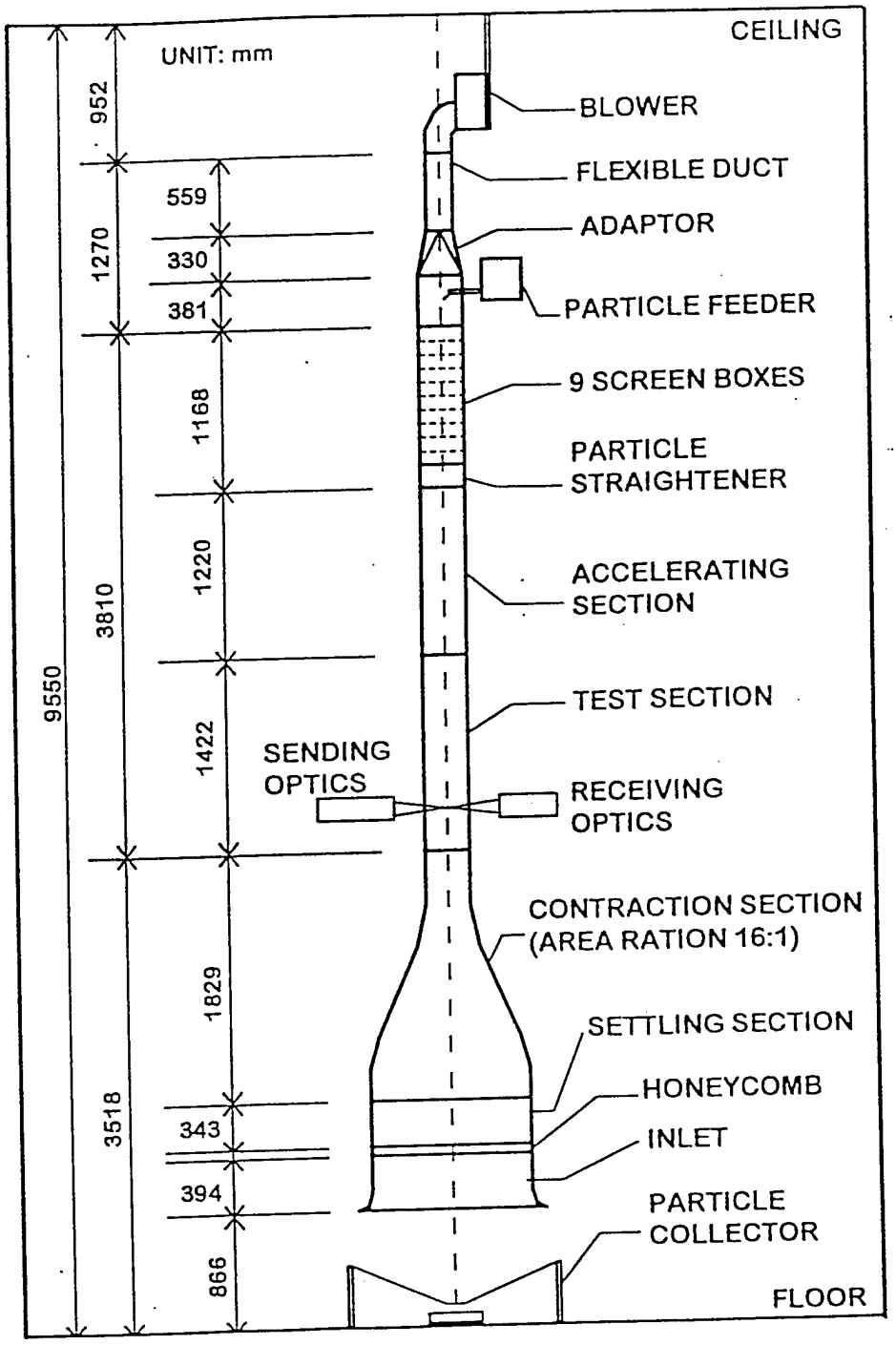

Fig. 7 Sketch of the counterflow particle/air wind tunnel. From Chen et al. (1998).

The test section has a 305 × 305 mm crossection with glass side walls to provide optical access.

Instrumentation. Particle number fluxes were measured by collecting particles in a thin-walled cylindrical container that could be traversed across the test section.

Gas and particle velocities were measured using a traversible laser velocimetry (LV) system. A single-channel dual-beam, forward-scatter, frequency-shifted LV was used, finding streamwise and crosstream velocities by rotating the optics accordingly. The air flow was seeded with oil particles for gas velocity measurements but was not seeded for particle velocity measurements. Particle velocity signals were readily determined due to their large signal amplitudes and nearly constant velocities.

Test Conditions. The experiments involved nearly monodisperse spherical glass particles having nominal diameters of 0.5, 1.1 and 2.2 mm. These particles yielded Reynolds numbers in the range 106-990. Turbulence intensities relative to the mean gas velocity (1.1 m/s) were less than 25%. The flows were dominated by turbulence generation with direct dissipation of turbulence due to particles less than 2%. Particle volume fractions were less than 0.003% so the flows were very dilute. The resulting relative turbulence intensities due to turbulence generation were in the range 0.2-5.0%.

3.3 Results and Discussion

Apparatus Evaluation. Sampling measurements showed that particle fluxes varied less than 10% over the central 205 × 205 mm crossection of the flow where velocity measurements were made. Mean and fluctuating particle and gas velocities were uniform over the same crossection for positions ± 100 mm from the normal measuring plane.

Particle Wake Properties. Direct temporal records of streamwise and crosstream velocities properly indicated wake disturbances that increased in frequency with increasing particle fluxes. Typical records indicating effects of particle Reynolds numbers for mid-range particle loadings are illustrated in Fig. 8 (Note that u and v records were not obtained at the same time). Relatively large negative spikes are observed on the streamwise velocity records indicating wake disturbances. Corresponding disturbances on the crosstream velocity records are absent for the 0.5 mm particles and have both negative and positive (or both) values for the larger particles. This behavior is expected based on the known properties of laminar-like turbulent wakes (Wu and Faeth 1994, 1995). In particular, mean crosstream velocities in these wakes are always small while the crosstream turbulence contribution is small for the 0.5 mm particles whose Re are below the onset of eddy shedding into the wake. In contrast, laminar-like turbulent wakes properties of the 1.1 and 2.2 mm particles have significant crosstream velocity fluctuations which explains the crosstream wake disturbances seen for these conditions. Thus, the results of Fig. 8 are strongly supportive of laminar-like turbulent wake behavior for the present test flows.

A further evaluation of particle wake properties is illustrated in Fig. 9. These results involve measurements of mean velocities in particle wakes for various particle sizes. Measurements were obtained for various maximum velocity defects which represent results for paths of the LV measuring volume at various radial distances from the wake axis. Effects of turbulence were handled by averaging several velocity records. Predictions for the same mean velocity defects, particle sizes and ambient turbulence intensities were obtained from the laminar-like turbulent wake properties reported by Wu and Faeth (1994, 1995). The agreement between measurements and predictions is excellent, supporting the

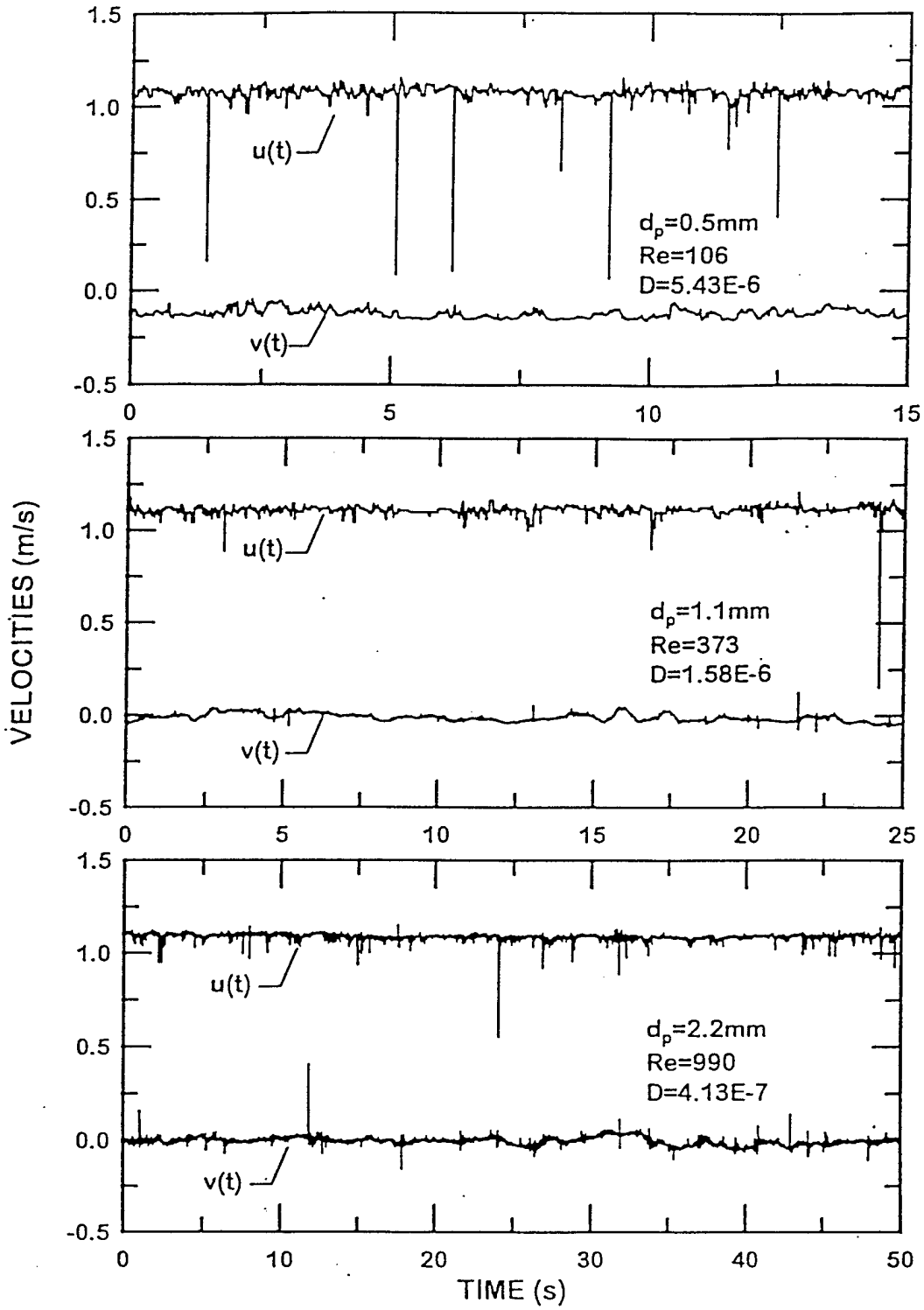

Fig. 8 Effect of particle Reynolds number on streamwise and crosstream.velocity records. From Chen et al. (1998).

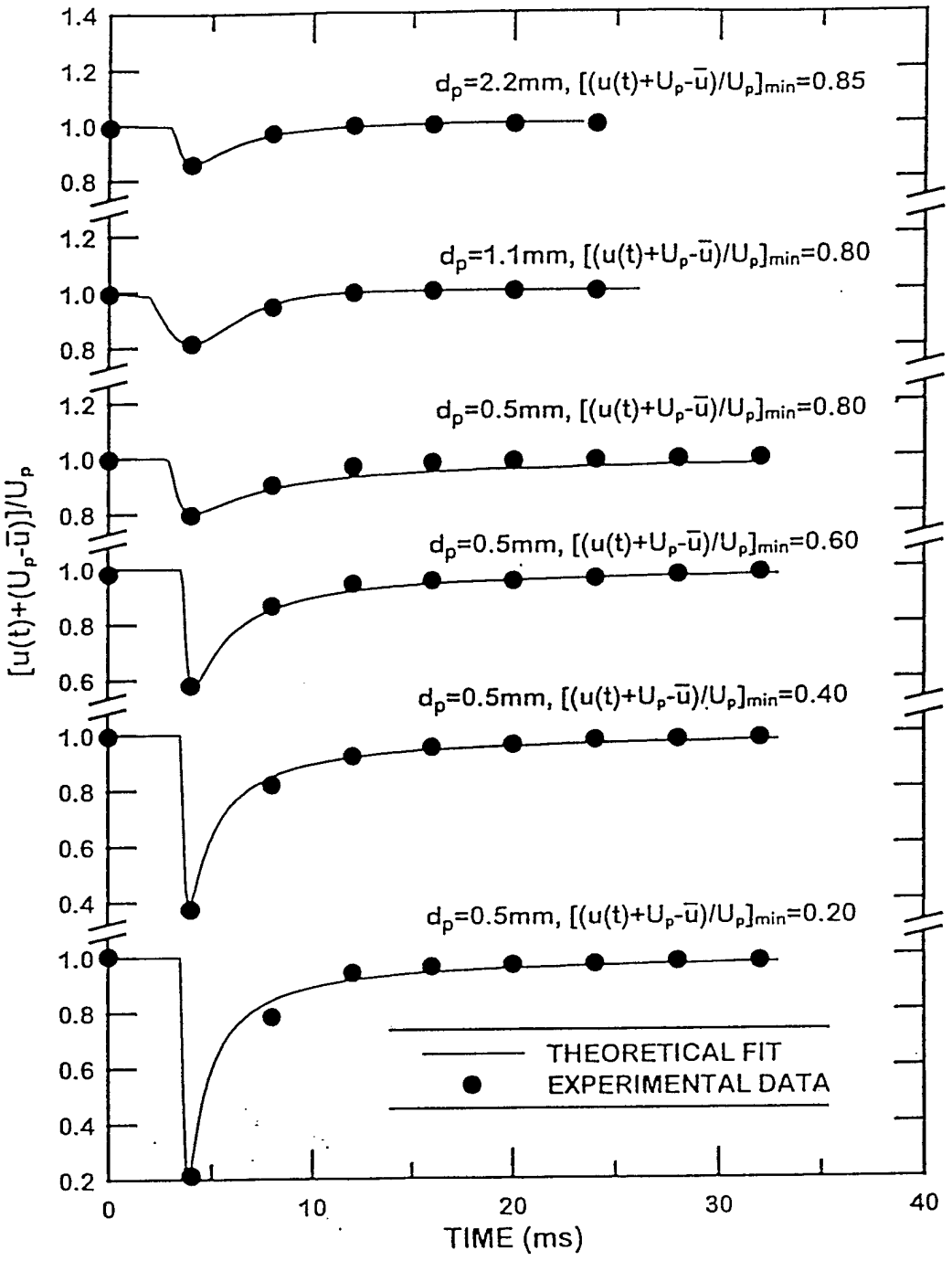

Fig. 9 Measured and predicted streamwise velocities in particle wakes as a function of time. From Chen et al. (1998).

presence of laminar-like turbulent wake properties for turbulence generation processes typical of sprays.

The proportions of wake and inter-wake regions were estimated based on the laminar-like turbulent wake properties combined with stochastic simulations to find realizations of particle positions. Laminar-like turbulent wakes were associated with each particle conservatively assuming that wake radii were equal to twice the characteristic wake radii and extended in the streamwise direction until the maximum mean velocity defect equaled the ambient rms turbulent fluctuations. These results indicated that wake crossectional areas generally were less than 30% of the available crossectional area and that less than 25% of the wakes experienced direct wake/wake interactions (mainly weak interactions far from both particles). Thus, the present test flows involve laminar-like turbulent wakes surrounded by relatively large inter-wake regions with occasional strong wake/wake interactions: actual dense sprays should be similar.

Probability Density Functions. More insight about the effects of wake disturbances on total turbulence properties can be obtained from PDF's of velocity fluctuations. Typical results along these lines for low and high particle loadings for 0.5 mm diameter particles are illustrated in Fig. 10. The PDF(u) are peaked with the peak shifted toward positive velocities compared to the mean velocity, which comes about due to the contribution of wake spikes according to the fundamental properties of PDF's, see Tennekes and Lumley (1972). In contrast, the PDF(v) is Gaussian, due to the absence of significant wake disturbances for this velocity component. Finally, the small effect of particle fluxes on the PDF's illustrated in Fig. 10 is expected because PDF's are generally effected by the shape rather than the frequency of the velocity signal. Similar results were observed for PDF's at other test conditions (Chen et al. 1998).

Velocity Fluctuations. Present measurements of streamwise and crosstream velocity relative turbulence intensities, i.e., rms velocity fluctuations normalized by the relative streamwise particle velocity, could be correlated in terms of the dissipation factor, D, similar to past observations of Parthasarathy and Faeth (1990) and Mizukami et al. (1992). These correlations show fair agreement among the three studies but there is significant scatter due to changes of particle sizes and even particle flux in some cases (Chen et al. 1998). Thus, these correlations are only tentative pending more information about inter-wake properties and the use of these results in a more rational conditional averaging procedure to summarize the properties of flows caused by turbulence generation.

Energy Spectra. Taylor's hypothesis was used to convert measured temporal spectra into energy spectra. As an example, the resulting streamwise energy spectra are illustrated in Fig. 11. Measurements are shown for various particle sizes and fluxes. A convenient approximation of isotropic turbulence spectra, where the -5/3 power decay in the inertial range follows a -2 power decay, is also shown on the plot.

The energy spectra correlate reasonably well when plotted in the manner of Fig. 11. The spectra actually extend beyond the range shown in the figure, to $kL_u \sim 100$ which is on the order of Kolmogorov frequencies. Thus, the spectra exhibit a rather large range of kL_u (roughly four decades) even though present particle Reynolds numbers are not large (less than 1000). Much of this behavior is typical of other homogeneous turbulence fields where disturbances due to grids (with relatively small grid element Reynolds numbers) yield turbulent flows having extended inertial ranges. Another feature of the present flows enhances this behavior, however, because both mean and turbulent contributions to wake disturbances affect the spectra because wake arrivals are random, which increases the range of length scales in the signal. Naturally, similar contributions are not present in grid-

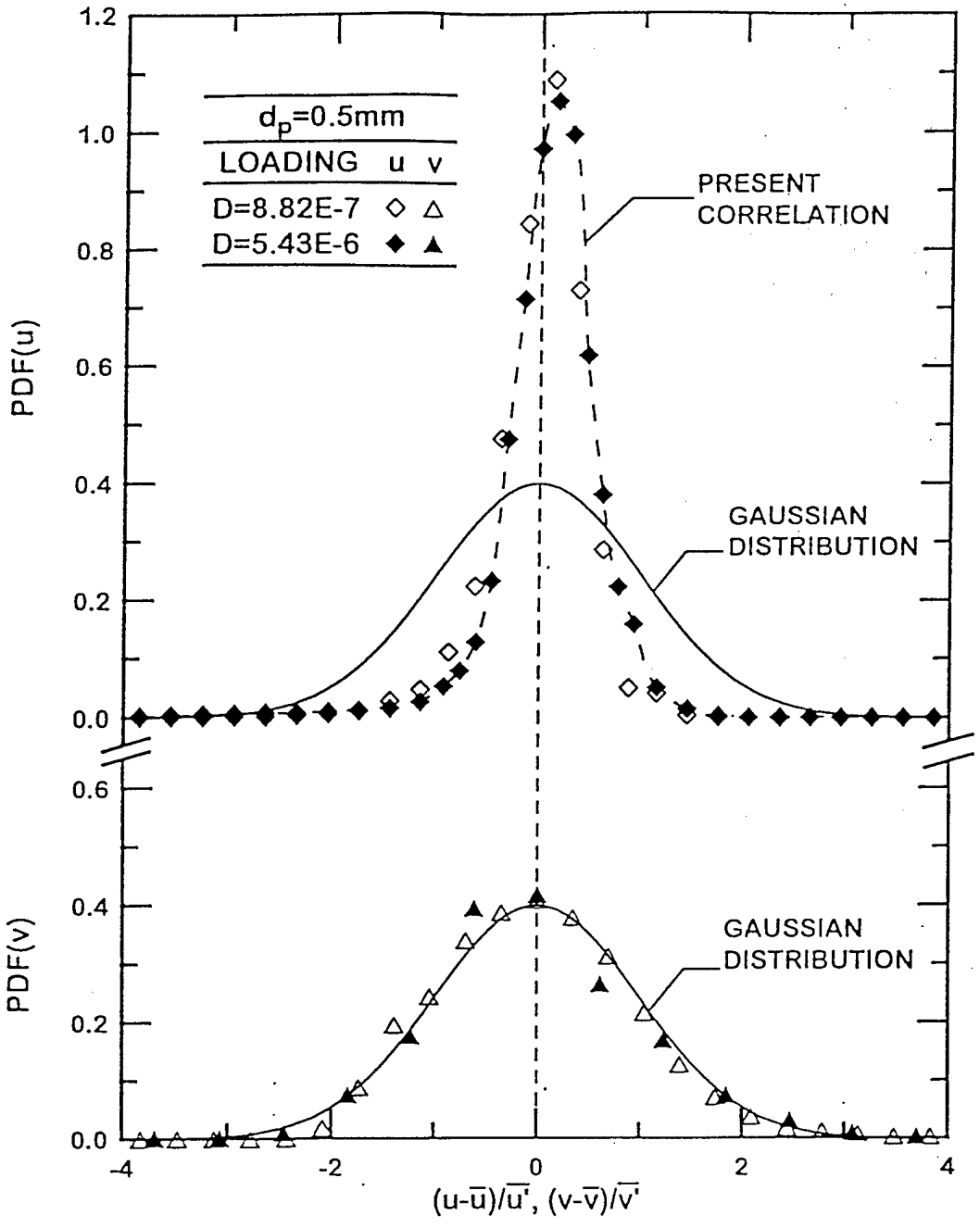

Fig. 10 Streamwise and crosstream velocity PDF's at low and high particle loadings for 0.5 mm particles. From Chen et al. (1998)

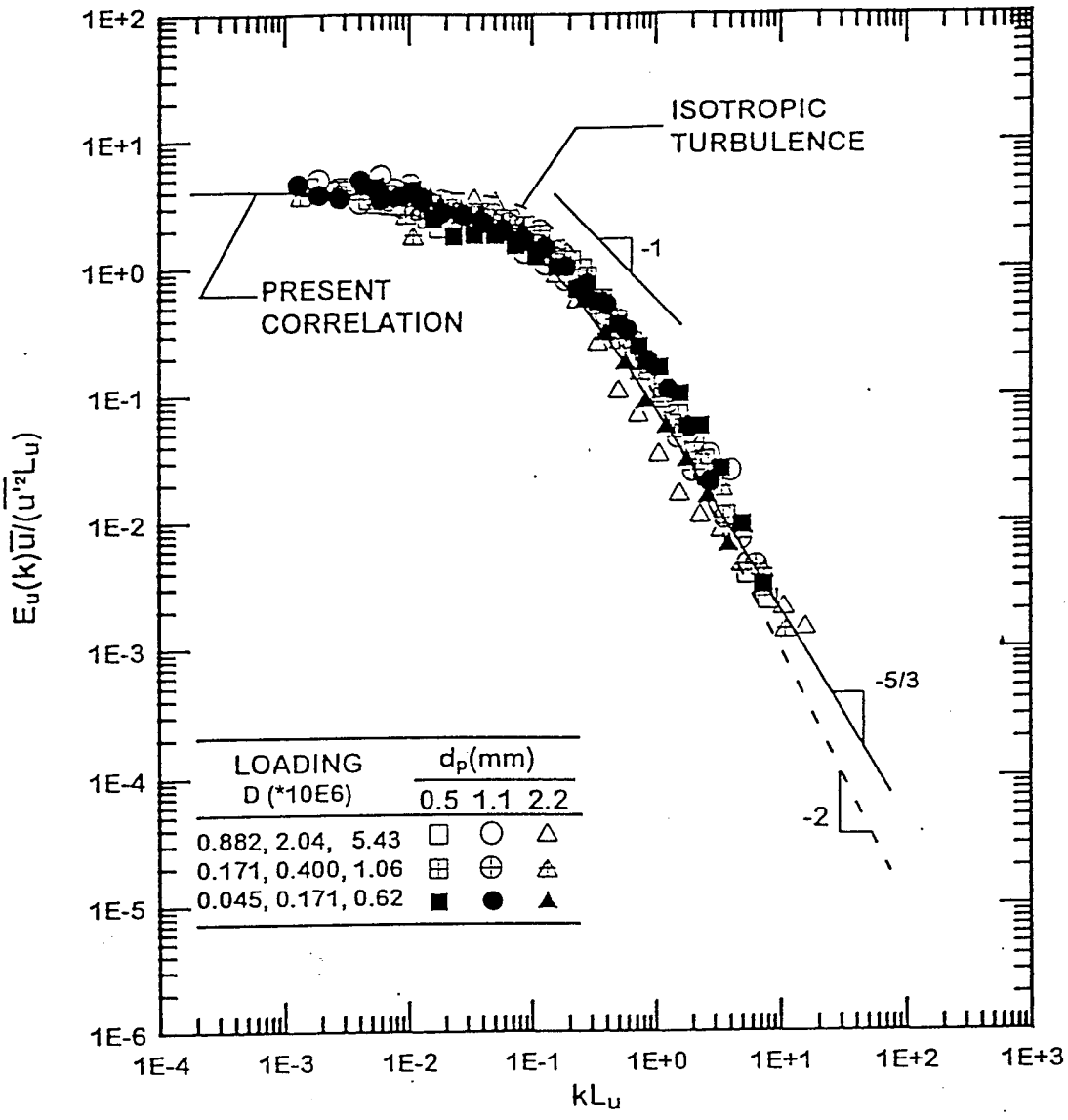

Fig. 11 Energy spectra of streamwise velocity fluctuations for various particle loadings and sizes. From Chen et al. (1998).

generated turbulence because measurements of these flows are made well downstream of the region that has significant direct wake disturbances.

The energy spectra of Fig. 11 also provide direct evidence of contributions from mean velocities in wake disturbances. In particular, the spectra exhibit prominent -1 and -5/3 decay regions with increasing wave numbers where the former is caused by mean velocity distributions in wakes and the latter is caused by turbulence contributions from both the wakes and the inter-wake region (Chen et al. 1998).

3.4 Conclusions

The major conclusions of the turbulence generation study thus far are as follows:

1. Measurements of gas velocities indicate that particle wake properties of the present turbulence generation processes correspond to the laminar-like turbulent wakes observed by Wu and Faeth (1994, 1995).

2. Dispersed flows typical of dense sprays involve wake disturbances (involving crossectional areas less than 30% of the whole) embedded into relatively large inter-wake turbulence regions with relatively few (less than 25%) direct wake/wake interactions (mainly limited to regions far from both wake-generating objects).

3. Present relative turbulence intensities agreed reasonably well with earlier observations of Parthasarathy and Faeth (1990) and Mizukami et al. (1992) for flows in nearly still liquids and gases (in the mean). The resulting correlations for various particle sizes and fluxes are somewhat scattered, however, and are only tentative pending development of more rational methods based on conditional averages for wake disturbances and inter wake regions.

4. PDF's and energy spectra provided direct evidence for effects of both wake disturbances and inter-wake turbulence regions, with wake disturbances contributing to peaked PDF's and to -1 power decay regions of energy spectra. The contributions from both wake disturbances and inter-wake regions also are responsible for the surprisingly large range of scales seen in flows caused by turbulence generation in spite of small particle Reynolds numbers.

Current work seeks a more rational basis to understand turbulence generation by studying the inter-wake region now that effects of wake disturbances are reasonably understood. Given detailed information about the inter-wake region, the use of conditional averages over the wake and inter-wake regions should provide a more fundamental estimate of flow properties than the past methods of Parthasarathy and Faeth (1990) and Mizukami et al. (1992).

References

Chen, J.-H., Wu, J.-S. and Faeth, G.M. (1998) AIAA J., submitted.

Chou, W.-H. and Faeth, G.M. (1998) Int. J. Multiphase Flow, in press.

Chou, W.-H., Hsiang, L.-P. and Faeth, G.M. (1997) Int. J. Multiphase Flow 23, 651.

Faeth, G.M. (1996) 26th Symp. (Intl.) Combustion, The Combustion Institute, Pittsburgh, p. 1593.

Faeth, G.M., Hsiang, L.-P. and Wu, P.-K. (1995) Int. J. Multiphase Flow 21 (Suppl.), 99.

Hinze, J.O. (1955) AICh J. 1, 289.

Hsiang,L.-P. and Faeth, G.M. (1995) Int. J. Multiphase Flow 18, 635,

Hsiang,L.-P. and Faeth, G.M. (1993) Int. J. Multiphase Flow 19, 721.

Hsiang, L.-P. and Faeth, G.M. (1995) Int. J. Multiphase Flow 21, 545.

Lance, M. and Bataille, J. (1982) Adv. Two-Phase Flow & Heat Trans. 1, Martinus Nijhof, Amsterdam, pp. 413.

Mizukami, M., Parthasarathy, R.N. and Faeth, G.M., (1992) Int. J. Multiphase Flow 18, 397.

Parthasarathy, R.N. and Faeth, G.M. (1987) Int. J. Multiphase Flow 13, 699.

Parthasarathy, R.N. and Faeth, G.M. (1990) J. Fluid Mech. 220, 485.

Rice, S. O. (1954) *Noise and Stochastic Processes* (N. Wax, ed.), Dover Publications, New York, p. 133.

Schlichting, H. (1975) *Boundary Layer Theory*, 7th ed., McGraw-Hill, New York, p. 234, p. 599,.

Tennekes, H. and Lumley, J.L., (1972) *A First Course in Turbulence*, MIT Press, Cambridge,p. 275.

Wu, J.-S. and Faeth, G.M. (1994) AIAA J. 32, 535.

Wu, J.-S. and Faeth, G.M. (1995) AIAA J. 33, 171.

Appendix A: Chou, W.-H., Hsiang, L.-P. and Faeth, G.M. (1997) Temporal Properties of Drop Breakup in the Shear Breakup Regime. Int. J. Multiphase Flow 23, 651-669,

Pergamon

PII: S0301-9322(97)00006-2

Int. J. Multiphase Flow Vol. 23, No. 4, pp. 651–669, 1997

Printed in Great Britain
0301-9322/97 $17.00 + 0.00

TEMPORAL PROPERTIES OF DROP BREAKUP IN THE SHEAR BREAKUP REGIME

W.-H. CHOU, L.-P. HSIANG and G. M. FAETH†

Department of Aerospace Engineering, The University of Michigan, Ann Arbor, MI 48109-2118, U.S.A.

(Received 2 June 1996; in revised form 27 January 1997)

Abstract—The temporal properties of drop breakup in the shear breakup regime were studied using pulsed shadowgraphy and holography for shock wave disturbances in air at normal temperature and pressure. Test conditions included Weber numbers of 125–375, Ohnesorge numbers of 0.003–0.040, liquid/gas density ratios of 670–990 and Reynolds numbers of 3000–12000. The size distributions of drops produced by breakup satisfied Simmons' universal root normal distribution function at each instant of time, with Sauter mean diameters independent of surface tension that exhibited transient and quasi-steady regimes as a function of time. The velocity distribution functions of drops produced by breakup were uniform, with mean drop velocities somewhat larger than the velocity of the parent drop and rms drop velocity fluctuations of 30–40% of the mean streamwise velocity of the gas relative to the parent drop, at each instant of time. The rate of liquid removal from the parent drop was correlated reasonably well by a clipped Gaussian function. The measurements showed that shear breakup is not a localized event; instead, it extends over streamwise distances of 0–100 initial drop diameters, which suggests that it should be treated as a rate process, rather than by jump conditions, in some instances. © 1997 Elsevier Science Ltd.

Key Words: drop breakup, drop dynamics, pulsed holography, sprays, atomization

1. INTRODUCTION

The breakup of individual drops, which is often called secondary breakup, is an important fundamental process of sprays. For example, drops formed by breakup of liquid surfaces, which is often called primary breakup, are intrinsically unstable to secondary breakup, while secondary breakup can be the rate controlling process within dense sprays in much the same way that drop vaporization can be the rate controlling process within dilute sprays (Faeth 1990, 1996; Wu *et al.* 1995). Motivated by these observations, the objective of the present investigation was to extend earlier studies of the regimes and outcomes of secondary breakup due to shock-wave disturbances (Hsiang and Faeth 1992, 1993, 1995), to consider the evolution of breakup as a function of time during breakup.

Earlier studies of drop breakup are discussed by Wu *et al.* (1995), Faeth (1990, 1996), Giffen and Muraszew (1953), Hinze (1955), Clift *et al.* (1979), Krzeczkowski (1980) and Wierzba and Takayama (1987, 1988), among others. Shock-wave disturbances were considered during most earlier studies, providing a step change of the ambient environment of the drop, similar to conditions experienced by drops at the end of primary breakup. The main findings of this work included the conditions required for particular deformation and breakup regimes, the times required for the onset and end of breakup, the drag properties of deformed drops, and drop size and velocity distributions at the end of the breakup process (i.e. the jump conditions). An interesting feature of these results is that drop breakup extended over appreciable regions of time and space and was not properly described by jump conditions in some instances. This behavior can be illustrated in terms of the characteristic breakup time, t^*, of Ranger and Nicholls (1968), defined as follows

$$t^* = d_o(\rho_L/\rho_G)^{1/2}/u_o, \qquad [1]$$

†To whom correspondence should be addressed.

where d is the drop diameter, ρ is density, u is streamwise drop velocity relative to the gas, the subscripts L and G denote liquid and gas properties, and the subscript o denotes conditions at the start of breakup. Liang *et al.* (1988) show that breakup times for a wide range of conditions are $5.5\,t^*$, which is comparable to flow residence times within the dense spray region where secondary breakup is a dominant process (Faeth 1990, 1996; Wu *et al.* 1995). Viewed another way, the original (or parent) drop moves roughly 40 initial drop diameters, while the smallest drops formed by breakup move up to 100 initial drop diameters, during the period of breakup within the shear breakup regime (Hsiang and Faeth 1992, 1993, 1995). Such distances can represent a significant fraction of the length of the dense spray region. These observations suggest that the time-resolved features of secondary breakup eventually must be understood. Thus, the present study seeks to provide some of this information by carrying out new measurements within the shear breakup regime, where breakup proceeds by the stripping of drop liquid from the periphery of the parent drop, because this regime tends to dominate drop breakup in practical sprays (Hsiang and Faeth 1995). Phenomenological theories also were developed to help interpret and correlate the measurements.

The present measurements were carried out using a shock tube facility, with the drop environment approximating air at normal temperature and pressure (NTP). Properties during breakup were observed using pulsed shadowgraphy and holography. Test conditions were limited to relatively large liquid/gas density ratios ($\rho_L/\rho_G > 500$) in order to minimize potential complications due to the inertia of the continuous phase. The test conditions also involved limited ranges of Weber and Ohnesorge numbers, which Hinze (1955) has shown define the boundaries of the shear breakup regime at large liquid/gas density ratios. The Weber number, We, is a measure of the relative importance of drop drag and surface tension forces, and is defined as follows

$$\mathrm{We} = \rho_G d_o u_o^2/\sigma, \qquad [2]$$

where σ is the surface tension of the drop liquid. The Ohnesorge number, Oh, is a measure of the relative importance of liquid viscous forces and surface tension forces, and is defined as follows

$$\mathrm{Oh} = \mu_L/(\rho_L d_o \sigma)^{1/2}, \qquad [3]$$

where μ is the molecular viscosity. The experiments involved relatively small initial Ohnesorge numbers ($\mathrm{Oh} < 0.04$) in order to minimize potential complications due to effects of liquid viscosity. For this range of Oh, operation in the shear breakup regime requires $\mathrm{We} > 90$, in order to exceed the multimode/shear breakup regime transition, and $\mathrm{We} < 800$, in order not to exceed the shear/drop-piercing (or shear/catastrophic) breakup regime transition (Giffen and Muraszew 1953; Hinze 1955; Reinecke and McKay 1969; Reinecke and Waldman 1970). Drop liquids included water, ethyl alcohol and various glycerol mixtures in order to provide information about effects of drop liquid properties.

2. EXPERIMENTAL METHODS

2.1. Apparatus

The test apparatus will be described briefly because it was similar to earlier work (Hsiang and Faeth 1992, 1993, 1995). A shock tube with the driven section open to the atmosphere was used for the measurements. The driven section had a rectangular cross-section (38 mm wide and 64 mm high) and was sized to provide test times of 17–21 ms in the uniform flow region behind the incident shock wave. The test location had quartz windows to allow observations of drop breakup.

A vibrating capillary tube drop generator, similar to the arrangement described by Dabora (1967), was used to generate a stream of drops having a constant diameter. An electrostatic drop selection system, similar to Sangiovanni and Kestin (1977), was used to control the spacing between drops. This drop stream passed vertically across the shock tube at the test location. The spacing between drops was 5–7 mm while drop sizes were ≤ 1 mm; therefore, drops always were present within the region observed while interactions between adjacent drops during shear breakup were negligible.

2.2. *Instrumentation*

Pulsed holography and shadowgraphy were used to observe the properties of the parent drop and the drops produced by breakup as a function of time during breakup. The holocamera used two frequency doubled YAG lasers (Spectra Physics Model GCR-130, 532 nm wavelength, 7 ns pulse duration, up to 300 mJ per pulse) which could be fired with pulse separations as small as 100 ns. An off-axis holocamera arrangement was used with the optics providing a 25 mm diameter field of view at the test drop location. Reconstruction of the double-pulse holograms yielded two images of the spray so that drop velocities could be found given the time of separation between the pulses (which was measured with a digital oscilloscope). The second laser pulse was somewhat weaker than the first, which allowed directional ambiguity to be resolved because stronger pulses yielded sharper reconstructed images. This arrangement also provided shadowgraphy by blocking the reference beam.

The hologram reconstruction system was modified from Hsiang and Faeth (1992, 1993, 1995). A helium–neon laser (Spectra Physics Model 124B, cw laser, 35 mW of optical power) was used to reconstruct the image, which was observed using a CCD camera (Sony, Model XC-77) with optics to yield a magnification of 300:1 and a field of view of the image (on the monitor) of 1.2 × 1.4 mm. The optical data was obtained using a frame grabber (Data Translation DT 2851) and processed using Media Cybernetics Image-Pro Plus software. Various locations in the hologram reconstruction were observed by traversing the hologram in two directions, and the videocamera of the image display in the third direction. Positions were selected for viewing using stepping motor driven linear traversing systems (Velmex, Model VP9000) having 1 μm positioning accuracies. The combined holocamera/reconstruction system allowed objects as small as 3 μm to be observed and objects as small as 5 μm to be measured with 5% accuracy.

Drop sizes and velocities were measured as described by Hsiang and Faeth (1992, 1993, 1995). Present results were found by summing over at least four realizations, and considering 50–100 liquid elements, in order to provide drop diameter and velocity correlations. These sample sizes were smaller than past studies of jump conditions in order to maintain a manageable test program while resolving drop properties as a function of time. Estimated experimental uncertainties (95% confidence) are less than 15% for drop diameters and less than 20% for streamwise mean drop velocities and rms drop velocity fluctuations; uncertainties of cross-stream mean velocities are larger due to the smaller values of these velocities, as discussed later.

2.3. *Test conditions*

The test conditions are summarized in table 1. The liquid properties were obtained from Lange (1952), except for the surface tensions of the glycerol mixtures which were measured in the same manner as Wu *et al.* (1991). Shock wave Mach numbers in the shock tube were relatively low, less than 1.15; therefore, the physical properties of the gas in the uniform flow region behind the shock wave, where drop breakup occurred, were nearly the same as air at NTP.

The specific range of the present tests is illustrated on the drop deformation and breakup regime map appearing in figure 1. This regime map is extended from Hsiang and Faeth (1995) to include new transitions measured during the present investigation, as follows: the shear/drop-piercing (or catastrophic) breakup regime transition at large We, first observed by Reinecke and McKay (1969), and the more qualitative shear/long-ligament breakup regime transition at large Oh, to be discussed later. Aside from experiments used to define the shear/drop-piercing and shear/long-ligament

Table 1. Summary of the test conditions†

Liquid	ρ_ℓ (kg/m^3)	$\mu_\ell \times 10^3$ (kg/ms)	σ (mN/m)	d_o (μm)	Oh × 10^3	Re
Water	997	8.94	70.8	590–1000	3.4–4.4	4930–11150
Ethyl alcohol	800	16.0	24.0	780–1000	11.5–13.1	3070–5740
Glycerol (42%)‡	1105	35.0	65.4	1000	13.0	6000–11180
Glycerol (63%)‡	1162	108.0	64.8	1000	39.4	5840–11240

†Air initially at 98.8 kPa and 298 ± 2 K in the driven section of the shock tube. Shock Mach numbers in the range 1.01–1.15 with We in the range 125–375. Properties of the air were taken at normal temperature and pressure: ρ_G = 1.18 kg/m^3, μ_G = 18.5 × 10^{-6} kg/ms.
‡Percentage glycerin by mass.

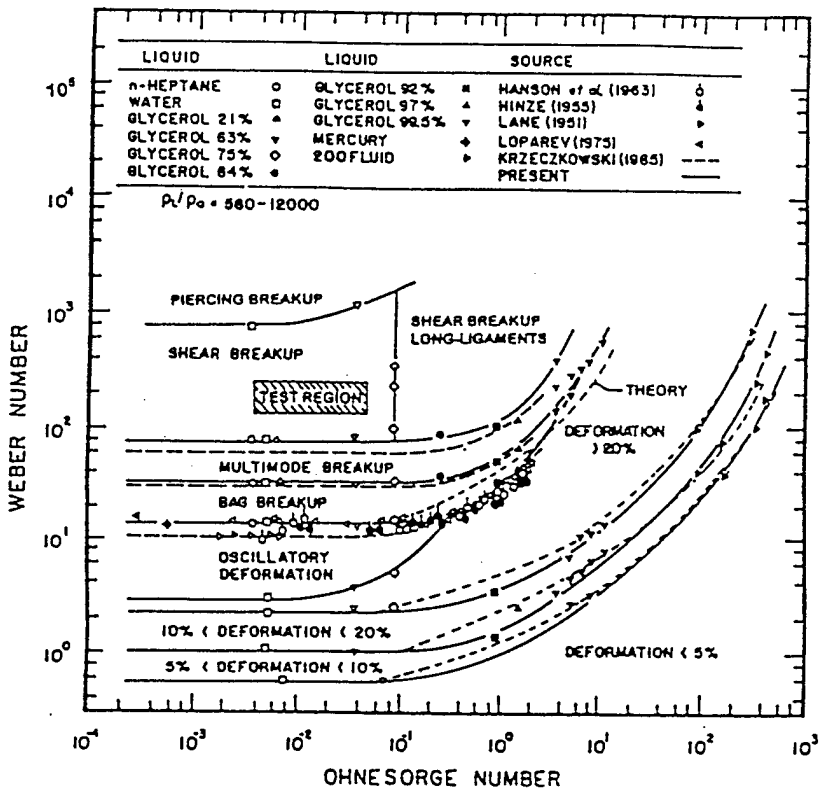

Figure 1. Drop deformation and breakup regime map for shock-wave disturbances, extended from Hsiang and Faeth (1995).

breakup regime transitions, however, present measurements were confined to the cross-hatched region which is conservatively located well within the shear breakup regime at small Ohnesorge numbers. This involved ρ_L/ρ_G of 670–990, We of 125–375 and Oh of 0.003–0.040. The range of initial drop Reynolds numbers, Re, was 3000–12000, where

$$\mathrm{Re} = \rho_G u_o d_o / \mu_G. \qquad [4]$$

These values of Re are higher than conditions where the gas viscosity has a significant effect on drop drag properties, e.g. the drag coefficient, C_D, for spheres only varies in the range 0.4–0.5 for this Reynolds number range (White 1974).

3. RESULTS AND DISCUSSION

3.1. *Flow visualization*

Pulsed shadowgraph flow visualizations provide an overview of the temporal properties of shear breakup. Figure 2 is an illustration of a series of these shadowgraphs for a condition toward the lower Oh values considered during the present study, see figure 1. It should be noted that the onset and end of breakup (where liquid removal from the parent drop begins and ends) occur at t/t^* of roughly 1.5 and 5.5, respectively (Liang *et al.* 1988), for reference purposes. The shock wave, and the flow velocities behind the shock wave, pass from the top to the bottom of the shadowgraphs.

The shadowgraph at $t/t^* = 0$ in figure 2 provides a size reference and illustrates the initial spherical shape of the drop. After passage of the shock wave, the drop deforms into a flattened shape, (see $t/t^* = 1$), because the liquid is drawn toward the drop periphery where the pressure is low due to acceleration of the gas flow over the drop surface. Ligaments and drops begin to be stripped from the drop when $t/t^* = 1.5$ (which is not shown in figure 2); even at $t/t^* = 2$, however, there is an extensive system of ligaments protruding from the periphery of the parent drop, with numerous individual drops present near the downstream end of the ligaments as a result of ligament breakup. Subsequently, the diameter and length of the ligaments, the diameters of the drops produced by breakup of the ligaments, the number of individual drops, and the range of streamwise distances where drops are observed, all increase as t/t^* increases; in contrast, the number of ligaments and the size of the parent drop both decrease as t/t^* increases—compare results at $t/t^* = 2$, 3, 4 and 5. Finally, the diameter of the parent drop, and the gas velocity relative to the parent drop, become small so that drop breakup ends at $t/t^* = 5.5$ (just beyond the range of photographs in figure 2). Subsequently the parent drop evolves toward a spherical shape as its relative velocity continues to decrease.

Increasing Ohnesorge numbers cause the maximum lengths of the ligaments to become progressively larger. This behavior follows from evolution of shear breakup toward large Oh conditions that are dominated by drop deformation and the formation of elongated single drops that are resistant to ligament breakup. Such configurations vastly complicate problems of temporally resolving drop breakup; therefore, present experiments were confined to $Oh < 0.1$, which was somewhat arbitrarily defined as the onset of the long ligament regime of shear breakup. Figure 3 is an illustration of breakup behavior at the transition condition to the long ligament regime. A series of shadowgraphs at the same values of t/t^* as figure 2 are shown for a glycerol (75% glycerin by mass) drop having $d_o = 1000\ \mu m$, $We = 250$ and $Oh = 0.099$. As before, both shock and flow velocities are directed from the top to the bottom of the shadowgraphs.

The shadowgraphs illustrated in figure 3 are qualitatively similar to those of figure 2. Ligament lengths and the extent of the region containing drops progressively increase, while the size of the parent drop progressively decreases, as t/t^* increases. Tracking and identifying intermediate

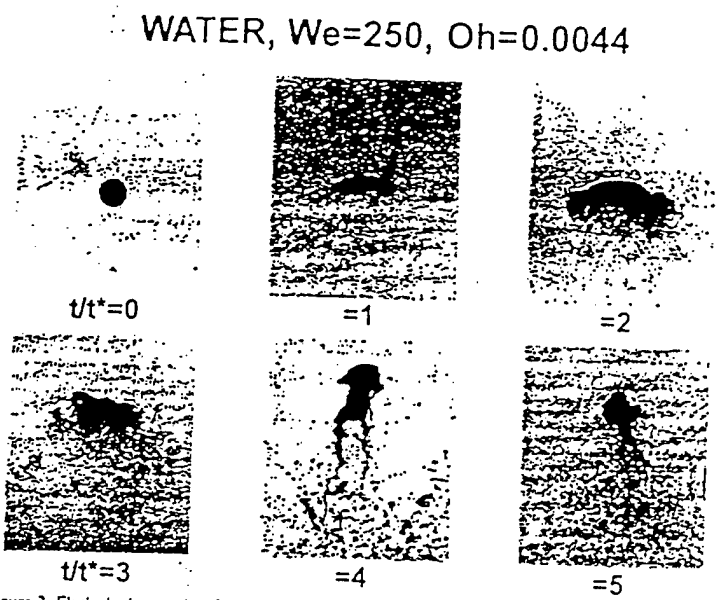

Figure 2. Flash shadowgraphs of the shear breakup of a water drop as a function of time: $d_o = 590\ \mu m$, $We = 250$ and $Oh = 0.0044$.

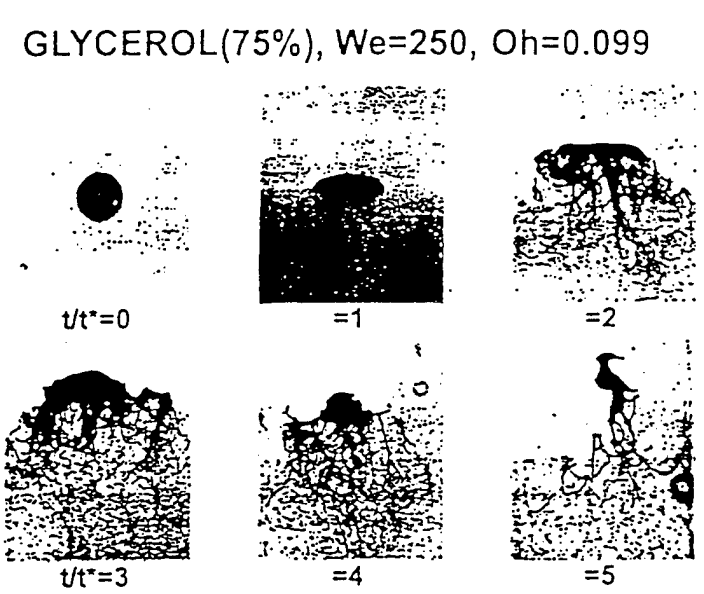

Figure 3. Flash shadowgraphs of the shear breakup of a glycerol drop (75% glycerin by mass) as a function of time: d_o = 1000 μm, We = 250 and Oh = 0.099.

breakup points along very long ligaments seen at these conditions, even when using holography, however, is very problematical. Thus, present test conditions were limited to Oh $\leq$ 0.04 which yielded manageable ligament lengths in a region somewhat below the transition to the long-ligament shear breakup regime.

3.2. Drop sizes

3.2.1. Drop size distribution. The evolution of drop size distributions during shear breakup was considered first because this affects the information needed to characterize secondary breakup properties. The main issue was to determine whether drop size distributions varied appreciably from the universal root normal distribution with MMD/SMD = 1.2, where MMD and SMD are the mass median and Sauter mean diameters of the distribution, respectively, proposed by Simmons (1977), which has been found to be satisfactory for a variety of drop breakup processes (Faeth 1990, 1996; Wu *et al.* 1995; Hsiang and Faeth 1992, 1993, 1995). See Belz (1973) for a discussion of the properties of the root normal distribution function.

Typical results from the drop size distribution measurements are illustrated in figure 4. The number of drops available to define the drop size distribution for each breakup condition and t/t^* is limited, which accounts for the significant scatter of drop size distribution properties seen in figure 4. Nevertheless, within the scatter of the data, drop sizes produced by secondary breakup are represented reasonably well by the universal root normal size distribution function with MMD/SMD = 1.2. This behavior is plausible because primary and secondary breakup processes, as well as drops at various positions within dense sprays, generally satisfy the universal root normal size distribution function, as mentioned earlier. With the two-parameter root normal size distribution function established for the temporal behavior of secondary drop breakup, drop size information can be summarized by the SMD alone (Hsiang and Faeth 1992).

3.2.2. Temporal evolution of the SMD. General description. Correlating expressions for the SMD as a function of time during secondary breakup in the shear breakup regime were sought using methods similar to Hsiang and Faeth (1992) and Wu *et al.* (1991). The present approach was motivated by the flow visualizations illustrated in figures 2 and 3. These results show that ligaments

(which subsequently break up into drops having comparable diameters) are stripped at the periphery of the parent drop from the liquid-phase vortical region (or boundary layer-like flow) that forms along the liquid surface on the upstream (windward) side of the drop during secondary breakup in the shear breakup regime. This behavior also was suggested by earlier work which showed that drop sizes after secondary breakup mainly depend on the viscosity, rather than the surface tension, of the liquid phase (Hsiang and Faeth 1992). In addition, initial measurements during the present investigation also suggested a strong effect of liquid viscosity on the drop sizes produced by secondary breakup. Finally, two basic types of behavior were observed during present experiments, as follows: (1) a regime where there was a progressive increase of ligament diameters, and a corresponding increase of the *SMD* of drops formed from these ligaments, as a function of time during breakup, which was mainly seen when the liquid viscosity and the time after the start of breakup were both small (this behavior is best characterized by the flow visualization of figure 2); and (2) a regime where the ligament diameters, and the SMD of drops formed from these ligaments, were relatively independent of time, which was mainly seen when the liquid viscosity and the time after the start of breakup were both large (this behavior is best characterized by the flow visualization of figure 3). Thus, liquid viscosity had an important effect on drop sizes even though all test conditions involved sufficiently small Ohnesorge numbers so that variations of liquid viscosity did not affect criteria for the onset of breakup, see figure 1. Both of these behaviors suggest that vorticity within the parent drop affects breakup; therefore, these effects will be considered similar to past study of drop size jump conditions due to Hsiang and Faeth (1992).

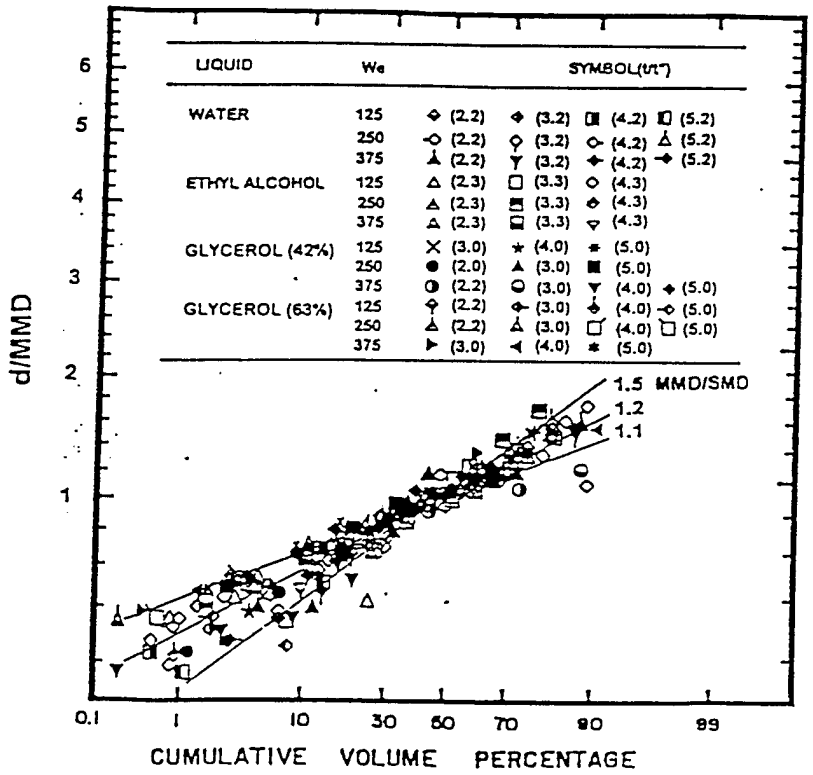

Figure 4. Diameter distribution of drops produced by shear breakup plotted according to the root normal distribution function.

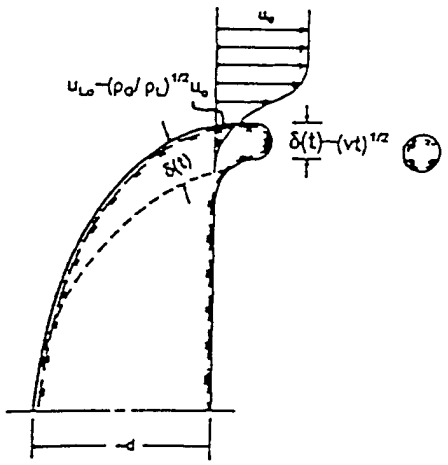

Figure 5. Sketch of the transient shear breakup mechanism at small Ohnesorge numbers ($t/t_c \leq 1$).

The phenomenological analyses to find the temporal variation of drop sizes during secondary breakup are based on the flow configurations appearing in figures 5 and 6. Both figures are sketches of the parent drop after the deformation period, when drops are being formed from the periphery of the parent drop. It is assumed that drops are formed from the vortical region in the liquid (or liquid boundary layer) that develops on the upstream side of the drop, that this layer is laminar, and that the thickness of this layer near the drop periphery, $\delta(t)$, is proportional to the *S.M.D* of

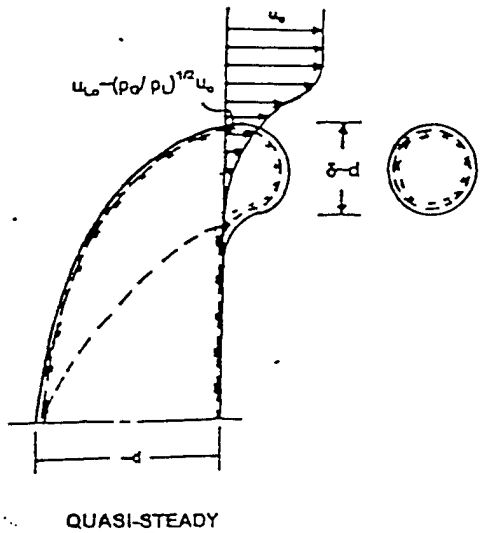

Figure 6. Sketch of the quasi-steady shear breakup mechanism at small Ohnesorge numbers ($t/t_c \geq 1$).

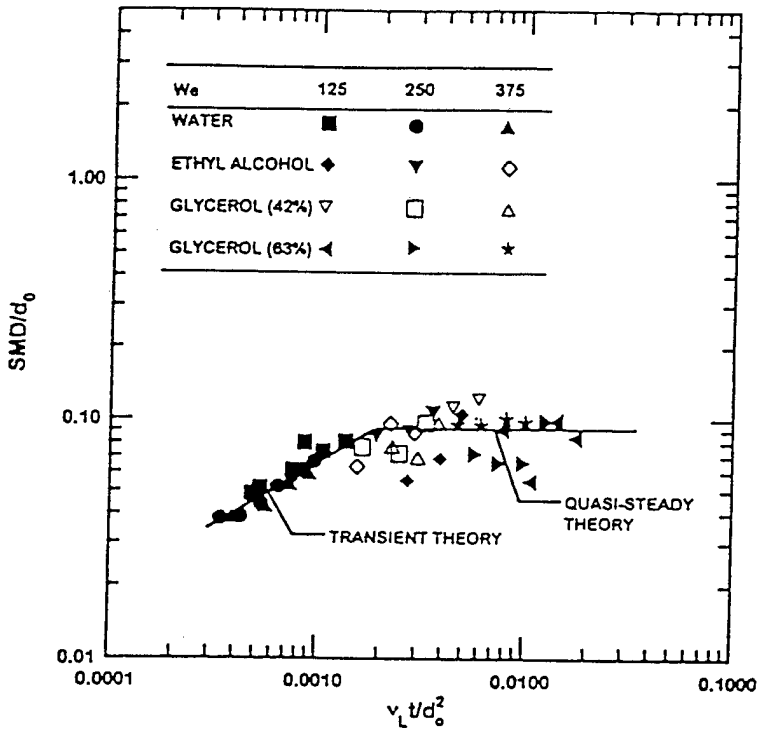

Figure 7. Temporal variation of the *SMD* of drops produced by shear breakup.

the drops currently being formed by shear breakup, similar to earlier considerations of jump conditions to find drop sizes after shear breakup due to Hsiang and Faeth (1992). Then, the two types of behavior noted earlier represent different states of the transient development of the vortical region, which will be denoted the transient and quasi-steady shear breakup regimes in the following. In order to fix ideas, the transition between the transient and quasi-steady shear breakup regimes will be assumed to occur at a time t_c to be quantified later.

Transient shear breakup. The transient breakup mechanism is illustrated in figure 5. This regime is observed at short times after the start of breakup, particularly for liquids that have a small viscosity so that the temporal rate of growth of the thickness of the boundary layer on the windward side of the drop is relatively slow. Then the thickness of the boundary layer, normalized by the initial boundary layer thickness, can be expressed as follows (Schlichting 1975)

$$\delta(t)/d_o = C_t(\nu_L t/d_o^2)^{1/2}, \quad t/t_c < 1, \tag{5}$$

where ν_L is the kinematic viscosity of the drop liquid and C_t is an empirical constant on the order of unity. Assuming $SMD(t) \sim \delta(t)$, an equation for the temporal variation of drop sizes in the transient shear breakup regime can be obtained from [5], as follows

$$SMD(t)/d_o = C_tC_t(\nu_L t/d_o^2)^{1/2}, \quad t/t_c < 1, \tag{6}$$

where C_t is another empirical constant on the order of unity.

Present measurements of $SMD(t)$ are correlated in terms of [6] for the transient shear breakup regime in figure 7. At small values of $\nu_L t/d_o^2$, the measurements exhibit an excellent correlation

according to the transient theory of [6]; the corresponding theoretical correlation, involving a least-squares fit based on [6] while maintaining the square root dependence of $(v_L t/d_o^2)$, is as follows

$$SMD(t)/d_o = 2.0(v_L t/d_o^2)^{1/2}, \quad t/t_c < 1. \qquad [7]$$

The best fit expression of [7] is also plotted in figure. 7. Limiting the data used to correlate [7] to $v_L t/d_o^2 < 0.00020$, yields a standard deviation of the coefficient on the right hand side of [7] of 13%, with the correlation coefficient of the fit being 0.96. If the power of $(v_L t/d_o^2)$ in [7] is found from a least-squares fit of the same data set, a value of 0.57 with a standard deviation of 0.04 is obtained, which is not statistically different from the 1/2 power based on the phenomenological theory used in [7]. In addition, the coefficient on the right hand side of [7] has an order of magnitude of unity as anticipated.

The experimental results illustrated in figure 7 exhibit a transition from the transient regime for values of $v_L t/d_o^2 > 0.0020$, which will be taken to represent conditions in the quasi-steady shear breakup regime in the following, as denoted on the figure. This transition completes the definition of t_c, which can be expressed as follows

$$t_c/t^* = 0.002(\rho_G/\rho_L)^{1/2} u_o d_o/\nu_L. \qquad [8]$$

Based on approximate conservation of momentum scaling, a characteristic initial liquid phase velocity, u_{Lo}, can be defined as $\rho_L u_{Lo}^2 = \rho_G u_o^2$; therefore, the factor on the right-hand side of [8] can be recognized as a characteristic initial liquid phase Reynolds number based on this velocity, i.e. $Re_L = u_{Lo} d_o/\nu_L$. Then, noting that the breakup period ends when $t/t^* = 5.5$ from Liang *et al.* (1988), [8] implies that transient behavior will be observed for the entire breakup process when $Re_L > 2750$. For present tests, such conditions were encountered for water drops having We = 250 and 375. At the other extreme, present measurements for ethyl alcohol and glycerol drops were mainly in the quasi-steady shear breakup regime.

The consistency of [7] with the earlier measurements of Hsiang and Faeth (1992) of the SMD at the end of shear breakup (or the jump conditions) for experiments dominated by large We and low viscosity liquids (which implies behavior mainly in the transient shear breakup regime) is also of interest. In particular, this relationship can be examined by assuming that drop sizes at the end of breakup are dominated by the largest drop sizes produced by breakup which also are generated at the end of breakup where $t = t_b = 5.5t^*$. Then, introducing [1] for t^* into [7] yields the following expression for SMD_s, the SMD for the entire secondary breakup process

$$SMD_s/d_o = 2C_s(t_b/t^*)^{1/2}(\rho_L/\rho_G)^{1/4}[\nu_L/(d_o u_o)]^{1/2} \qquad [9]$$

where C_s is an empirical factor to correct for the fact that jump conditions for drop sizes involve the entire breakup process, and the contribution of the remaining parent drop, rather than just the size of drops produced at the end of shear breakup. Nevertheless, [9] becomes identical to the jump conditions of Hsiang and Faeth (1992) if $2C_s(t_b/t^*)^{1/2} = 6.2$. Recalling that $t_b/t^* = 5.5$, implies that $C_s = 1.3$, which is a value on the order of unity as expected. Thus, present findings for the evolution of SMD as a function of time during shear breakup are consistent with the jump conditions found by Hsiang and Faeth (1992) for secondary breakup in the shear breakup regime.

An interesting feature of both [7] for $SMD(t)$ and [9] for SMD_s is that neither result depends on the surface tension, and thus We, even though conditions required for the appearance of the shear breakup regime at low Oh and large ρ_L/ρ_G are controlled by We, and thus σ. In a sense, this behavior is analogous to the role of Reynolds numbers for turbulent mixing, where the presence of turbulent mixing for jets, wakes, etc. depends on the Reynolds number of the flow, even though the rate of mixing itself is essentially independent of the Reynolds number once the flow is turbulent.

Similar to the correlation of SMD_s of Hsiang and Faeth (1992), [7] can be put into a form emphasizing the Weber number of drops produced by secondary breakup, as follows

$$\rho_G SMD(t) u_o^2/\sigma = 2(t/t^*)^{1/2} We/Re_L^{1/2}, \quad t/t_c < 1, \qquad [10]$$

where the left-hand side of [10] can be recognized as the Weber number of drops formed by secondary breakup based on the SMD and the initial relative velocity. Then, similar to previous considerations of the jump conditions to yield SMD_s (Hsiang and Faeth 1992, 1993), [10] shows

that the Weber number based on $SMD(t)$ and u_o can exceed values of We needed to initiate secondary breakup by shock-wave disturbances. As discussed by Hsiang and Faeth (1993, 1995), however, subsequent tertiary breakup does not occur because these drops have had time to adjust to the disturbance and are subject to different criteria for breakup in addition to effects of reduced relative velocities compared to u_o. Finally, even though [10] involves surface tension, it should be recalled that the surface tension only affects requirements for the onset of secondary breakup regimes for present conditions, while drop sizes produced by secondary shear breakup are independent of surface tension, see [7]–[9].

Quasi-steady shear breakup. The next issue that must be addressed with respect to the temporal evolution of SMD during shear breakup involves behavior in the quasi-steady shear breakup regime. There are two main possibilities for defining behavior in the quasi-steady shear breakup regime, as follows: (1) stabilization of the flow within the drop at the end of the transient period implies $\delta \sim d$, relatively independent of properties like Re_L, as illustrated in figure 6; and (2) complete development of the boundary layer near the surface of the liquid on the windward side of the drop yields δ proportional to the thickness of this boundary layer near the drop periphery, along the lines of the analysis of Hsiang and Faeth (1992). The somewhat increased scatter of the data for the quasi-steady shear breakup regime illustrated in figure 7 suggests the potential for complications due to contributions from both these limits; nevertheless, based on this information, it is reasonable to accept the approach illustrated in figure 6 for the quasi-steady shear breakup regime and adopt the approximation $SMD(t) \sim d_o$ to yield

$$SMD(t)/d_o = 0.09, \quad t/t_c > 1. \qquad [11]$$

which is illustrated on the plot. Limiting the data used to correlate [11] to $t/t_c > 1$, or $\nu_L t/d_o^2 > 0.0020$, yields a standard deviation of the coefficient on the right hand side of [11] of 22%, with the correlation coefficient of the fit being 0.91. If the power of $\nu_L t/d_o^2$ in [11] is found from a least-squares fit using the same data set, a value of -0.06 with a standard deviation of 0.10 is obtained, which is not statistically different from the power of zero based on the phenomenological description of [11].

It is also of interest to compare the approximation $\delta \sim d$ used to find [11] with estimates of the thickness of the boundary layer formed near the surface of the liquid on the windward side of the drop. For flows typical of the interior of drops this boundary layer is laminar and its thickness was estimated as the characteristic thickness of a laminar boundary layer on a flat plate having an ambient velocity of $u_{L,o}$ and a length d_o, which implies (Schlichting 1975)

$$\delta(d_o)/d_o = 4.0/[(\rho_G/\rho_L)^{1/2} u_o d_o/\nu_L]^{1/2}. \qquad [12]$$

The values of $\delta(d_o)/d_o$ computed from [12] for present test conditions are summarized in table 2. The tabulation indicates that for measurements involving the quasi-steady shear breakup regime (e.g. alcohol and glycerol drops), $\delta(d_o)/d_o$ from [12] was generally larger than SMD/d_o from [11] and much more variable than the range of SMD/d_o seen in figure 7 for these liquids. In contrast, only results for water drops, which generally did not reach quasi-steady conditions, yield boundary layer thicknesses less than the estimate of [10], which is also consistent with the behavior seen in figure 7. Taken together, these results support the present phenomenological approach where the transient regime ends when the thickness of the vortical region reaches a fraction of the parent drop diameter, as a result of the confined internal flow configuration of the deformed parent drop. Naturally, this limit does not yield formulas for the jump conditions for SMD that are consistent with the earlier results of Hsiang and Faeth (1992), similar to the transient shear breakup regime.

Table 2. Summary of quasi-steady liquid boundary layer thicknesses ($\delta(d_o)/d_o$)†

	Drop liquid			
We	Water	Ethyl alcohol	Glycerol (42%)	Glycerol (68%)
125	0.079	0.137	0.154	0.237
250	0.067	0.115	0.115	0.200
375	0.060	0.104	0.110	0.180

†Estimated from [11].

As mentioned earlier, however, this behavior is not surprising because the measurements of Hsiang and Faeth (1992) were dominated by results from the transient shear breakup regime. Another factor is that drop sizes toward the end of the transient shear breakup regime are comparable to those in the quasi-steady breakup regime, see figure 7; therefore, both sets of results tend to correlate in a similar manner.

3.3. Parent drop velocities

The temporal behavior of the velocity distributions of drops produced by shear breakup is closely associated with the temporal behavior of the velocity of the parent drop; therefore, this issue will be considered first. A correlating expression for the velocity of the parent drop with time was based on the phenomenological analysis of Hsiang and Faeth (1993). The major assumptions of this analysis are as follows: virtual mass, Bassett history and gravitational forces ignored; gas velocities assumed to be constant; mass removal from the parent drop ignored; and constant average drag coefficient assumed over the period of breakup. For present conditions, virtual mass and Bassett history forces are small due to the large values of ρ_L/ρ_G of the flow (Faeth 1990). Similarly, gravitational forces were not a factor because drop motion was nearly horizontal and drag forces were much larger than gravitational forces. In addition, uniform gas properties were a condition of the present experiments. In contrast, the uniform parent drop size approximation was not really justified for present conditions because parent drop diameters at the end of breakup were only 12–30% of the original drop diameters and vary considerably over the period of breakup (Hsiang and Faeth 1993). Nevertheless, accounting for these changes by adopting the original drop diameter and selecting a mean drag coefficient, $\overline{C_D}$, to best fit the measurements yielded reasonably good results in the past (Hsiang and Faeth 1993), and was continued during the present study.

The analysis to find parent drop velocities in a laboratory reference frame, u_p, as a function of time under the preceding approximations is presented by Hsiang and Faeth (1993). These results can be placed in the following form

$$(u_p - u_{p_0})/(u_G - u_{p_0}) = 3\overline{C_D}(t/(4t^*))(\rho_G/\rho_L)^{1/2}, \qquad [13]$$

where for present conditions $u_{p_0} = 0$ and u_G is the gas velocity in a laboratory reference frame. Earlier evaluation of parent drop velocities at the end of secondary breakup yielded a best fit value of $\overline{C_D} = 5$ in [13] (Hsiang and Faeth 1993).

Measurements of parent drop velocities for various secondary breakup conditions, and times during secondary breakup, were obtained from both the present investigation and from the earlier work of Hsiang and Faeth (1993). These results are plotted according to [13] in figure 8. A best-fit correlation according to [13] also is shown on the figure. The comparison between the measurements and the correlation is seen to be quite good in spite of the approximations of the simplified analysis. This yields the same best-fit value $\overline{C_D} = 5.0$, as the results found earlier by Hsiang and Faeth (1993), with an experimental uncertainty (95% confidence) of the fit of 15%.

3.4. Drop velocity distributions

Mean velocities. The velocity distributions of drops produced by shear breakup were measured as a function of time for all test conditions. It was found that the velocities of drops produced by secondary breakup, relative to the velocity of the parent drop, were related to the characteristic velocity of the liquid at each instant of time, i.e. $(\rho_G/\rho_L)^{1/2}(u_G - u_p)$. In addition, it was found that drop velocities were relatively independent of drop size, i.e. the drop velocity distributions were nearly uniform. Thus, volume-averaged mean streamwise and cross-stream velocities for shear breakup, u_L and v_L, normalized by the characteristic liquid velocity, are plotted as a function of t/t^* in figure 9. Similar to the drop diameters illustrated in figure 7, there is appreciable scatter of the drop velocities in figure 9. This behavior comes about because relatively few drops are available to find appropriate average drop velocities for a given breakup condition and time. In addition, random motions of the ligaments and the parent drop, see figures 2 and 3, yield turbulent-like velocity variations that cause corresponding variations of mean velocities. Nevertheless, it is evident that the mean volume-averaged streamwise and cross-stream velocities

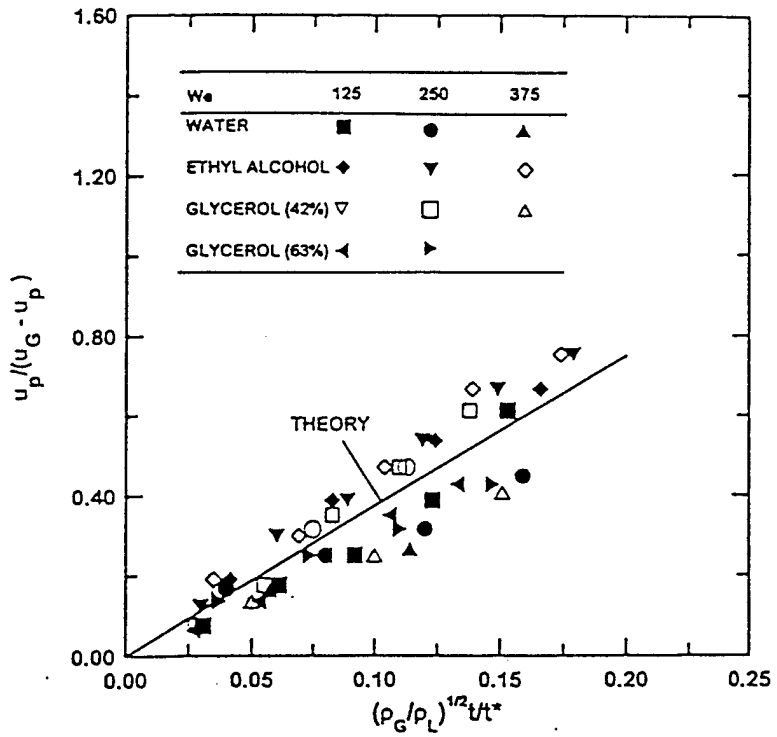

Figure 8. Streamwise velocities of the parent drop as a function of time during shear breakup.

are relatively independent of time as well as drop size and can be correlated reasonably well, as follows

$$(\rho_L/\rho_G)^{1/2}(\bar{u}_L - u_p)/(u_G - u_p) = 9.5 \quad [14]$$

and

$$(\rho_L/\rho_G)^{1/2}\bar{v}_L/(u_G - u_p) = 0 \quad [15]$$

with a standard deviation of the constant on the right-hand side of [14] of 28%. The corresponding standard deviation of the constant on the right hand side of [15] is 4.7; therefore, the mean value of v_L is not statistically different from zero. A difficulty with the correlation of streamwise velocity in [14] is that the actual value of the relative velocity increase of the drops produced by shear breakup is not easily compared with the relative velocity of the parent drop due to the effect of the density ratio. Thus, correlating the streamwise velocity data directly in terms of velocities relative to the velocity of the parent drop yields

$$(\bar{u}_L - u_p)/(u_G - u_p) = 0.37 \quad [16]$$

with the standard deviation of the constant on the right-hand side of [16] of 0.08. This result suggests that there is appreciable acceleration of the drop liquid during breakup, mainly as a result of acceleration of the liquid in the vortical layer near the surface of the parent drop as well as acceleration of liquid in the ligaments prior to final breakup into drops. The relatively large variations of v_L seen in figure 9 certainly tend to support significant effects of liquid acceleration in the ligaments. The corresponding values for v_L yield $\bar{v}_L/(u_G - u_p) = -0.01$ with a standard deviation of 0.15, which implies that mean radial velocities are not statistically different from zero, as before.

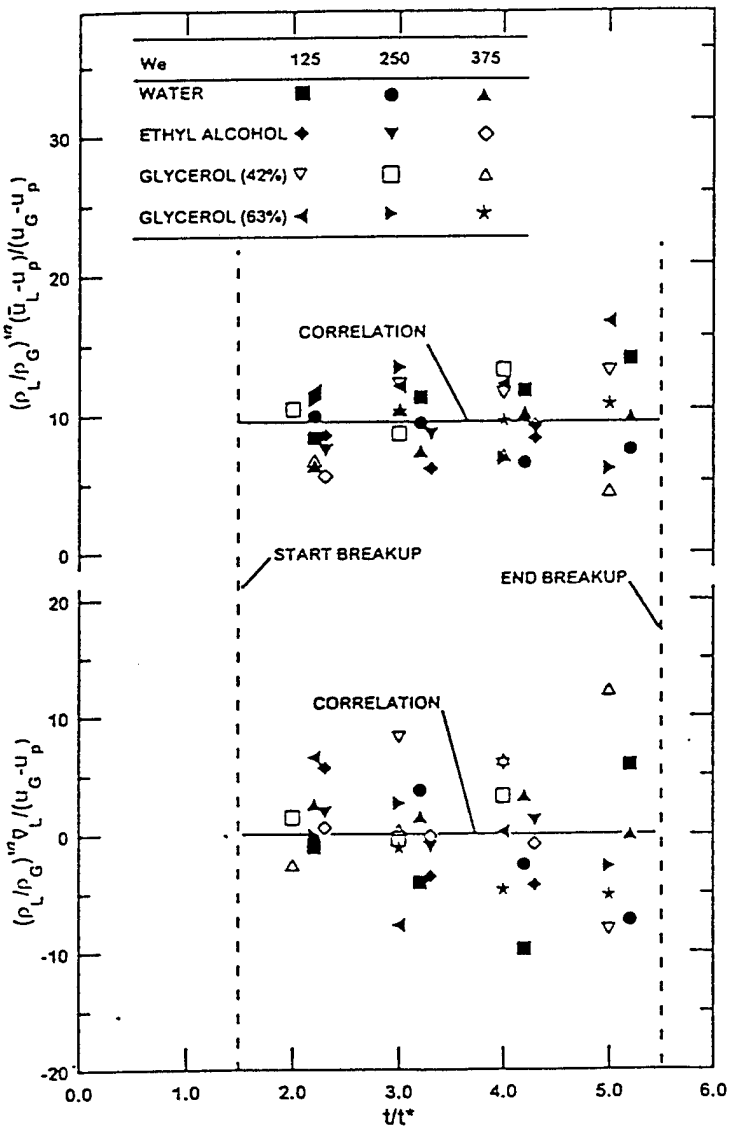

Figure 9. Streamwise and cross-stream mean velocities of drops produced by shear breakup as a function of time during breakup.

The behavior of drop velocities as the drops are formed as a function of time, given by [14] and [15], is in marked contrast to the drop velocity distribution as a function of drop size at the end of breakup (the jump conditions) discussed by Hsiang and Faeth (1993, 1995). For the jump conditions, drop velocities relative to the gas became progressively smaller as the drop sizes become smaller, rather than remaining constant compared to the relative velocity of the gas with respect to the parent drop, similar to the results illustrated in figure 9. This behavior comes about because the characteristic relaxation times of small drops are smaller than those of large drops (Hsiang and

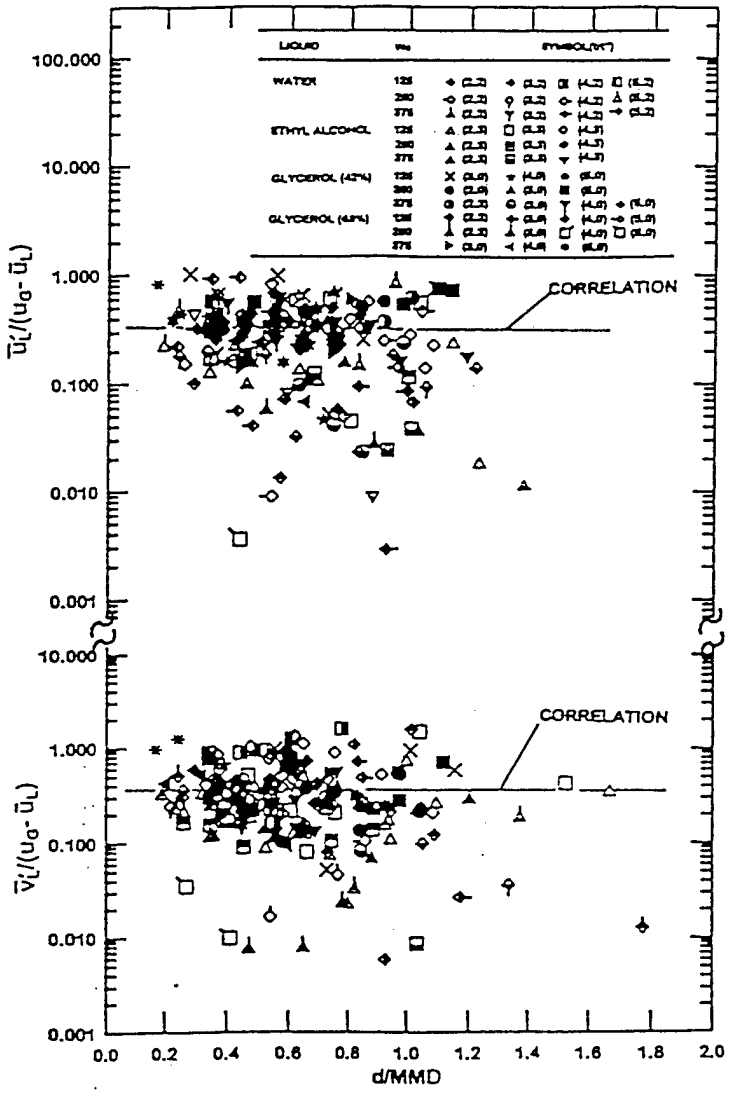

Figure 10. Streamwise and cross-stream rms velocity fluctuations of drops produced by shear breakup as a function of drop size.

Faeth 1992); therefore, small drops undergo a greater acceleration after they are formed than large drops, and more closely approach the gas velocity as a result.

Velocity fluctuations. Volume-averaged rms streamwise and cross-stream velocity fluctuations, $\overline{u_L'}$ and $\overline{v_L'}$ are plotted as a function of d/MMD, with We and t/t^* as parameters, in figure 10. Individual data points on this figure exhibit significant scatter, mainly because each test condition involves a limited number of test drops. Nevertheless, effects of drop size, We and t/t^* appear to be small over the entire data set, when volume-averaged fluctuations are normalized by the mean streamwise

velocity of the drops relative to the gas. The resulting volume-averaged rms streamwise and cross-stream drop velocity fluctuations can be summarized, as follows

$$\overline{u_L'^2}/(u_G - \overline{u_L}) = 0.31 \quad [17]$$

and

$$\overline{v_L'^2}/(u_G - \overline{u_L}) = 0.37. \quad [18]$$

where the standard deviations of the numbers on the right-hand sides of these equations are 22%. In view of these uncertainties, the magnitudes of u_L' and v_L' are not statistically different. Taking the data sets as a whole, however, the large number of total samples available to find u_L' and v_L' reduce the experimental uncertainties of these estimates (95% confidence) to less than 10%.

3.5. Drop formation rates

Drop formation rates were estimated using a simplified analysis. This involved the following major assumptions: liquid removal rates were proportional to the thickness of the boundary layer in the liquid on the upstream surface of the drop; liquid removal rates were proportional to the velocity of the drops formed relative to the velocity of the parent drop, estimated from [14]; liquid removal rates were proportional to the perimeter of the drop at its periphery; and breakup begins and ends at $t/t^* = 1.5$ and 5.5, respectively, as determined by Liang *et al.* (1988). The resulting formulation for the rate of production of dispersed liquid drops by secondary breakup, for the transient and quasi-steady drop breakup regimes, is relatively complex. It was noted, however, that the amount of liquid removed from the drop could be approximated by a clipped Gaussian function which simplifies the treatment of the onset and end of secondary breakup. Thus, only the simplified approach will be presented here because it should be useful for detailed analysis of drop breakup processes.

Present measurements of the cumulative volume of liquid removed from the parent drop as a function of time are plotted in figure 11. These results include all test conditions considered during the present investigation. The best-fit correlation of these results, according to a clipped Gaussian function, also is shown on the plot. It is evident that the clipped Gaussian function provides a good fit of the cumulative loss of volume of the parent drop as a function of t/t^*. This formula also provides a reasonably good fit of the rate of removal of drop liquid from the parent drop, except for the singular points at the beginning and end of the period where drop mass is being removed.

The results illustrated in figure 11 can be correlated to provide the mass rate of formation of dispersed drops due to shear breakup, $\dot{m}_s$, normalized by the initial drop mass and t^*, as follows

$$6\dot{m}_s t^*/(\pi\rho_L d_o^3) = 0.42\exp\{0.8(t/t^* - 3.5)^2\}, \quad 1.5 \le t/t^* \le 5.5. \quad [19]$$

3.6. Extent of drop-containing region

The region in the streamwise direction that contains drops will be considered in the following in order to provide information needed to evaluate when secondary breakup should be treated as a rate process rather than by jump conditions. This information can be summarized most compactly by plotting the boundaries of the drop-containing region in the streamwise direction, normalized by the initial drop diameter, as a function of t/t^*, based on mean relative velocities only. These boundaries are given by the motion of the parent drop, and the motion of the smallest drop formed at the onset of breakup. Thus, it is evident that these boundaries are fixed by the motion of the parent drop whose velocity is given by [13]. Based on this result, recalling that C_D was found to be a constant for present test conditions, it is evident that ρ_L/ρ_G is the only parameter of the problem. Thus, the sizes of the drop-containing region were found for $\rho_L/\rho_G = 500$ and 1000, which bound the range of conditions considered during the present investigation.

The growth of the spray-containing region in terms of distance in the streamwise direction, x, is plotted as a function of t/t^* in figure 12. Results are shown for the two different values of ρ_L/ρ_G that bound the present measurements, with the limiting values of t/t^* at the onset and end of drop breakup marked on the plot for reference purposes. The span of the drop-containing region increases with both the liquid/gas density ratio and time. For example, the drop-containing region at the end of breakup is in the range $x/d = 40$–120 for $\rho_L/\rho_G = 1000$ but only $x/d = 38$–85 for

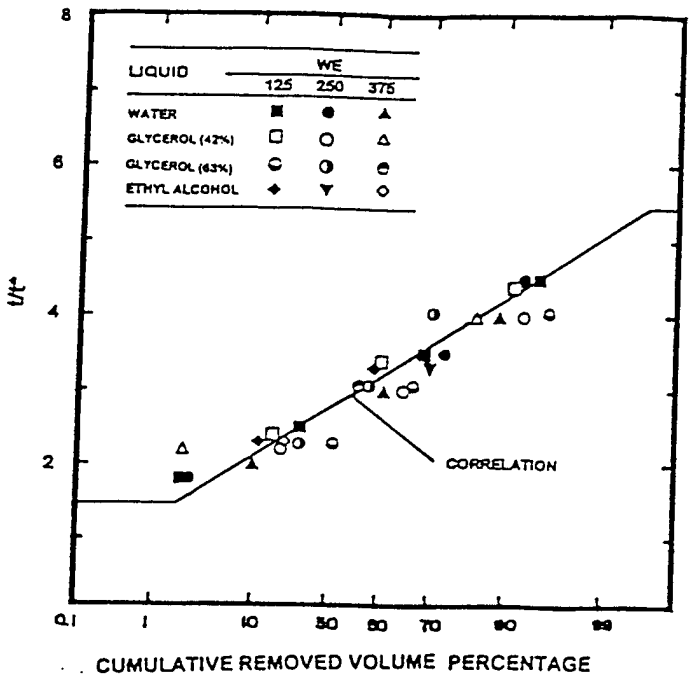

Figure 11. Degree of mass removal from the parent drop as a function of time during shear breakup.

$\rho_L/\rho_G = 500$. Similarly, the mean drop-containing region increases from zero at $t/t^* = 1.5$ to roughly $x/d = 40$–100 at $t/t^* = 5.5$. As noted earlier, the span of the secondary breakup times, the distance traveled by the parent drop, and the span of streamwise distances where drops are present at the end of breakup can be significant in some instances. In such cases, the information found during the present investigation about the temporal evolution of the sizes and velocities of drops produced by secondary breakup, as well as the rate of liquid removal from the parent drop during secondary breakup, should be helpful.

4. CONCLUSIONS

The properties of drop breakup in the shear breakup regime were studied as a function of time for shock-wave disturbances in air at NTP, for the test conditions summarized in table 1. The major conclusions of the study are as follows:

(1) The maximum lengths of ligaments protruding from the periphery of the drops progressively increase with increasing Ohnesorge number causing transition to a long-ligament shear breakup regime at Oh ≈ 0.1; present results are limited to the conventional shear breakup regime at small Ohnesorge numbers (Oh < 0.1).

(2) Drops produced by shear breakup at small Ohnesorge numbers satisfy the universal root normal drop size distribution function with $MMD/SMD = 1.2$, of Simmons (1977), at each instant of time.

(3) The SMD of drops produced by shear breakup at small Ohnesorge numbers exhibit transient and quasi-steady regimes as a function of time, based on the development of the liquid boundary layer within the parent drop; this behavior was correlated based on a phenomenological analysis

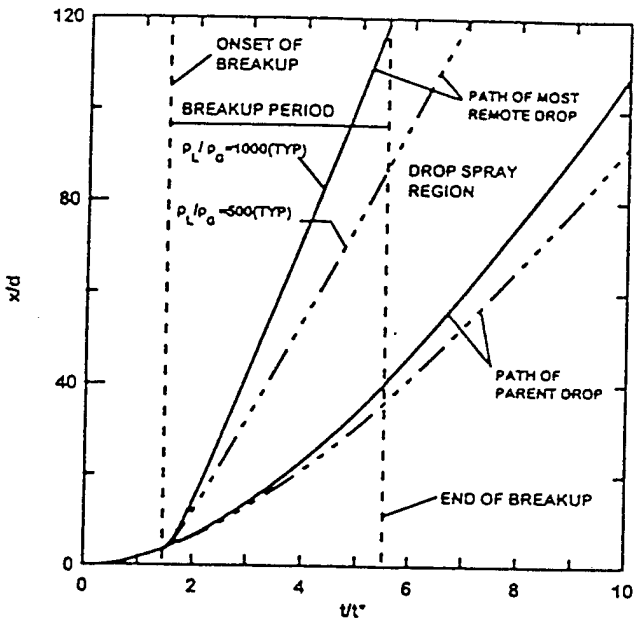

Figure 12. Growth of the spray-containing region during shear breakup.

which implied that drops produced by breakup had diameters comparable to the thickness of this liquid viscous region.

(4) The parent drop accelerates rapidly due to the large drag coefficient caused by its deformation; a phenomenological analysis provided an effective correlation of the resulting parent drop velocities.

(5) The mean velocities of drops produced by shear breakup at small Ohnesorge numbers were relatively independent of drop size, and were somewhat larger than the velocities of the parent drop, at each instant of time.

(6) The rms velocity fluctuations of drops produced by shear breakup at small Ohnesorge numbers were relatively independent of drop size, and were on the order of 30–40% of the mean streamwise velocity of the gas relative to the parent drop, at each instant of time.

(7) The rate of liquid removal from the parent drop could be interpreted reasonably well based on the variations of parent drop diameter and the size and velocity of drops leaving the periphery of the parent drop; these results were correlated concisely in terms of an empirical clipped Gaussian function.

(8) Shear breakup at small Ohnesorge numbers extends over streamwise distances of 0–100 initial drop diameters, and 0–5.5 characteristic drop breakup times; this behavior suggests that shear breakup should be treated as a rate process, rather than by jump conditions, in some instances.

Acknowledgements—This research was sponsored by the Air Force Office of Scientific Research Grant Nos. F49620-92-J-0399 and F49620-95-1-0364, under the technical management of J. M. Tishkoff. The authors would like to thank C. W. Kauffman for the loan of the shock tube facility and advice concerning its operation. The U.S. Government is authorized to reproduce and distribute copies of this article for governmental purposes notwithstanding any copyright notation thereon.

REFERENCES

Belz, M. H. (1973) *Statistical Methods in the Process Industries*, pp. 103–104. Wiley, New York.

Clift, R., Grace, J. R. and Weber, M. E. (1978) *Bubbles, Drops and Particles*, pp. 26 and 339–347. Academic Press, New York.

Dabora, E. K. (1967) Production of monodisperse sprays. *Rev. Scient. Instrum.* 38, 502–506.

Faeth, G. M. (1990) Structure and atomization properties of dense turbulent sprays. In *Proc. 23rd Symp. (Int.) on Combustion*. The Combustion Institute, Pittsburgh, PA, pp. 1345–1352.

Faeth, G. M. (1996) Spray combustion phenomena. In *Proc. 26th Symp. (Intl) on Combustion*. The Combustion Institute, Pittsburgh, PA, in press.

Giffen, E. and Muraszew, A. (1953) *The Atomization of Liquid Fuels*. Chapman & Hall, London.

Hanson, A. R., Domich, E. G. and Adams, H. S. (1963) Shock-tube investigation of the breakup of drops by air blasts. *Phys. Fluids* 6, 1070–1080.

Hinze, J. O. (1955) Fundamentals of the hydrodynamic mechanism of splitting in dispersion processes. *AIChE J.* 1, 289–295.

Hsiang, L.-P. and Faeth, G. M. (1992) Near-limit drop deformation and secondary breakup. *Int. J. Multiphase Flow* 18, 635–652.

Hsiang, L.-P. and Faeth, G. M. (1993) Drop properties after secondary breakup. *Int. J. Multiphase Flow* 19, 721–735.

Hsiang, L.-P. and Faeth, G. M. (1995) Drop deformation and breakup due to shock wave and steady disturbances. *Int. J. Multiphase Flow* 21, 545–560.

Krzeczkowski, S. A. (1980) Measurement of liquid droplet disintegration mechanism. *Int. J. Multiphase Flow* 6, 227–239.

Lane, W. R. (1951) Shatter of drops in streams of air. *Ind. Engng Chem.* 43, 1312–1317.

Lange, N. A. (1952) *Handbook of Chemistry*, 8th edn, pp. 1134 and 1709. Handbook Publishers, Inc., Sandusky, OH.

Liang, P. Y., Eastes, T. W. and Gharakhari, A. (1988) Computer simulations of drop deformation and drop breakup. AIAA Paper No. 88-3142.

Loparev, V. P. (1975) Experimental investigation of the atomization of drops of liquid under conditions of a gradual rise of the external forces. *Izvestiya Akad. Nauk SSSR, Mekh. Zhidkosti i Gaza* 3, 174–178.

Ranger, A. A. and Nicholls, J. A. (1969) The aerodynamic shattering of liquid drops. *AIAA J.* 7, 285–290.

Reinecke, W. G. and McKay, W. L. (1969) Experiments on waterdrop breakup behind Mach 3 to 12 shocks. Sandia Corp. Report SC-CR-70-6063.

Reinecke, W. G. and Waldman, G. D. (1970) A study of drop breakup behind strong shocks with applications to flight. Avco Report AVSD-0110-70-77.

Sangiovanni, J. and Kestin, A. S. (1977) A theoretical and experimental investigation of the ignition of fuel droplets. *Combust. Sci. Technol.* 6, 59–70.

Schlichting, H. (1975) *Boundary Layer Theory*, 7th edn, pp. 234–235 and 599. McGraw-Hill, New York.

Simmons, H. C. (1977) The correlation of drop-size distributions in fuel nozzle sprays. *J. Engng Power* 99, 309–319.

White, F. M. (1974) *Viscous Fluid Flow*. McGraw-Hill, New York.

Wierzba, A. and Takayama, K. (1987) Experimental investigations on liquid droplet breakup in a gas stream. *Report Inst. High Speed Mech.*, Tohoku Univ., Vol. 53, No. 382, pp. 1–99.

Wierzba, A. and Takayama, K. (1988) Experimental investigation of the aerodynamic breakup of liquid drops. *AIAA J.* 26, 1329–1335.

Wu, P.-K., Ruff, G. A. and Faeth, G. M. (1991) Primary breakup in liquid/gas mixing layers for turbulent liquids. *Atom. Sprays* 1, 421–440.

Wu, P.-K., Hsiang, L.-P. and Faeth, G. M. (1995) Aerodynamic effects on primary and secondary breakup. *Prog. Astro. Aero.* 169, 247–279.

Appendix B: Chou, W.-H. and Faeth, G.M. (1998) Temporal Properties of Secondary Drop Breakup in the Bag Breakup Regime. Int. J. Multiphase Flow, in press.

TEMPORAL PROPERTIES OF SECONDARY DROP BREAKUP IN THE BAG BREAKUP REGIME

W.-H. Chou* and G. M. Faeth†
Department of Aerospace Engineering
The University of Michigan
Ann Arbor, Michigan 48109-2140, U.S.A.

Abstract — The temporal properties of secondary drop breakup in the bag breakup regime were measured as a function of time for shock-wave-initiated disturbances in air at normal temperature and pressure. The test liquids included water, ethyl alcohol and various glycerol mixtures to yield liquid/gas density ratios of 633-893, Weber numbers of 13-20, Ohnesorge numbers of 0.0043-0.0427 and Reynolds numbers of 1550-2150. Single- and double-pulse shadowgraphy and holography were used to measure the structure, size and velocity of the parent drop, and the sizes and velocities of drops produced by secondary breakup. The parent drop undergoes significant deformation and lateral growth during breakup before forming a thin bag having a basal ring that is characteristic of the bag breakup regime. The basal ring contains roughly 56% of the initial drop volume (mass) and eventually yields drops having mean diameters of roughly 30% of the initial drop diameter by a Rayleigh breakup process; the size variations of drops formed from the basal ring increases with increasing Weber number due to the appearance of large "node" drops that are characteristic of the onset of the multimode breakup regime. Breakup of the bag yields nearly monodisperse drops having diameters of roughly 4% of the initial drop diameter. The velocity distributions of the drops formed from breakup of the basal ring and the bag were individually independent of drop size but varied as a function of time and differed between the two groups. Many features of these phenomena were successfully correlated using phenomenological analyses. Finally, bag breakup requires considerable time (5-6 characteristic secondary drop breakup times) and extends over considerable

*Currently with the Trane Corporation, LaCrosse, Wisconsin, U.S.A
†To whom correspondence should be addressed.

streamwise distances (50-100 initial drop diameters) by the end of breakup, which suggests that bag breakup should be treated as a rate process, rather than by jump conditions, in some instances.

Key Words: drop breakup, drop dynamics, pulsed holography, sprays, atomization.

1. INTRODUCTION

The secondary breakup of drops is important because primary breakup yields drops that are intrinsically unstable to secondary breakup, while secondary breakup often is the rate controlling process within dense sprays in much the same way that drop vaporization often is the rate controlling process within dilute sprays (Faeth 1997; Faeth et al. 1995; Wu et al. 1995). Motivated by these observations, the objective of the present investigation was to extend recent studies of the regimes and outcomes of secondary breakup caused by shock-wave disturbances due to Hsiang and Faeth (1992, 1993, 1995), and Chou et al. (1997), to consider the evolution of bag breakup as a function of time.

Several recent reviews of secondary breakup are available, see Faeth (1997), Faeth et al. (1995), Hsiang and Faeth (1992,1993,1995), Wu et al. (1995) and references cited therein; therefore, the following discussion of past work will be brief. Shock-wave disturbances were considered during most earlier studies, providing a step change of flow properties around the drop, similar to conditions experienced by drops at the end of primary breakup. Secondary breakup properties that have been considered include the conditions required for particular deformation and breakup regimes, the time required for the onset and end of breakup, the drag properties of deformed drops and the size and velocities of the drops produced by secondary breakup (i.e., the secondary breakup jump conditions). An interesting feature of these results is that secondary breakup extended over appreciable regions of time and space and was not properly described by jump conditions in some instances. For example, Liang et al. (1988) show that breakup times are equal to

5.5t* for a wide range of breakup conditions, where t* is the characteristic secondary breakup time for shear breakup defined by Ranger and Nicholls (1969) as follows:

$$t^* = d_o(\rho_L/\rho_G)^{1/2}/u_o \qquad [1]$$

In [1], d_o and u_o are the initial drop diameter and relative velocity, ρ denotes density and the subscripts L and G denote liquid and gas properties, respectively. Such times are comparable to flow residence times within the dense spray region where secondary breakup is a dominant process (Faeth 1997; Faeth et al. 1995; Wu et al. 1995). Viewed another way, the original (or parent) drop moves roughly 50 initial drop diameters, while the smallest drops formed by secondary breakup move up to 100 initial drop diameters, during the period of breakup for typical shear breakup processes (Hsiang and Faeth 1993,1995). Such distances can represent a significant fraction of the length of the dense spray region. These observations suggest that the time-resolved features of secondary breakup eventually must be understood, i.e., the size and velocity distributions of the drops, and the rate at which liquid is removed from the parent drop, must be known as a function of time during secondary breakup. Motivated by this observation, the authors and their associates are concentrating on studies of the temporal properties (dynamics) of particular secondary breakup processes.

The first phase of the study of the temporal properties of secondary breakup considered the shear breakup regime where secondary breakup proceeds by the stripping of drop liquid from the periphery of the parent drop (Chou et al. 1997). Other conditions of the shear breakup study included $\rho_L/\rho_G > 680$, where gas-phase processes approximate quasi-steady behavior, and small Ohnesorge numbers, $Oh = \mu_L/(\rho_L d_o \sigma)^{1/2} < 0.04$, where μ and σ denote viscosity and surface tension, respectively. It was found that the size distributions of drops produced by secondary breakup at each instant of time satisfied the universal root normal distribution function, with MMD/SMD = 1.2, due to Simmons

(1977), where MMD and SMD denote the mass median and Sauter mean diameters of the drop size distributions respectively. This behavior is very helpful because this two-parameter distribution function is fully defined by the SMD alone, given the MMD/SMD ratio. In contrast, the velocity distribution functions of drops produced by secondary breakup were uniform. Other measurements of shear breakup properties as a function of time included the size and velocities of the parent drop; the SMD and mean and fluctuating velocities of drops produced by secondary breakup, and the rate of liquid removal from the parent drop due to secondary breakup. All these properties were correlated and interpreted using phenomenological theories, providing the information needed to treat shear breakup as a rate process during computations of spray structure.

The present study seeks to extend information about the temporal properties of secondary breakup from the shear breakup regime to the bag breakup regime. Within the bag breakup regime, secondary breakup proceeds by deformation of the center of the drop into a thin balloon-like bag that extends in the downstream direction from a thicker ring-like structure of its base (the basal ring), with both the bag and the basal ring subsequently dividing into drops. An understanding of bag breakup is important for two reasons: (1) the bag breakup regime bounds the region where drops only deform and do not break up, which provides fundamental clues about the mechanism of the onset of secondary breakup, and (2) the complex multimode breakup regime is bounded by the bag- and shear-breakup regimes which clearly must be understood before addressing the important multimode breakup mechanism (Hsiang and Faeth 1992, 1993,1995). Similar to the earlier study of shear breakup, the present study emphasized new measurements of the temporal properties of bag breakup and used phenomenological theories to help interpret and correlate the measurements.

The present measurements were carried out using a shock tube facility, with the environment of the test drops during breakup roughly approximating air at normal temperature and pressure (NTP). Single- and double-pulse shadowgraphy and holography

were used to find the properties of the parent drop, the size and velocity properties of drops produced by secondary breakup and the rate of liquid removal from the parent drop as a function of time during breakup. Test conditions were limited to relatively large liquid/gas density ratios ($\rho_L/\rho_G > 500$) and relatively small Ohnesorge numbers ($Oh < 0.1$), within the bag breakup regime where the Weber number, $We = \rho_G d_o u_o^2/\sigma$, is in the range 13-35 (Hsiang and Faeth 1993). As a result, the present test conditions are most representative of bag breakup within sprays near atmospheric pressure. Drop liquids included water, ethyl alcohol and various glycerol mixtures, in order to provide information about effects of drop liquid properties.

The paper begins with a description of experimental methods. Results are then discussed considering the properties of the parent drop, the properties of the basal ring, the properties of drops formed from the bag itself and the overall properties of bag breakup, in turn. The following description of the study is brief, see Chou (1997) for more details and a complete tabulation of data.

2. *EXPERIMENTAL METHODS*

2.1 Apparatus and Instrumentation

The test apparatus and instrumentation will be described only briefly because it was similar to earlier work (Hsiang and Faeth 1992, 1993, 1995; Chou et al. 1997). The arrangement consisted of a rectangular shock tube with the driven section open to the atmosphere. The test location was windowed to allow observations of drop breakup. A vibrating capillary tube drop generator, combined with an electrostatic drop selection system, provided a stream of drops at the test location with sufficient spacing between drops accommodate bag breakup with negligible drop/drop interactions.

Single- and double-pulsed shadowgraphy and holography were used to observe the properties of the parent drop and the size and velocity distribution functions of drops produced by secondary breakup. Laser pulse times were sufficiently short (7 ns) to stop

the motion of drops on the film while using a weaker second laser pulse allowed directional ambiguity to be resolved for velocity measurements. The combined holocamera and reconstruction system allowed objects as small as 3 μm to be observed and as small as 5 μm to be measured with 5% accuracy. Results at each condition were summed over at least four realizations, considering 100-200 liquid elements, in order to obtain drop diameter and velocity correlations. Estimated experimental uncertainties (95% confidence) were less than 10% for drop diameters and less than 15% for streamwise drop velocities.

2.2 Test Conditions

The test conditions are summarized in Table 1. The liquid properties were obtained from Lange (1952), except for the surface tensions of the glycerol mixtures which were measured in the same manner as Wu et al. (1991). The ranges of the test variables were as follows: d_o = 0.62-0.85 mm, ρ_L/ρ_G = 633-893, Oh = 0.0043-0.0427, We = 13-20 and Re = 1550-2150, where the Reynolds number, $Re = \rho_G d_o u_o/\mu_G$. The present We test range is narrow but this is consistent with the narrow We range of the bag breakup regime. The Re range of the present experiments is higher than conditions where gas viscosity has a significant effect on drop drag properties, e.g., the drag coefficient, C_D, for spheres only varies in the range 0.4-0.5 for this Reynolds number range (White 1973). Shock Mach numbers were relatively low, less than 1.04; therefore, the physical properties of the gas in the uniform flow region behind the shock wave were nearly the same as room air.

3. RESULTS AND DISCUSSION

3.1 Parent Drop Properties

3.1.1 Parent Drop Size

Figure 1 is a composite illustration of several aspects of the temporal evolution of bag breakup. The illustration includes: measurements of the parent drop cross-stream diameter, d_p, as a function of time, t, for water, ethyl alcohol and glycerol drops having We of 13-20 and Oh $\leq$ 0.043; delineation of the time periods of various portions of the bag breakup process; and inset photographs of the appearance of the parent drop at various times during breakup. The photographs are for a water drop in air subjected to a shock wave disturbance with We = 20 and Oh = 0.0044. Note that the shock wave passes from left to right in the inset photographs. The various positions of the bag breakup process are defined as follows: the deformation period where the drop deforms from a spherical to a disk-like shape for t/t* of 0-2; the bag growth period where the center of the disk deforms into a thin membrane-like bag with a much thicker basal ring surrounding its open (upstream) end for t/t* of 2-3; the bag breakup period where the bag progressively breaks up from its closed downstream end toward the basal ring for t/t* of 3-4; and the ring breakup period where a series of relatively large node drops form along the ring followed by breakup of the ring into a circular array of relatively large drops to end the breakup process for t/t* of 4-5. Note that the bag growth and ring breakup periods include a temporal range that is dominated by these processes. The actual time periods when bag and ring breakup occurs are contained in these periods, respectively, but are much shorter. The value of d_p is taken to be the cross-stream diameter of the disk before the basal ring forms ($0 \leq t/t^* \leq 2$) and the outer diameter of the basal ring when it is present ($2 \leq t/t^* \leq 5$).

The transition between a spherical drop and a relatively thin disk aligned normal to the flow direction occurs during the deformation period ($0 \leq t/t^* \leq 2$) illustrated in figure 1. The deformation of the parent drop is caused by increased static pressures near the upstream and downstream stagnation points along the axis of the drop, combined with decreased static pressures near the drop periphery due to increased flow velocities in this region. This pressure distribution tends to squeeze the drop into a thin disk-like shape. A

detailed analysis of this process was not undertaken; instead, it was found that the deformation process could be expressed reasonably well according to the following empirical correlation suitable for the present range of test conditions:

$$d_p/d_o = 1.0 + 0.5\, t/t^*, \quad 0 \le t/t^* \le 2 \qquad [2]$$

Subsequent consideration of parent drop size parameters will focus on the properties of the basal ring. This interest is motivated by the fact that the size of the basal ring ultimately controls the size of the drops formed by basal ring breakup while these drops tend to dominate the size properties of drops formed by bag breakup because they are the largest drops in the size distribution. In addition, subsequent considerations will show that the basal ring, and thus the drops formed from the basal ring, comprise a major fraction of the original volume of liquid in the parent drop.

The results illustrated in figure 1 show that the rate of lateral acceleration of the basal ring diameters is largest in the period where the bag is present, with subsequent lateral acceleration progressively becoming small toward the end of the period where the bag itself breaks up. This behavior suggests that the higher pressure within the bag, caused by stagnation of the gas flow relative to the drop by the bag, is mainly responsible for the outward acceleration of the basal ring, as well as for the growth of the bag. This pressure difference progressively disappears as the breakup of the bag itself proceeds so that the basal ring simply continues to coast outward in the latter stages of the breakup process; this behavior is supported by the relatively constant outward velocity of the basal ring diameter toward the end of the entire breakup process. These ideas are developed in the following to obtain the predicted variation of d_p/d_o as a function of t/t^* for the period $2 \le t/t^* \le 5$ that is illustrated in figure 1.

Analysis of basal ring growth was carried out ignoring acceleration of the parent drop, i.e., it was assumed that the relative velocity of the basal ring with respect to the gas is equal to the initial relative velocity, u_o; the variation of the diameter of the basal ring tube

itself, d_r, was also neglected even though later considerations will show that this diameter decreases by almost a factor of two during the time period of interest; and circumferential surface tension forces were ignored due to the relatively large diameter of the basal ring at the start of the ring acceleration process. Other assumptions will be discussed as they are introduced. Considering the radial acceleration of the basal ring tube, conservation of momentum yields:

$$\rho_L(\pi^2 d_p d_r^2/4)d^2(d_p/2)/dt^2 = C_r(\rho_G u_o^2/2)(\pi d_p d_r) \qquad [3]$$

where C_r is an empirical constant, somewhat analogous to a drag coefficient, to account for the fact that the pressure difference across the basal ring is only a fraction of the ideal stagnation pressure increase due to effects of gas motion across the basal ring and the motion of the gas in the bag, particularly as breakup of the bag itself proceeds. In [3] it is also assumed that the aspect ratio of the ring, d_p/d_r is relatively large when approximating the ring volume and crossectional area. Adopting d_p/d_o and t/t^* as normalized dependent and independent variables, [3] becomes:

$$d^2(d_p/d_o)/d(t/t^*)^2 = (4C_r/\pi)(d_o/d_r), \quad 2 \le t/t^* \le 4 \qquad [4]$$

where the time interval of concern is the period when the bag (or at least a portion of it) is present and where the right-hand-side of this equation is taken to be a constant under the assumptions of the present approximate analysis. The initial conditions for [4] were chosen to match the value of d_p/d_o at $t/t^* = 2$ from [2] while adjusting the initial outward velocity of the basal ring to best fit the present measurements, as follows:

$$t/t^* = 2: d_p/d_o = 2.0, d(d_p/d_o)/d(t/t^*) = 0.8 \qquad [5]$$

Finally, integrating [4] subject to the initial conditions of [5] and adjusting the value of the constant on the right-hand side of [4] to best fit the present measurements, yields:

$$d_p/d_o = 0.25(t/t^*)^2 - 0.18(t/t^*) + 1.43, 2 \le t/t^* \le 4 \qquad [6]$$

which is the form that is plotted in figure 1. The result implies $C_r \approx 0.04$ in [3], which is reasonable in view of the residual motions of the gas within the bag (particularly toward the end of bag breakup) and the fact that the relative velocity of the parent drop with respect to the gas is only roughly 70-90% of the initial relative velocity during the period of bag growth and breakup.

Proceeding to the basal ring breakup period, it is assumed that the basal ring, and the drops that are formed by breakup of the basal ring, simply coast outward with a constant radial velocity once the bag, and thus the mechanism for a pressure difference across the basal ring, has disappeared. This behavior agrees with the observed variation of d_p in this time period, and involves neglecting the relatively small drag forces on drop liquid elements in the radial direction. Finally, the value of d_p/d_o at $t/t^* = 4$ is matched to the results of [6] and the outward coasting velocity in the ring breakup period is re-optimized to best fit the measurements. The final variation of d_p/d_o in the ring breakup period then becomes:

$$d_p/d_o = 1.79(t/t^*) - 2.51, \quad 4 \le t/t^* \le 6 \qquad [7]$$

which is the form that is plotted in figure 1.

Taken together, [2], [6] and [7] provide a reasonable correlation of the measured variations of d_p/d_o as a function of t/t^* in figure 1. These results suggest that the flow resistance caused by the bag, and the remaining portions of the bag during its breakup period, are mainly responsible for the cross-stream spread of drops formed by breakup of the parent drop, including the large drops resulting from breakup of the basal ring. Stabilization of this motion by surface tension within the deformation period can be important; after all, this mechanism is responsible for controlling drop deformation and for preventing drop breakup in the deformation regime at We smaller than the bag breakup regime. Nevertheless, effects of surface tension on the radial dispersion of liquid during bag breakup appear to be relatively small.

3.1.2 Parent Drop Velocities

The velocity of the parent drop, u_p, is plotted as a function of normalized time in figure 2. The various breakup periods — deformation, bag growth and basal ring growth (the last combining the bag breakup and ring breakup periods of figure 1) — are marked on the plot for reference purposes. The parent drop exhibits considerable acceleration during the breakup period, similar to past observations of the motion of parent drops for shear breakup (Hsiang and Faeth 1992,1993,1995). In fact, the absolute, u_p, and relative, $(u_o - u_p)$, velocities of the parent drop are comparable at the end of the ring growth period, which implies a reduction of the relative velocity of the parent drop of roughly 50% during the time of breakup, which is quite substantial. This behavior comes about due to growth of the cross-stream dimensions of the deformed parent drop, as a result of deformation and bag formation, as well as due to increased drag coefficients of the deformed parent drop, both of which significantly increase the drag forces on the parent drop compared to the original spherical drop.

3.1.3 Drag Coefficients

In order to provide a common basis for comparing the drag coefficients of the parent drops during the various breakup periods, they were based on the current (local) cross-sectional area of the drop normal to the flow and relative velocity of the deformed parent drop with respect to the ambient gas. The position of the parent drop was taken to be either the centroid of the deforming drop ($0 \le t/t^* \le 2$) or the axis of the basal ring ($2 \le t/t^* \le 5$). The temporal variation of the temporal drag coefficients are plotted in figure 3. The drag coefficients of spheres $C_D = 0.4$, and thin disks, $C_D = 1.2$, at similar Reynolds numbers are also shown on the plot for reference purposes. In the deformation period ($0 \le t/t^* \le 2$), the drag coefficient increases rapidly as the degree of deformation increases,

reaching a maximum value when the bag begins to form. This maximum value approximates the drag coefficient of a thin disk, which is reasonable in view of the shape of the parent drop at this condition. In the bag growth period ($2 \leq t/t^* \leq 3$), the continuous increase of the cross-stream diameter of the parent drop, along with bag growth (which reduces the transfer of drag forces to the basal ring) causes parent drop drag coefficients to become smaller. The reduced drag of the ring growth and breakup periods ($3 \leq t/t^* \leq 5$) is then representative of the lost flow resistance of the parent drop once the bag is no longer present.

3.2 Basal Ring Properties

3.2.1 Basal Ring Volume

Drop sizes formed from the bag and the basal ring of the bag are substantially different; therefore, it is important to know the relative volumes of the bag and its basal ring in order to estimate drop sizes produced by the bag breakup. Thus, measurements were undertaken to establish the distribution of the parent drop liquid between the bag and the basal ring over the complete range of the present data. These measurements were made by characterizing the ring at the end of bag breakup, including the volume of the nodal drops as well as the cylindrical sections of the ring in the region between the nodal drops. The ratio of the liquid volume in the basal ring, V_r, to the initial volume of the parent drop, V_o, is summarized in Table 2 (other parameters in this table include the Ohnesorge number based on the tube diameter of the ring $Oh_r = \mu_L/(\rho_L d_r \sigma)^{1/2}$, and the diameter of drops formed from the ring, d_{rd}, limited to the properties of the ring between node drops). For present test conditions, each value of Oh corresponds to a particular drop liquid; nevertheless, it can be seen that V_r/V_o is essentially independent of Oh over the present test range, yielding the correlation:

$$V_r/V_o = 0.56 \qquad [8]$$

with a standard deviation of 0.04. Lane (1951) carried out early measurements of bag breakup and mentions a determination of $V_r/V_o = 0.75$; nevertheless, this earlier value is only mentioned in passing with no information provided about its accuracy and method of determination so that its reliability is uncertain.

3.2.2 Tube Axis Diameter

Given that the volume of the ring as a fixed fraction of the initial drop volume, it should be possible to determine the diameter of the tube axis of the ring as a function of the ring diameter. In particular, if the presence of node drops along the basal ring is ignored:

$$V_r/V_o = (\pi^2 d_p d_r^2/4)/(\pi d_o^3/6) \qquad [9]$$

which implies:

$$d_r/d_o = (2V_r/(3\pi V_o))^{1/2}/(d_p/d_o)^{1/2} = 0.35/(d_p/d_o)^{1/2} \qquad [10]$$

where d_p/d_o is known as a function of time either from figure 1 or from [6] and [7].

Present measurements of $d_r/d_o$are plotted as a function of t/t^* in figure 4. The predictions of d_r/d_o from [10] using [6] and [7] to find d_p/d_o, are also shown on the plot. There is significant scatter of the measurements due to problems of observing the basal ring, particularly when the bag is present, and effects of the presence of node drops. Nevertheless, the measurements are in reasonably good agreement with [10], supporting a relatively slow reduction of d_r/d_o with increasing time due to the increased diameter of the tube axis of the basal ring itself.

3.2.3 Basal Ring Drop Diameters

Two types of drops are formed from the basal ring: node drops and drops from the cylindrical portions of the ring between the nodes that are somewhat smaller than the node drops. The drops formed from the cylindrical portion of the basal ring are not subject to

strong strain and appear to result from classical Rayleigh breakup of a nearly constant-diameter liquid column. In addition, the Ohnesorge numbers of the rings observed during the present investigation were relatively small ($Oh \leq 0.13$ based on values given in Table 2) so that effects of liquid viscosity should be small as well. Under these circumstances, the ratio of the diameter of the drops formed by ring breakup, and the ring diameter, should be a constant, as follows (Dombrowski and Hooper 1962):

$$d_{rd}/d_r = 1.88, \quad \text{predicted.} \qquad [11]$$

The Rayleigh breakup condition of [11] was evaluated using the present measurements. In doing this, the complication of the node drops was ignored (they will be considered later) and only drops formed from the intervening constant-diameter portions of the ring were considered. In addition, d_r was determined for this expression at the time of ring drop breakup, i.e., $t/t^* = 5$ where $d_r/d_o = 0.13$ from figure 4 with a 16% uncertainty.

The values of d_{rd}/d_r measured during the present investigation are summarized as a function of Oh in Table 2. As before, the present experiments involved a nearly constant Oh (and Oh_r) for each liquid because the variation of We is small in the bag breakup regime. The measurements do not suggest a significant effect of Oh over the present test range and yield

$$d_{rd}/d_r = 2.2, \quad \text{measured} \qquad [12]$$

Clearly, [12] is in reasonably good agreement with the Rayleigh breakup prediction at small Oh given by [11], supporting Rayleigh breakup as the mechanism producing drops from the ring-like portions of the basal ring. Finally, given $d_r/d_o = 0.13$, as just discussed, implies:

$$d_{rd}/d_0 = 0.29. \qquad [13]$$

The effect of the node drops on the mean size of drops produced by the ring will be considered next. In general, there were 4-6 node drops, having diameters of $(1.3\text{-}1.6)d_{rd}$.

Thus, if this contribution is added to that of the drops from the tubular portions of the ring, the final average size of drops formed from the basal ring, d_{trd}, can be correlated as follows:

$$d_{trd}/d_o = 0.30 \qquad [14]$$

with the uncertainty of this constant being less than 20%. Finally, the total number of drops produced by the basal ring, N_{trd}, can be found from the mean size of the basal ring drops given by [14] and the volume of the basal ring given by [8], as follows:

$$N_{trd} = 22.1$$

3.2.4 Basal Ring Breakup Time

As discussed by McCarthy and Molloy (1974), the Rayleigh breakup times, t_{rt}, of liquid columns have been shown to be

$$t_{rt} = C(\rho_t d_r/\sigma)^{1/2}(1+3Oh_r)d_r \qquad [16]$$

where d_r is the column diameter, Oh_r is the Ohnesorge number based on this dimension, and C is a stability constant that must be determined. Smith and Moss (1996) found C to be 13 for different liquids and column diameters. Associating the time required for the Rayleigh breakup with the time required for the basal ring to breakup, by replacing the column diameter with the tube axis diameter in [16], yields:

$$t_{rt} = CC_{rt}(\rho_L d_r/\sigma)^{1/2}(1+3Oh_r)d_r \qquad [17]$$

where C_{rt} is an unknown constant of proportionality expected to be on the order of unity. For the conditions of the present study, Oh_r is small so that the effect of liquid viscosity represented by the Oh term can be neglected. Then, normalizing [17] by t* yields:

$$t_{rt}/t^* = 13C_{rt}\,We^{1/2}(d_r/d_o)^{1/2} \qquad [18]$$

For bag breakup, We = 13-25, while d_r/d_o = 0.17-0.19 in the region where the basal ring is present (i.e., $2 \leq t/t^* \leq 5$) as seen in figure 4. Substituting averages of these parameters into [18] then yields:

$$t_\pi/t^* = 3.88C_\pi \qquad [19]$$

Finally, it is assumed that the Rayleigh breakup process of the basal ring begins when the ring has just formed ($t/t^* \approx 2$) and ends upon ring breakup ($t/t^* \approx 5$), based on the results illustrated in figure 1. This implies that the time required from initial basal ring formation to basal ring breakup is $t_\pi = 3t^*$, so that $C_\pi = 0.77$. Since C_π is on the order of unity, as expected, this finding provides good support for the idea that basal ring breakup involves a relatively passive Rayleigh breakup process. Thus, given that the time required to reach maximum deformation, where basal ring formation is completed, is $2t^*$, the Rayleigh breakup time of the basal ring of roughly $3t^*$ fixes the entire bag breakup time to be roughly $5t^*$. This breakup time is nearly the same as for shear breakup (Liang et al. 1988) but the previous reasoning suggests that this agreement is fortuitous due to the very different breakup phenomena that comprise the bag and shear breakup processes.

3.2.5 Ring Drop Velocity Distributions

Ring drop velocity distributions were essentially independent of drop size, except for a slight tendency for node drops to move slower than the smaller ring drops formed from portions of the basal ring between the node drops. This effect is evident from the downstream deflection of the basal ring in the region between nodes seen in the inset figure at $t/t^* = 4$ in figure 1. This variation, however, is less than present experimental uncertainties for velocity measurements so that initial ring drop velocities can be computed from the results illustrated in figure 2 with little error.

3.3 Bag Properties

3.3.1 Bag Drop Diameters

The properties of drops formed by breakup of the bag, along with a few determinations of bag thickness, h, by measurements from holograms, are summarized in Table 3. It should be noted that the values of h given in Table 3 are not very reliable because they approach present limits of spatial resolution and involve additional problems of estimating film thicknesses from the region where the bag breaks up into drops (in particular, later considerations will show that unbalanced surface tension forces in the region where bag drops are forming are important so that these effects probably locally increase bag thicknesses as well). In view of these problems, it is estimated that the values of h in Table 3 might be too large by as much as a factor of two, although the corresponding drop diameter measurements for drops found from bag breakup are felt to be reliable within the uncertainties stated earlier. Entries provided in Table 3 include d_o, the time when drop sizes were measured (except for one condition at $t/t^* = 3$, these results were averaged over the entire breakup period of $t/t^* = 3$-4), the number-averaged bag drop diameter, d_{bda}, and the Sauter mean diameter SMD_{bd}, of drops formed from the breakup of the bag, several normalizations of these properties and the Ohnesorge number based on the dimension d_{bda}.

Comparing mean drop diameters at the start of bag breakup and averaged over the entire bag breakup period for glycerol (42%) indicates an increase of the drop sizes as the basal ring of the bag is approached. This is not unexpected as some stretch of the bag membrane, and a corresponding reduction of the size of drops formed by breakup of the membrane, is expected as the farthest downstream location is approached. Nevertheless, the variation of drop diameters is not large, with drops formed initially from the bag being only 15% smaller than the mean size of drops formed from the bag.

A second issue of interest about drops formed by breakup of the bag itself is the variation of mean drop sizes with Oh. The results of Table 3 show that both d_{bda}/d_o and SMD_{bd}/d_o increase as Oh increases over the test range. Characterizing this behavior by the

Ohnesorge number based on the average size of drops formed from the bag, it is seen that d_{bda}/d_o increases from 3.5% to 4.9% as Oh_{bda} increases from 0.023 to 0.193. This behavior suggests an effect of liquid viscosity on bag properties, and thus on the properties of drops formed from the bag; such behavior is not surprising in view of past observations (Hsiang and Faeth 1992, 1993, 1995) of strong effects of liquid viscosity on the drop sizes formed by secondary breakup.

Mean drop sizes resulting from breakup of the bag vary somewhat with initial Oh as just noted, but yield an average value of d_{bda}/d_o of 4.2%, over the present test range. Thus, bag drops generally are relatively small and do not have as strong an effect on spray transport properties as the drops produced by breakup of the basal ring. For example, based on the diameter-squared behavior that tends to dominate drop properties in sprays (Faeth 1997), the lifetime of drops formed from the basal ring would be nearly 60 times longer than the lifetime of drops formed from the bag. Another issue concerning mean drop sizes is that SMD_{bd} and d_{bda} are nearly the same, e.g., the average value of the ratio $SMD_{bd}/d_{bda} = 0.89$. This behavior implies a nearly monodisperse size distribution for these drops, a property that will be considered in more detail next. To summarize, the correlation of bag drop sizes becomes:

$$d_{bda}/d_o = 0.042 \qquad [20]$$

The size distribution function of drops formed by breakup of the bag is illustrated in figure 5. These results are plotted according to the root normal distribution function that has proven to be successful for a variety of drop and spray breakup processes (Faeth 1997). Results for various values of MMD/SMD for the bag drops are shown on the plot for comparison with the measurements. In the past, this distribution function with MMD/SMD = 1.20 has been successful for correlating drop size distributions in sprays. The bag drops themselves, however, while correlating reasonably well according to the root normal distribution function, do so only with a much smaller value of MMD/SMD = 1.04. As discussed earlier, however, this result is not unexpected due to the nearly monodisperse

size distribution of drops formed from the bag because the bag membrane itself appears to have a relatively uniform thickness. The behavior of the drop size distribution function changes when drops formed from both the bag and the ring are considered, however, as discussed later in connection with overall breakup properties.

3.3.2 Bag Breakup Time

The time required for breakup of bag, t_{bt}, is also an important parameter that must be known. This issue will be considered in the following, assuming a constant bag thickness during bag growth period with an average bag velocity, u_b, as shown in Table 4, by relating the bag breakup time to the breakup time of a thin film.

From Dombrowski and Hooper (1962), the time required from breakup of a thin film, t_{ft}, can be correlated as follows:

$$t_{ft}/t^* = 3.73\ We^{-1/2}\ (u_o/u_L)^2(h/d_0)^{1/2} \qquad [21]$$

where u_L is the liquid film velocity. For the bag growth period, the liquid film velocity can be approximated by u_b to yield the time required for breakup of bag as follows:

$$t_{bt}/t^* = 3.73\ C_{bt}\ We^{-1/2}\ (u_o/u_b)^2(h/d_0)^{1/2} \qquad [22]$$

where C_{bt} is a constant of proportionality expected to be on the order of unity. Applying [22], using a constant value of $h/d_0 = 1\%$, yields the bag breakup times summarized in Table 4. From figure 1, the time required for breakup of the bag is typically $t_{bt}/t^* = 1.0$, thus, averaging the results in Table 4 implies that the $C_{bt} = 0.91$ which is on the order of unity, as expected. This finding strongly supports the idea that breakup of the bag itself involves a simple thin film breakup of the membrane-like bag, and that the bag inflation time is controlled by the breakup time of the first part of the bag that is formed, i.e., the tip of the bag.

3.3.3 Bag Drop Velocity Distribution

Initial velocities of bag drops exhibit negligible variation with size over the narrow range of sizes of these drops. In addition, even though portions of the bag move at somewhat different velocities than the parent drop (which is taken to be the basal ring for $2 \leq t/t^* \leq 5$ when parent drop velocities are found) these velocity variations are small compared to the parent drop velocity. Thus, within present experimental uncertainties, initial bag drop velocities can be estimated as the parent drop velocity at the time they are formed from figure 2. Present observations indicate that the time of breakup of the bag extends over the range $t/t^* = 3.2 - 3.5$, thus, in view of the relatively slow variation of parent drop velocities seen in Fig. 2, initial bag drop velocities are essentially monodisperse within present experimental uncertainties.

3.4 Overall Breakup Properties

3.4.1 Drop Size Distributions

Past work yielded different observations about overall drop size distributions resulting from bag breakup, for example, Hsiang and Faeth (1992, 1993, 1995) find that drop size distribution functions represented reasonably well by the universal root normal size distribution function while Gel'fand et al. (1974) report a bimodal drop size distribution function with one nearly monodisperse group associated with drops formed from the ring and a second nearly monodisperse group associated with drops formed from the bag. The overall drop size distribution function properties were studied during the present investigation in order to help resolve these differences. As a practical matter it was found that in spite of the nearly monodisperse drops formed from the bag no bimodal behavior for the drop size distribution function was evident. Thus, present results concerning the drop size distribution function were correlated in terms of the universal root normal distribution function of Simmons (1977). It will be shown later, however, that this behavior probably is due to undersampling the small drops formed from the bag, tending to support the findings of Gel'fand et al. (1974) at least to the extent that an overall drop size distribution is useful for treating bag breakup processes.

The drop size distribution results for the present measurements of bag breakup properties are plotted in terms of the universal root normal distribution function in figure 6. These results emphasize behavior over the entire test range rather more statistically significant results at a fewer number of conditions. Thus, the measurements illustrated in figure 6 are scattered due to inadequate statistics. In particular, bag breakup of individual drops yields a relatively small number of large drops that dominate the size distribution function because they represent a large fraction of the drop volume produced by breakup. In addition, the small drops formed from breakup of the bag itself tend to be undersampled because they are small and poorly resolved and also are rapidly swept downstream due to their rapid acceleration to gas velocities. The results shown in figure 6 however, are reasonably represented by the root normal distribution function, with MMD/SMD = 1.2, which is similar to earlier findings for other spray breakup processes (Faeth 1997).

A second issue of interest about the drop size distribution is the SMD after bag breakup. The SMD is mainly dominated by the largest drop sizes in the distribution; thus, by neglecting the small drops from bag, the present measurements of SMD/d_o after bag breakup are summarized in Table 5, along with the average ring drop size from [14] and the average bag drop size from Table 3. Clearly, the SMD after bag breakup is dominated by the node drop size (the largest drop size of ring drops) and is essentially independent of Oh over the present range to yield:

$$SMD_{total}/d_o = 0.36 \qquad [23]$$

with a standard deviation of 0.05 for [23].

The present correlation of the SMD for the entire bag breakup process from [23] differs from the earlier findings of Hsiang and Faeth (1992). The correlating expression for the SMD for bag breakup from Hsiang and Faeth (1992) was found as an empirical extension of the boundary layer stripping analysis developed for the shear breakup regime to yield the following expression:

$$\rho_G SMD u_o^2/\sigma = 6.2(\rho_L/\rho_G)^{1/4}(\nu_L/d_o u_o)^{1/2} We \qquad [24]$$

The SMD after bag breakup for the present measurements is plotted in figure 7 as suggested by [24], along with the data of Hsiang and Faeth (1992) for the bag breakup region. Both sets of measurements roughly agree with each other, however, the results of the present study, characterized by the results of [23], yield a constant value of SMD/d_o for the bag region instead of the correlation of [24]. This implies that the SMD after bag breakup only fortuitously agreed with the boundary layer analogy, over the narrow range of We of the bag breakup regime. Thus, a more rational approach would be to treat bag breakup as dominated by Rayleigh breakup of the basal ring, including the complications due to the presence of node drops to yield [23].

The small drops (which mainly are formed from the bag) can have a large effect on the SMD, however, even though they are often ignored, because there are a large number of small drops due to the reasonably large mass fraction and small size of drops formed from the bag. In the same way that the number of drops formed from ring was estimated in [15], the number of drops formed from the bag can be estimated as follows:

$$\pi/6\, d_o^3 (\text{mass fraction of bag drops}) = N_b\, \pi/6\, d_{bd}^3 \qquad [25]$$

Using the mass fraction of the basal ring from [8] and the average bag drop size given by [20], the number of drops formed from the bag can be computed from [25] to yield N_b = 5940 bag drops per initial drop. Summarizing the results from [8] and [25], and estimating the number of node drops as 6 per initial drop, then the number distribution involves fixed fractions for the bag, node and ring drops as follows: f_b = 0.996, f_n = 0.001 and f_r = 0.003. It is obvious, that the small drops dominate the number of drops in the distribution.

Given this information, the overall SMD including the small drops can be estimated from the fundamental definition of the SMD as follows:

$$SMD/d_o = \frac{f_b(d_{bd}/d_o)^3 + f_r(d_{rd}/d_o)^3 + f_n(d_{nd}/d_o)^3}{f_b(d_{bd}/d_o)^2 + f_r(d_{rd}/d_o)^2 + f_n(d_{nd}/d_o)^2} \qquad [26]$$

Substituting the values of f_b, f_r and f_n, and the ratios d_{bd}/d_o, d_{rd}/d_o, d_{nd}/d_o, found earlier, yields $SMD/d_o = 0.11$, which is much smaller than the result given by [23] where the bag drops have been ignored. This implies that the small drops do affect the SMD substantially when the overall, SMD is sought. This behavior suggests that such gross averages for the entire bag breakup process are not very helpful, although the drops formed from the bag are still important in spite of their small size because they amount to 44% of the initial mass of the drop. Taken together, a more effective approach is to use [23] to estimate the size of the ring drops, and [20] to estimate the size of the bag drops, while treating these drops as separate populations.

3.4.2 Drop Breakup Rate

In order to find drop breakup rates, the fact that the entire bag breakup process involves two separate periods of liquid removal from the parent drop must be considered: one period associated with breakup of the bag itself, and the other period associated with breakup of the basal ring. The first period involves 44% of the original drop mass from [8], with this process approximated by a constant rate of liquid removal over the time period, $t/t^* = 3.2\text{-}3.5$, when the bag itself was observed to break up based on present measurements. The second period involves 56% of the original drop mass from [8], with this process assumed to occur by the nearly simultaneous formation of drops from the basal ring at $t/t^* = 5.0$, when the basal ring was observed to break up based on present measurements.

Present measurements of the cumulative volume percentage of liquid removed from the parent drop, based on the assumptions just discussed, are plotted in figure 8. Thus, unlike shear breakup, bag breakup involves two relatively short breakup periods, separated by periods of development of Rayleigh breakup processes. An interesting feature of the results illustrated in figures 1 and 8 is that the bag forms for a time period 1.0 t^* with bag formation ending due to Rayleigh breakup of the tip of the bag. Thus, if the entire process of breakup of the bag proceeded by passive Rayleigh breakup, a total breakup period of the

bag 1.0 t* might be expected as well. Instead, the bag actually breaks up in a much shorter time, 0.3 t*. This suggests that once breakup of the bag starts, the unbalanced surface tension forces on the broken bag enhance its motion toward the basal ring so that its time of breakup (or disappearance) is reduced. This behavior also helps to explain the tendency for bag drop sizes to be larger than suggested by estimates of bag thickness, and to increase as the basal ring is approached due to a corresponding increase of the membrane thickness. Finally, the liquid removal properties of bag breakup highlights why separate treatment of drops formed from the bag and from the basal ring is preferable to attempting to treat all the drops as a single population.

3.4.3 Temporal and Spatial Breakup Region

The spatial and temporal properties of bag breakup based on the velocity results of figure 2 are illustrated in figure 9. These findings involve the streamwise positions of the drops and the tip of bag, denoted by x, as functions of the time after the start of breakup. The positions of the parent drop (which is slowest drop to relax toward gas velocities), the tip of the bag (when it is present in the period $2<t/t^*<3$) and the most remote drop (which is the first drop formed from breakup of the tip of the bag and which responds relatively rapidly to the gas motion due to its relatively small size) are illustrated in the figure. The most remote drop separates from the parent drop at roughly $t/t^* = 3$ (actually $t/t^* = 3.2$) when the bag begins to break up, and begins its streamwise travel from the tip of the bag. The breakup process itself typically is ended when breakup of the ring is completed, which occurs roughly at $t/t^* = 5$ for present test conditions. In the coordinate system of figure 9, there is a small effect of ρ_L/ρ_G on drop motion; therefore, results at the limits of the present test range, $\rho_L/\rho_G = 630$ and 890, have been illustrated on the plot.

The results illustrated in figure 9 indicate that the temporal and spatial ranges of bag breakup are comparable to the findings for shear breakup observed by Chou et al. (1997). In particular, the breakup period requires t/t^* in the range 0-5; in this period, the most

remote drop moves a streamwise distance of roughly 60 initial drop diameters and the parent drop moves a streamwise distance of roughly 50 initial drop diameters. Finally, the results plotted in figure 1 (based on the value of d_p/d_o at the time of breakup of the basal ring) imply that the largest drops formed by breakup of the ring spread laterally to a diameter of roughly 7 initial drop diameters. These times and distances are comparable to characteristic times and distances associated with the dense region of pressure-atomized sprays (Faeth, 1997); therefore, both bag and shear breakup should be treated as rate processes rather than by jump conditions, in many instances.

4. CONCLUSIONS

The objective of the present study was to experimentally investigate the temporal properties of bag breakup for shock-wave initiated disturbances in air at normal temperature and pressure. The test liquids included water, ethyl alcohol and various glycerol mixtures to yield liquid/gas density ratios of 633-893, Weber numbers of 13-20, Ohnesorge numbers of 0.0043-0.0427 and Reynolds numbers of 1550-2150. The major conclusions of the study are as follows:

1. The basal ring formed from the parent drop contains roughly 56% of the initial drop volume (mass) and eventually yields drops having mean diameters of roughly 30% of the initial drop diameter due to a Rayleigh-like breakup process of the basal ring that occurs relatively abruptly near $t/t^* = 5$.

2. The bag formed from the parent drop contains roughly 44% of the initial drop volume (mass) and eventually yields nearly monodisperse drops having mean diameters of roughly 4% of the initial drop diameter due to a breakup process of the membrane-like bag. This breakup process propagates progressively from the tip to the basal ring end of the bag over the period $t/t^* = 3.2 - 3.5$ and yields a nearly

monodisperse drop size distribution; this behavior suggests a relatively uniform bag thickness of roughly 2-3% of the initial drop diameter.

3. The distinct properties of the drops formed from the bag and from the basal ring suggest that they should be treated as separate drop populations rather than merged as in past determinations of bag breakup jump conditions, e.g., the approach developed by Hsiang and Faeth (1992). Thus, the two drop populations should be represented by separate size distribution functions with the bag drops assumed to be formed at a uniform rate over the period $t/t^* = 3.2 - 3.5$ and the basal ring drops assumed to be formed abruptly at $t/t^* = 5.0$, with initial drop velocities at these conditions relatively independent of drop size and approximated by corresponding parent drop velocities at the time of drop formation.

4. The parent drop experiences large acceleration rates due to the development of both large cross-sectional areas and large drag coefficients caused by drop deformation and bag formation. Phenomenological analyses provided reasonably good correlations of parent drop velocities similar to earlier considerations of jump conditions for drop velocities due to Hsiang and Faeth (1992, 1993, 1995).

5. Bag breakup causes significant temporal and spatial dispersion of drops during the breakup period, as follows: the breakup process requires a total time of $t/t^* = 5$; the cross-stream dispersion, based on the diameter of the ring axis when ring breakup is completed, amounts to roughly 7 initial drop diameters; and the streamwise dispersion when breakup is completed involves a streamwise motion of the parent drop of roughly 50 initial drop diameters and corresponding motion of the most remote drop of roughly 60 initial diameters. These times and distances are not always small in comparison to the characteristic times and distances of dense spray processes, implying that bag breakup should be treated as a rate process, rather than

by jump conditions, in some instances, in agreement with earlier findings for shear breakup due to Chou et al. (1997).

Acknowledgments — This research was sponsored by the Air Force Office of Scientific Research, Grant No. F49620-95-1-0364, under the technical management of J.M. Tishkoff, and the Office of Naval Research under the technical management of E.P. Rood. The authors would like to thank C.W. Kauffman for the loan of the shock tube facility and advice concerning its operation. The U.S. Government is authorized to reproduce and distribute copies of this article for governmental purposes notwithstanding any copyright notation thereon.

REFERENCES

Chou, W.-H. (1997) Temporal variation of drop properties and formation rates during secondary breakup. Ph.D. Thesis, The University Of Michigan, Ann Arbor, Michigan, U.S.A.

Chou, W.-H., Hsiang, L.-P. and Faeth, G.M. (1997) Temporal properties of secondary drop breakup in the shear breakup regime. *Int. J. Multiphase Flow*, in press.

Dombrowski, H. and Hooper, P.C. (1962) The effect of ambient density on drop formation in sprays. *Chem. Engr. Sci.* 19, 291-305.

Faeth, G.M. (1997) Spray combustion phenomena. In *Twenty-Sixth Symposium (International) on Combustion*, The Combustion Institute, Pittsburgh, Pennsylvania, U.S.A., pp. 1593-1612.

Faeth, G.M., Hsiang, L.-P. and Wu, P.-K. (1995) Structure and breakup properties of sprays. *Int. J. Multiphase Flow* 21 (Suppl.), 99-127.

Gel'fand, B.E, Gubin, S.A. and Kogarko, S.M. (1974) Various forms of drop fractionation in shock waves and their special characteristics. *Inzhenerno-Fizicheskii Zhurnal* 27, 119-126.

Hsiang, L.-P. and Faeth, G.M. (1992) Near-limit drop deformation and secondary breakup. *Int. J. Multiphase Flow* 18, 635-652.

Hsiang, L.-P. and Faeth, G.M. (1993) Drop properties after secondary breakup. *Int. J. Multiphase Flow* 19, 721-735.

Hsiang,L.-P. and Faeth, G.M. (1995) Drop deformation and breakup due to shock wave and steady disturbances. *Int. J. Multiphase Flow* 21, 545-560.

Lane, W. R. (1951) Shatter of drops in streams of air. *Ind. Engr. Chem.* 43, 1312-1317.

Lange, N.A. (1952) *Handbook of Chemistry*, 8th ed., Handbook Publishers, Inc., Sandusky, Ohio, U.S.A., pp. 1134 and 1709.

Liang, P.Y., Eastes, T.W. and Gharakhari, A. (1988) Computer simulations of drop deformation and drop breakup. AIAA Paper No. 88-3142.

McCarthy, M.J. and Malloy, N.A.(1974) Review of stability of liquid jets and the influence of nozzle design. *Chem. Engr. J.* 7, 1-20.

Ranger, A.A. and Nicholls, J.A. (1969) The aerodynamic shattering of liquid drops. *AIAA J.* 7, 285-290.

Simmons, H.C. (1977) The correlation of drop-size distributions in fuel nozzle sprays. *J. Engr. for Power* 99, 309-319.

Smith, S.W.J. and Moss, H. (1916-1917) *Proc. Phys. Soc. A* 93, 373.

White, F.M. (1974)*Viscous Fluid Flow*, McGraw-Hill, New York, U.S.A..

Wu, P.-K., Ruff, G.A. and Faeth, G.M. (1991) Primary breakup in liquid/gas mixing layers for turbulent liquids. *Atomization and Sprays* 1, 421-440.

Wu, P.-K., Hsiang, L.-P. and Faeth, G.M. (1995) Aerodynamic effects on primary and secondary breakup. *Prog. Astro. Aero.* 169, 247-279.

Table 1 Summary of the test conditions for bag breakup[a]

Liquid[b]	d_o (μm)	ρ_L (kg/m^3)	ρ_L/ρ_G (-)	$\mu_L \times 10^4$ (kg/ms)	$\sigma \times 10^3$ (N/m)	Oh x 10^3 (-)	Re (-)
Water	620	997	755	8.94	70.8	4.3	1670-1910
Ethyl alcohol	630	800	633	16.0	24.0	15.0	1830-2080
Glycerol (21%)	650	1050	806	16.0	67.3	7.5	1550-1660
Glycerol (42%)	650	1105	857	35.0	65.4	16.1	1550-1910
Glycerol (63%)	850	1162	893	108.0	64.8	42.7	1850-2150

[a]With We in the range 13-20 in air initially at 98.8 kPa and 298± 2K in the driven section of the shock tube. Shock Mach numbers in the range of 1.01-1.04. Properties of air taken for conditions downstream of shock wave: with pressures of 119.7 - 129.8 kPa, ρ_G of 1.25-1.31 kg/m^3 and μ_G of 18.5 x 10^{-6} kg/ms.
[b]Glycerol compositions given in parentheses are percent glycerin (by mass) in water.s

Table 2 Summary of properties of basal ring[a]

Liquid[b]	We	Oh	V_r/V_0	Oh_r	d_{rd}/d_r
Water	15	0.0043	0.57	0.013	2.53
Ethyl Alcohol	15	0.0150	0.52	0.045	2.54
Glycerol (21%)	15	0.0075	0.59	0.021	1.91
Glycerol (42%)	17	0.0161	0.57	0.045	1.87
Glycerol (63%)	15	0.0427	0.54	0.130	2.21

[a]Result based on the properties of the bag during the bag breakup period for the test conditions summarized in Table 1
[b]Glycerol compositions given in parentheses are percent glycerin (by mass) in water

Table 3 Summary of properties of drops formed from the bag[a]

Liquid[b]	d_o (μm)	t/t* (-)	h (μm)	d_{bda} (μm)	SMD_{bd} (μm)	Oh_{bda}	h/d_o (%)	d_{bda}/h (-)	d_{bda}/d_o (%)	SMD_{bd}/d_o (%)
Water	620	3-4	16.4	21.9	23.8	0.023	2.65	1.33	3.5	3.8
Glycerol (21%)	650	3-4	—	22.1	23.9	0.077	—	—	3.8	3.5
Glycerol (42%)	650	3	23.2	25.8	28.9	0.038	3.57	1.12	4.0	4.5
Glycerol (42%)	650	3-4	—	29.6	33.2	0.075	—	—	4.6	5.1
Glycerol (63%)	850	3-4	35.4	42.1	48.8	0.193	4.16	1.17	4.9	5.2
					averages =		3.46	1.21	4.2	4.4

[a]Results based on the properties of the bag and the properties of drops formed by breakup of the bag during the bag breakup period for the test conditions summarized in Table 1.
[b]Glycerol compositions given in parentheses are percent glycerin (by mass) in water.

Table 4 Summary of properties of bag during bag formation period[a]

Liquid[b]	We	t/t*	h/d_0	u_b/u_o	t_{bf}/t^*
Water	15	2.0-3.5	0.01	0.266	1.36
Glycerol (21%)	15	3.0-3.5	0.01	0.288	1.16
Glycerol (42%)	17	3.0-3.5	0.01	0.324	0.92
Glycerol (63%)	15	3.0-3.5	0.01	0.317	0.96

[a]Result based on the properties of the bag during the bag breakup period for the test conditions summarized in Table 1
[b]Glycerol compositions given in parentheses are percent glycerin (by mass) in water

Table 5 Summary of SMD after bag breakup[a]

Liquid[b]	We	Oh	SMD_{total}/d_0	d_{trd}/d_0	d_{bd}/d_0
Water	15	0.0043	0.34	0.30	0.035
Ethyl alcohol	15	0.015	0.32	0.30	—
Glycerol (21%)	15	0.0075	0.41	0.30	0.038
Glycerol (42%)	17	0.016	0.37	0.30	0.040
Glycerol (63%)	15	0.042	0.38	0.30	0.041
		averages=	0.36	0.30	0.041

[a]Result based on the properties of the bag during the bag breakup period for the test conditions summarized in Table 1
[b]Glycerol compositions given in parentheses are percent glycerin (by mass) in water

List of Figures

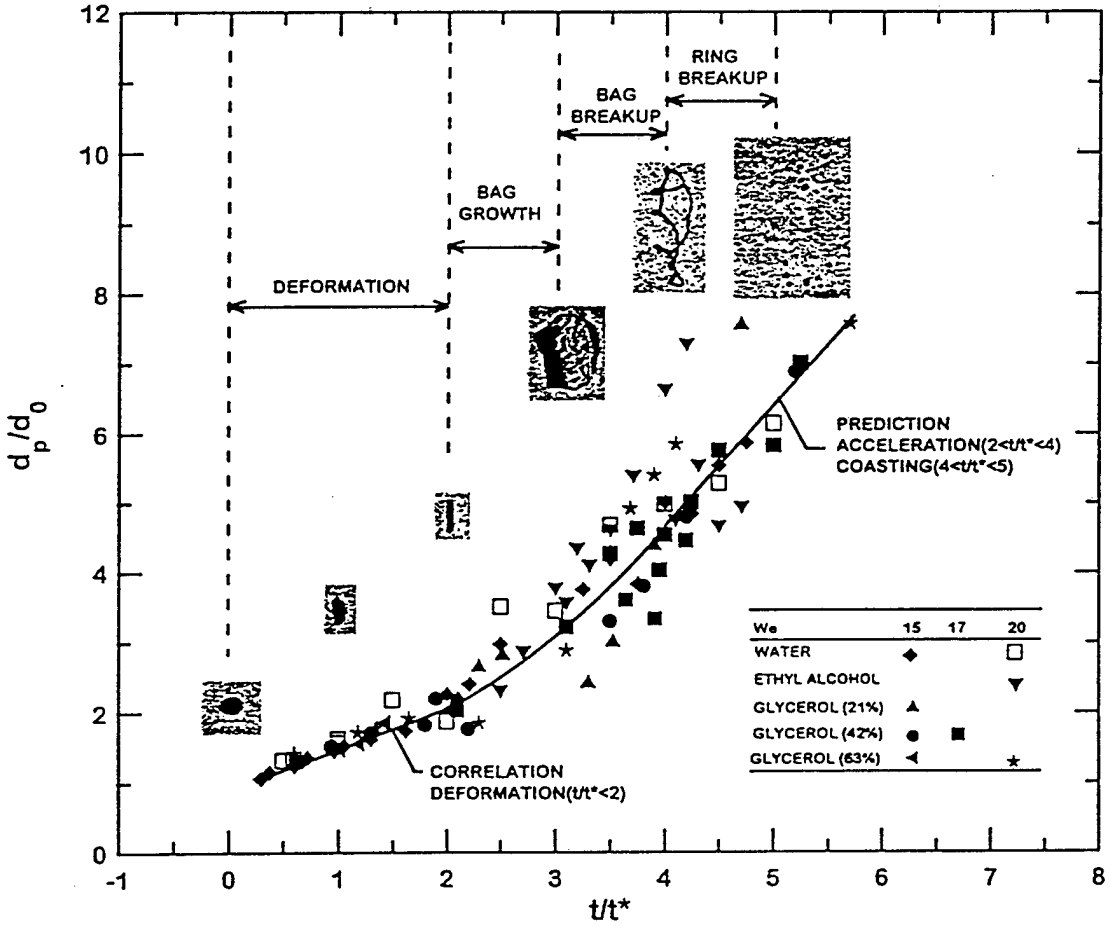
RING BREAKUP
BAG BREAKUP
BAG GROWTH
DEFORMATION
PREDICTION
ACCELERATION(2<t/t*<4)
COASTING(4<t/t*<5)
CORRELATION
DEFORMATION(t/t*<2)
We 15 17 20
WATER
ETHYL ALCOHOL
GLYCEROL (21%)
GLYCEROL (42%)
GLYCEROL (63%)
d_p/d_0
t/t*
0 2 4 6 8 10 12
-1 0 1 2 3 4 5 6 7 8

FIG. 1

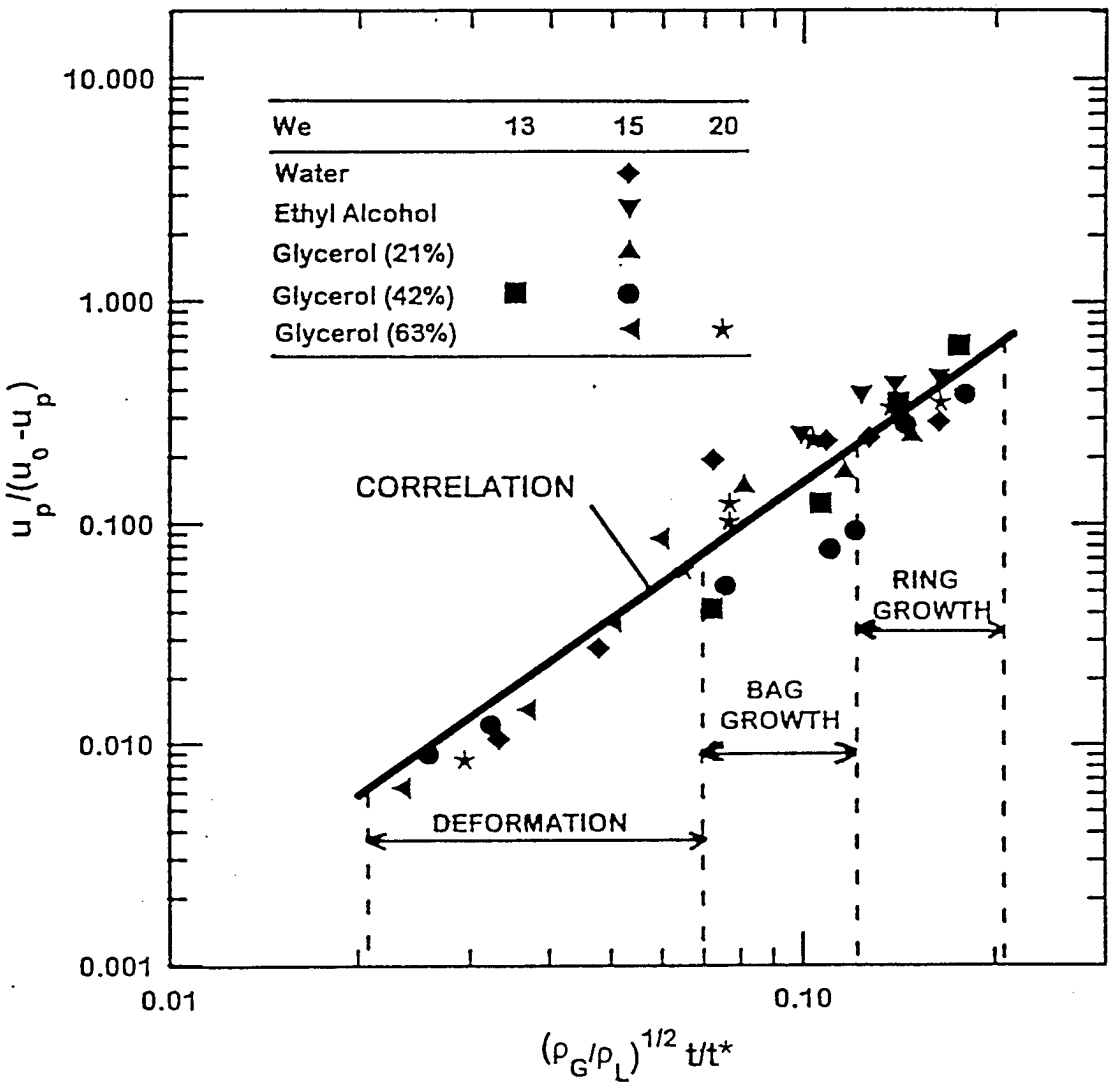
10.000
1.000
0.100
0.010
0.001
0.01
0.10
$u_p/(u_o-u_p)$
$(\rho_G/\rho_L)^{1/2}\ t/t^*$
We 13 15 20
Water
Ethyl Alcohol
Glycerol (21%)
Glycerol (42%)
Glycerol (63%)
CORRELATION
DEFORMATION
BAG GROWTH
RING GROWTH

FIG. 2

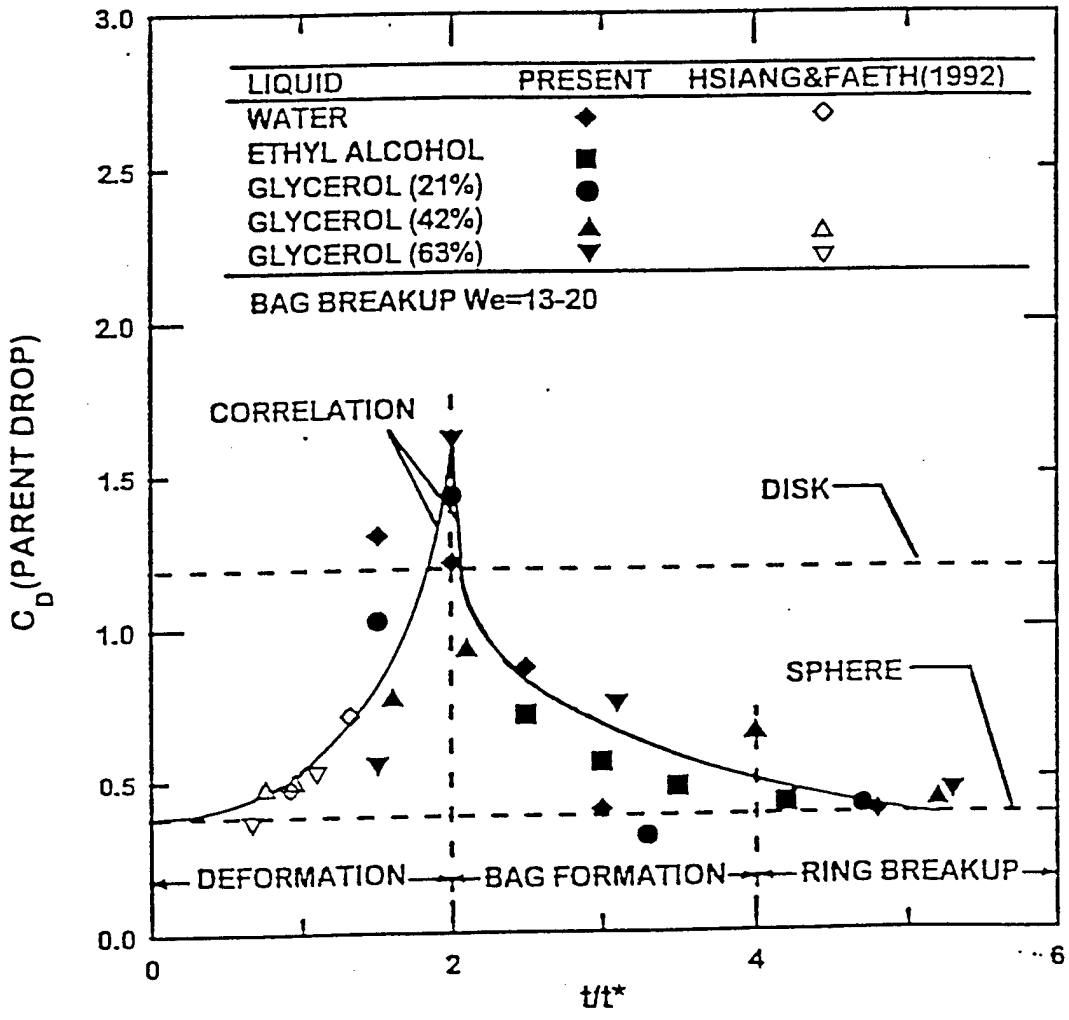
LIQUID
PRESENT
HSIANG&FAETH(1992)
WATER
ETHYL ALCOHOL
GLYCEROL (21%)
GLYCEROL (42%)
GLYCEROL (63%)
BAG BREAKUP We=13-20
CORRELATION
DISK
SPHERE
DEFORMATION
BAG FORMATION
RING BREAKUP
C_D(PARENT DROP)
t/t*
3.0
2.5
2.0
1.5
1.0
0.5
0.0
0
2
4
6

FIG. 3

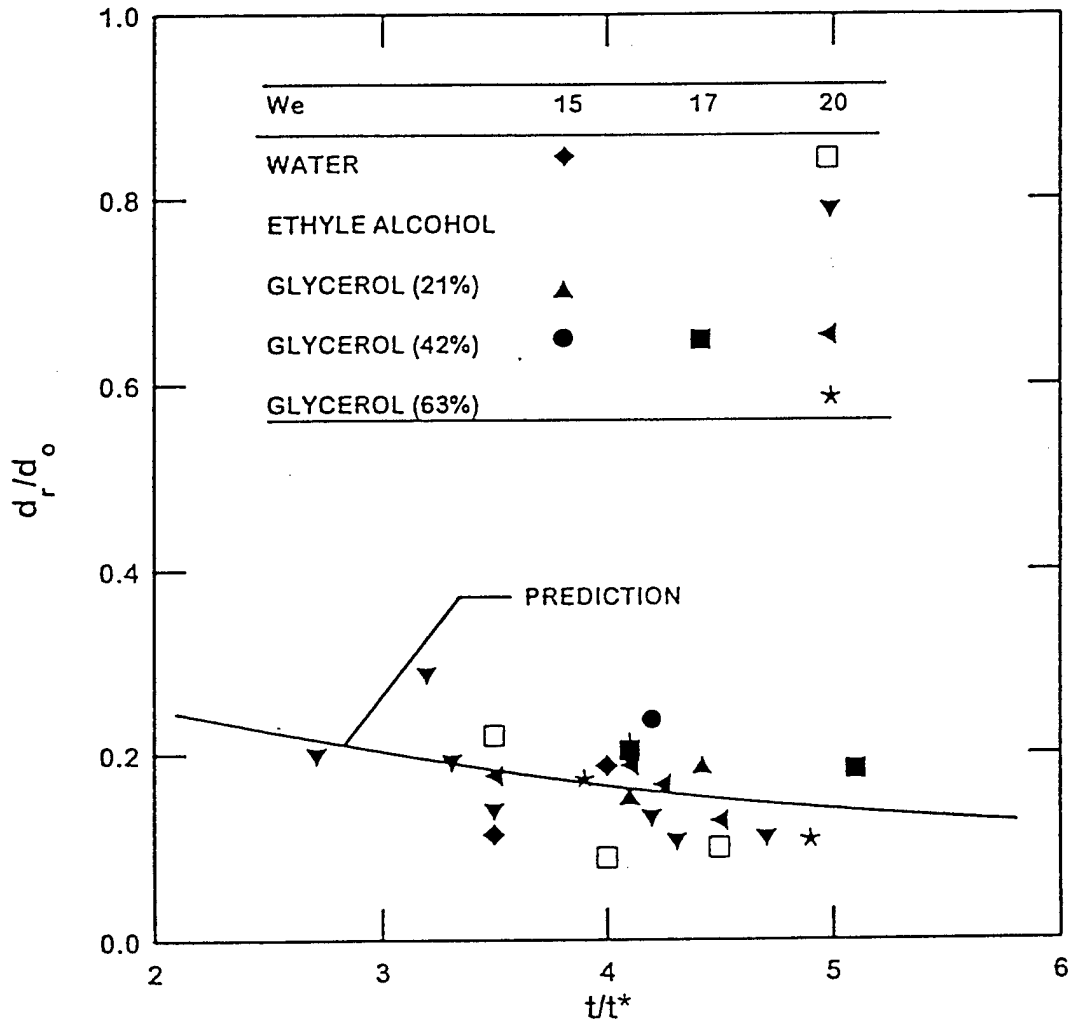
1.0
0.8
0.6
0.4
0.2
0.0
d_r/d_o
We
15
17
20
WATER
ETHYLE ALCOHOL
GLYCEROL (21%)
GLYCEROL (42%)
GLYCEROL (63%)
PREDICTION
2
3
4
5
6
t/t*

FIG. 4

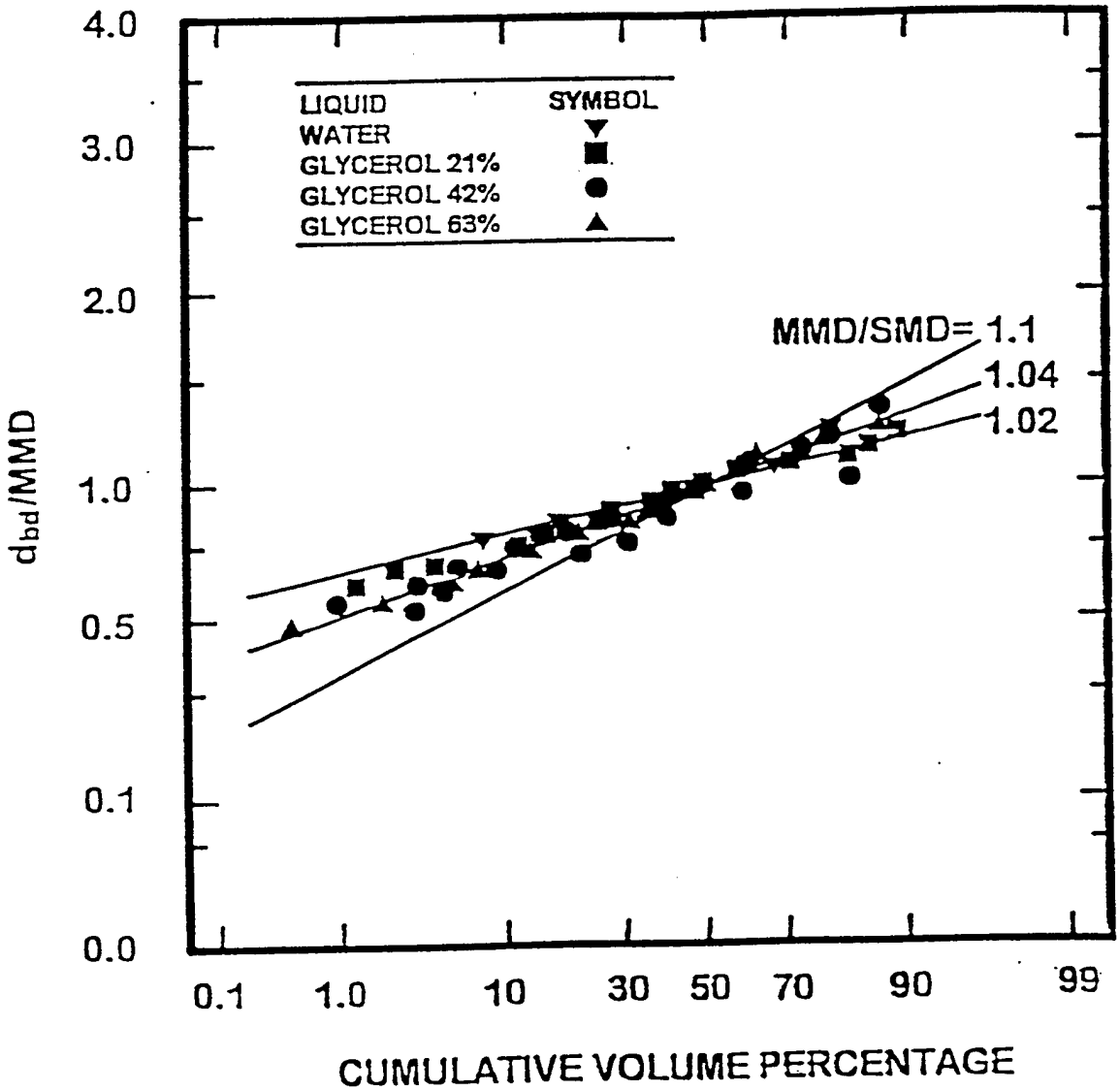
4.0
3.0
2.0
1.0
0.5
0.1
0.0
d_{bd}/MMD
LIQUID
SYMBOL
WATER
GLYCEROL 21%
GLYCEROL 42%
GLYCEROL 63%
MMD/SMD= 1.1
1.04
1.02
0.1
1.0
10
30
50
70
90
99
CUMULATIVE VOLUME PERCENTAGE

FIG. 5

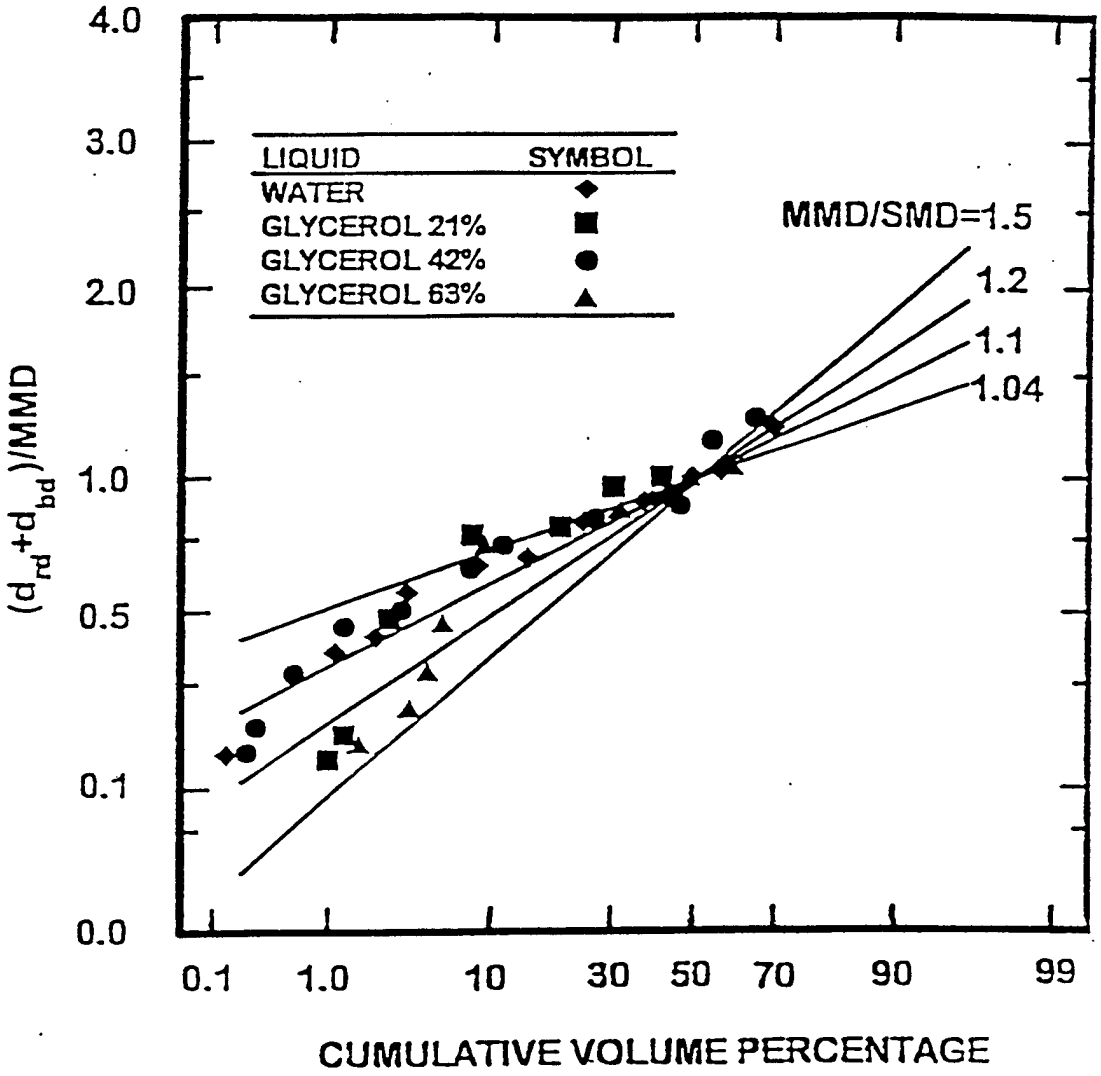
4.0
3.0
2.0
1.0
0.5
0.1
0.0
$(d_{rd}+d_{bd})/MMD$
LIQUID
SYMBOL
WATER
GLYCEROL 21%
GLYCEROL 42%
GLYCEROL 63%
MMD/SMD=1.5
1.2
1.1
1.04
0.1
1.0
10
30
50
70
90
99
CUMULATIVE VOLUME PERCENTAGE

FIG. 6

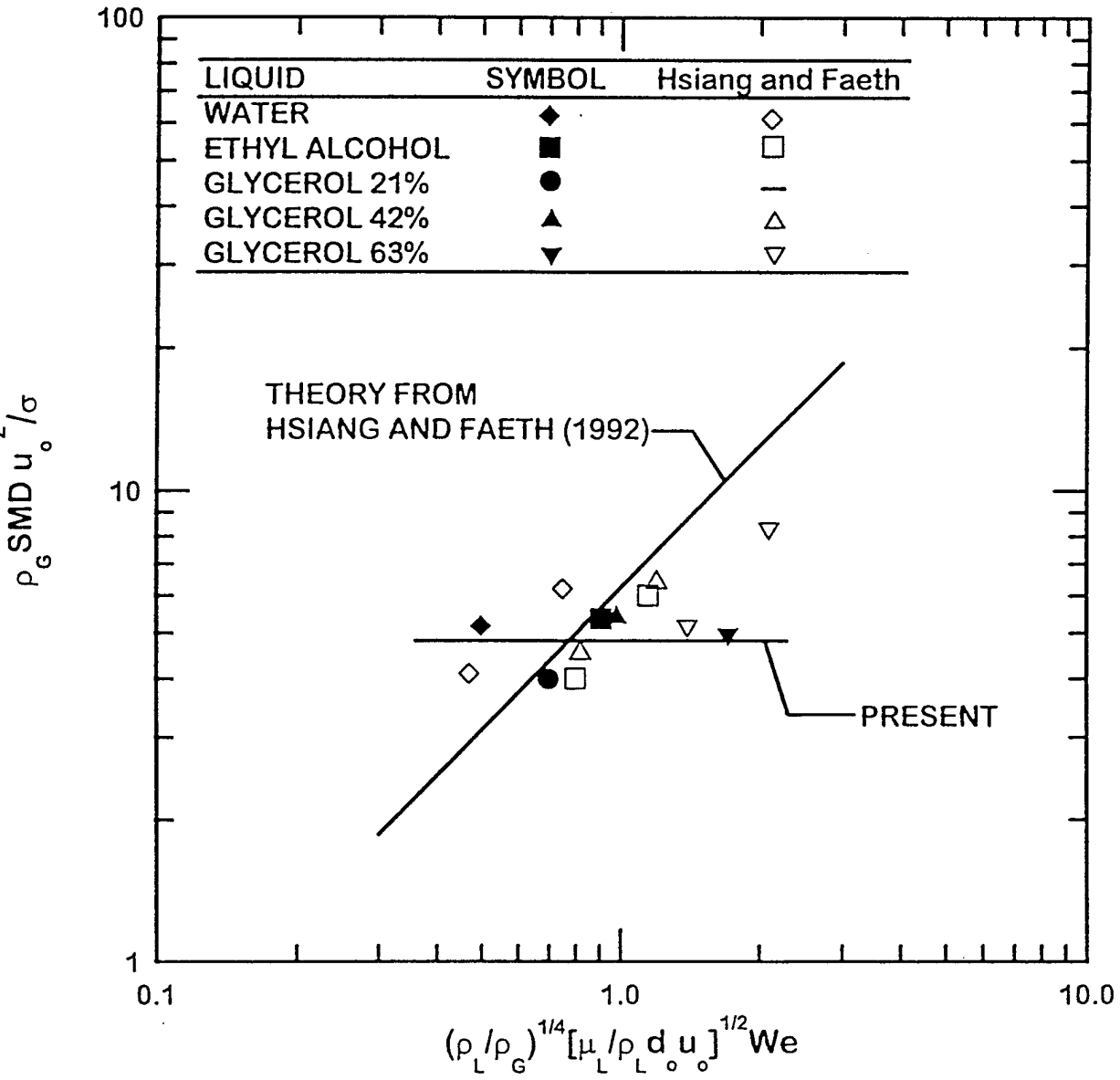
100
10
1
0.1
1.0
10.0
LIQUID
SYMBOL
Hsiang and Faeth
WATER
ETHYL ALCOHOL
GLYCEROL 21%
GLYCEROL 42%
GLYCEROL 63%
THEORY FROM
HSIANG AND FAETH (1992)
PRESENT
$\rho_G SMD\, u_o^2/\sigma$
$(\rho_L/\rho_G)^{1/4}[\mu_L/\rho_L d_o u_o]^{1/2}We$

Fig 7

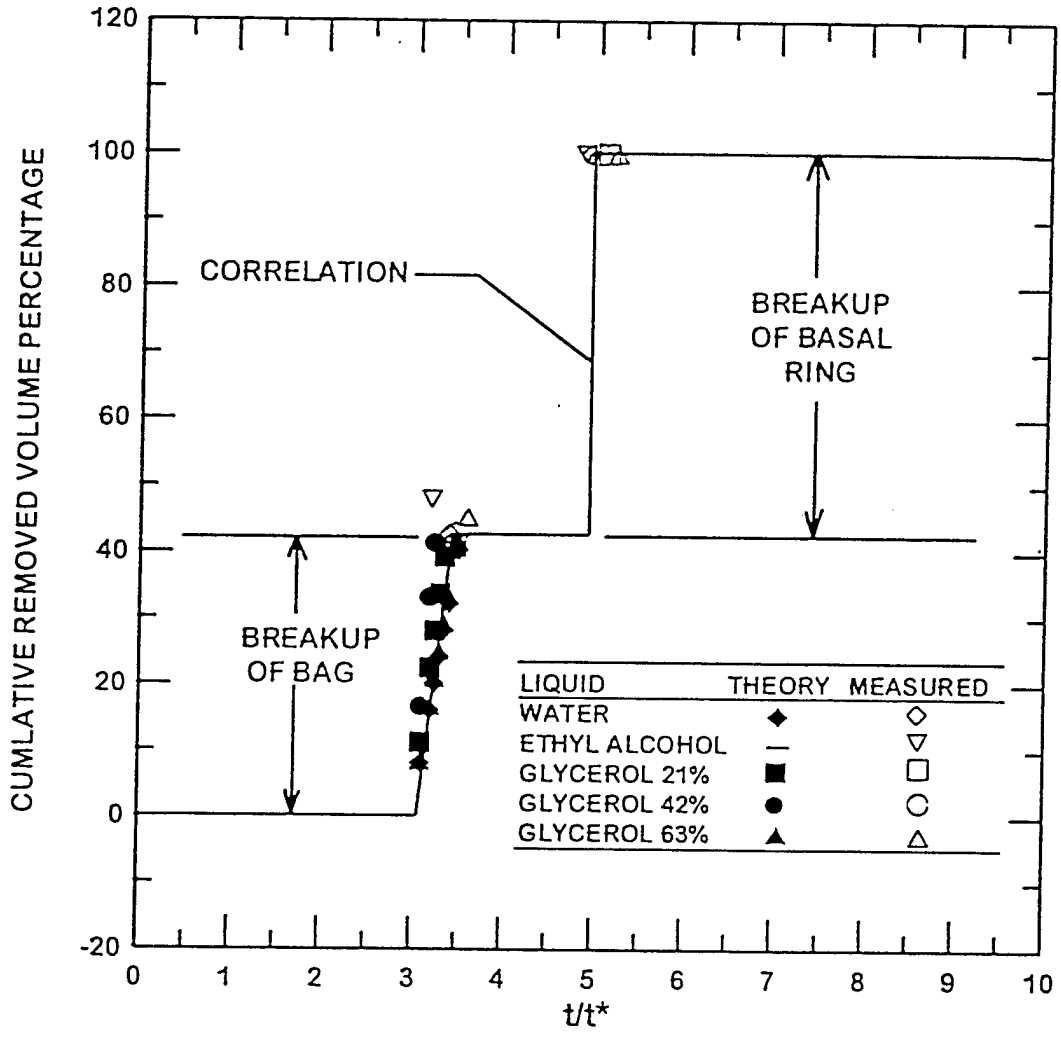
CUMLATIVE REMOVED VOLUME PERCENTAGE
120
100
80
60
40
20
0
-20
0
1
2
3
4
5
6
7
8
9
10
t/t*
CORRELATION
BREAKUP OF BASAL RING
BREAKUP OF BAG
LIQUID
THEORY
MEASURED
WATER
ETHYL ALCOHOL
GLYCEROL 21%
GLYCEROL 42%
GLYCEROL 63%

FIG. 8

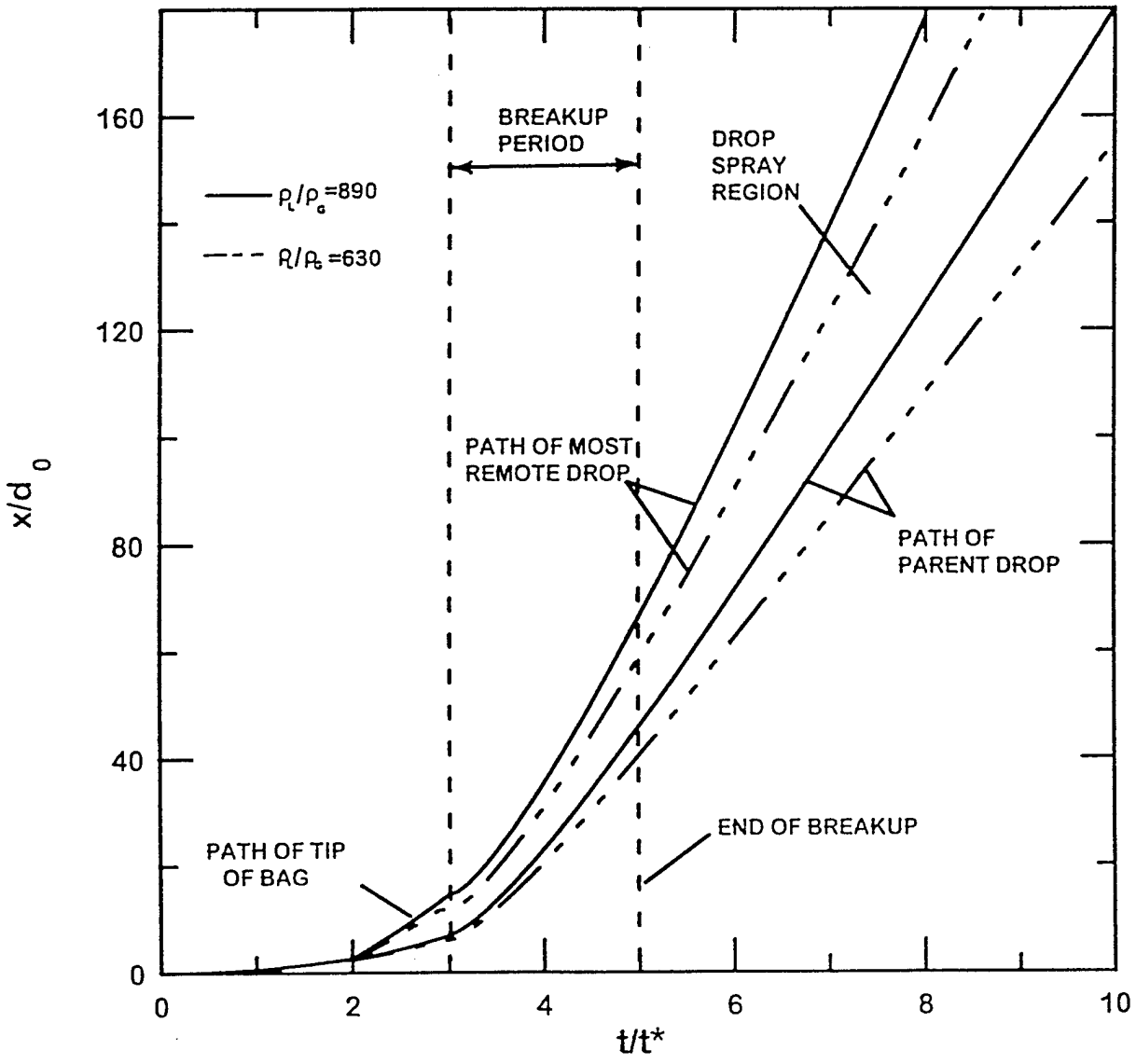
160
120
80
40
0
0
2
4
6
8
10
x/d 0
t/t*
BREAKUP PERIOD
DROP SPRAY REGION
ρL/ρg=890
ρL/ρg=630
PATH OF MOST REMOTE DROP
PATH OF PARENT DROP
PATH OF TIP OF BAG
END OF BREAKUP

FIG. 9

Appendix C: Chen, J.-H., Wu, J.-S. and Faeth, G.M. (1998) Turbulence Generation in Homogeneous Particle-Laden Flows. AIAA J., submitted.

Turbulence Generation in Homogeneous Particle-Laden Flows

J.-H. Chen*, J.-S. Wu† and G.M. Faeth‡
The University of Michigan, Ann Arbor, Michigan 48109-2140

The generation of turbulence by uniform fluxes of monodisperse spherical particles moving through a uniform flowing gas was studied experimentally. Phase velocities, moments, probability density functions and energy spectra were measured within a counterflowing particle/gas wind tunnel using phase-discriminating laser velocimetry. Test conditions included particle Reynolds numbers of 106-990, particle volume fractions less than 0.003% and direct rates of dissipation of turbulence by particles less than 2% with turbulence generation rates sufficient to yield relative turbulence intensities in the range 0.2-5.0%. Velocity records showed that the flow consisted of randomly-arriving wake disturbances within an inter-wake turbulence field and that the particle wake properties corresponded to recent observations of laminar-like turbulent wakes for spheres at intermediate Reynolds numbers in turbulent environments. Probability density functions of velocities were peaked for streamwise velocities due to contributions from mean streamwise velocities in particle wakes but were Gaussian for crosstream velocities which only involve turbulence contributions from the wakes. Relative intensities of streamwise and crosstream velocity fluctuations were roughly correlated in terms of a dimensionless rate of turbulence dissipation factor. Finally, energy spectra exhibited prominent -1 and -5/3 power decay regions associated with contributions from mean velocities in particle wakes, and particle and inter-wake turbulence, respectively.

---

*Graduate Student Rsearch Assistant, Department of Aerospace Engineering.
†Research Fellow; currently Assistant Professor, Department of Mechanical Engineering, National Chiao-Tung University, Taiwan.
‡A.B. Modine Professor, Department of Aerospace Engineering, 3000 François-Xavier Bagnoud Building, 1320 Beal Avenue, Fellow AIAA.

Nomenclature

C_D = sphere drag coefficient

D = dissipation factor, $\varepsilon d_p C_D^{1/3} / (2 U_p^3)$

d_p = sphere diameter

$E_u(k), E_v(k)$ = streamwise and crosstream energy spectra

f = frequency

k = wave number, $2\pi f / \bar{u}$

L_u = streamwise integral length scale

ℓ_K = Kolmogorov length scale

ℓ_p = mean particle spacing

$\dot{n}''$ = particle number flux

Re = particle Reynolds number, $d_p U_p / \nu$

t_K = Kolmogorov time scale

U_p = mean streamwise relative velocity of particle

u = streamwise gas velocity

u_K = Kolmogorov velocity scale

v = crosstream gas velocity

ε = rate of dissipation of turbulence kinetic energy

ν = kinematic viscosity

Superscripts

$(\bar{\ })$ = mean value

$(\bar{\ })'$ = r.m.s. fluctuating value

Introduction

A study of the modification of continuous-phase turbulence properties due to the presence and motion of a dispersed phase is described. Hinze[1] identifies several turbulence modification mechanisms that are observed in dispersed flows. Of these, the least understood turbulence modification mechanisms involve direct effects of dispersed phases on continuous-phase turbulence properties, as follows: the exchange of kinetic energy between the dispersed and continuous phases as the dispersed-phase motion accommodates to the continuous-phase motion, denoted turbulence modulation, which generally decreases turbulence fluctuations;[2-4] and the direct disturbance of the continuous-phase velocity field by particle wakes, denoted turbulence generation, which generally increases turbulence fluctuations.[3-7] Evaluating the relative magnitude of these two effects to determine whether turbulence modification will increase or decrease turbulence levels has been addressed by a number of investigations.[2,8-11] These studies generally show that turbulence generation (modulation) dominates effects of turbulence modification, tending to increase (reduce) turbulence levels, when dispersed-phase elements have large (small) relaxation times compared to characteristic turbulence time scales. As a result, turbulence generation tends to dominate turbulence modification in many practical dispersed flows having significant separated-flow effects, such as sprays, particle-laden jets, bubbly jets and rainstorms, among others. Thus, the present study addresses turbulence generation in view of its importance to practical applications.

Past studies of turbulence generation have considered dilute dispersed flows in both shear flow[3-5,11] and homogeneous flow[6,7,12] configurations; however, the latter offer a convenient experimental configuration because they avoid problems of separating effects of turbulence generation from mechanisms of continuous-phase turbulence production in shear flows. One of the first studies along these lines was Lance and Bataille [12] who considered homogeneous air/water bubbly flows downstream of a turbulence-generating grid. Effects of turbulence generation caused a progressive increase of continuous-phase

turbulence levels with increasing void fractions; unfortunately, these results still are difficult to interpret due to combined effects of bubble- and grid-generated turbulence.

Earlier studies treating homogeneous flows where turbulence generation was the only mechanism of turbulence production considered uniform number fluxes of nearly monodisperse beads falling at their terminal velocities in nearly stagnant (in the mean) water and air.[6,7] Measurements included phase velocities and turbulence properties for various particle number fluxes. Particle sizes were selected to yield intermediate Reynolds number conditions (Re of 100-800) that are typically encountered for practical dispersed turbulent flows. The flows were analyzed using a simplified stochastic method involving superposition of randomly-arriving particle velocity fields, by extending the method Rice[13] used to analyze noise. The stochastic approach provided some useful interpretations of flow properties, however, the analysis was problematical because information about particle wakes at intermediate Reynolds numbers, particularly in turbulent environments typical of homogenous dispersed flows, was limited. Thus, it was necessary to estimate wake properties by extrapolating available results at large Reynolds numbers in nonturbulent environments, which is questionable and caused convergence problems of the Rice[13] approach similar to those encountered during stochastic analysis of sedimentation.[14] Other questions about approximate analysis concerned the extent that particle wakes interacted with each other and the nature of the flow field between wakes (the inter-wake region) if water-wake interactions were small. These studies were also problematical because the nearly stagnant (in the mean) continuous phases caused significant experimental uncertainties due to the resulting very large turbulence intensities (up to 1000%) along with problems of buoyant disturbances.

Related work involved studies of sphere wakes at intermediate Reynolds numbers in both nonturbulent and turbulent environments in order to provide information needed to better understand turbulence generation.[14-16] Wakes in nonturbulent environments yielded

anticipated behavior for self-preserving turbulent and laminar wakes,[18,19] with transition between these flows at wake Reynolds numbers on the order of unity.[15] Findings more relevant to turbulence generation involved sphere wakes at intermediate Reynolds numbers in turbulent (roughly isotropic) environments which showed that these wakes scaled in the same manner as self-preserving laminar wakes but with significantly enhanced viscosities due to the presence of turbulence (termed "laminar-like turbulent wakes").[16,17] Naturally, the properties of laminar-like turbulent wakes differed considerably from the wake properties assumed in the earlier turbulence generation studies.[6,7] In addition, estimates of flow properties suggested that the probability of direct wake-to-wake interactions was small; instead, it was likely that wake disturbances were imbedded in relatively large inter-wake turbulent regions. A concern about this behavior, however, was whether laminar-like turbulent wakes were actually observed during turbulence generation processes because such turbulence fields have rather different properties from the conventional isotropic turbulence that was considered during the wake studies of Refs. 16 and 17.

In summary, review of past work has highlighted deficiencies of past studies of turbulence generation, even for the relatively simple and fundamental homogenous dispersed-flow configuration. In particular, were wake disturbances during turbulence generation equivalent to the laminar-like turbulent wakes observed in Refs. 16 and 17, does the flow involve wake disturbances imbedded in an inter-wake region or does it involve strongly interacting wakes, and can turbulence generation properties measured at large turbulence intensities be confirmed for moderate turbulence intensities where experimental uncertainties are much reduced? These issues were addressed during the present investigation which had the following specific objectives: (1) to complete new measurements of stationary homogenous dispersed flows involving nearly monodisperse spherical solid (glass) particles at intermediate Reynolds numbers in air, using a counterflow particle/air wind tunnel, (2) to use the measurements to determine the nature of wake disturbances and wake-to-wake interactions during turbulence generation, and (3)

to use the measurements to highlight differences between turbulence fields associated with turbulence generation and more conventional turbulence.

In the following, experimental methods are described first. Results are then considered, treating apparatus evaluation, particle wake properties and continuous-phase properties (probability density functions, velocity fluctuations and energy spectra), in turn. The article ends with a summary of the major conclusions of the study.

Experimental Methods

Apparatus

The apparatus consisted of a vertical counterflow wind tunnel with upflowing air moving toward the suction side of a blower and freely-falling particles introduced at the top of the apparatus using a particle feeder, see the sketch of the arrangement in Fig. 1. The air flow system consisted of a rounded inlet, a honeycomb flow straightener (10 mm hexagonal cells 76 mm long) and a 16:1 contraction ratio to the 305 × 305 mm crossection windowed test section. The particle dispersion section was located just above the test section. The upper part of the particle dispersion section involved 9 equally spaced screens (square pattern with 0.9 mm diameter wires spaced 4.2 mm apart) to disperse the particles and achieve a uniform particle flux. This was followed by a honeycomb flow straightener (10 mm hexagonal cells 76 mm long) to remove lateral particle motion caused by the screens. The particle inlet section and the transition section to the blower were at the upper end of the wind tunnel. The wind tunnel air flow was provided by a single inlet variable spaced blower having a SCR speed controller.

The particle flow was provided by a variable-speed screw feeder (Accurate, Model 310/04). After passing through the wind tunnel, the particles impacted on a plastic sheet within a particle collector. Microscope inspection showed that the particles were not damaged by passing through the wind tunnel; therefore, they were reused.

Instrumentation

Measurements included particle number fluxes and gas and particle velocities. Particle number fluxes were measured by collecting particles in a thin-walled cylindrical container having a 25 mm diameter that was closed at the bottom. The container was mounted on a rod so that it could be traversed across the test section. The accuracy of these measurements was dominated by finite sampling times which were selected to keep experimental uncertainties (95% confidence) less than 10%.

Gas and particle velocities were measured using a traversible (5 μm accuracy) laser velocimetry (LV) system. The LV was based on the 514.5 nm line of an argon-ion laser having an optical power of 1900 mW. A single-channel dual-beam, forward-scatter, frequency-shifted LV arrangement was used, finding streamwise and crosstream velocities by rotating the optics accordingly. For gas velocities, the sending optics included a 3.75:1 beam expander to yield a measuring volume diameter and length of 55 and 425 μm, respectively. Due to the small measuring volume the frequency of test particles passing through the measuring volume was small; the few that were observed were readily detected and eliminated from the sample due to their large signal amplitudes and relatively fixed velocities. The air flow entering the wind tunnel was seeded with oil drops having a 1 μm nominal diameter. Velocities were found from the low-pass filtered analog output of a burst-counter signal processor. The combination of frequency shifting plus a constant sampling rate of the analog output of the signal processor eliminated effects of directional bias and ambiguity as well as velocity bias. Sampling periods were adjusted to provide the following experimental uncertainties (95% confidence): mean velocities less than 2%, rms velocity fluctuations less than 10%, probability density functions (PDF's) within one standard deviation of the most probable velocity less than 10% and temporal power spectral

densities less than 20% (at frequencies smaller than the reciprocal of the temporal integral scale with uncertainties smaller elsewhere).

Particle velocity measurements were made with the same LV arrangement as the gas velocities except that the optics were changed to provide a larger measuring volume having a diameter of 1.5 mm and a length of 10 mm. This provided a reasonable sampling rate of particle velocities. Optics were rotated to measure streamwise and crosstream velocities. The gas was not seeded for the particle velocity measurements and the large amplitude signals from particles were easily separated from background signals due to dust in the air. Sampling periods were adjusted to provide experimental uncertainties less than 5% for streamwise mean velocities and less than 10% for rms streamwise and crosstream velocity fluctuations. Mean cross stream velocities were nearly zero and only were an order of magnitude accurate due to their small magnitudes.

Test Conditions

Test conditions are summarized in Table 1. The particles were nearly monodisperse with Reynolds numbers were in the range 106-990, which is representative of the intermediate Reynolds number conditions of drops in sprays.[15] Terminal velocities and drag coefficients were measured, yielding values that agreed with the standard drag curve for spheres due to Putnam[20] within 15%. Test conditions were adjusted so that turbulence intensities relative to the mean gas velocity were less than 15% so that LV measuring conditions were excellent. The particles approached but did not reach terminal velocity conditions during the present turbulence generation measurements while mean crosstream particle velocities were small. Particle velocity fluctuations were small due to their poor response to air motion and were mainly caused by variations of particle sizes.

Assuming that the particles are falling randomly, the mean particle spacing can be found from

$$\ell_p = ((U_p - \bar{u})/\dot{n}'')^{1/3} \quad (1)$$

which yields values of 13-208 mm, and particle volume fractions less than 0.003%, for the present experiments. The direct dissipation of turbulence kinetic energy (dissipation) by particles is less than 2% for present test conditions. Thus, dissipation can be equated to the rate of turbulence generation by particles, which in turn is equal to the rate of transfer of mechanical energy to the gas as the particles move through the flow, i.e.,

$$\varepsilon = \pi \dot{n}'' d_p^2 C_D U_p^2/8 \quad (2)$$

Given ε, the Kolmogorov scales can be computed from their definitions,[19] yielding the ranges summarized in the table. Relative turbulence intensities due to turbulence generation were in the range 0.2-5.0%.

Results and Discussion

Apparatus Evaluation

The apparatus was evaluated to determine whether the dispersed-and continuous-phase flows where properly stationary and homogeneous, and that velocity fluctuations were due to effects of turbulence generation rather than disturbances of the wind tunnel flow. The temporal and spatial uniformity of the particle flows were evaluated by traversing the sampling probe along the two perpendicular axes of symmetry at the lowest crossection where measurements were made. These measurements were carried out for all three particle sizes considered, spanning the ranges of particle fluxes for each size. Samples obtained from multiples of the shortest sampling period showed that the particle fluxes were statistically stationary. Finally, the sampling measurements showed that mean particle fluxes varied less than 10% over the central 205 × 205 mm crossection of the flow where velocity measurements were made. Mean and fluctuating particle velocities were also uniform within experimental uncertainties over the same region. Thus, particle properties were properly stationary and homogenous for present test conditions.

The properties of the continuous (gas) phase were established by measurements of mean and fluctuating streamwise velocities over the central 205 × 205 mm crossection of the flow, considering streamwise distances up to ± 100 mm from the normal crossection where measurements were made. The results of these measurements did not vary significantly with upflow velocities in the range 500-1300 mm/s. For these conditions, gas flow properties were statistically stationary and homogeneous within experimental uncertainties.

Measurements of streamwise velocities for various particle sizes, particle fluxes and upflow velocities were also used to establish minimum allowable particle fluxes. In particular, very low particle fluxes for a given upflow velocity yielded rather large relative turbulence intensities due to thermal disturbances associated with the large vertical height of the apparatus. Increasing the particle flux, however, disrupted the thermal disturbances and caused relative turbulence intensities to decrease for a time as particle fluxes increased before increasing once again in a manner similar to the behavior of turbulence generation seen in Refs. 6 and 7. Thus, present measurements were only undertaken for particle fluxes somewhat larger than the minimum relative turbulence intensity condition. Relative turbulence intensities at low particle fluxes were also affected by the upflow velocity. An upflow velocity of 1.1 m/s was finally selected in order to maximize the range of particle fluxes that could be considered while avoiding the excessive particle concentrations in the flow that are observed when upflow velocities approach the terminal velocity of the particles, see Eq. (1).

Particle Wake Properties

Given satisfactory evaluation of the apparatus, the experiments turned to observation of flow velocities for various particle sizes and fluxes. The objectives of these measurements were to identify the direct contributions of particle wakes to gas-phase flow

properties, and to assess whether velocity distributions within these wakes were similar to the past observations of laminar-like turbulent wakes within isotropic turbulence observed in Refs. 16 and 17.

Typical temporal records of present streamwise and crosstream gas velocities are illustrated in Fig. 2. When interpreting this data, it should be recalled that streamwise and crosstream gas velocities were observed at different times and there is no correlation between the two records. Results are shown for 0.5 mm particles at low and high particle loadings, characterized by both the dimensionless dissipation factor of Refs. 6 and 7 and the particle flux. The most obvious features of the velocity signals are that the streamwise velocities exhibit large negative spikes, with spike frequencies increasing with increasing with particle loading, whereas crosstream velocities exhibit no spikes and are similar to streamwise velocities in the time interval between spikes. This behavior is consistent with the spikes being velocity disturbances of particle wakes at this particle Reynolds number. Naturally, increasing numbers of spikes with increasing particle fluxes is an obvious property that should be satisfied by particle wake disturbances. In addition, the maximum velocity disturbances of the spikes were comparable to relative particle velocities within experimental uncertainties. The presence of spikes in only the streamwise velocity record is also consistent with known particle wake properties at these conditions. In particular, mean crosstream velocities are always small compared with both mean streamwise velocities and rms velocity fluctuations of laminar-like turbulent wakes also are small at Re = 106, see Refs. 16 and 17. Thus, velocity disturbances due to particle wakes should limited to the streamwise direction, for the conditions of Fig. 2, if these disturbances behave similar to laminar-like turbulent wakes.

Additional temporal records of present streamwise and crosstream gas velocities are illustrated in Fig. 3, considering mid-range particle loadings for all three particle sizes. Similar to the results of Fig. 2, relatively large negative spikes associated with wake

velocity disturbances are observed on the streamwise velocity records while corresponding spikes are not observed on the crosstream velocity for the 0.5 mm particles which have Re = 106. On the other hand, an interesting property of the crosstream velocity records is that spikes having both positive and negative velocity disturbances are observed on the crosstream velocity records for the 1.1 and 2.2 mm particles that have Re = 373 and 990, respectively. This behavior, however, is exactly what should be observed based on observations of the behavior of laminar-like turbulent wakes in Refs. 16 and 17. In particular, while crosstream turbulent velocity fluctuations are absent at small Reynolds numbers, eddy shedding occurs for Re > 300 and this is accompanied by crosstream turbulent velocity fluctuations. This behavior accounts for the observations seen in Fig. 3 and strongly suggests that the wake properties observed during the present turbulence generation experiments are similar to the past observations of laminar-like turbulent wakes of Refs. 16 and 17.

A final assessment of the similarities between the wake disturbances observed during the present turbulence generation studies and the laminar-like turbulent wakes observed in Refs. 16 and 17 involved direct comparison of mean streamwise velocities. This comparison was carried out for all three particle sizes at relatively large particle loadings so that representative samples of particle wakes could be observed in reasonable test times. Measurements were made for various maximum velocity defects, which represent results for paths of the LV measuring volume at various radial distances from the wake axis. Effects of turbulence were handled by averaging several velocity records to obtain an estimate of mean streamwise wake velocities (the averaging criterion was an experimental uncertainties (95% confidence) of the maximum mean velocity defect less than 10%). Predictions assuming vertical wake axes (which is reasonable based on the particle velocity measurements), and having the same maximum mean velocity defects, were obtained from the correlations for the mean properties of laminar-like turbulent wakes of Refs. 16 and 17 (at the same particle Reynolds number and relative turbulence intensity).

The resulting measured and predicted mean streamwise velocities in the particle wakes are illustrated in Fig. 4. These results involve plots of normalized streamwise velocities as a function of time for various particle diameters and maximum velocity defects. Results for 0.5 mm particles are relatively comprehensive and involve dimensionless velocity defects in the range 0.20-0.80 because sampling rates were relatively large for these small particles. Results for particle diameters of 1.1 and 2.2 mm are limited to a single velocity defect (representative of the outer edge of the wakes) in order to obtain reasonable sampling rates for these small particle flux conditions. It is evident that the agreement between measurements and predictions is excellent in Fig. 4, which supports the use of the laminar-like turbulent wake properties of Refs. 16 and 17 to help interpret present observations of turbulence generation.

Based on the previous findings, it seems reasonable to assume that the present wake disturbances are similar to the laminar-like turbulent wakes described in Refs. 16 and 17. This information was then used to estimate of proportions of the wake and inter-wake regions as well as the extent of direct wake/wake interactions. This was done by carrying out stochastic simulations to find realizations of particle positions in space for various particle fluxes and the three particle sizes. This was done by random selections in three dimensions while accounting for the slight compression particle spacing in the vertical direction due to gas upflow as discussed in connection with Eq. (1). Appropriate laminar-like turbulent wakes were then associated with each particle, assuming that wake radii were equal to twice the characteristic wake width at each streamwise distance behind the particle and that the wake extended in the streamwise direction until the maximum mean velocity defect was equal to the ambient rms streamwise velocity fluctuations. These results indicated that wake crossectional areas generally were less than 30% of the available crossectional area, and that less than 25% of the wakes experienced wake/wake interactions at any one time (with these interactions mainly confined to conditions far from both

particles) over the present test range. Thus, the present flows involve laminar-like turbulent wakes surrounded by a relatively large inter-wake turbulence region, with occasional wake/wake interactions. This view agrees with the velocity traces of Figs. 2 and 3, if it recognized that only a relatively small portion of each wake can generate the large velocity spikes seen on these plots. Further evidence of combined effects of the wake and inter-wake regions on overall flow properties will be sought from consideration of probability density functions and spectra in the following.

Probability Density Functions

More insight about the effect of particle wake disturbances on the total turbulence properties of homogeneous dispersed flows dominated by turbulence generation can be obtained from the PDF's of velocity fluctuations. Typical results along these lines are presented in Figs. 5 and 6 for 2.2 and 0.5 mm particles, respectively, which bound results for 1.1 mm particles. On each of these plots, PDF's are shown for streamwise and crosstream velocities at the low and high particle loadings specified by dissipation factor values. Fits of the measurements are also shown on the plots, corresponding to least-squares sectional fits for the PDF(u) and best Gaussian fits for the PDF(v).

The present PDF's plotted in Figs. 5 and 6 do not agree with earlier observations of Refs. 6 and 7 for dispersed flows in stagnant baths, which yielded Gaussian PDF's for both velocity components, with at most a slight upward bias (roughly 10% when averaged over all test conditions) of the PDF(u) near its most probable value. This behavior agrees with present behavior of PDF(v), which is nicely fitted by Gaussian PDF's for both loadings of all particle sizes. In contrast, the present PDF(u) are more peaked and somewhat skewed toward negative velocities compared to the mean velocity, i.e., the PDF(u) exhibit greater kurtosis and skewness than the nearly Gaussian PDF(v).[19] In addition, the PDF(u) for each particle size tends to be independent of particle loading, similar to PDF(v), but the PDF(u) becomes progressively more peaked (or has

progressively increasing kurtosis) as the particle size (or Re) decreases. All these characteristics can be explained from the properties of the streamwise and crosstream velocity records (and the spike disturbances due to particle wakes seen in the velocity records) of Figs. 2-4, as discussed next.

The main reason for the different PDF(u) of Refs. 6 and 7 and the present study follows from the much improved laser velocimetry conditions of the present study which allowed the near wake region of the spike disturbances due to particle wakes seen in Fig. 4 to be resolved for the streamwise velocity records. This point was easily demonstrated during the present experiments by reducing seeding levels so that the spikes seen in Figs. 2 and 3 were rarely resolved; the corresponding PDF(u) then became more Gaussian similar to the results of Refs. 6 and 7. The other properties of PDF(u) in Figs. 5 and 6 then follow from the well known effects of the properties of the velocity signal on the values of the skewness and kurtosis of the PDF(u). In particular, the spikes always contribute a streamwise negative velocity signal based on the results illustrated in Figs. 2 and 3; this implies a corresponding positive bias of the PDF(u), or negative skewness, based on the well known properties of PDF's.[19] The more rapid reduction of streamwise velocities in the radial direction for small d_p (or Re) conditions (yielding narrower wake disturbances) implies a more peaked PDF(u), or a larger kurtosis of the PDF(u), for similar reasons.[19] In addition, the small effect of particle flux on the PDF(u) and the PDF(v) is consistent with the generally observed behavior of these functions, where the *shape* of the velocity signal as a function of time affects the skewness and kurtosis of the PDF but not the characteristic frequency of the signal,[19] e.g., homogeneous, isotropic dispersed flows have Gaussian PDF's irrespective of their characteristic time or frequency scales. Finally, either the absence of discernible spikes for the crosstream velocity records for the 0.5 mm particles, or the presence of both positive and negative spikes due to wake turbulence for the crosstream velocity records for the 2.2 mm particles, are entirely consistent with the Gaussian behavior of the PDF(v) seen in Figs. 5 and 6. Taken together, the combined

findings of Figs. 2-6 suggest that both particle wake disturbances and the inter-wake region provide significant contributions to the overall apparent turbulence properties of the present turbulence generated flows.

Velocity Fluctuations

The measurements of velocity fluctuations in Refs. 6 and 7 were correlated based on an approximate stochastic approach assuming that velocity fluctuations were entirely due to wake disturbances. This approach yielded reasonably effective correlations of relative turbulence intensities of streamwise and crosstream velocity fluctuations in terms of a dissipation factor, D, resulting from the approximate stochastic theory. Recent results, however, suggest more complex behavior, involving conditional averages over wake and inter-wake regions having rather different properties. Nevertheless, the correlation of Refs. 6 and 7 will be considered in the following due to its past success.

Measurements of streamwise and crosstream relative turbulence intensities are plotted as a function of the dissipation factor in Fig. 7. Measurements shown on the figure include results for particles in still (in the mean) water due to Parthasarathy and Faeth,[6] results for particles in still (in the mean) air due to Mizukami et al.,[7] and the present results for particles in counterflowing air. All three experiments used the same 0.5, 1.1 and 2.2 mm spherical glass particles. Correlations in terms of $D^{1/2}$, as suggested by the stochastic theory of Ref. 6, are fitted to the combined data sets for each velocity component. The correlations are seen to provide only fair agreement with the measurements. This is particularly true for the measurements of Mizukami et al.,[7] which exhibit significant scatter when plotted in the manner of Fig. 7. The results suggest some relationship between the properties of the wakes and the inter-wake region but clearly a correlation solely in terms of D cannot capture features such as the onset of crosstream wake disturbances for Re > 300 seen in Fig. 3. Thus, the correlations illustrated in Fig. 7 are only tentative pending more information about flow properties in the inter-wake region, and the use of these results in a

more rational conditional averaging procedure to summarize the properties of flows caused by turbulence generation.

Energy Spectra

Taylor's hypothesis was used to convert measured temporal power spectra and temporal integral scales into energy spectra and spatial integral scales. The resulting streamwise and crosstream energy spectra are plotted as functions of normalized wave numbers in Figs. 8 and 9, respectively. Results are shown for various particle sizes and fluxes, with the latter represented by values of the dissipation factor. The LV conditions for these measurements were good so that effects of step noise were deferred until Kolmogorov wave numbers were approached (this condition is roughly shown by the large wave number terminations of the crosstream energy spectra in Fig. 9). The values of L_u for the measurements were found by setting $E_u(k)\,\bar{u}/(\bar{u}^{-2}L_u) = 4$ as kL_u becomes small, as discussed by Hinze.[21] Correlations of energy spectra for isotropic turbulence are also shown on the plots, for comparison with the present measurements. These spectra represent a simplification of isotropic turbulence discussed by Hinze.[21], where the -5/3 power decay in the inertial range is approximated by a -2 power decay.

The energy spectra provide reasonably good correlations of present measurements as plotted in Figs. 8 and 9. The upper end of the normalized crosstream energy spectra illustrated in Fig. 9 is more scattered than the rest. This behavior is caused by the fact that $E_v(k)$ reaches a maximum at a finite values of kL_u rather than reaching a maximum as kL_u becomes small similar to $E_u(k)$. This behavior tends to broaden the data band of $E_v(k)$ for various test conditions in the region where this function reaches maximum.

An interesting feature of the spectra of Figs. 8 and 9 is that they decay over a rather large range of kL_u (roughly four decades) even though present particle Reynolds numbers are not large (less than 1000). Much of this behavior is typical of other homogeneous turbulence fields where disturbances due to grids (with relatively small grid element

Reynolds numbers) yield turbulent flows having extensive inertial ranges.[4,19,21] Another feature of the present flows enhances this behavior, however, as pointed out in earlier work.[6,7] In particular, the spectra of Figs. 8 and 9 include contributions from both particle wake disturbances and the inter-wake region. Then since the wake arrivals are random, mean velocities in the wakes contribute to the spectra increasing the range of scales that are present. Naturally, similar contributions are not present for grid-generated turbulence because measurements of these flows are made well downstream of the region of significant direct wake disturbances from the turbulence-generating grid.

The energy spectra of Figs. 8 and 9 also provide other evidence of direct contribution of mean velocities in wake disturbances. In particular, the spectra exhibit prominent -1 and -5/3 decay regions as kL_u increases. The -1 power decay region is not seen in conventional turbulent flows but based on the approximate stochastic analysis of Ref. 6 such behavior is typical of the contribution of mean velocities in wake disturbances to temporal power spectra (and thus energy spectra under present approximations). Other evidence for this explanation is that the -1 decay region is associated with values of kL_u on the order of unity which is characteristic of wake dimensions. Larger wave numbers exhibit -5/3 power decay regions which are representative of conventional turbulence and probably involves contributions from both the wake disturbances and the inter-wake region as discussed earlier in connection with Figs. 2 and 3. For example, crosstream spectra for 0.5 mm particles do not exhibit significant wake contributions to turbulence so that the large wave number portion of the spectra must be caused by the inter-wake region. The crosstream spectra for 0.5 mm particles generally decay more rapidly than the rest at large wake numbers in Fig. 9, however, which can be explained by the loss of the direct contribution from wake turbulence to the overall behavior of the flow.

Conclusions

This investigation considered the properties of homogeneous turbulence generated by uniform fluxes of monodisperse spherical particles moving through air at standard temperature and pressure. The experimental configuration involved particles falling in counterflowing air to supplement earlier measurements for particles falling in stagnant water, Ref. 6, and stagnant air, Ref. 7. Present test conditions included: particle Reynolds numbers of 106-990, particle volume fractions less than 0.003% and direct rates of dissipation of turbulence by particles less than 2%, with particle fluxes sufficient to yield relative turbulence intensities of 0.2-5%. The major conclusions of the study are as follows.

1. Measurements of gas velocities indicate that the particle wake properties of the present turbulence generation processes correspond to the laminar-like turbulent wakes observed in Refs. 16 and 17 for spheres similar to intermediate Reynolds numbers in isotropic turbulence.

2. Estimates of the character of the present flows based on the properties of laminar-like turbulent wakes suggest that wake disturbances (generally involving crossectional areas less than 30% of the total available crossectional area) are embedded in a relatively large inter-wake turbulent region with relatively few (less than 25%) direct wake/wake interactions, with the latter confined to regions far from both particles.

3. Present measurements of relative turbulence intensities were in fair agreement with earlier measurements of turbulence generation in still liquids and gases from Refs. 6 and 7, and all these measurements could be correlated in terms of the dissipation factor. These correlations are only considered tentative, however, pending development of a more rational approach that properly accounts for the relative contributions of wake disturbances and inter-wake turbulent regions that fundamentally have very different flow properties.

4. Other properties measured during the present study, probability density functions and spectra, were not in good agreement with the earlier observations of Refs. 6 and 7. In particular, present observations provided direct evidence of effects of both wake disturbances and inter-wake regions (as nonGaussian PDF's and prominent -1 and -5/3 decay regions of energy spectra) that were either absent or less evident during the earlier studies. These differences were shown to result from the improved LV measuring conditions of the present study.

5. Contributions from both the wake disturbance and inter-wake turbulent regions also were responsible for the surprisingly large range of scales seen in the present flows in spite of relatively small particle Reynolds numbers. In particular, mean velocities in particle wake disturbances contribute to present apparent turbulence properties because wake arrivals are random and this contribution is generally not present in turbulence generated in other ways, e.g., by grids or shear flows.

Acknowledgments

This investigation was supported by the Air Force Office of Scientific Research, Grant Nos. F49620-92-J-0399 and F49620-95-I-0364, under the technical management of J.M. Tishkoff. The U.S. Government is authorized to reproduce and distribute copies of the paper for governmental purposes notwithstanding any copyright notation therein.

References

[1]Hinze, J.O., "Turbulence Fluid and Particle Interaction," Prog. Heat Mass Transfer, Vol. 6, 1972, pp. 433-452.

[2]Hetsroni, G., "Particle-Turbulence Interaction," Int. J. Multiphase Flow , Vol. 15, No. 5, 1989, pp. 735-746.

[3]Squires, K.D., and Eaton, J.K., "Particle Response and Turbulence Modification in Isotropic Turbulence," Phys. Fluids A, Vol. 2, No. 6,1990, pp. 1191-1203.

[4]Rogers, C.B., and Eaton, J.K, "The Effect of Small Particles on Fluid Turbulence in a Flat-Plate Turbulent Boundary Layer in Air," Physics Fluids A, Vol. 3, No. 5, 1991, pp. 928-937.

[5]Parthasarathy, R.N., and Faeth, G.M., "Structure of Particle-Laden Turbulent Water Jets in Still Water," Int. J. Multiphase Flow, Vol. 13, No. 5, 1987, pp. 699-716.

[6]Parthasarathy, R.N., and Faeth, G.M. "Turbulence Modulation in Homogeneous Dilute Particle-Laden Flows, " J. Fluid Mech., Vol. 220, Pt.2, 1990, pp. 485-514.

[7]Mizukami, M., Parthasarathy, R.N., and Faeth, G.M., "Particle-Generated Turbulence in Homogeneous Dilute Dispersed Flows," Int. J. Multiphase Flow, Vol. 18, No. 2, 1989, pp. 397-412.

[8]Gore, R.A., and Crowe, C.T., "Effect of Particle Size on Modulating Turbulent Intensity," Int. J. Multiphase Flow, Vol. 15, No. 2, 1989, pp. 279-285.

[9]Kenning, V.M., and Crowe, C.T., "On the Effect of Particles on Carrier Phase Turbulence in Gas-Particle Flows," Int. J. Multiphase Flow, Vol. 23, No. 2, 1997, pp. 403-408.

[10]Yuan, Z., and Michaelides, E., "Turbulence Modulation in Particulate Flows — A Theoretical Approach," Int. J. Multiphase Flow, Vol.18, No. 5, 1992, pp. 779-785.

[11]Rashidi, M., Hetsroni, G., and Banerjee, S., "Particle-Turbulence Interaction in a Boundary Layer," Int. J. Multiphase Flow, Vol. 16, No. 6, 1990, pp. 935-949.

[12]Lance, M., and Bataille, J., "Turbulence in the Liquid Phase of a Uniform Bubbly Air-Water Flow," J. Fluid Mech., Vol. 222, Pt. 1, 1991, pp. 95-119.

[13]Rice, S. O., "Mathematical Analysis of Random Noise," *Noise and Stochastic Processes* (N. Wax, ed.), Dover Publications, New York, 1954, pp. 133-294.

[14]Batchelor, G.K., "Sedimentation in a Dilute Dispersion of Spheres," J. Fluid Mech., Vol. 52, 1971, pp. 245-268.

[15]Wu, J.-S., and Faeth, G.M., "Sphere Wakes in Still Surroundings at Intermediate Reynolds Numbers," AIAA J., Vol. 31, No. 8, 1993, pp. 1448-1455.

[16]Wu, J.-S., and Faeth, G.M., "Sphere Wakes at Moderate Reynolds Numbers in a Turbulent Environment," AIAA J., Vol. 32, No. 3, 1994, pp. 535-541.

[17]Wu, J.-S., and Faeth, G.M., "Effects of Ambient Turbulence Intensity on Sphere Wakes at Intermediate Reynolds Numbers," AIAA J., Vol. 33, No. 1, 1995, pp. 171-173.

[18]Schlichting, H., *Boundary Layer Theory*, 7th ed., McGraw-Hill, New York, 1979, pp. 234-235 and 599.

[19]Tennekes, H., and Lumley, J.L., *A First Course in Turbulence*, MIT Press, Cambridge, Massachusetts, 1972, pp. 113-124 and 196-201.

[20]Putnam, A., "Integrable Form of Droplet Drag Coefficient," ARS Journal, Vol. 31, 1961, pp. 1467-1468.

[21]Hinze, J.O., *Turbulence*, 2nd Ed., McGraw-Hill, New York, 1975, Chapt. 3, and p. 204.

Table 1. Summary of test conditions[a]

Nominal Particle Diameter (mm)	0.5	1.1	2.2
U_p (mm/s)[b]	3370 (280)	5530 (340)	7000 (200)
Re (-)[b]	106 (9)	373 (23)	990 (28)
C_D(-)	1.22	0.79	0.54
$\dot{n}''$(kpart/m^{2}s)	71-950	4-56	0.5-10
ℓ_p (mm)	32-13	97-41	208-77
ε (m^2/s^3)	0.081-1.083	0.032-0.42	0.014-0.29
ℓ_K (mm)	0.5-0.2	0.6-0.3	0.7-0.4
t_K (ms)	14-4	22-6	33-8
u_K (mm/s)	34-66	28-54	21-44
$\overline{u}'/U_p$ (%)	0.5-5.0	0.2-0.9	0.2-0.8
$\overline{v}'/U_p$ (%)	0.5-1.3	0.2-1.2	0.2-0.9

[a]Round glass beads (density of 2500 kg/m^3) falling in upflowing air at standard temperature and pressure (air density of 1.16 kg/m^3 and kinematic viscosity of 15.9 mm/s) having a mean velocity of 1.1 m/s.
[b]Standard deviations given in parentheses.

List of Figures

FIG. 1

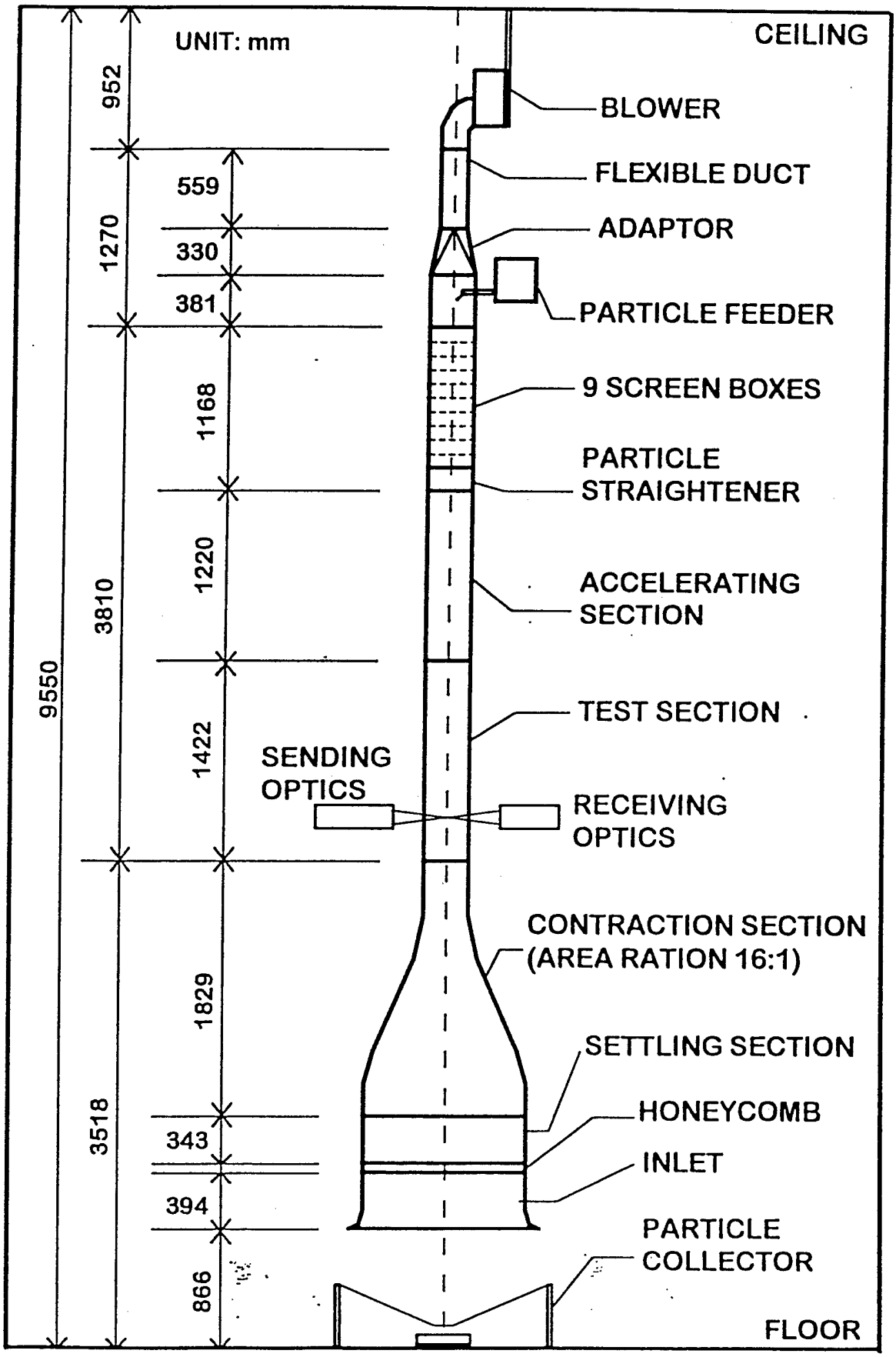
UNIT: mm
CEILING
952
559
1270
330
381
1168
3810
1220
9550
1422
1829
3518
343
394
866
BLOWER
FLEXIBLE DUCT
ADAPTOR
PARTICLE FEEDER
9 SCREEN BOXES
PARTICLE STRAIGHTENER
ACCELERATING SECTION
TEST SECTION
SENDING OPTICS
RECEIVING OPTICS
CONTRACTION SECTION (AREA RATION 16:1)
SETTLING SECTION
HONEYCOMB
INLET
PARTICLE COLLECTOR
FLOOR

FIG. 2

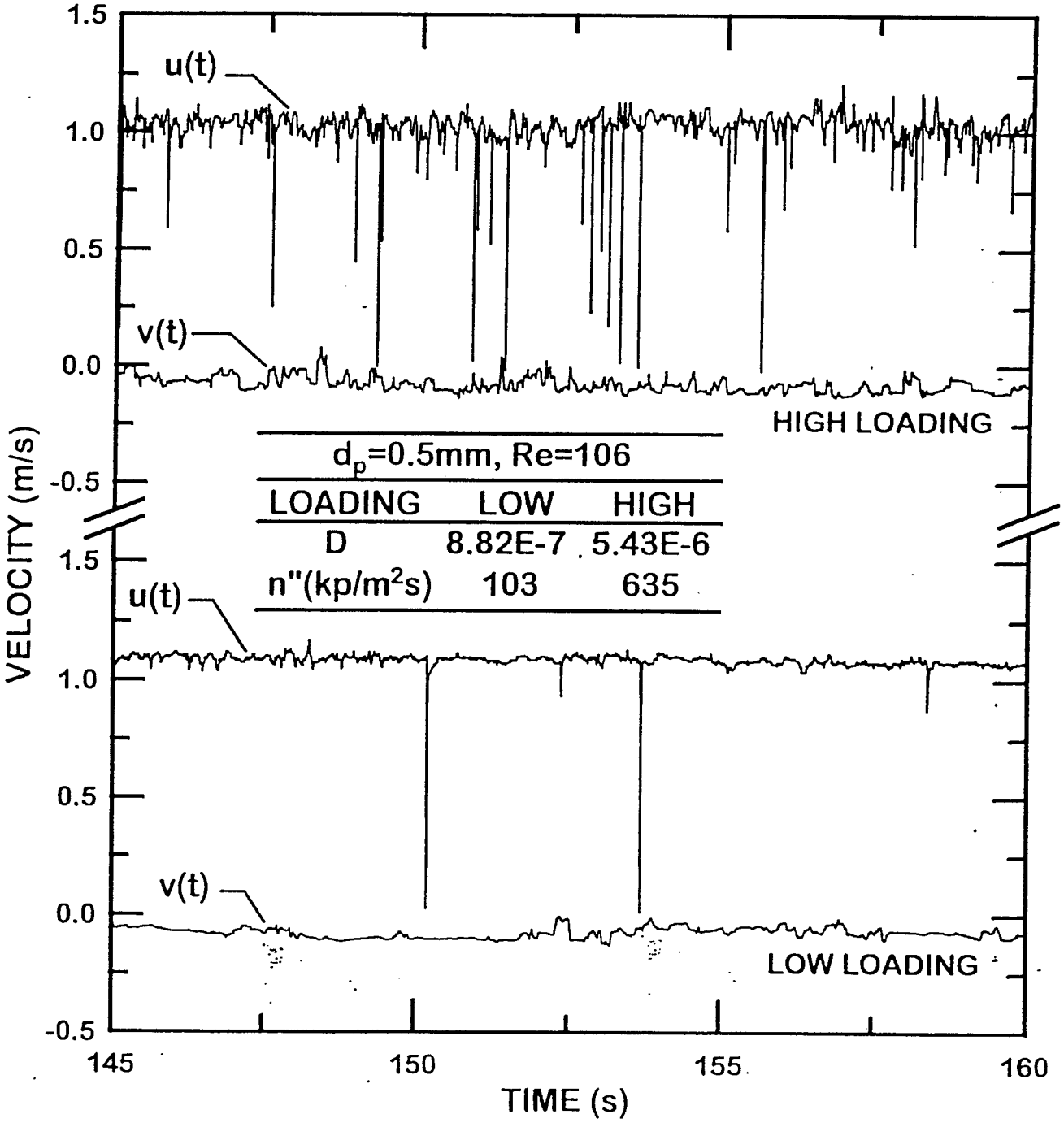
1.5
1.0
0.5
0.0
-0.5
u(t)
v(t)
HIGH LOADING
d_p=0.5mm, Re=106
LOADING LOW HIGH
D 8.82E-7 5.43E-6
n"(kp/m²s) 103 635
u(t)
v(t)
LOW LOADING
VELOCITY (m/s)
145
150
155
160
TIME (s)

FIG-3

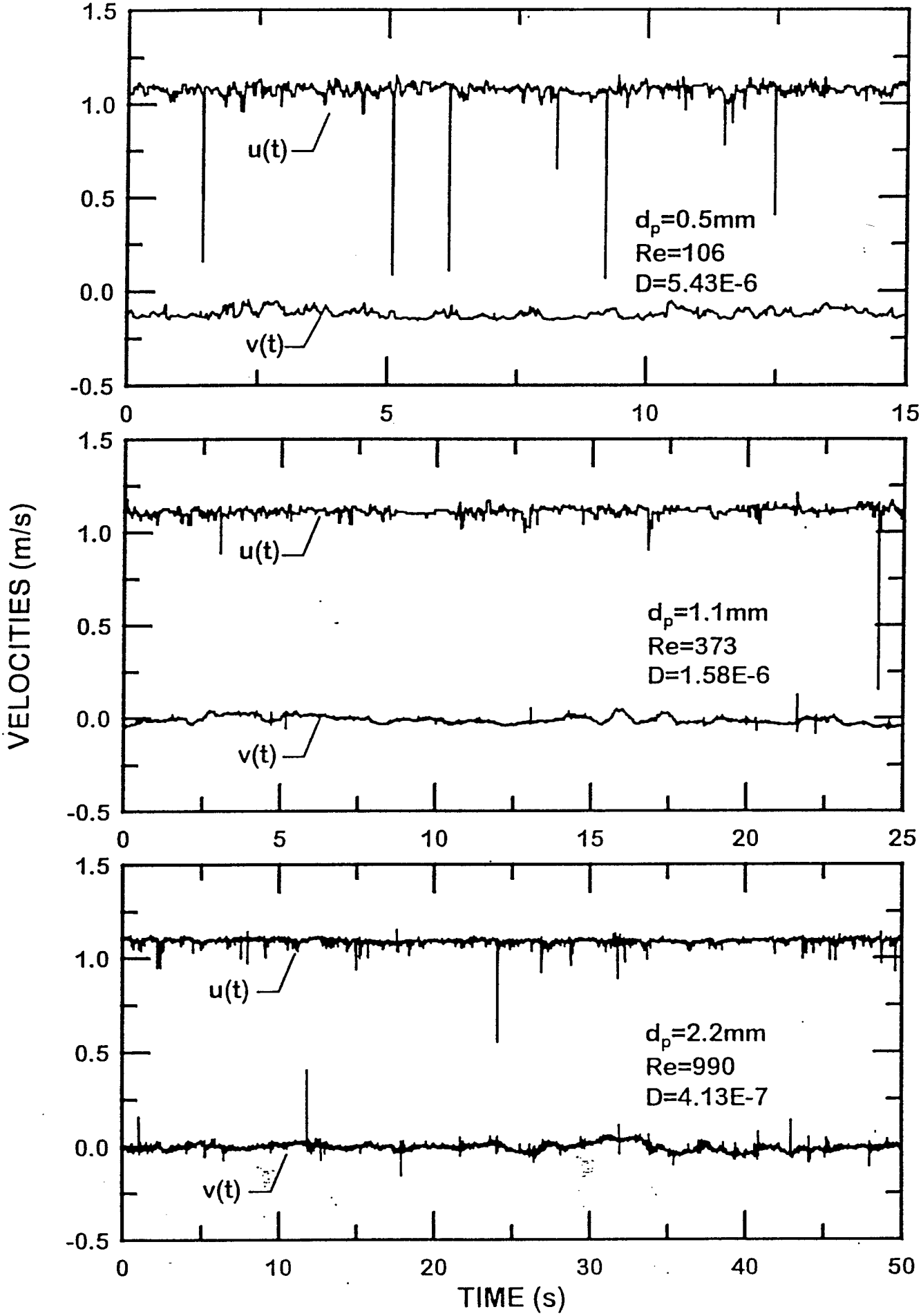
1.5
1.0
0.5
0.0
-0.5
u(t)
v(t)
d_p=0.5mm
Re=106
D=5.43E-6
0
5
10
15
1.5
1.0
0.5
0.0
-0.5
u(t)
v(t)
d_p=1.1mm
Re=373
D=1.58E-6
0
5
10
15
20
25
1.5
1.0
0.5
0.0
-0.5
u(t)
v(t)
d_p=2.2mm
Re=990
D=4.13E-7
0
10
20
30
40
50
VELOCITIES (m/s)
TIME (s)

FIG. 4.

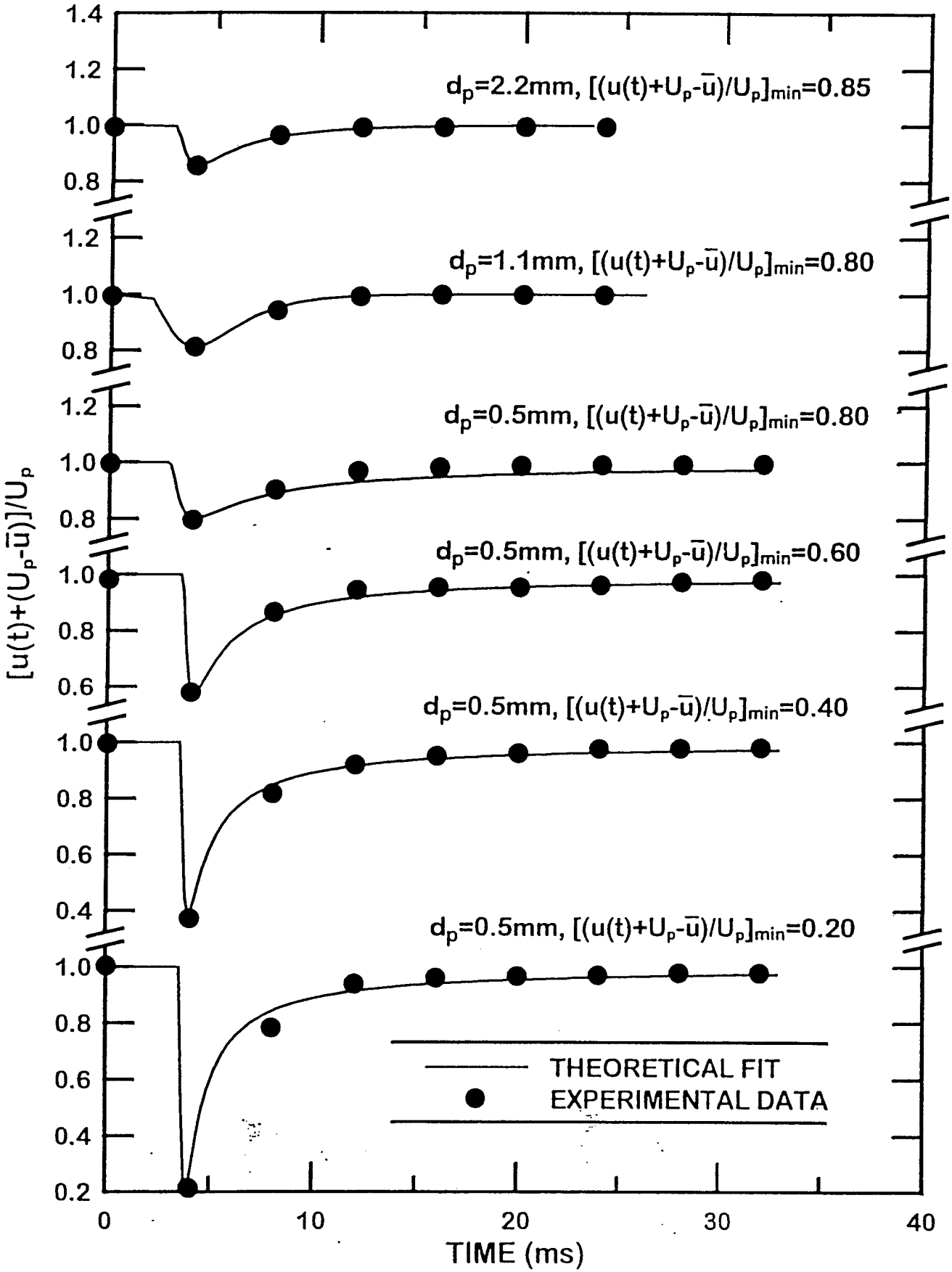
d_p=2.2mm, $[(u(t)+U_p-\bar{u})/U_p]_{min}$=0.85
d_p=1.1mm, $[(u(t)+U_p-\bar{u})/U_p]_{min}$=0.80
d_p=0.5mm, $[(u(t)+U_p-\bar{u})/U_p]_{min}$=0.80
d_p=0.5mm, $[(u(t)+U_p-\bar{u})/U_p]_{min}$=0.60
d_p=0.5mm, $[(u(t)+U_p-\bar{u})/U_p]_{min}$=0.40
d_p=0.5mm, $[(u(t)+U_p-\bar{u})/U_p]_{min}$=0.20
THEORETICAL FIT
EXPERIMENTAL DATA
$[u(t)+(U_p-\bar{u})]/U_p$
TIME (ms)
0
10
20
30
40

FIG. 5

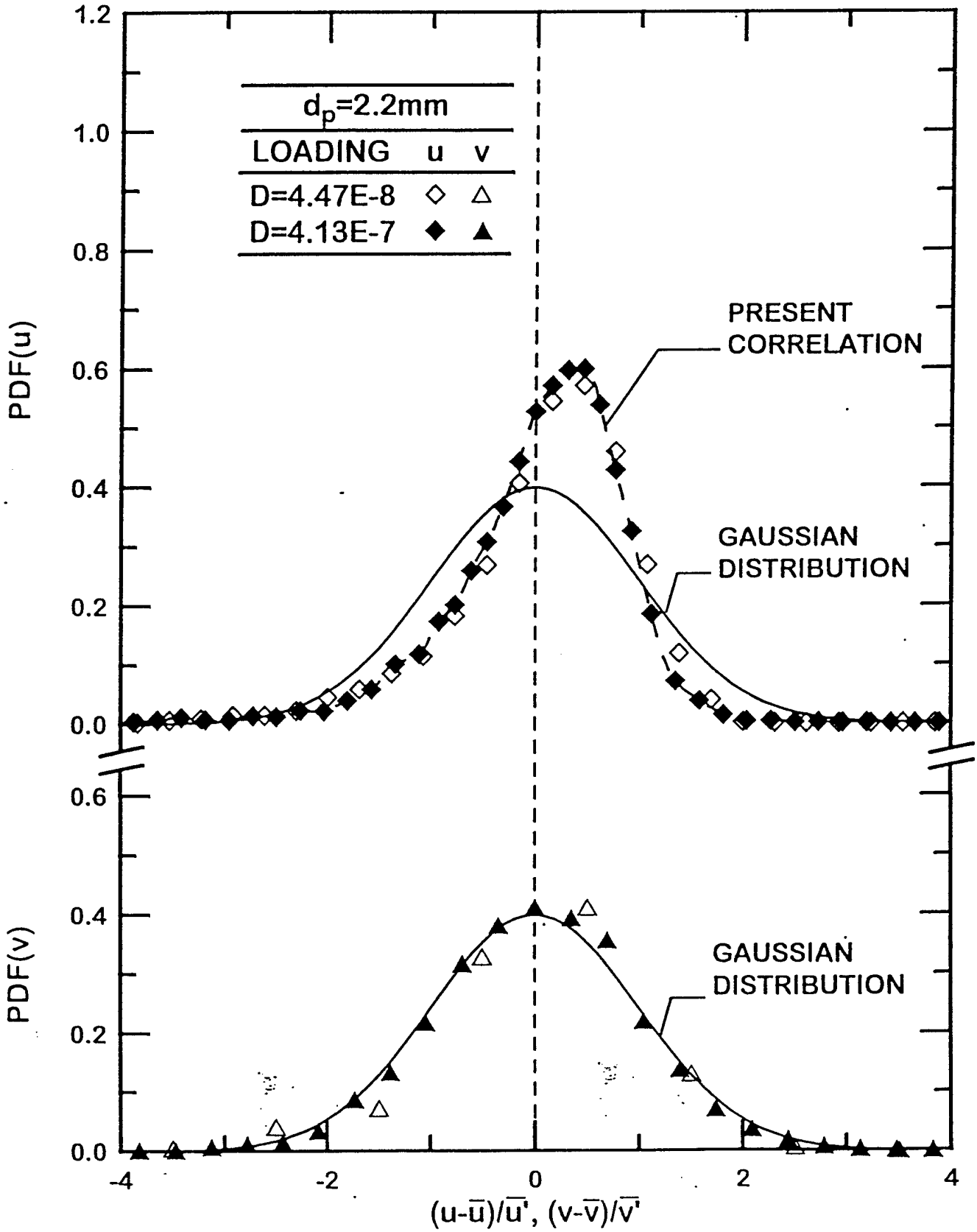
d_p=2.2mm
LOADING u v
D=4.47E-8
D=4.13E-7
PRESENT CORRELATION
GAUSSIAN DISTRIBUTION
GAUSSIAN DISTRIBUTION
PDF(u)
PDF(v)
1.2
1.0
0.8
0.6
0.4
0.2
0.0
0.6
0.4
0.2
0.0
-4
-2
0
2
4
(u-ū)/ū', (v-v̄)/v̄'

FIG. 6

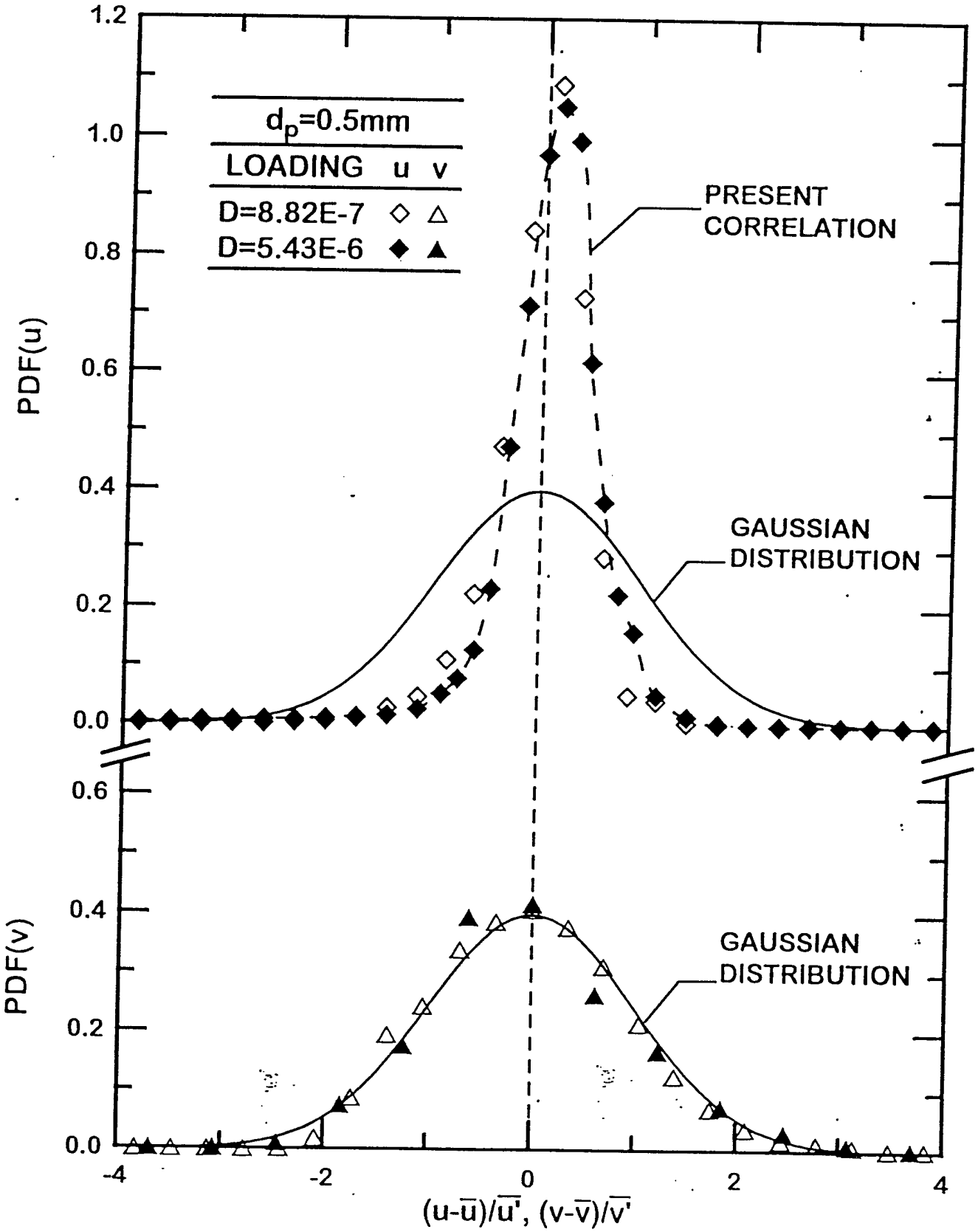
d_p=0.5mm
LOADING u v
D=8.82E-7 ◇ △
D=5.43E-6 ◆ ▲
PRESENT CORRELATION
GAUSSIAN DISTRIBUTION
GAUSSIAN DISTRIBUTION
PDF(u)
PDF(v)
1.2
1.0
0.8
0.6
0.4
0.2
0.0
0.6
0.4
0.2
0.0
-4
-2
0
2
4
(u-ū)/ū', (v-v̄)/v̄'

FIG. 7

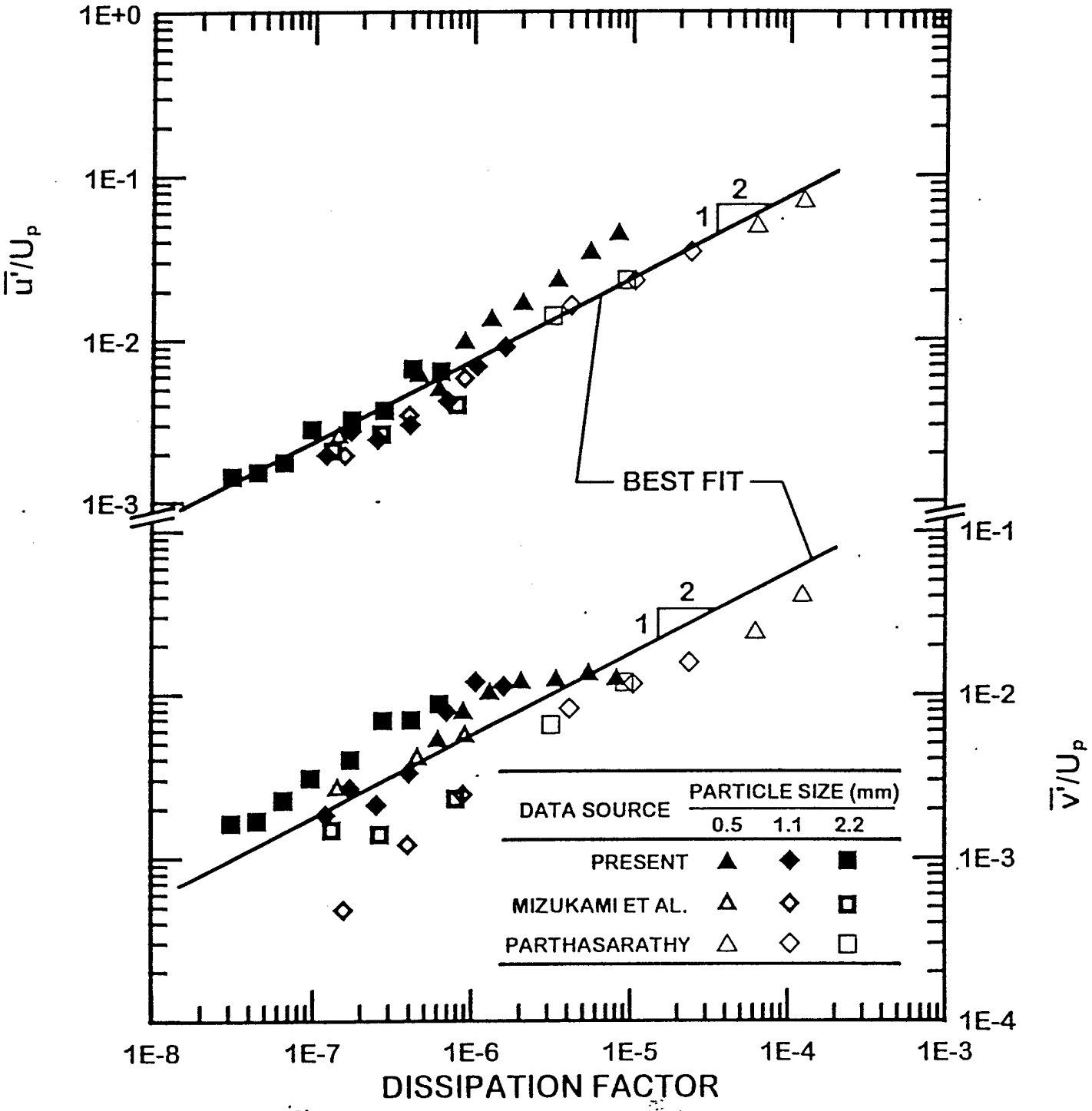
1E+0
1E-1
1E-2
1E-3
$\overline{u'}/U_p$
2
1
BEST FIT
2
1
1E-1
1E-2
1E-3
1E-4
$\overline{v'}/U_p$
DATA SOURCE
PARTICLE SIZE (mm)
0.5 1.1 2.2
PRESENT
MIZUKAMI ET AL.
PARTHASARATHY
1E-8
1E-7
1E-6
1E-5
1E-4
1E-3
DISSIPATION FACTOR

FIG. 8

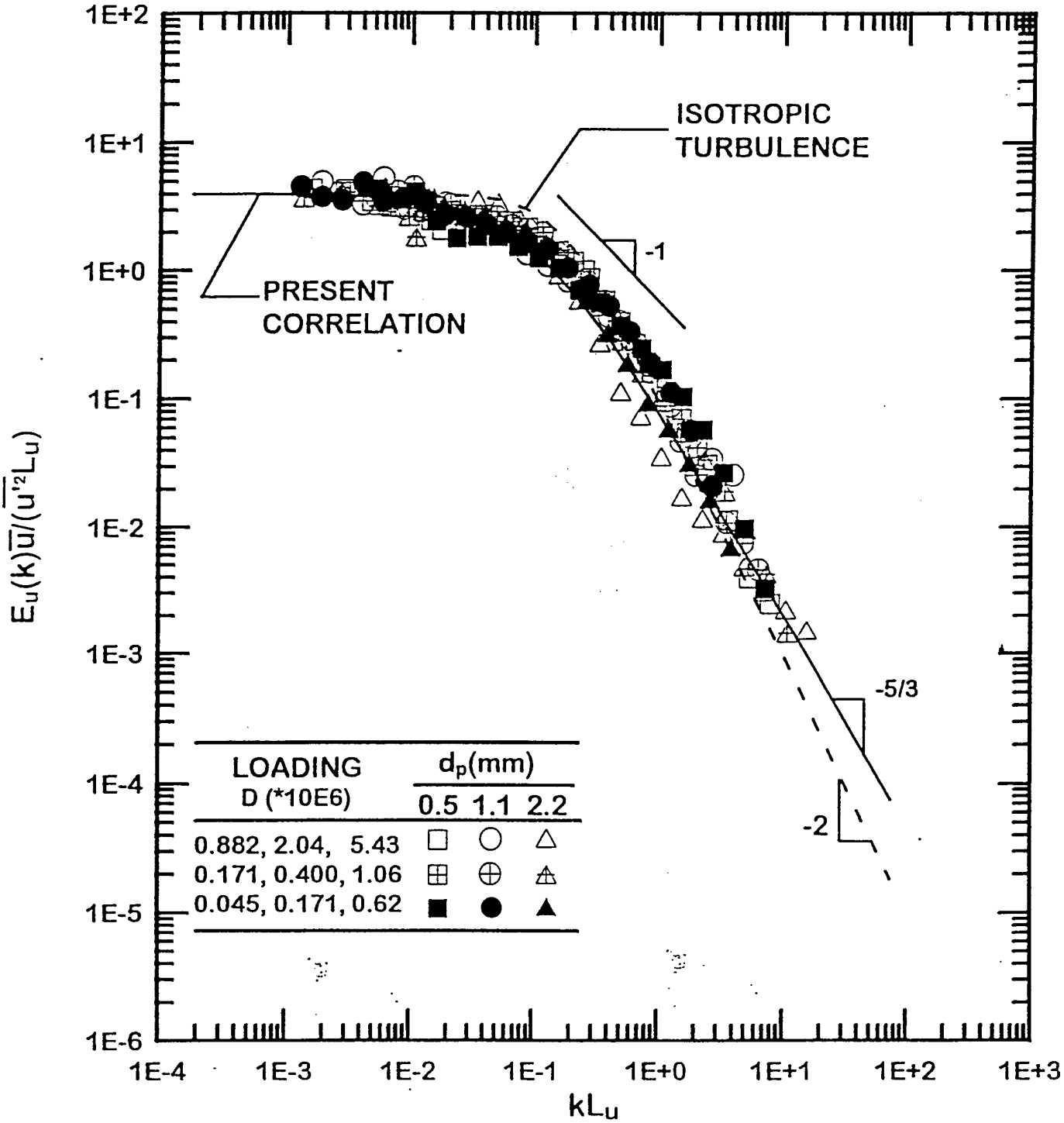
1E+2
1E+1
1E+0
1E-1
1E-2
1E-3
1E-4
1E-5
1E-6
1E-4
1E-3
1E-2
1E-1
1E+0
1E+1
1E+2
1E+3
$E_u(k)\overline{u}/(\overline{u'^2}L_u)$
kL_u
ISOTROPIC TURBULENCE
PRESENT CORRELATION
-1
-5/3
-2
LOADING D (*10E6)
d_p(mm) 0.5 1.1 2.2
0.882, 2.04, 5.43
0.171, 0.400, 1.06
0.045, 0.171, 0.62

FIG. 9

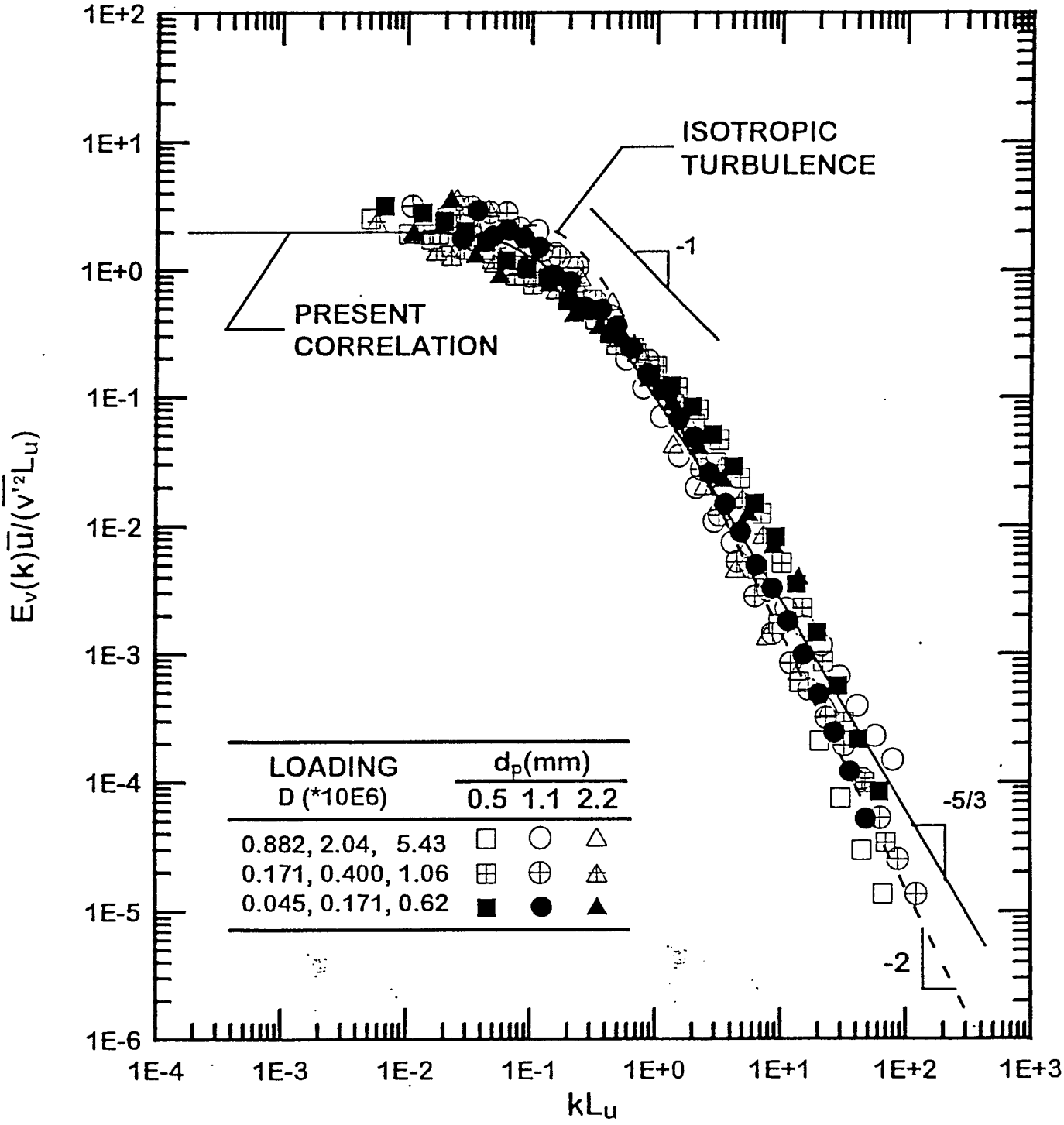
1E+2
1E+1
1E+0
1E-1
1E-2
1E-3
1E-4
1E-5
1E-6
1E-4
1E-3
1E-2
1E-1
1E+0
1E+1
1E+2
1E+3
$E_v(k)\bar{u}/(\overline{v'^2}L_u)$
kL_u
ISOTROPIC TURBULENCE
PRESENT CORRELATION
-1
-5/3
-2
LOADING D (*10E6)
d_p(mm) 0.5 1.1 2.2
0.882, 2.04, 5.43
0.171, 0.400, 1.06
0.045, 0.171, 0.62

Appendix D: Wu, P.-K., Hsiang, L.-P. and Faeth, G.M. (1995) Aerodynamic Effects on Primary and Secondary Breakup. Prog. Astro. Aero. 169, 247-279.

Chapter 9

Aerodynamic Effects on Primary and Secondary Spray Breakup

P.-K. Wu,* L.-P. Hsiang,† and G. M. Faeth‡
University of Michigan, Ann Arbor, Michigan 48109-2118

Nomenclature

a = drop acceleration
C_D = drop drag coefficient
$\bar{C}_D$ = mean drop drag coefficient over breakup period
C_i = empirical coefficient
d = drop or injector diameter
d_c = cross stream drop diameter
d_{cmax} = maximum cross stream drop diameter
$e_{p\ell}$ = ellipticity of drop
Eo = Eötvös number, $a\rho_f d^2/\sigma$ or $a|\rho_f - \rho_g|d^2/\sigma$
g = acceleration of gravity
ℓ = characteristic eddy size
ℓ_K = Kolmogorov length scale of turbulence
MMD = mass median drop diameter
Oh = Ohnesorge number of a drop, $\mu_f/(\rho_f d_0 \sigma)^{1/2}$
Oh_{cr} = Ohnesorge number of core drop, $\mu_f/(\rho_f d_b \sigma)^{1/2}$
Oh_d = jet Ohnesorge number, $\mu_f/(\rho_f d\sigma)^{1/2}$
p = pressure
Re = Reynolds number, $\rho_g d u/\mu_g$
Re_{fd} = jet Reynolds number, $\bar{u}_0 d/\nu_f$
$Re_{f\Lambda}$ = Reynolds number, $\bar{u}_0 \Lambda/\nu_f$
r = radial distance
SMD = Sauter mean diameter
SMD_p = Sauter mean diameter after primary breakup for a merged primary breakup

*Research Fellow, Department of Aerospace Engineering.
†Graduate Student Research Assistant, Department of Aerospace Engineering.
‡Professor, Department of Aerospace Engineering.

t = time
t^* = characteristic breakup time, $d_0(\rho_f/\rho_g)^{1/2}/u_0$
u = streamwise relative velocity
u' = streamwise absolute velocity
u_p = streamwise drop velocity
v = radial velocity
v_ℓ = radial velocity associated with eddy of size ℓ
v_p = radial drop velocity
We = initial Weber number of drop, $\rho_g d_0 u_0^2/\sigma$
We_{cr} = Weber number of core drop, $\rho_g d_b(u_0' - u_b)^2/\sigma$
We_{fd} = jet Weber number, $\rho_f d\bar{u}_0^2/\sigma$
We_{gd} = jet Weber number, $\rho_g d\bar{u}_0^2/\sigma$
x = streamwise distance
δ = liquid boundary-layer thickness
Λ = radial integral length scale
μ = molecular viscosity
ν = kinematic viscosity
ρ = density
σ = surface tension
τ_b = characteristic secondary breakup time, $(\rho_f/\rho_g)^{1/2}SMD/u_0$
τ_R = characteristic Rayleigh breakup time, $(\rho_f SMD^3/\sigma)^{1/2}$

Subscripts and Superscripts

b = property at end of breakup
cr = critical conditions for onset and end of breakup
f = liquid-phase property
g = gas-phase property
i = at point of breakup initiation
o = initial condition
$\bar{(\ )}$ = time-averaged mean property
$\tilde{(\ )}$ = mass-averaged mean property
$\bar{(\ )}'$ = time-averaged rms fluctuating property

I. Introduction

PRIMARY and secondary breakup are important classical multiphase flow problems that have motivated numerous past studies. Primary breakup involves the initial formation of drops and other liquid fragments at the surface of a liquid. Primary breakup is important because it controls the initial dispersion of liquid into the gas phase and, through the strong effect of drop sizes on interphase transport rates, the subsequent mixing properties of sprays. Secondary breakup involves any subsequent breakup of drops or liquid fragments present as dispersed liquids. Secondary breakup is important because drops after primary breakup are intrinsically unstable to secondary breakup, which affects subsequent mixing rates by influencing drop sizes as well. In addition, effects of liquid heating or acceleration of the gas phase can lead to conditions where drops undergo secondary breakup. In spite of their importance, however, current understanding of primary and secondary breakup is limited due to problems of making measurements within

dense dispersions of drops. In particular, measurements of primary breakup involve observations near an undulating liquid surface having protruding ligaments, and frequently generating irregular liquid fragments, which prevents the use of methods convenient for spherical drop fields such as Fraunhofer diffraction and phase Doppler anemometry.[1,2] Additionally, secondary breakup involves the individual drop generating a relatively localized drop field that is not convenient to characterize using line-of-sight or single-point measurements. Recent development of pulsed holography techniques for measurements within dense sprays, however, has provided an alternative experimental approach that has removed some of the experimental limitations.[1,2] Thus, the objective of this chapter is to briefly describe what has been learned about primary and secondary breakup using pulsed holography thus far and to highlight aspects of these phenomena that merit more attention in the future.

Harrje and Reardon[3] review early work on primary and secondary breakup as related to the problem of liquid rocket engine combustion and combustion instability. Other more general reviews of aspects of liquid atomization processes are available as well.[4–9] This chapter will focus specifically on the properties of primary and secondary breakup disclosed by pulsed holography measurements that are not treated in these earlier reviews. The studies of primary breakup focused on breakup along the surfaces of round liquid jets in still gases, whereas the studies of secondary breakup were limited to simple shock-wave disturbances. Thus, the findings do not directly address the complexities of most practical atomization processes. In particular, many instances of primary breakup involve thin liquid sheets, interacting with gas flows having a range of relative velocities, which will not be considered here. Furthermore, practical processes of secondary breakup in sprays often involve gradual variations of disturbances imposed on drops, which will not be addressed as well. Nevertheless, primary breakup of relatively deep liquids, along the surface of round liquid jets, and secondary breakup following shock-wave disturbances, are classical liquid breakup problems that provide well-defined experimental conditions which help to simplify the interpretation of measurements. References 3–9 should be consulted for an introduction to the more extensive literature concerning general processes of primary and secondary breakup.

Some aspects of secondary breakup affect primary breakup; in particular, conditions can be encountered where processes of primary and secondary breakup overlap or merge. Thus, secondary breakup is considered before primary breakup in the following. The discussion is brief, see Refs. 8–15 for additional details.

II. Secondary Breakup

A. Introduction

Because of numerous applications, secondary breakup has received significant attention in the past. Early work in the field is reviewed by Harrje and Reardon,[3] Giffen and Muraszew,[4] Clift et al.,[5] and Hinze[16]; therefore, the following discussion will be limited to more recent studies. The definition of the onset of secondary breakup, secondary breakup dynamics, and the outcome of secondary breakup will be considered in turn.

Most earlier work on secondary breakup has at least touched on the definition and conditions for the onset of various breakup regimes. The breakup regime observed at the onset of secondary breakup has been termed bag breakup; it involves

deflection of the drop into a thin disk normal to the flow direction, followed by deformation of the center of the disk into a thin balloonlike structure extending in the downstream direction, both of which subsequently divide into drops (see Refs. 16–23 for photographs of all the breakup regimes discussed here). The shear breakup regime is observed at higher relative velocities; it involves deflection of the periphery of the disk in the downstream direction, rather than the center, and stripping of drops from the periphery of the disk. The transition between the bag and shear breakup regimes involves complex breakup processes, with portions of this regime termed parachute breakup, chaotic breakup, bag-jet breakup, transition breakup,[19,24–26] etc.; this regime will be denoted the multimode breakup regime in the following. A complex breakup mechanism also has been observed at very large relative velocities, which is called the catastrophic breakup regime[21,22]; however, this regime is associated with very strong disturbances, such as detonation waves, rather than spray processes and will not be considered here.

Existing observations of secondary breakup have generally involved liquid/gas density ratios greater than 500 and Reynolds numbers greater than 100. For these conditions, Hinze[16] has shown that transitions between breakup regimes are largely functions of the Weber ($We = \rho_g d_0 u_0^2/\sigma$) and Ohnesorge ($Oh = \mu_f/(\rho_g d_0 \sigma)^{1/2}$) numbers, which are measures of the ratios of drop drag and liquid viscous forces to surface tension forces, respectively. He found that progressively larger disturbances, i.e., larger Weber numbers, were required for the onset of breakup as Ohnesorge number increased because viscous forces in the liquid tend to inhibit drop deformation at large Ohnesorge number, which is the first step in the breakup process. In fact, viscous forces essentially suppressed secondary breakup for the available range of Weber number ($We < 40$) for $Oh > 2$ (Ref. 16). Among others, Loparev[25] showed that the properties of the disturbances also affected the onset of breakup, with more slowly applied disturbances requiring higher values of Weber number for breakup at a particular value of Ohnesorge number. Subsequent considerations will be limited to shock-wave disturbances to avoid this complication. Borisov et al.[24] proposed an alternative breakup regime map in terms of Weber and Reynolds numbers ($Re = \rho_g d u/\mu_g$), considering both the bag and shear breakup regimes, which is best suited to conditions where $Oh \ll 1$. Krzeczkowski[19] extended the breakup regime map of Hinze[16] to locate transitions to the bag, bag jet, multimode (also called transition breakup) and shear breakup regimes as a function of Weber and Ohnesorge numbers.

Another aspect of secondary breakup that has been studied is the time required to complete breakup. Liang et al.[27] summarize past measurements of breakup times, including the findings of Simpkins and Bales[28] and Ranger and Nicholls[20] for shear breakup, Reinecke and Mckay[21] and Reinecke and Waldman,[22] for catastrophic breakup—all for shock-wave disturbances at large liquid/gas density ratios and low Ohnesorge number. For these conditions, breakup times could be normalized by a characteristic breakup time, $t^* = d_0(\rho_f/\rho_g)^{1/2}/u_0$, finding that the normalized breakup time was constant within experimental uncertainties over a large range of Weber number ($10 < We < 10^6$) that includes both the shear and catastrophic breakup regimes.

Finally, due to the problems of observing drops after secondary breakup, there is very little information available about the outcome of secondary breakup even though this information is vital for understanding the structure of dense sprays.[9]

An exception is some limited results reported by Gel'fand et al.[18] for the bag breakup regime. A bimodal drop size distribution was observed with small drops resulting from breakup of the bag and large drops associated with breakup of the liquid ring at the base of the bag. However, this information is too limited to provide general guidance about the drop sizes produced by secondary breakup.

The preceding review indicates that there are several gaps in the literature concerning secondary breakup. In particular, conditions for the onset of various breakup regimes have been defined reasonably well by Krzeczkowski,[19] but analogous deformation regimes have not been defined. Results at large Ohnesorge numbers where liquid viscosity effects are important are also limited. Breakup times and drop deformation have been studied as well, however, available information is limited for the bag and transition breakup regimes that are important for drop breakup in dense sprays. Finally, measurement problems have limited study of the outcome of secondary breakup so that virtually no information is available for this critical breakup property. Thus, the objectives of the present investigation were to extend the earlier work to provide measurements of the onset of various deformation and breakup regimes, the evolution of breakup processes, and the resulting drop sizes and velocities after secondary breakup. Phenomenological descriptions of these processes were used to help interpret the data. The measurements involved pulsed shadowgraph photography and holography limited to conditions which are representative of sprays near atmospheric pressure: $\rho_f/\rho_g > 500$ and $Re > 100$. The following discussion is brief, more details can be found in Refs. 10–12.

B. Experimental Methods

1. Apparatus

The measurements of secondary breakup properties were carried out using a shock tube apparatus with the driven section open to the atmosphere.[10–12] The driven section had a rectangular cross section (38 mm wide × 64 mm high) and a length of 6.7 m with the test location 4 m from the downstream end. This provided test times of 17–21 ms in the uniform flow region behind the incident shock wave. The test location had quartz windows mounted flush with the interior side walls of the shock tube in order to allow observation of drop breakup. Drop breakup was observed in air initially at 98 kPa and 297 ± 2 K in the driven section of the shock tube with shock Mach numbers in the range 1.08–1.31.

Two different drop generator systems were used for the shock tube experiments. Operation at low and moderate Ohnesorge numbers involved use of a vibrating capillary tube drop generator which generated a stream of drops. Electrostatic deflection of a fraction of the drops out of the stream yielded a drop stream with sufficient separation so that interactions between drops during secondary breakup were eliminated.

Drop generation at large Ohnesorge numbers required a different approach because such drops are very difficult to form. Instead, a low Ohnesorge number drop was formed from a liquid solution consisting of a volatile solvent having a low viscosity and a nonvolatile viscous liquid. This drop then was levitated at the test location until the volatile solvent evaporated away. This yielded a small drop of a highly viscous liquid to provide the desired large Ohnesorge number condition. For work reported here, Dow Corning 200 Fluids were used for the viscous liquids with *n*-heptane used as the volatile solvent.

2. *Instrumentation*

Drops were observed using pulsed shadowgraph photographs and motion pictures to study the overall dynamics of breakup and single- and double-pulsed holography to study the outcome of breakup. The pulsed shadowgraph photographs were obtained using a xenon lamp having a 1-μs pulse duration. The image was recorded using a Graphlex camera at a 6:1 magnification. These photographs were obtained in a darkened room with a variable time delay between shock passage and operation of the flash lamp so that various portions of the breakup process could be observed.

Motion picture shadowgraphs were obtained using a copper vapor laser having a 30-nm-pulse duration, in conjunction with a 35-mm rotating drum camera. Laser triggering was controlled to yield 5–14 motion picture shadowgraphs with 120–160 μs separation times between images.

The holocamera and reconstruction systems were similar to those described by Ruff et al.[1,2] An off-axis holocamera arrangement was used with a 2–3:1 magnification of the hologram image and a 20-ns-laser pulse time. This arrangement was coupled with reconstruction optics that allowed drop diameters as small as 25 μm to be measured with 5% accuracy and drops as small as 10–15 μm to be observed. Reconstruction of double-pulsed holograms yielded two images of the spray with separation times as short as 1 μs so that drop velocities could be measured.

The diameters of mildly irregular drops were found by measuring their maximum and minimum diameters. It then was assumed that the drop had an ellipsoidal shape; taking the effective diameter to be the diameter of a sphere having the same volume as the ellipsoid. More irregular liquid fragments were sized by finding the cross-sectional area and perimeter of the image and proceeding as before for an ellipsoid having the same properties. The velocity of each drop was found by measuring the distance between the centroid of its two images and dividing by the known time between laser pulses. Results at each test condition were summed over at least three realizations, in order to provide drop size and velocity correlations.

3. *Test Conditions*

Test drops of water, *n*-heptane, mercury, two Dow Corning 200 Fluids, and various glycerol mixtures were studied. Initial drop diameters were in the range 150–1550 μm. Ranges of other variables are as follows: $\rho_f/\rho_g = 580$–12,000, $Oh = 0.006$–560, $We = 0.5$–680, and $Re = 340$–15,760. The Reynolds number range of these measurements is higher than conditions where gas viscosity plays a strong role on drop drag properties, e.g., within this Reynolds number range, the drag coefficient of solid spheres only varies in the range 0.4–0.6 (Refs. 10–12).

C. Presentation of Results on Secondary Breakup

1. *Deformation and Breakup Regimes*

The presentation of secondary breakup results will begin with definition of deformation and breakup regime transitions in order to help organize the remainder of the findings. The deformation and breakup regime map, showing transitions as functions of Weber and Ohnesorge numbers similar to Hinze[16] and Krzeczkowski[19] is illustrated in Fig. 1. Present evaluation of the onset of breakup (the transition to

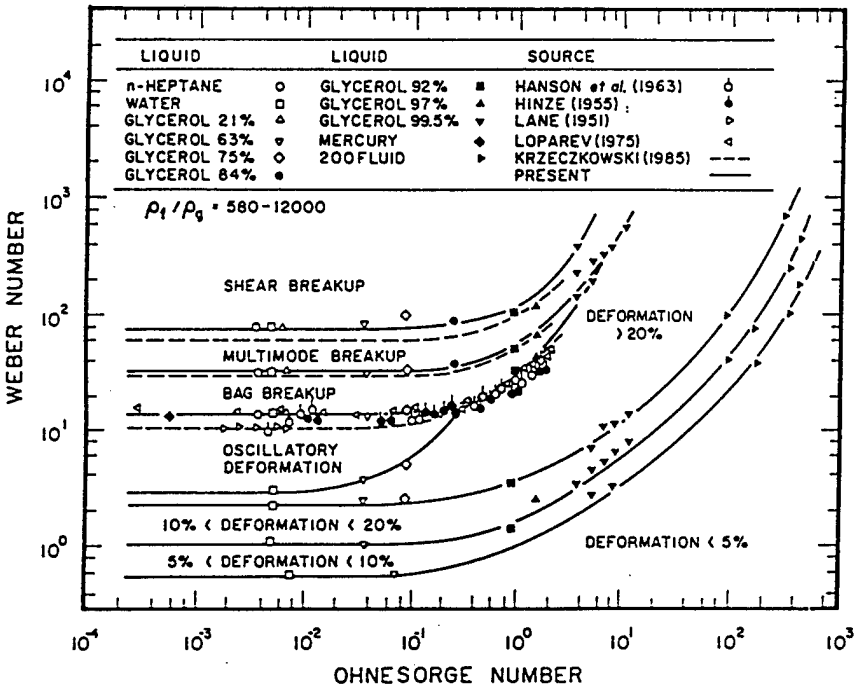

Fig. 1 Drop deformation and breakup regime map for liquid/gas density ratios greater than 500.

the bag breakup regime) is identical to the findings of Hinze[16] and Krzeczkowski[19] within experimental uncertainties. Present results also agree quite well with transitions found by Krzeczkowski[19] to the shear breakup regime and the multimode breakup regime (which Krzeczkowski[19] called the transition breakup regime). In view of the somewhat subjective identifications of breakup regimes and their transitions, this level of agreement is quite satisfying.

Observations of transitions to the various deformation and oscillatory deformation regimes illustrated in Fig. 1 have not been reported before. The definition of transition to the various deformation regimes was taken to be the condition where the drop deformed so that the ratio of its maximum (cross stream) dimension to its initial diameter was within the given range. Following these transitions, there was a range of Weber numbers at each Ohnesorge number where the drop decayed back to a spherical shape much like an overdamped oscillation. For $Oh > 0.4$, this regime ended by the onset of bag breakup, however, for $Oh < 0.4$, there was a range of Weber numbers where the drop oscillated with progressively decaying ratios of maximum to initial diameters before the bag breakup regime was reached; this regime is denoted the oscillatory deformation regime in Fig. 1.

The most striking feature of the flow regime map of Fig. 1 is that progressively higher Weber numbers are needed for the various transitions as Ohnesorge number increases. In fact, for $We < 1000$, breakup is no longer possible for $Oh > 10$ whereas 5% deformation is no longer possible for $Oh > 1000$. Recalling that Ohnesorge number characterizes the ratio between liquid viscous forces and surface tension forces, the inhibition of deformation and breakup at large Ohnesorge

numbers clearly is due to increased damping by liquid viscous forces. This increased viscous damping slows the deformation process so that drag forces can reduce relative velocities and the potential for breakup. This high-Ohnesorge number regime is encountered during spray combustion processes at high pressures, where values of surface tension become small but viscosity remains finite as the drop surface nears its thermodynamic critical point. Thus, the findings illustrated in Fig. 1 suggest that drops at these conditions would not necessarily shatter due to small surface tension near the thermodynamic critical point as often thought[9]; instead, they might only deform or even remain spherical. However, additional study of drop breakup processes at high pressure is needed before definitive conclusions about this behavior can be obtained. In particular, specific drop trajectories across the flow regime map depend on atomization and mixing properties of the spray whereas near-critical drop processes involve much lower values of ρ_f/ρ_g than those considered in Fig. 1.

2. *Breakup Times*

The discussion of deformation and breakup regime transitions highlights the importance of breakup time, which is defined as the time between initiation of the velocity disturbances and the last fragmentation of drop liquid. In particular, as drop velocity relaxation times and breakup times approach one another, the propensity for drop breakup decreases due to reduction of relative velocities between the drop and the gas. Present measurements of breakup times, along with earlier measurements for shock-wave disturbances from Refs. 20–22, 28, and 29, are plotted as a function of Weber number in Fig. 2. The breakup times t_b in the figure are normalized by the characteristic breakup time for shear breakup defined by Ranger and Nicholls[20] as follows:

$$t^* = d_0(\rho_f/\rho_g)^{1/2}/u_0 \tag{1}$$

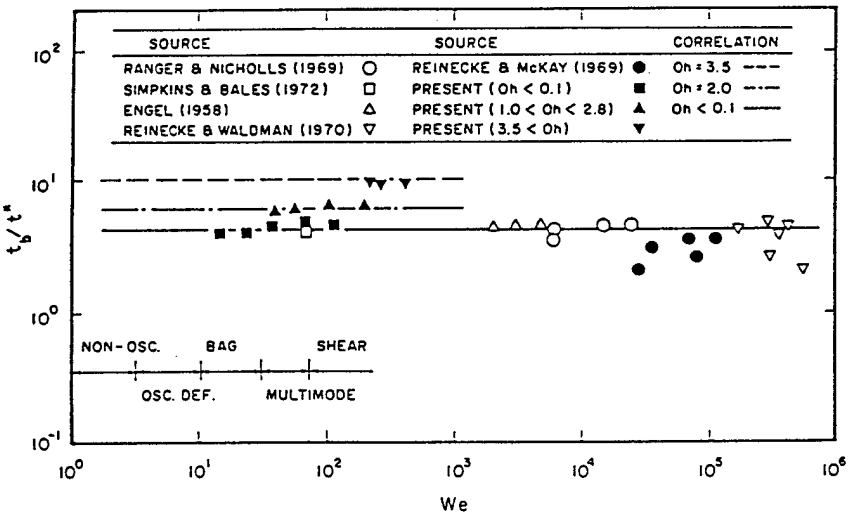

Fig. 2 Drop breakup times as a function of Weber and Ohnesorge numbers.

Except for the present results, which are grouped according to Ohnesorge number, the measurements are for $Oh < 0.1$ and effects of liquid viscosity are small. Thus, the deformation and breakup regimes at small Ohnesorge numbers are illustrated in the figure for reference purposes.

A remarkable feature of the breakup time results of Fig. 2 at $Oh < 0.1$ is that t_b/t^* varies very little even though Weber number varies over a large range (roughly 10–10^6) and a variety of breakup regimes are involved. In fact, the breakup time correlation of Ranger and Nicholls[20] developed for the shear breakup regime

$$t_b/t^* = 5.0 \tag{2}$$

provides a reasonably good correlation of all of the measurements for $Oh < 0.1$. When the present results for $Oh > 0.1$ are considered, however, it is seen that t_b/t^* progressively increases with increasing Ohnesorge number. This reflects the importance of liquid viscosity on breakup evident from the breakup regime map of Fig. 1.

3. *Drop Deformation*

The first stage of drop deformation, in the period where the drop flattens and first reaches a maximum cross stream dimension, was studied due to its influence on drop velocity relaxation and breakup. In particular, the distortion of the drop should affect its drag properties, and thus relative velocities during the breakup process, which undoubtedly plays a role in the onset of breakup.

Drop distortion correlates reasonably well as a linear function of time with the maximum distortion reached at roughly $t/t^* = 1.6$ when $Oh < 0.1$ (Ref. 10). Notably, measurements plotted by Wierzba and Takayama[23] exhibit very similar behavior. Measurements of drop distortion at $Oh > 0.1$, however, show progressive delay in the time required for the drop to reach maximum distortion.

The next parameter of interest is the maximum cross stream diameter of the drop $d_{c\,\max}$. An approximate expression for the variation of $d_{c\,\max}$ with flow conditions can be obtained for conditions where effects of liquid viscosity are small, $Oh < 0.1$, by considering the interaction between surface tension and pressure forces when the drop is drawn into a flattened shape. This yields the following expression for the maximum deformation[10]:

$$d_{c\,\max}/d_0 = 1 + 0.19We^{1/2}, \quad Oh < 0.1, \qquad We < 10^2 \tag{3}$$

Figure 3 is an illustration of present measurements of $d_{c\,\max}/d_0$ as a function of Weber number, with Ohnesorge number as a parameter. The correlating expression of Eq. (3) for $Oh \leq 0.1$ also is plotted in the figure; it is evident that Eq. (3) provides a reasonable fit of the data. Effects of increasing Ohnesorge number can be seen, with $d_{c\,\max}/d_0$ tending to decrease at a particular Weber number as Ohnesorge number is increased. Because the deformation motions of the drop cease at the point where $d_{c\,\max}$ is reached, this behavior is not thought to be a direct effect of viscous forces on the force balance fixing $d_{c\,\max}$. Instead, the increased time of deformation due to effects of liquid viscosity is a more probable mechanism. This allows drag forces to act for a longer time before the maximum deformation condition is reached, which tends to reduce the relative velocity, and correspondingly $d_{c\,\max}$.

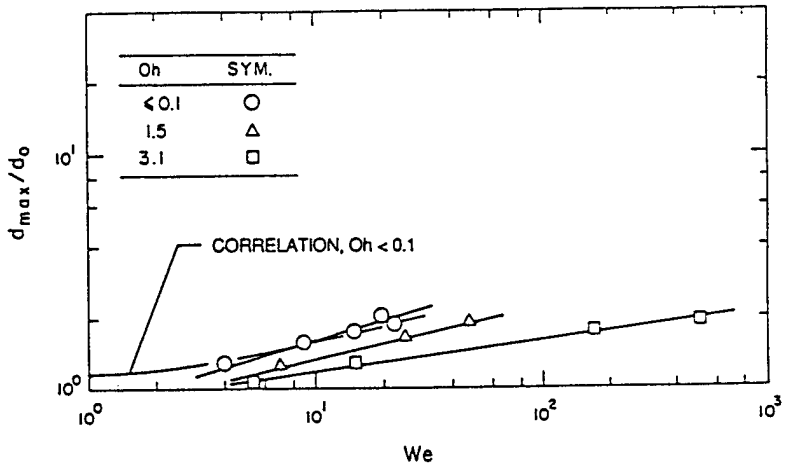

Fig. 3 Maximum cross stream drop diameters prior to breakup as a function of Weber and Ohnesorge numbers.

4. *Drop Drag*

Drop drag properties were found by measuring the motion of the centroid of the drop in the uniform flowfield behind the shock wave. This approach is only approximate because it neglects the forces involved as the mass of the drop is redistributed during drop deformation, however, this effect is not expected to be large for present test conditions because characteristic velocities in the liquid phase are small as discussed subsequently.[10]

The experiments to find C_D involved the initial deformation of the drops up to the time $d_{c\,max}$ was reached for $Oh < 0.1$ and for a moderate range of Reynolds number (1000–2500) where effects of Reynolds number on the drag of the drops are expected to be small.[8] Thus, it was found that C_D largely was a function of the degree of deformation of the drop for present test conditions. To highlight this behavior, the results are plotted in terms of d_c/d_0 in Fig. 4. Measurements of C_D for solid spheres and thin disks, drawn from White[30] for the same range of Reynolds number as the present tests, also are illustrated on the plot. In spite of the relatively large uncertainties of the measurements, the trend of the data is quite clear: for d_c/d_0 near unity, C_D approximates results for solid spheres and then increases to approach results for thin disks at $d_c/d_0 = 2$. Thus, behavior in the period observed appears to be dominated by distortion of the drop, rather than internal circulation which would cause reductions of C_D from values appropriate for solid spheres. This seems reasonable because liquid-phase velocities are relatively small for present test conditions. In particular, conservation of momentum considerations suggest that characteristic liquid-phase velocities are on the order of $(\rho_g/\rho_f)^{1/2}u_0$, see Ranger and Nicholls.[20] Thus, for $(\rho_f/\rho_g) > 500$, liquid velocities are roughly 5% of the initial relative velocity.

5. *Drop Sizes*

Measurements of drop sizes after breakup were limited to conditions where $Oh < 0.1$. This was necessary in order to capture the entire drop field after breakup on a single hologram, because larger values of the Ohnesorge number yielded

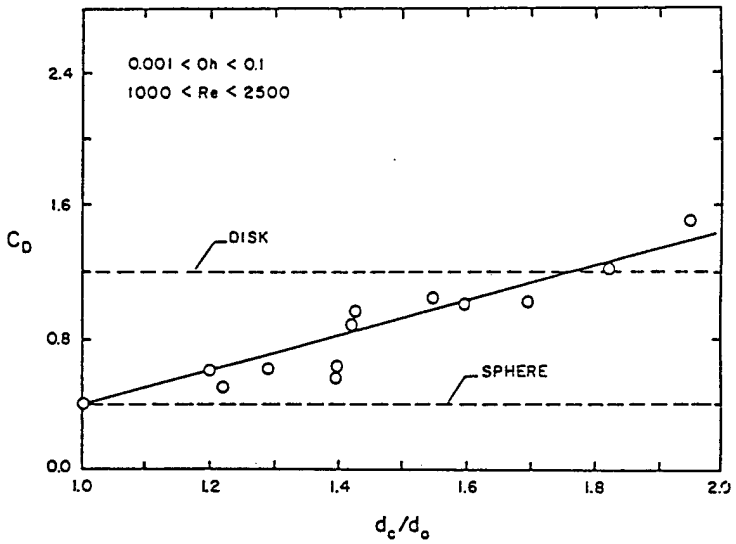

Fig. 4 Drop drag coefficient prior to breakup as a function of the normalized cross stream diameter.

regions containing drops that were too large for the present optical arrangement. The measurements included $We < 10^3$, which corresponds to the bag, transition, and shear breakup regimes.

Past work on the structure of dense sprays and processes of primary breakup of nonturbulent and turbulent liquids[2,13,14] indicated that local drop size distributions generally satisfied the universal root normal distribution function of Simmons,[31] with *MMD/SMD* = 1.2 (see Belz[32] for a discussion of the properties of the root normal distribution function). This vastly simplifies the presentation of data because the root normal distribution only has two moments, and with *MMD/SMD* equal to a constant, is specified entirely by the Sauter mean diameter alone. Thus, initial measurements of drop sizes after breakup focused on evaluating the root normal distribution function.

Typical measurements of drop size distributions are illustrated in Fig. 5 for bag breakup. Results for the other breakup regimes were similar, although for shear breakup trends illustrated in Fig. 5 they were achieved only after removing the core or drop-forming drop from the distribution as discussed in the following (the core drop will be handled separately). The results are plotted in terms of the root normal distribution function, with the function itself illustrated for values of *MMD/SMD* = 1.1, 1.2, and 1.5. The data are somewhat scattered at large drop sizes because of the limited number of large drops. The results are represented reasonably well by the universal root normal distribution function with *MMD/SMD* = 1.2, similar to the earlier findings.[2,13,14] In contrast to the present findings, Gel'fand et al.[18] observed a bimodal distribution of drop sizes after bag breakup for the two conditions they considered. The reason for this discrepancy is unknown and clearly merits additional study.

A correlating expression for the Sauter mean diameter after secondary breakup is obtained by noting the similarity between primary breakup of nonturbulent liquids[13] and secondary breakup due to stripping originating from the windward

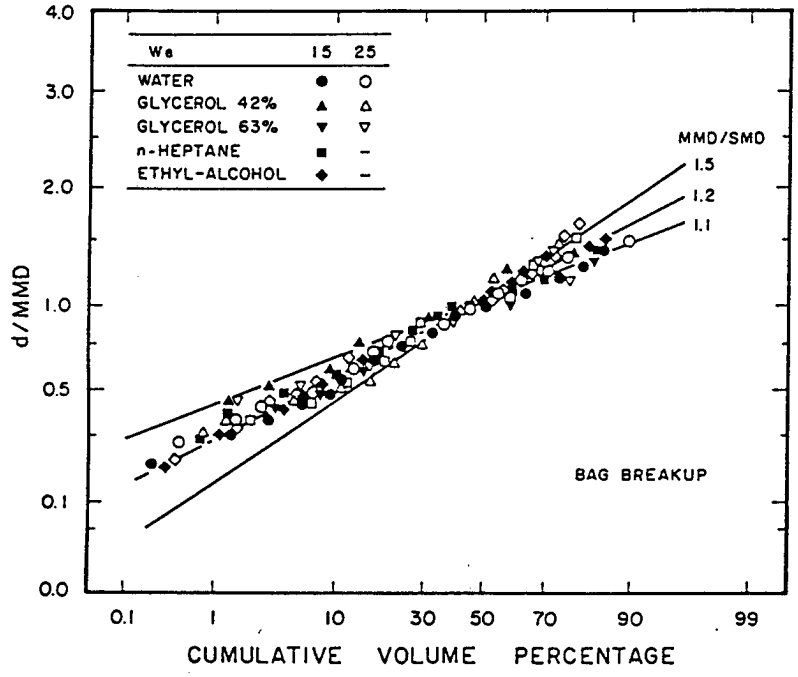

Fig. 5 Distribution of drop diameters after bag breakup.

side of the drop in the shear breakup regime. The configuration for secondary breakup in the shear breakup regime is shown in Fig. 6, where the core (drop-forming) drop is illustrated. It is assumed that the relative velocity at the time of breakup can be represented by the initial relative velocity, that drop sizes after breakup are comparable to the thickness of the boundary layer as it reaches the periphery of the drop, that the liquid boundary layer is laminar, and that the Sauter mean diameter is dominated by the largest drop sizes in the distribution. The length of development of the liquid boundary layer is taken to be proportional to d_0, which should be the condition tending to yield the largest drop sizes.[10]

Present measurements of the Sauter mean diameter after secondary breakup are plotted in terms of the variables from the secondary breakup model in Fig. 7. These results are for $Oh < 0.1$ and $We < 10^3$, including the bag, transition, and shear breakup regimes. A correlation of the data based on the approximate theory also is shown on the plot. The best empirical fit of the data to the theoretical variables is as follows:

$$\rho_g SMD\, u_0^2/\sigma = 6.2(\rho_f/\rho_g)^{1/4}[\mu_f/(\rho_f d_0 u_0)]^{1/2} We \tag{4}$$

with the correlation coefficient of the fit being 0.91. It should be noted, however, that ρ_f/ρ_g does not vary greatly over the present test range, and additional measurements are needed to explore density ratio effects.

It is probably fortuitous, and certainly surprising, that a single correlation can express the Sauter mean diameter after bag, transition, and shear breakup since the three breakup mechanisms appear to be rather different. On the other hand, similar behavior for the three breakup regimes is consistent with the observation

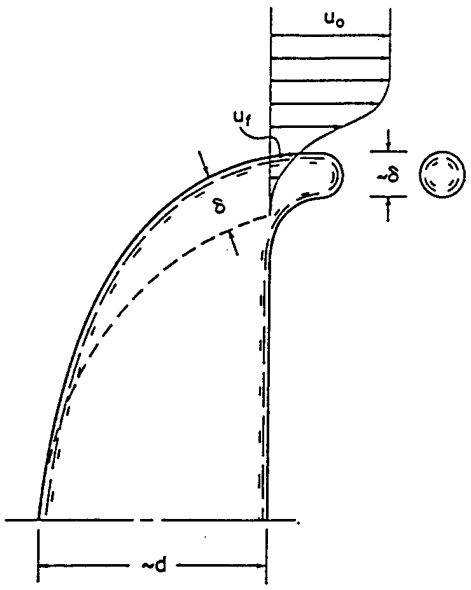

Fig. 6 Shear breakup process of drops.

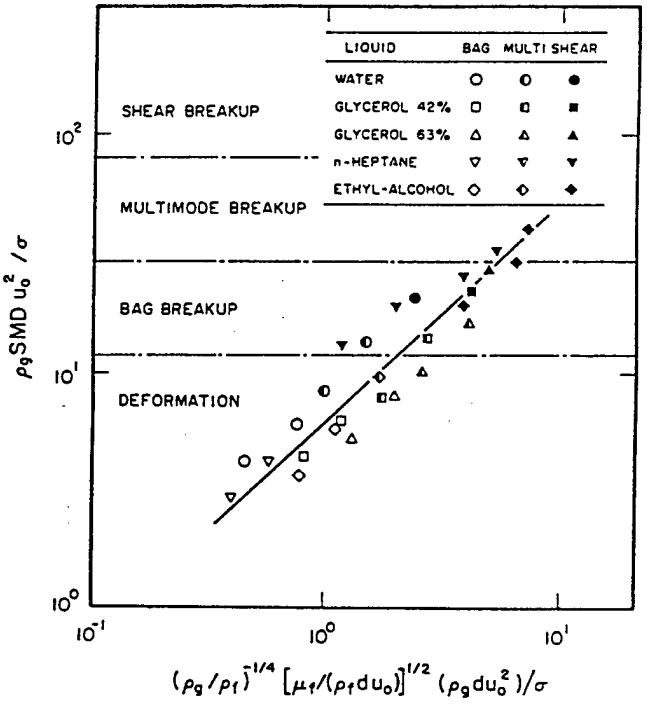

Fig. 7 Correlation of the *SMD* after secondary breakup.

that their breakup times correlated in the same way, as discussed in connection with Fig. 2

6. *Core Drop Properties*

The velocity and size of the core drop at the end of breakup must be known in order to treat it separately from the rest of the drop population after shear breakup. Since drops stripped from the core drop were not observed to undergo subsequent breakup, the end of shear breakup coincides with the end of drop stripping from the core drop. In the following, the velocity of the core drop at the end of breakup will be considered first. Given this information about core drop velocities, subsequent stability considerations yield a method for correlating measurements of core drop sizes. These considerations are limited to the streamwise velocity of the core drop because these drops did not exhibit appreciable cross stream velocities during the present experiments (aside from their cross stream motion due to operation of the drop generator system).

To assist data correlation, a simplified analysis was used to estimate core drop velocities at the end of breakup. The major assumptions of the analysis[11,12] are as follows: virtual mass, Bassett history, and gravitational forces were ignored; gas velocities were assumed to be constant; mass stripping from the core drop was ignored; and a constant average drag coefficient was used over the period of breakup.

Based on the preceding assumptions, the following expression for the absolute velocity of the core drop at the end of breakup, $u_b' = u_0 - u_b$, can be found[11,12]:

$$(u_b'/u_0)(\rho_f/\rho_g)^{1/2}(1+3C) = 3\bar{C}_D(t_b/t^*)/4 \tag{5}$$

where

$$C = (3\bar{C}_D t_b/4t^*)(\rho_g/\rho_f)^{1/2} \tag{6}$$

Earlier work has shown that $t_b/t^* = 5$ for $10 < We < 10^6$ and $Oh < 0.1$ (Refs. 10 and 27). Thus, the right-hand side of Eq. (5) should be a constant if a constant average value of C_D for the shear breakup process can be found. A reasonable correlation of the present measurements of u_b/u_0 was obtained by taking $\bar{C}_D = 5$, which is comparable to values observed near the maximum deformation condition.[10] This yields $3\bar{C}_D(t_b/t^*)/4 = 19$ on the right-hand side of Eq. (5).

The measurements of core drop velocities at the end of breakup, normalized as suggested by Eq. (5), are plotted as a function of Weber number in Fig. 8. Measurements are shown for all of the drop liquids over the test range of the shear breakup regime, $100 < We < 600$, along with the fitted predictions of Eq. (5). The correlation for u_b'/u_0 is relatively independent of Weber number over this range and is in fair agreement with Eq. (5), based on the estimates of t_b/t^* and $\bar{C}_D$ discussed earlier.

The velocity measurements indicated that the relative velocity of the core drop at the end of breakup was 30–40% lower than the initial relative velocity. This implied that the local Weber numbers of the core drop when breakup ended generally were greater than the critical Weber number for the onset of drop breakup due to shock-wave disturbances ($We = 13$). Thus, the criterion for the end of drop stripping from the core drop differs from the criterion for the onset of breakup.

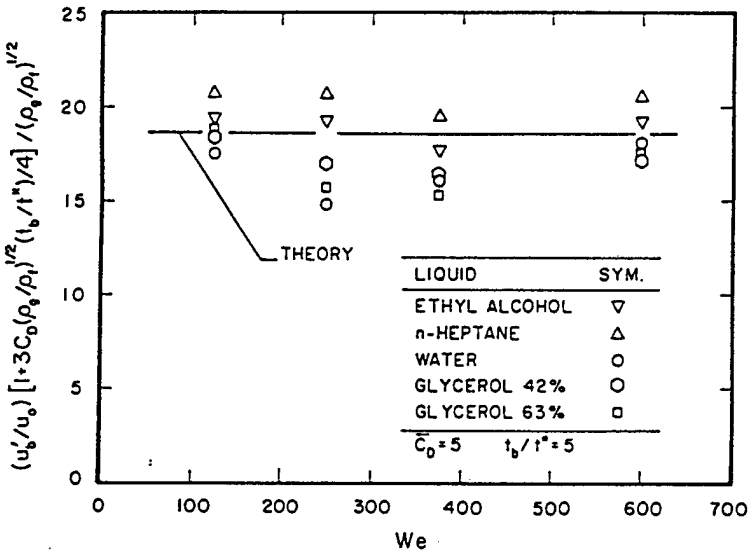

Fig. 8 Velocities of the core drop at the end of shear breakup.

The dynamic state of a drop at the start of secondary breakup, where the drop is round and the drop liquid is motionless, clearly differs from the state of the core drop when shear breakup ends, where the drop is deformed and liquid motion associated with drop stripping is present. Thus, it is not surprising that local Weber numbers of the core drop at the end of shear breakup were different from (and generally exceeded) the critical Weber number associated with the onset of secondary breakup. Instead, conditions defining the end of drop stripping for shear breakup appear to be related more closely to the onset of breakup for more gradual drop motions, like the breakup of freely falling drops. This correspondence is exploited in the following to find a criterion for the end of core drop stripping and a method for estimating the size of the core drop at this condition.

The deformation and size of freely falling drops generally are correlated in terms of the Eötövs number *Eo*. The appropriate expression when the drop acceleration a is due to gas motion relative to the drop is as follows[5]:

$$Eo = a|\rho_f - \rho_g|d^2/\sigma = a\rho_f d^2/\sigma \tag{7}$$

where the latter approximation follows because $\rho_f/\rho_g \gg 1$ for present test conditions. It is anticipated that drop stripping ends when a critical value of Eötvös number Eo_{cr} is reached, based on the behavior of freely falling drops. The values of Eo_{cr} were found for all shear breakup conditions, as defined in Refs. 11 and 12, and are plotted as a function of Weber number in Fig. 9. The critical Eötvös number of the core drop at the end of shear breakup is seen to be relatively independent of Weber number and liquid type over the range of the measurements, yielding a mean value, $Eo_{cr} = 16$. This behavior also is similar to the breakup requirements of freely falling drops, as discussed later.

The previous considerations suggest that Weber number, Eötvös number, and time all are factors in drop breakup events at low-Ohnesorge number. These interactions are highlighted by the local values of critical Weber number, critical Eötvös number, and t_{cr}/t^* for various breakup events summarized in Table 1.

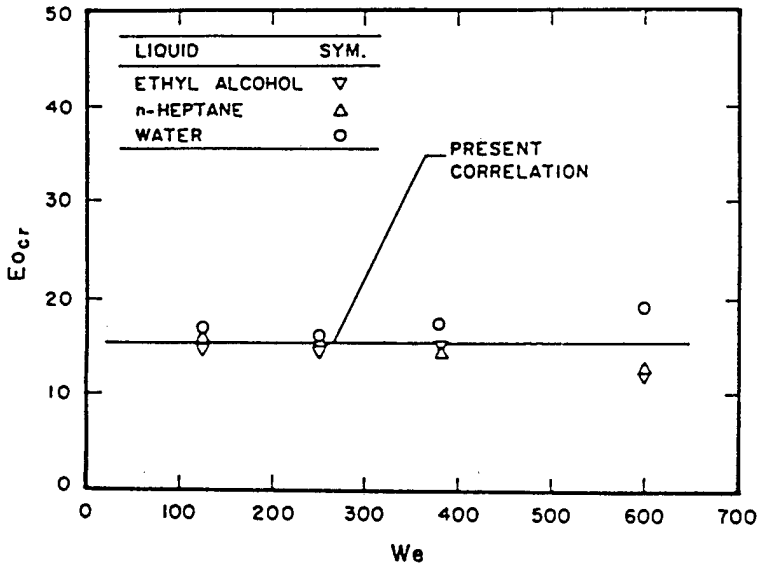

Fig. 9 Critical Eötvös number of the core drop at the end of shear breakup.

For abrupt disturbances, like the onset of secondary breakup due to shock-wave disturbances, local values of critical Weber numbers and critical Eötvös numbers were estimated at the time of breakup using measured values of drop drag in the deformation period.[11,12] Thus, these values are lower than criteria normally given for breakup regime transitions due to drop acceleration prior to the onset of breakup. Similar to the normalized breakup time, the normalized time at the onset of breakup for shock-wave disturbances is a constant over a wide range of Weber number, $t_{cr}/t^* = 1.6$. For this process, drops in the deformation period have local values of Weber and Eötvös numbers that exceed the limits for the onset of breakup, however, breakup does not begin until the drop has had time to deform and achieve a dynamical condition in the liquid that allows drops to separate from the parent drop. The characteristics of critical Weber number, critical Eötvös number and t_{cr}/t^* are somewhat different for gradual disturbances.[33–36] In the case

Table 1 Criteria for secondary breakup processes[a]

Process	We_{cr}	Eo_{cr}	t_{cr}/t^*
Abrupt (shock-wave) disturbances:			
Start of bag breakup, in gases	8–23	24–70	1.6
Start of multimode breakup, in gases	23–53	70–160	1.6
Start of shear breakup, in gases	53 <	160 <	1.6
Gradual disturbances:			
Start of bag breakup, in gases[b]	11–13	11	large
Start of bag breakup, in liquids[b]	7–9	15	large
End of shear breakup, in gases	8–29[c]	16	5.5

[a] $Oh < 0.05$, We_{cr} and Eo_{cr} subsequently increase with increasing Ohnesorge number.
[b] Freely falling drops in a motionless environment, from Refs. 33–36.
[c] Present test range with wider range probable.

of bag breakup for a freely falling drop, Eötvös number, based on the actual drop acceleration, is a maximum at the start of free fall, whereas t_{cr}/t^* is large due to the relatively slow acceleration of the drop. Thus, liquid properties are roughly quasisteady at each relative velocity condition and breakup only occurs when forces on the drop surface due to drag are too large to be stabilized by surface tension, i.e., when the Weber number of the drop reaches a critical value. Finally, the end of drop stripping for shear breakup also involves near quasisteady liquid behavior with the dynamical state of the drop being stabilized by surface tension once the forces on the surface, represented by the drop acceleration, became lower than a critical value represented by the critical Eötvös number. A range of critical Weber number is associated with this condition due to the large variation of the drag coefficient with the degree of deformation of the drop. Thus, various breakup events are associated with required minimum values of Weber number, Eötvös number, and time, with one of these parameters frequently serving as the controlling parameter for a particular process.

7. *Drop Velocities*

The last aspect of secondary breakup considered was the drop-size/velocity correlation at the completion of secondary breakup. These results will include all of the drops in the bag and multimode breakup regimes. The core drop will be excluded in the shear breakup regime, however, because its properties have already been established. A simplified analysis, similar to the approach used for core drop velocities, was used to assist the correlation of drop velocity data.[11,12] Although the analysis was rather crude, it did yield results that were useful for correlating the velocity measurements. Similar to consideration of core drop velocities, attention was limited to streamwise drop velocities.

The drop-size/velocity correlation based on the variables from the simplified analysis is plotted in Fig. 10. The test results involve a variety of drop liquids over the bag, multimode, and shear breakup regimes. Results for the core drops have been shown as dark symbols, for comparison purposes, but they are not included in the following drop-size/velocity correlation. The measured results clearly are independent of the breakup regime and can be correlated reasonably well using the following empirical fit based on the simplified analysis[11,12]:

$$u_0/u_b - 1 = 2.7\left[(\rho_g/\rho_f)^{1/2} d_0/d\right]^{2/3} \tag{8}$$

Equation (8) appears to be rather robust over the three breakup regimes, the range of liquid types, and the flow conditions considered during the present experiments. Even the results for core drops are in fair agreement with Eq. (8), however, the specific relationships for core drops discussed earlier provide a better estimate of their velocities. Additionally, the results indicate that relative velocities are reduced 30–70% over the period of breakup, with the smallest drops experiencing the largest reduction of relative velocity due to their smaller relaxation times. Finally, this variation of drop velocities with size implies that the secondary breakup process extends over a considerable region of space; for example, core drops move 30–40 initial droplet diameters during the period of breakup.[11] Thus, secondary breakup corresponds to a rate process, somewhat like drop vaporization, rather than to an instantaneous process that can be characterized by jump conditions.

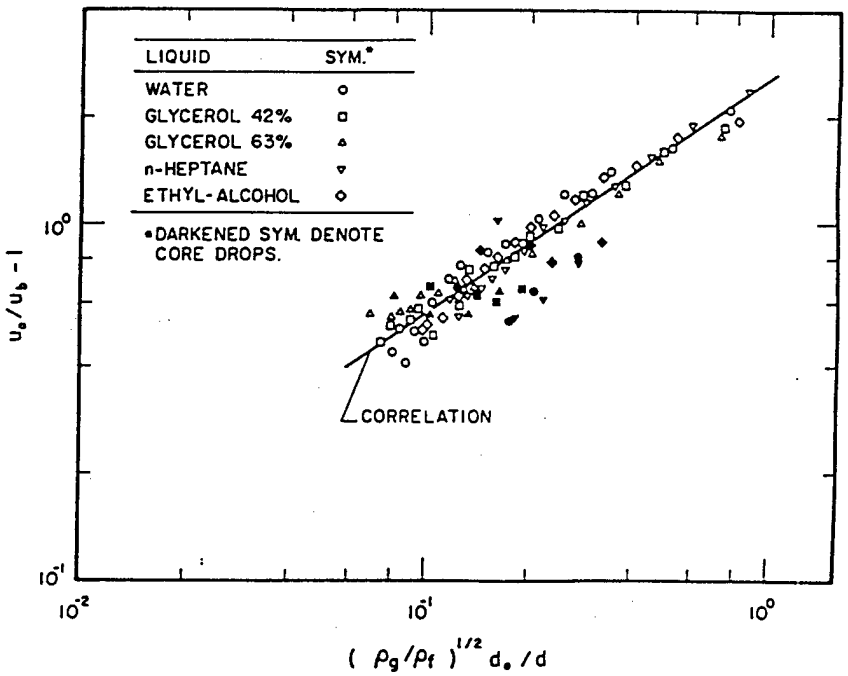

Fig. 10 Correlation of drop velocities with drop size at the end of secondary breakup.

D. Conclusions

Drop deformation and secondary breakup after shock-wave initiated disturbances were studied, considering a variety of liquids in air at normal temperature and pressure ($We = 0.5$–600, $Oh = 0.006$–600, $\rho_f/\rho_g = 580$–12000, and $Re = 340$–15760). The major conclusions of the study are as follows.

1) Drop deformation and breakup begin at $We \sim 1$ and 10, respectively, at low Ohnesorge number. Effects of liquid viscosity, however, inhibit deformation and breakup at high Ohnesorge numbers, e.g., for $We < 1000$, breakup and deformation were no longer possible for $Oh > 10$ and 1000, respectively. This inhibition of deformation and breakup should be important for high-pressure combustion processes where drops reach large Ohnesorge numbers as the liquid surfaces approach the thermodynamic critical point. see Fig. 1.

2) Drop size distributions after secondary breakup satisfy the universal root normal distribution of Simmons[31] with $MMD/SMD = 1.2$, similar to other observations in dense sprays and after primary breakup.[1,2,13] An exception was shear breakup where the core drop must be treated separately. Thus, the size distribution is completely defined by the Sauter mean diameter alone, see Fig. 5.

3) The Sauter mean diameter after secondary breakup could be correlated in terms of a characteristic liquid boundary-layer thickness for all three breakup regimes, see Fig. 7 and Eq. (4).

4) The streamwise velocity and size of the core drop after shear breakup were correlated successfully based on simplified considerations of drop motion during breakup, and the observation that the Eötvös number at the end of drop stripping was a constant, i.e., $Eo_{cr} = 16$, see Figs. 8 and 9 and Eq. (5).

5) The relative streamwise velocities of the drop liquid are significantly reduced during secondary breakup (30–70%, depending on drop size) due to the large drag coefficients during the drop deformation stage and the reduced relaxation times of smaller drops. These effects were correlated successfully based on variables found from simplified analysis of drop motion, see Fig. 10 and Eq. (8).

6) At low Ohnesorge numbers, criteria for various drop breakup processes can be represented by critical values of Weber number, Eötvös number, and t/t^*. Although certain minimum values are required for all three parameters, reaching a critical local value of one of the parameters tends to control the onset of particular breakup events: t_{cr}/t^* for the onset of breakup after a shock-wave disturbance, critical Weber number for the onset of breakup of a freely falling drop, and critical Eötvös number for the end of drop stripping from the core drop during shear breakup.

Aside from the deformation and breakup regime map, the present findings generally were limited to $Oh < 0.039$, with results concerning core drop properties limited to $Oh < 0.011$. Increasing the Ohnesorge number tends to impede drop deformation and breakup processes and should modify secondary breakup behavior considerably from the results observed during the present study. The liquid/gas density ratios of present work also were relatively limited and are most appropriate for sprays at atmospheric pressure. Effects of both Ohnesorge number and ρ_f/ρ_g clearly merit additional study in order to better understand secondary breakup properties for practical combusting sprays, particularly at the conditions of liquid rocket engines. Finally, the rate aspects of secondary breakup, e.g., the evolution of dispersed drop liquid as a function of time, needs to be explored because secondary breakup extends over a significant region in space and time and is not completely characterized by jump conditions.

III. Turbulent Primary Breakup

A. Introduction

Primary breakup to form drops near liquid surfaces is an important fundamental process of sprays. Unfortunately, current understanding of primary breakup is limited due to problems of observing the process in dense spray environments, effects of secondary breakup that modify drop size distributions prior to the drop field reaching conditions where drop sizes can be measured readily, and effects of liquid-phase disturbances that can vastly alter primary breakup properties. Recently, pulsed holography techniques have provided optical access to primary breakup properties; thus, findings using these methods will be discussed in the following.[13–15] This work has been limited to primary breakup along the surfaces of round liquid jets in still gases. This region corresponds to the near-injector dense-spray region of pressure-atomized sprays for atomization breakup conditions, in the absence of significant gas velocities relative to the injector passage.

Past studies of pressure-atomized sprays have established that spray properties are influenced by turbulence at the jet exit. First of all, the early studies of pressure atomization by De Juhasz et al.[37] and Lee and Spencer[38] showed that both atomization quality and mixing rates differed for laminar and turbulent flow at the jet exit. Next, Grant and Middleman[39] and Phinney[40] observed that jet stability and the onset of breakup were affected by turbulence at the jet exit as well. Additionally, Hiroyasu et al.[41] studied the length of the all-liquid core near the

jet exit, which resembles the potential core region of single-phase jets. They conclude that turbulence generated in the flow passage has a significant effect on jet breakup properties, with even relatively short injectors exhibiting effects of turbulence due to disturbances generated at the reattachment points of separated flow regions. Chehroudi et al.[42] criticized the measurements of all-liquid core lengths of Hiroyasu et al.,[41] typically finding values roughly half as long. Nevertheless, several other studies with reasonably good characterization of turbulence properties at the jet exit and alternative methods for measuring all-liquid core lengths and jet properties also have reported effects of jet exit turbulence on liquid jet breakup properties.[43–49]

The recent studies of Ruff et al.[1,2,43] and Tseng et al.[44,45] also have helped to quantify effects of turbulence at the jet exit on the mixing rates and structure of the dispersed phase region of pressure-atomized sprays. These studies involved liquid jets in still air at various pressures with both nonturbulent slug flow and fully developed turbulent pipe flow at the jet exit. Measurements of liquid volume fraction distributions showed much faster mixing rates for fully developed turbulent pipe flow than for nonturbulent slug flow. Additionally, drop sizes after primary breakup were larger for turbulent than nonturbulent liquids even though the other properties of these flows were nearly identical. Finally, drop sizes were relatively independent of liquid/gas density ratios for values greater than 500. However, drop sizes progressively decreased as liquid/gas density ratios were reduced below 500, so that aerodynamic effects appear to be limited to this low-density ratio regime.

Other studies also found that disturbances within the liquid phase, i.e., the presence of liquid turbulence, has dominated observations of breakup in pressure-atomized sprays and that aerodynamic effects are not very important at liquid/gas density ratios typical of observations at normal pressure and temperature. First of all, Hoyt and Taylor[46–48] found that the breakup of liquid jets in air at atmospheric pressure was associated with the presence of turbulent boundary layers along the walls near the jet exit. Additionally, large changes in the aerodynamic environment, including both coflowing the counterflowing air, had little effect on breakup properties. Finally, Wu et al.[49] observed the complete suppression of primary breakup along the liquid surface when boundary layers that develop along the injector passage walls for slug flow conditions are removed; instead, the entire liquid column breaks up as a whole at some distance from the jet exit, due to growth of large-scale disturbances. Thus, even the so-called slug flows considered in the past,[1,2,13,44,45] probably involved effects of breakup enhanced by turbulent boundary layers near the liquid surface.

The preceding review of the literature shows that liquid properties affect primary breakup on the surface of the round jet and that aerodynamic effects, or at least the onset of conditions where they are important, are controlled by the liquid/gas density ratio and are not very significant for surface breakup at liquid/gas density ratios greater than 500. Thus, the objective of the present investigation was to observe primary breakup along liquid surfaces with well-defined liquid disturbance levels at various liquid/gas density ratios. Measurements involved round liquid jets in still gases with fully developed turbulent pipe flow at the jet exit. Effects of flow dynamics and liquid physical properties were studied by considering various gases as the jet environment. The measurements included pulsed shadowgraph photography and holography to find the location of the onset of turbulent primary

breakup as well as drop sizes and velocities after primary breakup as a function of distance from the jet exit. Additionally, phenomenological theories were used to help interpret and correlate the results. The following discussion is brief; more details can be found in Refs. 14, 15, and 49.

B. Experimental Methods

1. Apparatus

The measurements of primary breakup properties along the surface of round liquid jets in gases were carried out using an injector within a windowed test chamber. The injector consisted of a pneumatically driven piston/cylinder arrangement containing a 600-ml sample of the test liquid. The outlet of the cylinder had a rounded contraction to prevent cavitation, followed by a constant-diameter passage having a length-to-diameter ratio ≥ 41, to yield nearly fully developed turbulent pipe flow at the jet exit. Injection was vertically downward with the liquid collected at the bottom of the test chamber and then discarded.

The windowed test chamber was cylindrical with a diameter of 300 mm and a length of 1370 mm. The chamber could be evacuated and refilled with various gases at pressures of 1 and 2 atm in order to change ρ_f/ρ_g while avoiding problems of cavitation and flashing at low-chamber pressures. Total test times were 200–10,000 ms, which was sufficient due to short flow development and data acquisition times. Jet exit velocities were calibrated using an impact plate.

2. Instrumentation

Instrumentation consisted of pulsed shadowgraph photography and single- and double-pulsed holography to measure drop sizes and velocities. These observations were confined to the region near the liquid surface in order to characterize the outcome of primary breakup. The holocamera was used for pulsed shadowgraph photography, operating in the single-pulse mode with the reference beam blocked to yield a shadowgraph rather than a hologram; these measurements were used to measure primary breakup properties near the onset of breakup. The arrangement of the holocamera as well as measurement techniques were identical to the secondary breakup measurements discussed in Sec. II. Results at each test condition were summed over 20–400 liquid fragments, to provide drop size and velocity correlations.

3. Test Conditions

The experiments involved relatively large, 3.6–9.5-mm-diam, liquid jets in still gases. Test liquids included water, *n*-heptane, and various glycerol mixtures. Test gases included helium, air, and freon 12 at pressures of 1–2 atm. Jet exit velocities were in the range 16–109 m/s, yielding the following ranges of jet and primary breakup dynamic parameters: $\rho_f/\rho_g = 104$–6230, $Re_{fd} = 90{,}000$–$780{,}000$, $We_{gd} = 12$–3790, $We_{fd} = 60{,}000$–$1{,}090{,}000$, and $Oh_d = 0.0011$–0.0052. Most test conditions involved $We > 8$ and $We_{gd} > 40$, which places them in the atomization breakup regime defined by Miesse[52] and Ranz,[53] where primary breakup should begin right at the jet exit. Actually, the onset of primary breakup always occurred at some distance from the jet exit, as will be discussed later in more detail.

C. Presentation of Results on Primary Breakup

1. *Drop Size Distributions*

Drop size distributions after primary breakup were measured for all test conditions. It was found that they satisfied the universal root normal distribution function with the ratio $MMD/SMD = 1.2$, similar to results after secondary breakup, discussed earlier. These results also are consistent with numerous other observations in dense sprays.[1,2,31,43–45] Thus, drop size distributions will be specified by the *SMD* diameter alone in the following.

2. *Drop Velocities*

The measurements of mass- (volume-) averaged streamwise and cross stream drop velocities after primary breakup are plotted as a function of distance from the jet exit in Fig. 11. To highlight potential aerodynamic effects, results for $\rho_f/\rho_g > 500$ are shown as open symbols whereas results for $\rho_f/\rho_g < 500$ are shown as darkened and half-darkened symbols.

The normalized drop velocities illustrated in Fig. 11 provide crude correlations in terms of x/d but other factors probably are involved as well. Near the jet exit, $\bar{u}_p/\bar{u}_0$, has a value of near 0.6, which increases to roughly 0.9 for $x/d > 20$. This behavior is consistent with drop velocities after turbulent primary breakup being roughly the same as streamwise liquid velocities near the liquid surface. Thus, the lower streamwise velocities are expected near the jet exit due to the retarding effect of the passage wall, evolving to higher values farther downstream where liquid velocities become more uniform. Superimposed on this behavior,

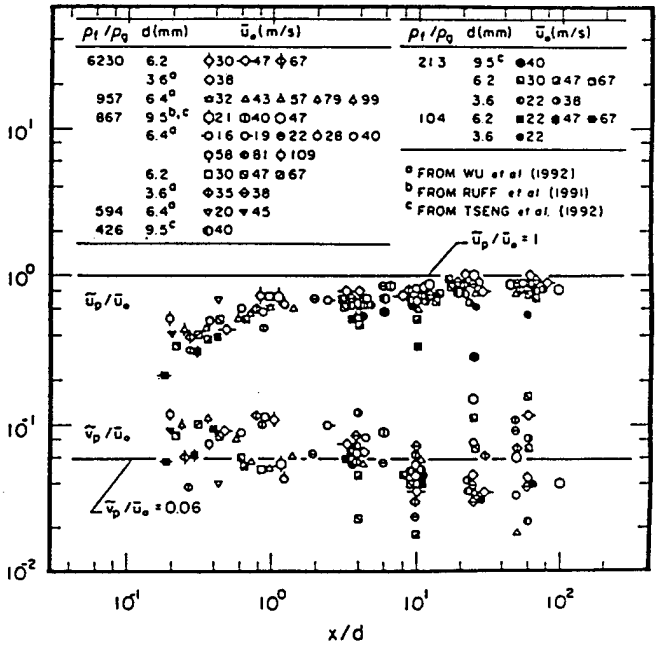

Fig. 11 Mass-averaged drop velocities after primary breakup as a function of distance from the injector exit.

however, is a clear trend that measurements for $\rho_f/\rho_g < 500$ have significantly lower mean streamwise velocities than the higher density ratio conditions—on the average roughly 20–40% lower. This can be attributed to aerodynamic drag if it is recalled that gas velocities near the liquid surface tend to be relatively low because the dispersed-phase region is very dilute (liquid volume fractions are less than 0.1%) so that momentum transfer to the gas phase is not very effective and relative velocities between the phases are large.[1,2]

Similar trends with respect to density variations are much less clear for the cross stream velocity component $\bar{v}_p/\bar{u}_0$ in Fig. 11, which are comparable to cross stream velocity fluctuations in the liquid. In particular, maximum values of $\bar{v}_0'/\bar{u}_0 = 0.058$ for fully developed turbulent pipe flow, even in the region near the wall[50,51] which is comparable to the cross stream drop velocity results seen in Fig. 11. An explanation of why the cross stream velocity component does not exhibit a reduction due to drag at low values of ρ_f/ρ_g, similar to the streamwise velocity component, is provided by an aerodynamic effect other than drag. In particular, the classical aerodynamic theories of primary drop breakup are based on the idea that flow velocities in the radial direction are increased for protuberances from the liquid surface due to acceleration of the gas over the tip of the protuberance,[52-56] which can be seen from the sketch appearing in Fig. 12. This yields a radial pressure drop across the protuberance that should increase the radial velocities of drops near the surface when aerodynamic effects are significant. This mechanism would tend to compensate for drag effects in the radial direction. Thus, it is plausible that radial drop velocities are not significantly changed by the presence of aerodynamic effects within the rather large scatter of the measurements.

3. *Onset of Breakup*

Phenomenological analysis to find drop properties at the onset of breakup was based on the configuration illustrated in Fig. 12. The onset mechanism was

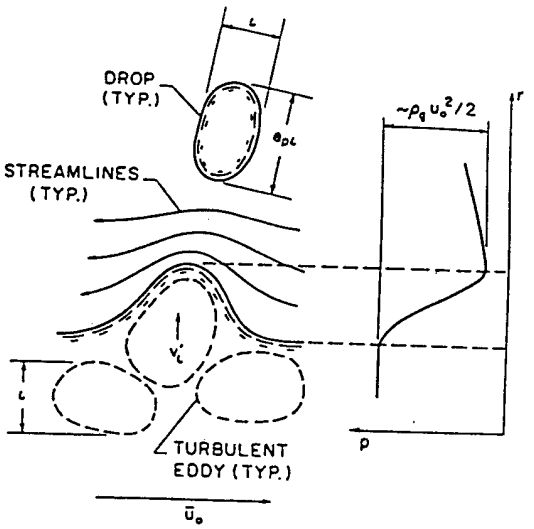

Fig. 12 Aerodynamically enhanced turbulent primary breakup at a liquid surface.

assumed to involve the formation of a drop from a turbulent eddy having a characteristic size ℓ, and a characteristic cross stream velocity relative to the surrounding liquid v_ℓ. The eddy is shown with an elongated shape because length scales in the streamwise direction are larger than in the cross stream direction for turbulent pipe flow.[50,51] The eddy is assumed to be convected in the streamwise direction at the local mean velocity, which is taken to be $\bar{u}_0$ based on the results discussed in connection with Fig. 11. The drop formed by the eddy also is assumed to have a diameter comparable to ℓ.

Drops formed at the onset of turbulent primary breakup are the smallest drops that can be formed by this mechanism.[14] The smallest drops that can be formed are either comparable to the smallest or Kolmogorov scales of turbulence, ℓ_K, or the smallest eddy that has sufficient mechanical energy to provide the surface energy needed to form a drop, whichever is larger. For present test conditions, ℓ_K was in the range 1–10 μm, which is much smaller than the smallest observed drop sizes; therefore, only the second criterion will be considered here, even though the first criterion may be relevant for some applications. The second criterion for the smallest drop that can be formed can be approximately quantified based on energy considerations. The mechanical energy available to form a drop includes the kinetic energy of an eddy of characteristic size, ℓ_i, relative to its surroundings, plus the added mechanical energy due to the pressure drop caused by acceleration of the surrounding gas over the tip of the protuberance, as illustrated in Fig. 12. It is reasonable to assume that ℓ_i is in the inertial range of the turbulence spectrum, which implies[53]

$$v\ell_i \sim \bar{v}_0'(\bar{v}_0'\ell_i/\Lambda)^{1/3} \tag{9}$$

where variations of turbulence properties in the liquid have been ignored, similar to Ref. 14. Formulation of these ideas, setting $SMD_i \sim \ell_i$, and assuming that turbulence properties in the liquid can be approximated by jet exit turbulence properties, yields the following implicit equation for SMD_i (Ref. 15):

$$\frac{SMD_i}{\Lambda}\left[1 + C_{sa}\left(\frac{\rho_g}{\rho_f}\right)\left(\frac{\bar{u}_0}{\bar{v}_0'}\right)^2\left(\frac{\Lambda}{SMD_i}\right)^{2/3}\right]^{3/5} = C_{si}\left(\frac{\bar{u}_0}{\bar{v}_0'}\right)^{6/5} We_{f\Lambda}^{-3/5} \tag{10}$$

where C_{sa} and C_{si} are empirical proportionality constants. With fully developed turbulent pipe flow at the jet exit, $\bar{v}_0'/\bar{u}_0$ essentially is a constant[50,51]; therefore, the effect of the aerodynamic enhancement term in Eq. (10) largely is controlled by the liquid/gas density ratio. This helps support past observations that the onset of aerodynamic effects depends on the liquid/gas density ratio rather than dynamic properties related to the liquid velocity.[14,45]

Present measurements of SMD_i are plotted in terms of the variables of Eq. (10) in Fig. 13. In doing this, C_{sa} was optimized to a value of 0.04, based on taking $\bar{v}_0'/\bar{u}_0 = 0.058$ for fully developed turbulent pipe flow.[51] In addition to present results, measurements from Ref. 14 also are shown on the plot, which involve a variety of liquids for conditions where aerodynamic effects are not important. As before, test conditions for $\rho_f/\rho_g > 500$, where aerodynamic effects could not be identified, are shown as open symbols. The correlation of the data for all conditions generally is within the scatter anticipated from experimental uncertainties. The power of $We_{f\Lambda}$ from the correlation of the data is not $-3/5$ as suggested by

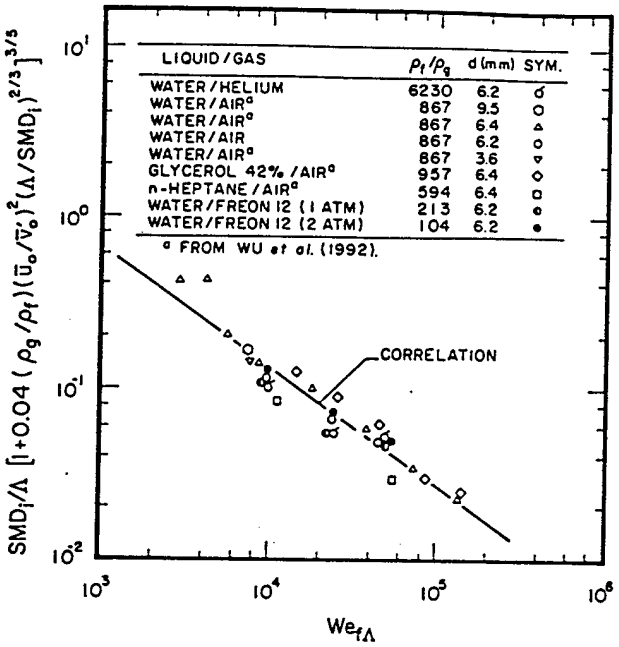

Fig. 13 ***SMD*** **at the initiation of turbulent primary breakup as a function of** $We_{f\lambda}$.

Eq. (9), however, and can be represented by the following empirical fit that is shown on the plot:

$$\frac{SMD_i}{\Lambda}\left[1+0.04\left(\frac{\rho_g}{\rho_f}\right)\left(\frac{\bar{u}_0}{\bar{v}_0'}\right)^2\left(\frac{\Lambda}{SMD_i}\right)^{2/3}\right]^{3/5}=76We_{f\Lambda}^{-0.69} \qquad (11)$$

Given SMD_i, the approach to find the location of the onset of turbulent primary breakup, x_i, was similar to Ref. 14. To find x_i, it is assumed that the drop-forming eddy convects along the liquid surface with a streamwise velocity $\bar{u}_0$ based on the results of Fig. 11. In addition, it was assumed that the onset of breakup was given by the time for growth of ligaments until their breakup into drops, taken to be the Rayleigh breakup time. The Rayleigh breakup time for a ligament of length ℓ_i, assuming that effects of liquid viscosity are small, is proportional to $(\rho_f \ell_i^3/\sigma)^{1/2}$, as discussed in Refs. 13 and 14. This yields the following expression for x_i (Ref. 15):

$$\frac{x_i}{\Lambda}\left[1+C_{sa}\left(\frac{\rho_g}{\rho_f}\right)\left(\frac{\bar{u}_0}{\bar{v}_0'}\right)^2\left(\frac{\Lambda}{SMD_i}\right)^{2/3}\right]^{9/10}=C_{xi}\left(\frac{\bar{u}_0}{\bar{v}_0'}\right)^{9/5}We_{f\Lambda}^{-4/10} \qquad (12)$$

where C_{xi} is a constant of proportionality. Similar to Eq. (9), aerodynamic effects on x_i from Eq. (12) are controlled by the liquid/gas density ratio alone.

Both the present measurements of x_i and those of Ref. 14 are plotted in terms of the variables of Eq. (12) in Fig. 14, adopting $C_{sa} = 0.04$ as before. The correlation of the data over the full range of aerodynamic effects is reasonably good in view of

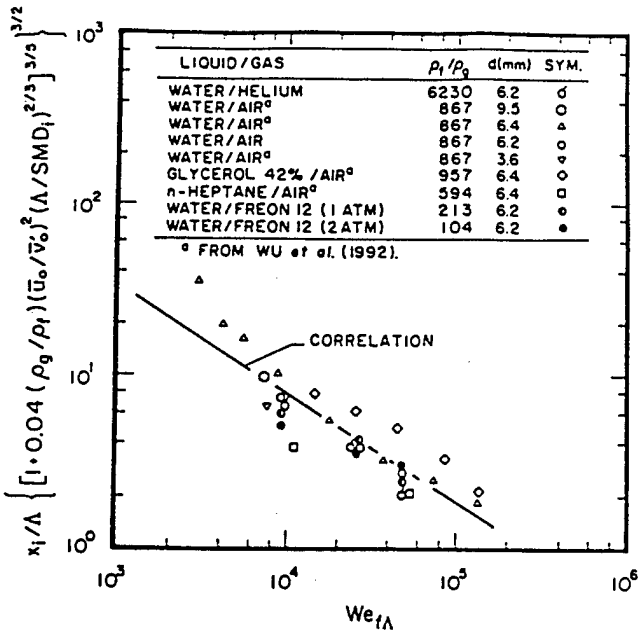

Fig. 14 Length to initiate turbulent primary breakup as a function $We_{f\Lambda}$.

the relatively large experimental uncertainties of x_i. As before, however, the power of $We_{f\Lambda}$ for the correlation of the data is not -0.4 as suggested by Eq. (12) but can be represented better by the following empirical expression, which is shown on the plot:

$$\frac{x_i}{\Lambda}\left[1+0.04\left(\frac{\rho_g}{\rho_f}\right)\left(\frac{\bar{u}_0}{\bar{v}_0'}\right)^2\left(\frac{\Lambda}{SMD_i}\right)^{2/3}\right]^{9/10} = 2570We_{f\Lambda}^{-0.63} \qquad (13)$$

4. Drop Sizes

Aerodynamic secondary breakup times scale proportional to $\ell_i(\rho_f/\rho_g)^{1/2}/\bar{u}_0$ for an object of size ℓ_i, if the velocity of the gas near the liquid surface is assumed to be small.[10] Thus, for conditions where aerodynamic effects are important, Rayleigh breakup times increase more rapidly than do secondary breakup times as ℓ_i, increases. This implies a tendency for secondary and primary breakup to occur simultaneously, or to merge, as distance from the jet exit increases—a mechanism that dominated drop sizes near the liquid surface when aerodynamic effects are important, except near the onset of turbulent primary breakup.

Within the merged primary and secondary breakup regime, turbulent primary breakup properties will be found using the results of Ref. 14 whereas aerodynamic secondary breakup properties will be found from Eq. (4). The variation of *SMD* with distance from the jet exit for turbulent primary breakup was found assuming that the *SMD* was proportional to the largest drop that could be formed at a particular position with the time of breakup determined from the Rayleigh breakup

time. Thus, the combined formulation yields the following expression for the *SMD* after merged primary and secondary breakup[15]:

$$\rho_g SMD\bar{u}_0^2/\sigma = C_s C_{sx}^{1/2}(x/\Lambda)^{1/3}(\rho_g/\rho_f)^{3/4}We_{f\Lambda}^{5/6}Re_{f\Lambda}^{-1/2} \tag{14}$$

where C_s and C_{sx} are empirical constants.

Present measurements of aerodynamic turbulent primary breakup, along with some results from Ref. 45, are plotted according to the variables of Eq. (14) in Fig. 15. The following best fit correlation of present measurements also is shown in the plot:

$$\rho_g SMD\bar{u}_0^2/\sigma = 12.0\left[(x/\Lambda)^{1/3}(\rho_g/\rho_f)^{3/4}We_{f\Lambda}^{5/6}Re_{f\Lambda}^{-1/2}\right]^{1.17} \tag{15}$$

Additionally, adopting the best fit values of C_s and C_{sx} in Eq. (14), the following theoretical prediction for *SMD* as a function of distance is obtained:

$$\rho_g SMD\bar{u}_0^2/\sigma = 12.9(x/\Lambda)^{1/3}(\rho_g/\rho_f)^{3/2}We_{f\Lambda}^{5/6}Re_{f\Lambda}^{-1/2} \tag{16}$$

with the standard deviation of the constant of 21%. Thus, the differences between Eqs. (15) and (16) are not statistically significant, within experimental uncertainties. Present measurements also are in good agreement with the predictions. The measurements of Tseng et al.[45] however, definitely yield smaller drop sizes after merged primary and secondary breakup. An explanation of this behavior is that these flows involved the highest concentrations of drops after turbulent primary breakup within the database, so that drop properties near the liquid surface could be influenced by small drops migrating from other parts of the multiphase mixing layer due to turbulent dispersion.

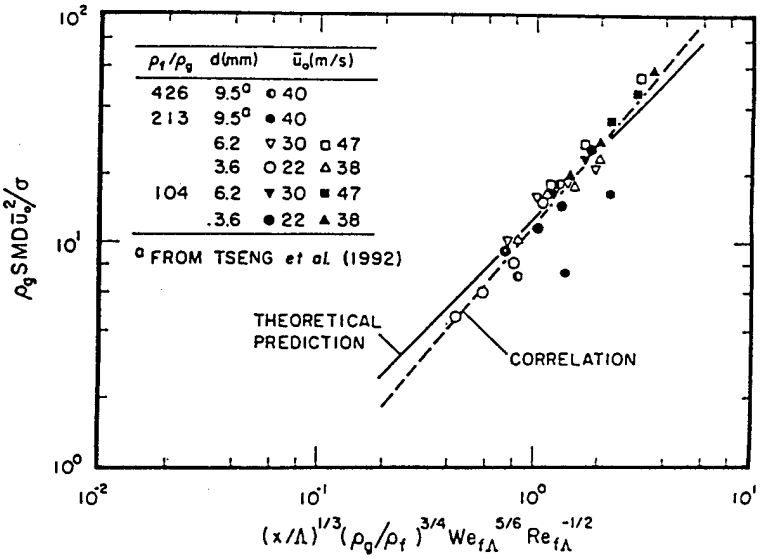

Fig. 15 ***SMD*** **after merged turbulent primary and secondary breakup as a function of distance from the injector exit.**

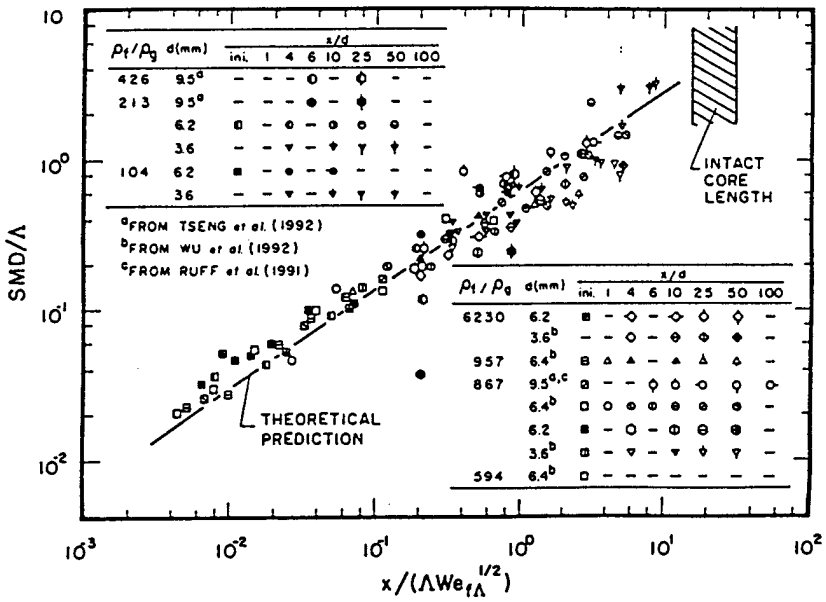

Fig. 16 ***SMD*** **after turbulent primary breakup as a function of distance from the injector exit, including inversion of merged secondary breakup effects.**

The consistency of the merged primary and secondary breakup process also can be examined by inverting the process; namely, by computing the drop sizes that should have been observed after primary breakup in the absence of aerodynamic effects, SMD_p, and comparing these results with other measurements at similar conditions. To do this, the nonaerodynamic turbulent primary breakup correlation was refitted to yield[14]

$$SMD_p/\Lambda = 0.65\left[x/\left(\Lambda We_{f\Lambda}^{1/2}\right)\right]^{2/3} \tag{17}$$

This implies reasonably consistent measurements of turbulent primary breakup with respect to Ref. 14, where the constant of Eq. (17) was 0.64. Then from the fit of the measurements illustrated in Fig. 15, the relationship between *SMD* and SMD_p is given by

$$SMD_p/\Lambda = 3.91 \times 10^{-3}(\rho_g/\rho_f)^{1/2} Re_{f\Lambda}(SMD/\Lambda)^2 \tag{18}$$

The measurements illustrated in Fig. 15, where primary and secondary breakup occurred, were inverted to get SMD_p, using Eq. (18). These results are plotted in Fig. 16, along with previous results for turbulent primary breakup where aerodynamic effects are not important from Ref. 14. Aside from the few results of Ref. 45 mentioned earlier in connection with Fig. 15, the inverted aerodynamic turbulent primary breakup measurements are seen to be in good agreement with the other results, supporting the idea of merging of primary and secondary breakup.

An interesting feature of the results of Fig. 16 is the progressive increase of *SMD* with distance from the injector. The largest *SMD* values observed in Fig. 16 approach the order of magnitude of the radial integral scale of the turbulence.

Whereas larger drops are feasible for liquid surfaces in general, this is not the case for round liquid jets due to the finite length of the liquid core. This is indicated in the figure using the correlation for liquid core length from Grant and Middleman.[39] The fact that the *SMD* approaches Λ near the end of the liquid core is consistent with the liquid column breaking up as a whole in this region.

5. *Breakup Regimes*

Present measurements suggested three regimes of turbulent primary breakup: 1) nonaerodynamic turbulent primary breakup, 2) aerodynamically enhanced turbulent primary breakup, observed at onset conditions, and 3) aerodynamic turbulent primary breakup, which involves merging of turbulent primary and secondary breakup. The results also indicted that the boundaries of these regimes are fixed by the liquid/gas density ratio and the relative magnitudes of characteristic Rayleigh breakup times of ligaments and the secondary breakup times of liquid fragments. The breakup times used to define these regimes were based on the *SMD* after primary breakup, or after the primary breakup stage of merged primary and secondary breakup, for conditions beyond the onset of breakup for present data. Thus, the characteristic Rayleigh breakup time was taken to be $\tau_R \sim (\rho_f SMD^3/\sigma)^{1/2}$, whereas the characteristic secondary breakup time was taken to be $\tau_b \sim (\rho_f/\rho_g)^{1/2}\ SMD/\bar{u}_0$. Then using Eq. (18) to eliminate *SMD* from the ratio, the characteristic time ratio was taken to be

$$\tau_R/\tau_b = (\rho_g/\rho_f)^{1/2}(x We_{f\Lambda}/\Lambda)^{1/3} \tag{19}$$

The resulting turbulent primary breakup regimes based on present measurements, as well as those from Refs. 1, 14, and 45, are illustrated in terms of ρ_f/ρ_g and τ_R/τ_b in Fig. 17. The total set of measurements yields $\rho_f/\rho_g = 500$ as the aerodynamic/nonaerodynamic transition, and $\tau_R/\tau_b = 4$ as the enhanced-aerodynamic/merged transition.

D. Conclusions

Primary breakup along the surface turbulent liquids was studied, considering liquid jets in still gases with fully developed turbulent pipe flow at the jet exit ($\rho_f/\rho_g = 104$–6230, $Re_{fd} = 90{,}000$–$780{,}000$, $We_{gd} = 12$–3790, $We_{fd} = 60{,}000$–$1{,}090{,}000$, and $Oh_d = 0.0011$–0.0052). The major conclusions of the study are as follows:

1) The presence of aerodynamic phenomena for turbulent primary breakup largely is controlled by the liquid/gas density ratio. When this ratio is less than 500, aerodynamic phenomena affect both conditions at the onset of breakup and drop sizes and velocities (to a lesser extent) after breakup.

2) Aerodynamic enhancement of the onset of turbulent primary breakup was due to the aerodynamic pressure reduction over the tips of protruding liquid elements. This effect assists the kinetic energy of a corresponding liquid eddy relative to its surroundings to provide the surface tension energy needed to form a drop, thus allowing smaller drops to form. Phenomenological analysis based on these ideas yielded reasonable correlations of onset properties, Eqs. (11) and (13), for the enhanced aerodynamic breakup regime (see Figs. 13 and 14).

3) For conditions where secondary breakup times become small in comparison to Rayleigh breakup of turbulence-induced ligaments protruding from the surface,

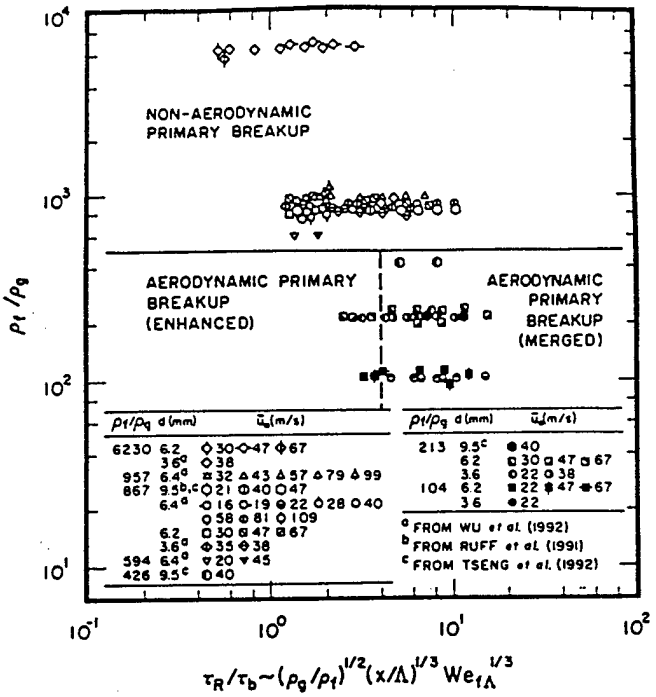

Fig. 17 Turbulent primary breakup regime map.

processes of primary and secondary breakup merge yielding smaller drops than when aerodynamic effects are absent. The reduction of drop sizes at these conditions correlated reasonably well with results for the secondary breakup of drops due to shock disturbances, yielding the correlation of Eq. (16), see Fig. 15.

4) Drop size distributions after aerodynamic turbulent primary breakup approximated Simmons'[31] universal root normal distribution with $MMD/SMD = 1.2$, similar to observations of other drop breakup processes as well as drops in the multiphase mixing layers of pressure-atomized sprays. Additionally, mass-averaged drop velocities after aerodynamic turbulent primary breakup approximate mean and rms velocity fluctuations of the liquid in the streamwise and cross stream directions, respectively, although there was a tendency for streamwise velocities to be somewhat reduced by aerodynamic effects.

A major issue still open involves primary breakup of nonturbulent liquids and the relevance of the classical primary breakup theories of Taylor[54] and Levich.[55] Current findings, and the observations of others,[46–49] all indicate that it is difficult to observe the nonturbulent primary breakup mechanism. The main problems are effects of liquid disturbances, the intrusion of secondary breakup, and weak aerodynamic effects for most liquids at normal pressure and temperature where measurements are most convenient. Until these experimental difficulties are resolved, understanding of this important primary breakup mechanism will remain limited. This is problematical because the classical nonturbulent aerodynamic primary breakup mechanism is likely to dominate breakup processes within combusting sprays at the pressures typically found in practical transportation and

propulsion systems.[3–9] Finally, the rate properties of primary breakup are not well known, which limits capabilities for rational models of the near-injector region of sprays.

Acknowledgments

This research was sponsored by the Air Force Office of Scientific Research, Grant 89-0516 and F49620-92-J-0399, under the technical management of J. M. Tishkoff; and by the Office of Naval Research, Grant N00014-89-J-1199, under the technical management of G.D. Roy. The U.S. Government is authorized to reproduce and distribute copies for governmental purposes notwithstanding any copyright notation thereon.

References

[1]Ruff, G. A., Bernal, L. P., and Faeth, G. M., "Structure of the Near-Injector Region of Non-Evaporating Pressure-Atomized Sprays," *Journal of Propulsion and Power,* Vol. 7, No. 2, 1991, pp. 221–230.

[2]Ruff, G. A., Wu, P.-K., Bernal, L. P., and Faeth, G.M., "Continuous- and Dispersed-Phase Structure of Dense Non-Evaporating Pressure-Atomized Sprays," *Journal of Propulsion and Power,* Vol. 8, No. 2, 1992, pp. 280–289.

[3]Harrje, D. T., and Reardon, F. H., "Liquid Rocket Combustion Instability," NASA SP-194, 1972, pp. 49–55.

[4]Giffen, E., and Muraszew, A., *The Atomization of Liquid Fuels,* Wiley, New York, 1953.

[5]Clift, R., Grace, J. R., and Weber, M. E., *Bubbles, Drops and Particles,* Academic, New York, 1978, pp. 26, 339–347.

[6]Lefebvre, A. H., *Atomization and Sprays,* Hemisphere, New York, 1989, pp. 27–78, 201–272.

[7]Chigier, N. A., "The Physics at Atomization," *Proceedings of the Fifth International Conference on Liquid Atomization and Spray Systems,* NIST SP-813, National Inst. of Standards and Technology, Washington, DC, 1991, pp. 1–15.

[8]Faeth, G. M., "Mixing, Transport and Combustion in Sprays," *Progress in Energy and Combustion Science,* Vol. 13, No. 4, 1987, pp. 293–345.

[9]Faeth, G. M., "Structure and Atomization Properties of Dense Turbulent Sprays," *Twenty-Third Symposium (International) on Combustion,* Combustion Inst., Pittsburgh, PA, 1990, pp. 1345–1352.

[10]Hsiang, L.-P., and Faeth, G. M., "Near-Limit Drop Deformation and Secondary Breakup," *International Journal of Multiphase Flow,* Vol. 18, No. 5, 1992, pp. 635–652.

[11]Hsiang, L.-P., and Faeth, G. M., "Drop Properties After Secondary Breakup," *International Journal of Multiphase Flow,* Vol. 19, No. 5, 1993, pp. 721–735.

[12]Hsiang, L.-P., and Faeth, G. M., "Drop Deformation and Breakup Due to Shock Wave and Steady Disturbances," *International Journal of Multiphase Flow* (to be published).

[13]Wu, P.-K., Ruff, G. A., and Faeth, G. M., "Primary Breakup in Liquid/Gas Mixing Layers," *Atomization and Sprays,* Vol. 1, No. 4, 1991, pp. 421–440.

[14]Wu, P.-K., Tseng, L.-K., and Faeth, G. M., "Primary Breakup in Gas/Liquid Mixing Layers for Turbulent Liquids," *Atomization and Sprays,* Vol. 2, No. 3, 1992, pp. 295–317.

[15]Wu, P.-K., and Faeth, G. M, "Aerodynamic Effects on Primary Breakup of Turbulent Liquids," *Atomization and Sprays,* Vol. 3, No. 3, 1993, pp. 265–289.

[16]Hinze, J. O., "Fundamentals of the Hydrodynamic Mechanism of Splitting in Dispersion Processes," *AIChE Journal,* Vol. 1, No. 3, 1955, pp. 289–295.

[17]Hanson, A. R., Domich, E. G., and Adams, H. S., "Shock-Tube Investigation of the Breakup of Drops by Air Blasts," *Physics of Fluids*, Vol. 6, No. 8, 1963, pp. 1070–1080.

[18]Gel'fand, B. E., Gubin, S. A., and Kogarko, S. M., "Various Forms of Drop Fractionation in Shock Waves and Their Special Characteristics," *Inzhenerno-Fizicheskii Zhurnal*, Vol. 27, No. 1, 1974, pp. 119–126.

[19]Krzeczkowski, S. A., "Measurement of Liquid Droplet Disintegration Mechanisms," *International Journal of Multiphase Flow*, Vol. 6, No. 2, 1980, pp. 227–239.

[20]Ranger, A. A., and Nicholls, J. A., "The Aerodynamic Shattering of Liquid Drops," *AIAA Journal*, Vol. 7, No. 2, 1969, pp. 285–290.

[21]Reinecke, W. G., and McKay, W. L., "Experiments on Waterdrop Breakup Behind Mach 3 to 12 Shocks," Sandia Corp. Rept. SC-CR-70-6063, 1969.

[22]Reinecke, W. G., and Waldman, G. D., "A Study of Drop Breakup Behind Strong Shocks with Applications to Flight," Avco Rept. AVSD-0110-70-77, 1970.

[23]Wierzba, A., and Takayama, K., "Experimental Investigation of the Aerodynamic Breakup of Liquid Drops," *AIAA Journal*, Vol. 26, No. 11, 1988, pp. 1329–1335.

[24]Borisov, A. A., Gel'fand, B. E., Natanzon, M. S., and Kossov, O. M., "Droplet Breakup Regimes and Criteria for Their Existence," Inzhenerno-Fizicheskii Zhurna Vol. 40, No. 1, 1981, pp. 64–70.

[25]Loparev, V. P., "Experimental Investigation of the Atomization of Drops of Liquid under Conditions of a Gradual Rise of the External Forces," *Izvestiya Akademii Nauk SSSR, Mekhanika Zhidkosti i Gaza*, No. 3, 1975, pp. 174–178.

[26]Lane, W. R., "Shatter of Drops in Streams of Air," *Industrial Engineering Chemistry*, Vol. 43, 1951, pp. 1312–1317.

[27]Liang, P. Y., Eastes, T. W., and Gharakhari, A., "Computer Simulations of Drop Deformation and Drop Breakup," AIAA Paper 88-3142, 1988.

[28]Simpkins, P. G., and Bales, E. J., "Water-Drop Response to Sudden Accelerations," *Journal of Fluid Mechanics*, Vol. 55, No. 4, 1972, pp. 629–639.

[29]Engel, O. G., "Fragmentation of Waterdrops in the Zone Behind an Air Shock," *Journal of Research of the National Bureau of Standards*, Vol. 6, No. 3, 1958, pp. 245–280.

[30]White, F. M., *Viscous Fluid Flow*, McGraw–Hill, New York, 1974.

[31]Simmons, H. C., "The Correlation of Drop-Size Distributions in Fuel Nozzle Sprays," *Journal of Engineering for Power*, Vol. 99, No. 3, 1977, pp. 309–319.

[32]Belz, M. H., *Statistical Methods in the Process Industries*, Wiley, New York, 1973, pp. 103–104.

[33]Merrington, A. C., and Richardson, E. G., "The Break-Up of Liquid Jets," *Proceedings of Physical Society of London*, Vol. 59, 1947, pp. 1–13.

[34]Finlay, B. A., Ph.D. Thesis, Univ. of Birmingham, England, UK, 1957.

[35]Ryan, R. T., "The Behavior of Large Low-Surface-Tension Water Drops Falling at Terminal Velocity in Air," *Journal of Applied Meterology*, Vol. 15, 1976, pp. 157–165.

[36]Hu, S., and Kintner, R. C., "The Fall of Single Drops Through Water," *AIChE Journal*, Vol. 1, 1955, pp. 42–48.

[37]DeJuhasz, K. J., Zahm, O. F., Jr., and Schweitzer, P. H., "On the Formation and Dispersion of Oil Sprays," Engineering Experiment Station, Bulletin No. 40, Pennsylvania State Univ., University Park, PA, 1932, pp. 63–68.

[38a]Lee, D. W., and Spencer, R. C., "Preliminary Photomicrographic Studies of Fuel Sprays," NACA Tech. Note 424, 1932.

[38b]Lee, D. W., and Spencer, R. C., "Photomicrographic Studies of Fuel Sprays," NACA Rept. 454, 1933.

[39]Grant, R. P., and Middleman, S., "Newtonian Jet Stability," *AIChE Journal*, Vol. 12, No. 4, 1966, pp. 669–678.

[40]Phinney, R. E., "The Breakup of a Turbulent Jet in a Gaseous Atmosphere," *Journal of Fluid Mechanics,* Vol. 60, Pt. 4, 1973, pp. 689–701.

[41a]Hiroyasu, H., Shimizu, M., and Arai, M., "The Breakup of a High Speed Jet in a High Pressure Gaseous Environment," Univ. of Wisconsin, Madison, ICLASS-82.

[41b]Arai, M., Shimizu, M., and Hiroyasu, H., "Break-Up Length and Spray Angle of High Speed Jet," Univ. of Wisconsin, Madison, WI, ICLASS-85, 1985, p. IB/4/1.

[42]Chehroudi, B., Onuma, Y., Chen, S.-H., and Bracco, F. V., "On the Intact Core of Full Cone Sprays," Society of Automotive Engineers, SAE Paper 850126, 1985.

[43]Ruff, G. A., Sagar, A. D., and Faeth, G. M., "Structure of the Near Injector Region of Non-Evaporating Pressure-Atomized Sprays," *AIAA Journal,* Vol. 27, No. 7, 1989, pp. 901–908.

[44]Tseng, L.-K., Ruff, G. A., and Faeth, G. M., "Effects of Ambient Gas Density on the Structure of Liquid Jets in Still Gases," *AIAA Journal,* Vol. 30, No. 6, 1992, pp. 1537–1544.

[45]Tseng, L.-K., Wu, P.-K., and Faeth, G. M., "Dispersed-Phase Structure of Pressure-Atomized Sprays at Various Gas Densities," *Journal of Propulsion and Power,* Vol. 8, No. 6, 1992, pp. 1157–1166.

[46]Hoyt, J. W., and Taylor, J. J., "Waves on Water Jets," *Journal of Fluid Mechanics,* Vol. 88, Pt. 1, 1977, pp. 119–123.

[47]Hoyt, J. W., and Taylor, J. J., "Turbulence Structure in a Water Jet Discharging in Air," *Physics of Fluids,* Vol. 20, Pt. 2, No. 10, 1977, pp. S253–S257.

[48]Hoyt, J. W., and Taylor, J. J., "Effect of Nozzle Boundary Layer on Water Jets Discharging in Air," *Jets and Cavities,* edited by J. H. Kim, O. Furuya and B. R. Parkin, ASME-FED, Vol. 31, American Society of Mechanical Engineers, New York, 1985, pp. 93–100.

[49]Wu, P.-K., Miranda, R. F., and Faeth, G. M., "Effects of Initial Flow Conditions on Primary Breakup of Nonturbulent and Turbulent Liquid Jets," AIAA Paper 94-0561, Jan. 1994.

[50]Schlichting, H., *Boundary Layer Theory,* 7th ed., McGraw–Hill, New York, 1979, p. 599.

[51]Hinze, J. O., *Turbulence,* 2nd ed., McGraw–Hill, New York, 1975, pp. 427 and 724–742.

[52]Miesse, C. C., "Correlation of Experimental Data on the Disintegration of Liquid Jets," *Industrial Engineering Chemistry,* Vol. 47, No. 9, 1955, pp. 1690–1697.

[53]Ranz, W. E., "Some Experiments on Orifice Sprays," *Canadian Journal of Chemical Engineering,* Vol. 36, No. 8, 1958, pp. 175–181.

[54]Taylor, G. I., "Generation of Ripples by Wind Blowing Over a Viscous Liquid," *The Scientific Papers of Sir Geoffrey Ingram Taylor,* edited by G.K. Batchelor, Vol. 3, Cambridge Univ. Press, Cambridge, England, UK, 1963, pp. 244–254.

[55]Levich, V. G., *Physicochemical Hydrodynamics,* Prentice-Hall, Englewood Cliffs, NJ, 1962, pp. 639–646.

[56]Reitz, R. D., and Bracco, F. V., "Mechanism of Atomization of a Liquid Jet," *Physics of Fluids,* Vol. 25, No. 10, 1982, pp. 1730–1742.

[57]Tennekes, H., and Lumley, J. L., *A First Course in Turbulence,* MIT Press, Cambridge, MA, 1972, pp. 113–124.

[58]Weber, C., "Zum Zerfall eines Flussigkeitsstrahles," *Zeitschrift für Z Angewesen Mathematik und Mechanik,* Vol. 2, 1931, pp. 136–141.

Appendix E: Faeth, G.M., Hsiang, L.-P. and Wu, P.-K., (1995)Structure and Breakup Properties of Sprays. Int. J. Multiphase Flow 21(Suppl.), 99-127.

Pergamon

0301-9322(95)00059-3

Int. J. Multiphase Flow Vol. 21, Suppl. pp. 99–127, 1995

0301-9322/95 $29.00 + 0.00

STRUCTURE AND BREAKUP PROPERTIES OF SPRAYS

G. M. FAETH, L.-P. HSIANG and P.-K. WU

Department of Aerospace Engineering, 3000 FXB Building, The University of Michigan, Ann Arbor, MI 48109-2118, U.S.A.

(Received 25 July 1995)

Abstract—Multiphase flow phenomena relevant to spray combustion are reviewed, emphasizing the structure of the near-injector dense-spray region and the properties of secondary and primary breakup. Existing measurements of dense-spray structure are limited to round pressure-atomized sprays in still gases and show that the dispersed flow region is surprisingly dilute, that separated flow effects are significant because the flow is dilute and developing, and that atomization involves primary breakup at the liquid surface followed by secondary breakup, while effects of collisions are small. Available information about secondary breakup emphasizes breakup due to shock wave disturbances at large liquid/gas density ratios and shows that secondary breakup is a dominant feature of dense sprays that must be resolved as a function of time so that secondary breakup can be properly treated as a rate process. Finally, available information about primary breakup has been dominated by effects of disturbances in the injector passage; therefore, while some understanding of turbulent primary breakup has been achieved, more information about aerodynamic primary breakup is needed to address practical spray combustion processes.

Key words: atomization, dispersed flow, injection, primary breakup, secondary breakup, sprays

1. INTRODUCTION

There have been numerous studies of non-combusting and combusting sprays, emphasizing the dilute region far from the injector exit, where observations and modeling are relatively tractable due to small liquid volume fractions. As a result, many features of dilute sprays are understood reasonably well, see the reviews due to Giffen & Muraszew (1953), Levich (1962), Harrje & Reardon (1972), Clift *et al.* (1978), Lefebrve (1980, 1983, 1989), Law (1982), Sirignano (1983), Wierzba & Takayama (1988), Annamalai & Ryan (1992), Faeth (1977, 1983, 1987, 1990) and references cited therein. Thus, attention now is being directed to the less accessible dense-spray region near the injector exit, in order to determine how injector design properties and the spray environment influence flow properties entering the dilute-spray region. Thus, the objective of this paper is to briefly review these efforts and to identify areas where additional research is needed.

Three aspects of multiphase flow relevant to spray combustion are reviewed as follows: (1) the structure of the near-injector dense-spray region, in order to help define the environment of various dense spray processes; (2) the properties of secondary breakup, which often is the rate controlling process of dense sprays in much the same way that drop vaporization often is the rate controlling process of dilute sprays; and (3) the properties of primary breakup, which define initial conditions for dense sprays and most directly connect injector design properties (hardware) and spray properties. Due to space limitations, however, present considerations will be limited to processes directly relevant to non-evaporating round pressure-atomized sprays in still gases. Ignoring evaporation is reasonable because the dense-spray region of combusting sprays generally involves cool portions of the flow where rates of heat and mass transfer are modest. Additionally jet flows in still gases are a simple classical flow configuration that exhibit most features of dense-sprays while only requiring a few defining parameters. Information about other spray processes and injection configurations can be found in the review articles cited earlier, and references cited therein.

In the following, dense-spray structure, secondary breakup and primary breakup will be considered in turn. The description of each topic is sufficiently complete so that it can be read independently, if desired.

2. DENSE SPRAY STRUCTURE

2.1. Introduction

Round pressure-atomized sprays in a still gas are a classical spray configuration that will be used to illustrate the environment of dense sprays, based on results described by Clift *et al.* (1978), Faeth (1987, 1990), Ruff & Faeth (1995), Ruff *et al.* (1989, 1991, 1992), Tseng *et al.* (1992a, b, 1995) and Wu *et al.* (1995b). Early studies of this spray configuration emphasized spray breakup regimes, including conditions required for the important atomization breakup regime where drop formation begins right at the jet exit, see Reitz & Bracco (1982), Miesse (1955), Ranz (1958) and Phinney (1973). Subsequent work concentrated on visualization of the near-injector region of the flow and definition of the properties of the liquid core, which is similar to the potential core of a single-phase jet, see Phinney (1973), Hoyt & Taylor (1977a, b), Hiroyasu *et al.* (1982) and Chehroudi *et al.* (1985). More recently, Wu *et al.* (1983, 1984) have studied the properties of the dilute spray region near the outer edge of the spray. Emphasis in the following, however, will be on the dense spray region, based on the measurements of Ruff *et al.* (1989, 1991, 1992) and Tseng *et al.* (1992a, b). For these conditions, flow regimes and flow structure will be considered, in turn.

2.2. Flow regimes

The atomization breakup regime of round pressure-atomized sprays is most important because it provides the fine atomization needed for rapid mixing of liquid and gas phases during practical combustion processes. A sketch of the flow within the near-injector region for this breakup regime is illustrated in figure 1. There are two main multiphase flow regions within dense sprays; namely, the liquid core and the dispersed flow region beyond the surface of the liquid core. As noted earlier, the liquid core is similar to the potential core of a single phase jet, although it is generally much longer. For example, Chehroudi *et al.* (1985) find the following expression for the length, L_c, of the liquid core:

$$L_c/d = C_c(\rho_L/\rho_G)^{1/2} \qquad [1]$$

where d is the injector diameter, ρ_L and ρ_G are the liquid and gas densities, respectively, and C_c is an empirical constant in the range 7–16. This implies L_c/d in the range 200–500 for typical sprays at atmospheric pressure, with this ratio generally being inversely proportional to the square root of pressure. Thus, liquid cores are a very prominent feature of round pressure-atomized sprays.

The dispersed flow region beyond the liquid surface involves a developing multiphase mixing layer in the region where the liquid core is present, followed by a multiphase jet that evolves into a dilute round spray flow. The multiphase mixing layer begins close to the jet exit within the atomization breakup regime. Primary breakup occurs due to the formation of ligaments and other irregular liquid elements along the surface of the liquid core. Thus, rates of primary breakup tend to control the length of the liquid core. The dense spray region generally is associated with the

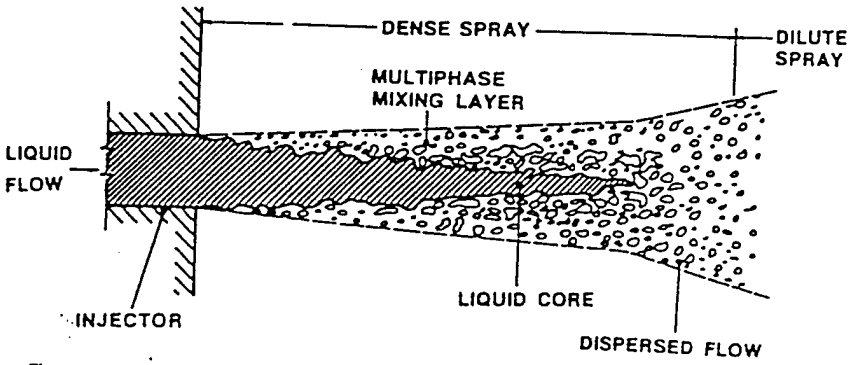

Figure 1. Sketch of the near-injector region of a pressure-atomized spray in the atomization breakup regime.

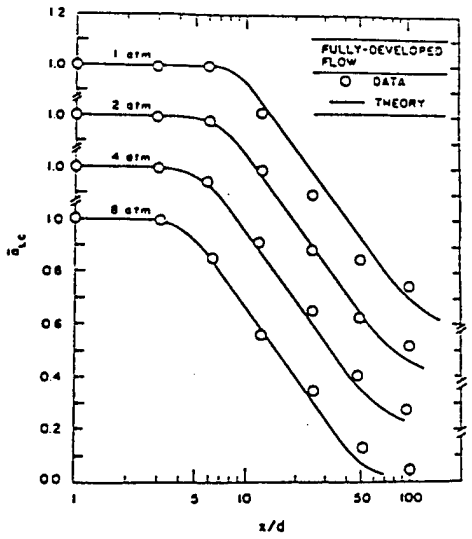

Figure 2. Time-averaged liquid volume fractions along the axis of round pressure-atomized water sprays in still air at various pressures for atomization breakup with fully-developed turbulent pipe flow at the jet exit. From Tseng *et al.* (1992a).

presence of the liquid core although this definition is not very precise, e.g. the edge of this region is a dilute spray while the region just downstream of the liquid core has large liquid volume fractions typical of a dense spray condition. The outcome of primary breakup frequently is irregular drops or ligaments while most liquid elements resulting from primary breakup are unstable to secondary breakup: these are features that are typical of dense sprays. Finally, the properties of dense sprays, or even the existence of the dense spray region, are strongly dependent upon liquid flow properties (disturbance levels, vorticity properties, turbulence levels, etc.) at the jet exit, as will be discussed later.

2.3. Flow structure

Ruff *et al.* (1989, 1991, 1992) and Tseng *et al.* (1992a, b) observe significant effects of the degree of development of turbulence at the jet exit on dense spray properties. Thus, in order to fix ideas, subsequent information about dense spray properties will be limited to conditions where there is fully-developed turbulent pipe flow at the jet exit. Measured and predicted time-averaged liquid volume fractions along the axis of the dense spray region, $\bar{x}_{L\ell}$, for water injected into air at various pressures, from Tseng *et al.* (1992a), are illustrated in figure 2 as a function of the distance from the jet exit, x. The measurements were completed by Ruff *et al.* (1989) and Tseng *et al.* (1992a) by deconvoluting gamma-ray absorption determinations for cord-like paths through the flow; notably, the two sets of measurements are in excellent agreement in the region where they overlap. The predictions are based on a Favre-averaged turbulence model under the locally-homogeneous flow (LHF) approximation, where relative velocities between the phases are assumed to be small in comparison to mean flow velocities, see Ruff *et al.* (1989), for a complete description of this model.

The region near the jet exit ($x/d < 3$–8) illustrated in figure 2, exhibits mean liquid volume fractions near unity, followed by a rapid reduction of the liquid volume fraction. The initial reduction of liquid volume fractions occurs at progressively smaller values of x/d as the pressure increases, indicating faster mixing rates at higher ambient gas densities, analogous to effects of flow density ratio for single-phase turbulent jets, see Ricou & Spalding (1961). There is good agreement between measurements and predictions; nevertheless, these conditions represent relatively low levels of mixing as will be discussed subsequently. For such conditions, LHF predictions generally are reasonably good, because separated flow effects due to relative velocity differences between the gas

and the liquid are not very significant when the flow is mainly liquid. Finally, although the variation of liquid volume fraction suggests a relatively short liquid core, this is not the case when viewed in terms of mixture fraction. Results to be considered next will show that Favre-averaged mixture fractions are near unity for all the conditions illustrated in figure 2, so that even low levels of flapping of the liquid core can explain the liquid volume fraction reductions.

Ricou & Spalding (1961) have shown that properties along the axis of single-phase variable-density jets should scale in terms of a normalized density-weighted streamwise distance, $(\rho_G/\rho_L)^{1/2}x/d$, while Chehroudi *et al.* (1985) recommend similar scaling based on their measurements of liquid core lengths as discussed in connection with [1]. Thus, predicted and measured Favre-averaged mixture fractions along the axis, $\tilde{f}_c$, where the subscript c denotes a property along the axis (mixture fraction simply corresponds to the mass fraction of water for these conditions) are plotted as a function of this variable in figure 3, for the same conditions as figure 2. When plotted in this manner, both measurements and predictions exhibit little effect of ambient pressure and also show that liquid volume fractions generally are near unity in this region, as noted earlier. Nevertheless, the LHF predictions vastly overestimate the subsequent rate of reduction of mass fractions with increasing streamwise distance, and thus the mixing rates. The corresponding slower rates of mixing along the axis than LHF predictions suggest significant effects of separated flow just downstream of the end of the liquid core. This behavior is plausible, because breakup of the end of the liquid core yields large drops that maintain significant relative velocities due to their large inertia. Thus, separated flow effects are an important feature of dense sprays. Another result illustrated in figure 3 is the effect of jet exit flow conditions on spray mixing rates as evidenced by the slower rate of development of the non-turbulent slug flow in comparison to the fully-developed turbulent pipe flow at the jet exit (most evident at the farthest downstream position).

Predicted and measured radial profiles of mean liquid volume fractions at atmospheric pressure are plotted as a function of radial distance, r, in figure 4, for the same conditions as figures 2 and 3. The independent measurements of Ruff *et al.* (1989) and Tseng *et al.* (1992a) agree within experimental uncertainties, except for $x/d = 100$ where the greater confinement of the flow studied by Tseng *et al.* (1992a) might be a factor. The measurements show a progressive increase of flow width with increasing distance from the jet exit. The comparison between LHF predictions and

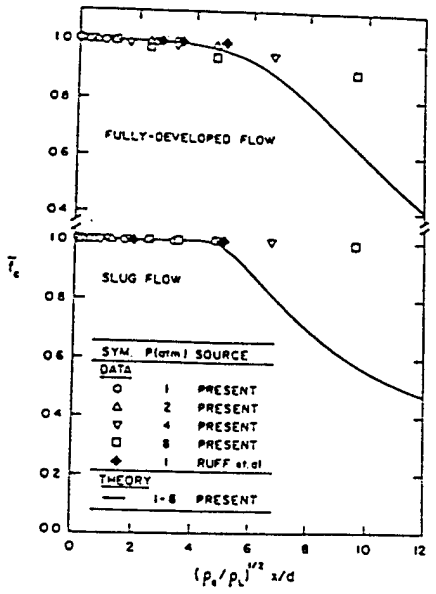

Figure 3. Favre-averaged mixture fractions along the axis of round pressure-atomized water sprays in still air at various pressures for atomization breakup with fully-developed turbulent pipe flow at the jet exit. From Tseng *et al.* (1992a).

measurements is reasonably good, except at larger values of x/d: Ruff *et al.* (1989) show that this difficulty is due to effects of separated flow as the flow becomes more dilute.

Tseng *et al.* (1992b) directly assess effects of separated flow in the dense spray region of round pressure-atomized sprays using double-pulsed holography to measure drop size and velocity distributions, in the mixing layer, as well as the position of the surface of the liquid core. These results allowed the determination of Favre-averaged flow velocities, for direct comparison with LHF predictions, assuming that the velocities of 5 μm diameter drops were representative of gas velocities. The resulting measured and predicted streamwise mean phase velocities (Favre-averaged and gas phase velocities) at a typical streamwise location ($x/d = 25$) are plotted in figure 5 for ambient pressures of 1, 2 and 4 atm. The velocities on this plot are normalized by the injector exit velocity, u_o. The range of measured positions of the liquid surface are also shown on the plots for reference purposes. In general, the measured Favre-averaged velocity is significantly greater than the gas velocity, although the differences between the two decrease as the ambient pressure increases. In addition, the LHF predictions are not very satisfactory, which is expected due to the presence of significant effects of separated flow.

Additional insight concerning separated-flow effects in dense sprays can be obtained from the structure properties plotted in figure 6. The results in this figure include the ellipticity of the drops, e_p, the Sauter mean diameter of the spray, SMD, and drop velocities, u_p for various drop diameters, d_p. These results are for the same conditions as figure 5, with both data and predictions obtained from Ruff *et al.* (1992), but they are typical of findings at other conditions within the dense spray region. The region near the liquid surface consists of large, irregular, ligament-like elements (large e_p and SMD), even though this spray had good atomization properties, while the dilute spray region near the edge of the flow involves smaller round drops. This provides direct evidence of significant levels of secondary breakup in the dense spray region near the liquid surface. In addition, the dispersed flow region, exterior to the liquid core, was surprisingly dilute (with mean liquid volume fractions less than 0.1%), see Ruff *et al.* (1992) and Tseng *et al.* (1992b); therefore, the large mean liquid volume fractions observed in some portions of the dense spray region are mainly due to the

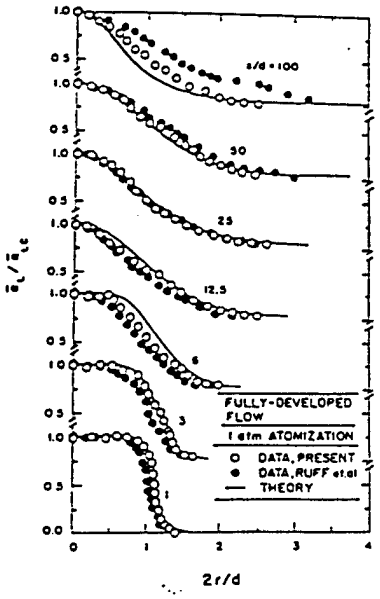

Figure 4. Radial profiles of time-averaged liquid volume fractions along the axis of round pressure-atomized water sprays in still air at atmospheric pressure for atomization breakup with fully-developed turbulent pipe flow at the jet exit. From Tseng *et al.* (1992a).

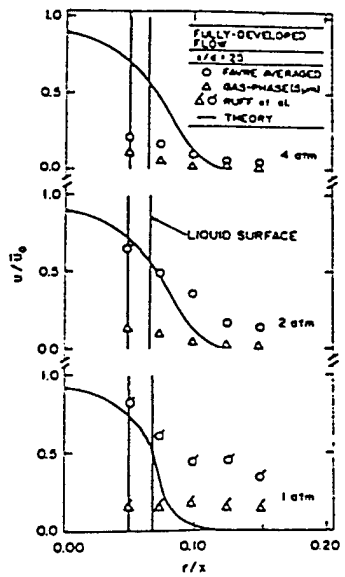

Figure 5. Radial profiles of mean phase velocities for round pressure-atomized water sprays in still air at various pressures for atomization breakup with fully-developed turbulent pipe flow at the jet exit. From Tseng *et al.* (1992b).

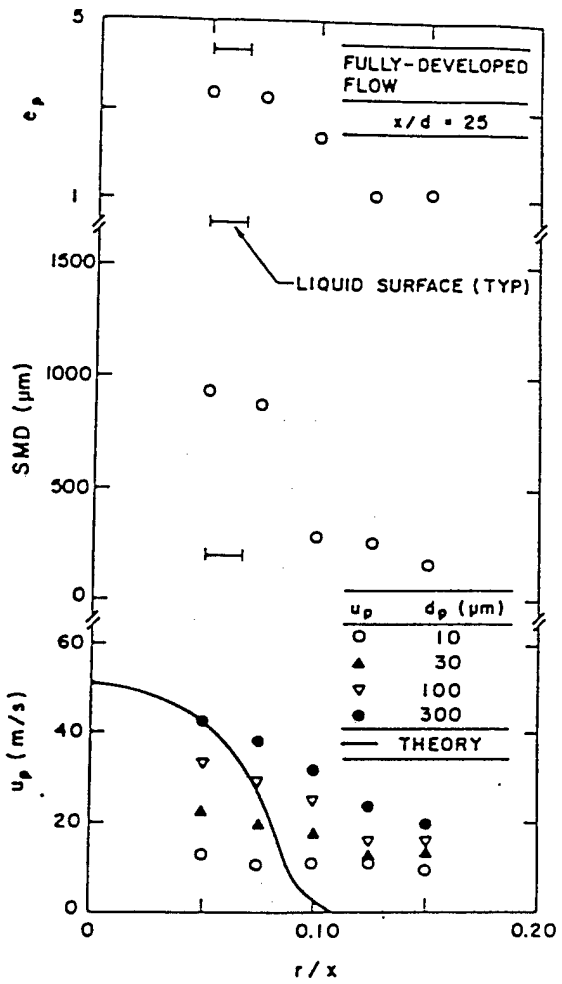

Figure 6. Radial profiles of dispersed-phase properties for round pressure-atomized water sprays in still air at atmospheric pressure for atomization breakup with fully-developed turbulent pipe flow at the jet exit. Data from Ruff *et al.* (1992).

presence of the liquid core. The low liquid volume fractions within the dispersed flow region imply that collisions between liquid elements are improbable, see Faeth (1977, 1983, 1987). Thus, these findings support the conventional picture of atomization within dense sprays, as discussed by Giffen & Muraszew (1953), which involves primary breakup into ligaments and large drops at the liquid surface followed by secondary breakup into smaller round drops, with negligible effects of collisions.

A useful experimental finding of the studies of Ruff *et al.* (1992) and Tseng *et al.* (1992b) was that drop size distributions throughout the dense spray region are well correlated by the universal root-normal distribution with MMD/SMD = 1.2 due to Simmons (1977), where MMD is the mass median drop diameter of the spray. See Belz (1973) for a discussion of the properties of this distribution function. Then, since this distribution only has two parameters, the entire size distribution can be represented by the SMD alone. Another observation was that the drop sizes after primary breakup, as well as mixing rates throughout the flow which was noted earlier, were

very dependent upon flow conditions at the injector exit—a finding that parallels the well known importance of jet exit conditions on the development region of single-phase turbulent jets.

The distributions of drop velocities illustrated in figure 6 show that they vary considerably with drop diameter at each point in the flow, providing direct evidence of significant separated flow effects in dense sprays. Near the liquid core, the largest drops have velocities comparable to mean liquid injection velocities, however, velocities decrease with both decreasing drop size and increasing radial distance. A surprising feature of these observations is that gas velocities (which approximate the velocities of the smallest drops) are low and are nearly constant across the width of the dispersed flow region. This implies relatively ineffective momentum exchange between the phases because the large drops contain most of the momentum and they respond slowly to drag forces due to their relatively large inertia. Finally, consistent with observations in connection with figures 2–5, the LHF predictions illustrated in figure 6 are poor because separated flow effects are important within most of the dense spray region.

2.4. Conclusions

Based on the study of the structure and mixing properties of dense sprays found near the injector for round pressure-atomized sprays in still gases, the following major conclusions are obtained:

(1) The large liquid volume fractions observed in dense sprays generally are due to the presence of the liquid core; in contrast, liquid volume fractions in the dispersed flow region beyond the liquid surface are small, less than 0.1%, so that the flow in this region corresponds to a dilute spray but with added complications due to the presence of irregular liquid elements and secondary breakup.

(2) Measurements generally support the traditional view of atomization expressed by Giffen & Muraszew (1953); namely, primary breakup at the liquid surface is followed by secondary breakup in a dilute spray environment where effects of drop collisions are negligible (except for spray conditions that strive for significant effects of collisions to enhance breakup rates, such as impinging injectors).

(3) Rates of mixing, drop properties and flow structure within dense sprays are strongly dependent on the degree of flow development and turbulence levels at the jet exit, and on the liquid/gas density ratio, somewhat analogous to the effect of these properties on the structure of the flow development region of single-phase jets.

(4) Effects of separated flow are important within dense sprays, with significant differences between the velocities of large drops and the gas due to the poor response properties of large drops. Thus, LHF predictions of the structure of dense sprays are not very effective, except at the highest liquid volume fractions where the momentum of the gas and small drops is negligible in any event.

(5) Drop size distributions after primary breakup, as well as after secondary breakup and on approach to the dilute spray region, all satisfied the universal root-normal drop size distribution with MMD/SMD = 1.2 due to Simmons (1977) at each point in dense sprays; therefore, the entire drop-size distribution can be characterized by a single moment, e.g. the SMD.

3. SECONDARY BREAKUP

3.1. Introduction

Based on the previous considerations of the structure of the dense spray region for round pressure-atomized sprays, secondary breakup clearly is an important process of dense sprays, through its effect on drop size distributions as the dilute spray region is approached. In particular, primary breakup at the surface of the liquid core yields drops that are intrinsically unstable to secondary breakup. In addition, high-pressure combustion for typical power and propulsion systems involves conditions where the surface tension of drops becomes small, because the liquid surface approaches the thermodynamic critical point; naturally, such conditions suggest potential for significant effects of drop deformation and secondary breakup. Prompted by these observations, current understanding of secondary breakup will be discussed in the following.

Giffen & Muraszew (1953), Levich (1962), Harrje & Reardon (1972), Clift *et al.* (1978), Wierzba & Takayama (1988), Hinze (1955) and Krzeczkowski (1980) have reviewed early work on secondary breakup; therefore, the following discussion will emphasize more recent studies. Of particular interest are the studies of Hsiang & Faeth (1992, 1993, 1995) and Hsiang *et al.* (1995) which have considered breakup regimes, breakup dynamics and the outcomes of breakup. In general, past work has been limited to two kinds of well defined disturbances that cause deformation and breakup of drops: shock wave disturbances that provide step changes in the ambient environment of a drop typical of a drop at the end of primary breakup; and steady disturbances typical of freely-falling drops in rainstorms or in spray drying processes. Effects of shock wave disturbances have received the most attention and approximate the secondary breakup environment of dense sprays; therefore, these disturbances will be emphasized in the following. Deformation and breakup regimes, breakup dynamics and breakup outcomes will be considered, in turn.

3.2. Deformation and breakup regimes

Numerous studies have considered the definitions and conditions for the onset of various deformation and breakup regimes of drops subjected to shock wave disturbances. When effects of liquid viscosity are small, the breakup regime observed at the onset of breakup has been termed bag breakup: it involves deflection of the drop into a thin disk normal to the flow direction, followed by deformation of the center of the disk into a thin, balloon-like structure, both of which subsequently divide into drops, see Wierzba & Takayama (1988), Hinze (1955), Krzeczkowski (1980), Hanson *et al.* (1963), Gel'fand *et al.* (1974), Ranger & Nicholls (1969) and Reinecke & McKay (1969) and Reinecke & Waldman (1970) for photographs of all the breakup regimes discussed here. The shear breakup regime is observed at higher relative velocities: it involves deflection of the periphery of the disk in the downstream direction, rather than deflection of the center of the disk, and the stripping of drops from the periphery of the disk. The transition between the bag and shear breakup regimes is a complex mixture of the two bounding regimes which will be denoted the multimode breakup regime in the following. A complex breakup mechanism also has been observed at very large relative velocities, which has been called catastrophic breakup by Reinecke & McKay (1969) and Reinecke & Waldman (1970), nevertheless, this regime is not seen in typical dense sprays and will not be considered here.

Existing observations of secondary breakup have generally involved $\rho_L/\rho_G > 500$ and $Re > 100$, where $Re = \rho_G d u/\mu_G$ and μ_G is the molecular viscosity of the gas. For these conditions, Hinze (1955) shows that breakup regime transitions are functions of the initial Weber number of a drop, $We = \rho_G d_o u_o^2/\sigma$, where σ is the drop surface tension and the subscript o denotes an initial condition, and the Ohnesorge number of a drop, $Oh = \mu_L/(\rho_L d_o \sigma)^{1/2}$, where μ_L is the molecular viscosity of the liquid, which are measures of the ratios of drag and liquid viscous forces to surface tension forces, respectively. The resulting deformation and breakup regime map based on available results from Hinze (1955), Krzeczkowski (1980), Hsiang & Faeth (1992,1993,1995), Hanson (1963), Lane (1951) and Loparev (1975) is illustrated in figure 7. The various breakup regimes identified by Hinze (1955), Krzeczkowski (1980) and Hsiang & Faeth (1992, 1995) are in excellent agreement in the regions where they overlap; in view of the subjective nature of identifying breakup regime transitions, this degree of agreement is quite satisfying. The transitions to the deformation regimes are important because they define conditions where drop drag departs significantly from that of a solid sphere: these regimes are defined by the ratio of the maximum (cross stream) dimension to the original drop diameter. The oscillatory deformation regime is defined by conditions where the drop oscillates with a weakly damped amplitude, see Hsiang & Faeth (1992) for discussion of this behavior.

All regime transitions illustrated in figure 7 are relatively independent of liquid viscous forces (or Oh) for $Oh < 0.01$. The order of the transitions with increasing We in this region from Hsiang & Faeth (1995) is as follows: 5% deformation, $We = 0.6$; 10% deformation, $We = 1.0$; 20% deformation, $We = 2.1$; oscillatory deformation, $We = 3.0$; bag breakup, $We = 13$; multimode breakup, $We = 35$; and shear breakup, $We = 80$. As noted earlier, the We at breakup regime transitions due to Hinze (1955) and Krzeczkowski (1980) are similar to these results. These findings suggest quite plausibly that significant levels of deformation and breakup occur when dynamic

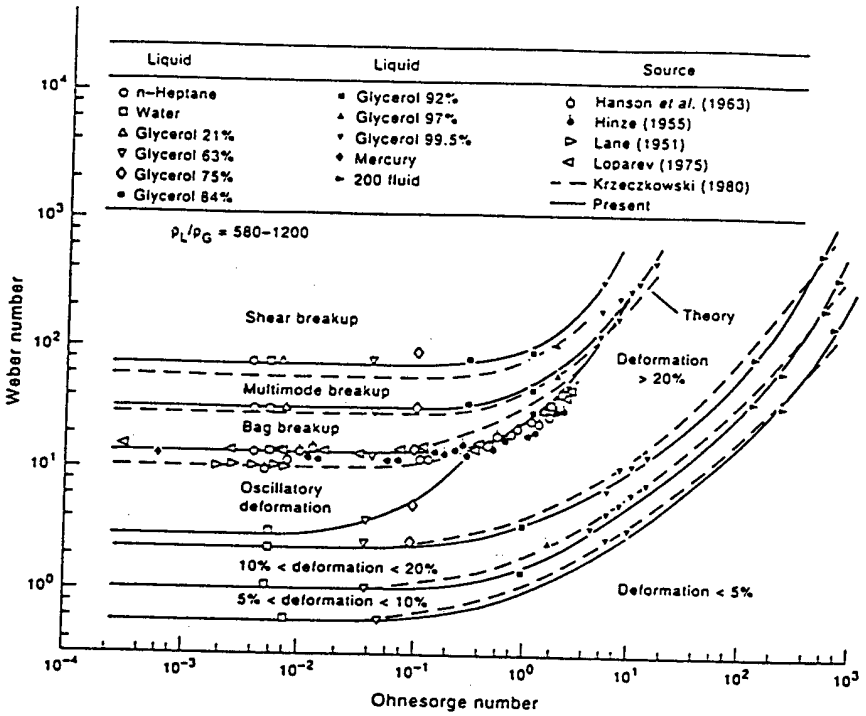

Figure 7. Drop deformation and breakup regime map for shock-wave disturbances with liquid/gas density ratios greater than 500. From Hsiang & Faeth (1995).

forces (or drag forces) are comparable to the stabilizing forces of surface tension if effects of liquid viscosity are small.

Perhaps the most striking feature of figure 7 is that while the values of We required for particular regime transitions are relatively constant for $Oh < 0.1$, they progressively increase with increasing Oh for $Oh > 1$. In addition oscillatory deformation disappears at $Oh \approx 0.3$ and bag breakup disappears at $Oh \approx 4$. Hinze (1955) and Levich (1962) observed this tendency for the limited ranges of Oh where data were available at the time, and conjectured that breakup might not be observed for $Oh > 1$ to 2. However, the large Oh behavior observed in figure 7 does not suggest such a limitation; rather, there is an almost linear increase of We at the deformation and breakup transitions with increasing Oh.

Clearly, it is crucial to establish whether large values of Oh imply no deformation or breakup as suggested by Hinze (1955) and Levich (1962), or simply rather large values of We at the transitions, as suggested by the measurements illustrated in figure 7; therefore, Hsiang & Faeth (1995) undertook phenomenological analysis in an attempt to explain the effect of Oh on deformation and breakup regime transitions. Their approach was based on the observation that the main effect of liquid viscosity for shock wave disturbances was to reduce the rate of deformation of the drop. This behavior allows more time for drop velocities to relax toward the local ambient velocity at large Oh, tending to reduce the relative velocity, and thus the driving potential for drop deformation, at each stage of the deformation process. The motion of the drop was analyzed for these circumstances, assuming $Oh \gg 1$ so that maximum deformation occurred at a multiple of the characteristic viscous time, τ, of Hinze (1948), defined as follows:

$$\tau = \mu_L/(\rho_G u_0^2) \qquad [2]$$

This analysis yielded the following relationship between We and Oh for particular deformation or breakup transitions at large Oh:

$$We = (We_{cr}/4)(1 + 4K'We_{cr}^{-1/2}(\rho_G/\rho_L)^{1/2}Oh) \quad [3]$$

In [3], We_{cr} is the local Weber number at the maximum deformation condition required for the transition of interest to occur, while K' is an empirical factor. Values of We_{cr} and K' were fitted to [3] to yield the best fit predicted transitions at large Oh illustrated in figure 7: in view of the simplifications of the theory, the agreement between the predicted and measured regime transitions is seen to be reasonably good. Notably, [3] suggests that transition We ~ Oh at large Oh rather than an ultimate limit for particular transitions as suggested by Hinze (1955) and Levich (1962). This is a very important difference in behavior that has significant relevance for processes of high-pressure combustion, where Oh becomes large as drops approach their thermodynamic critical point (because their surface tension approaches zero while their viscosity remains finite). Another issue concerning [3] is the effect of liquid/gas density ratio, which suggests further increases in We at a given transition as ρ_G/ρ_L increases, a parameter variation that has not been explored thus far. Thus, the large Oh regime transition criteria of [3] clearly merit additional study, emphasizing the large Oh and ρ_G/ρ_L conditions relevant to high-pressure spray combustion processes.

3.3. Breakup dynamics

The discussion of deformation and breakup regime transitions highlights the importance of breakup times and already has introduced the characteristic breakup time, τ, when liquid viscous forces are large in comparison to surface tension forces at large Oh, see [2]. Available measurements of drop breakup times from Engel (1958), Simpkins & Bales (1972), Ranger & Nicholls (1969) Reinecke & Waldman (1970) and Hsiang & Faeth (1992) are plotted as a function of We and Oh in figure 8. In this plot, the breakup times, t_b, are normalized by the characteristic breakup time for shear breakup at low Oh, t^*, defined by Ranger & Nicholls (1969) as follows:

$$t^* = d_o(\rho_L/\rho_G)^{1/2}/u_o \quad [4]$$

Except for the results of Hsiang & Faeth (1992), which are grouped according to Oh, the measurements are for Oh < 0.1; therefore, the deformation and breakup regimes defined earlier for these conditions are marked on the plot for reference purposes.

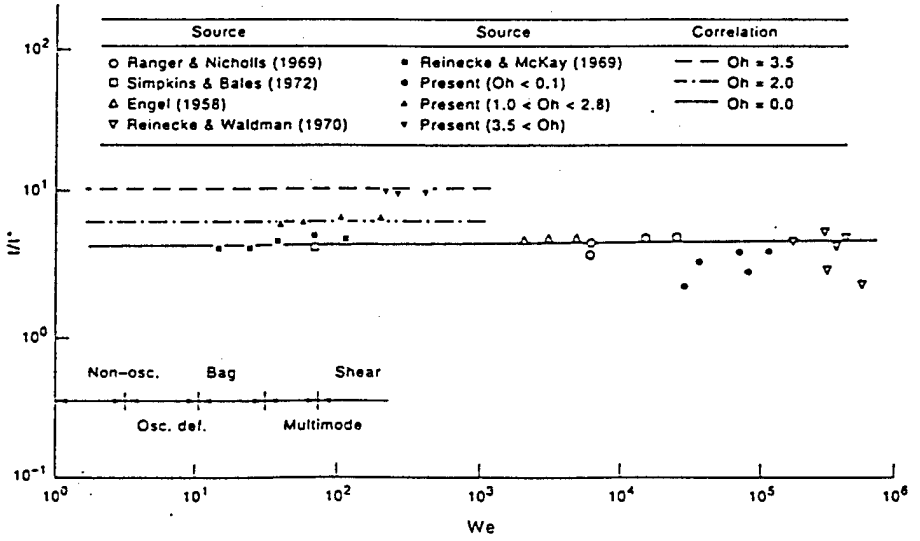

Figure 8. Drop breakup times as a function of the Weber and Ohnesorge numbers for shock-wave disturbances with liquid gas density ratios greater than 500. From Hsiang & Faeth (1992).

A remarkable feature of the breakup time results illustrated in figure 8 for Oh < 0.1 is that t_b/t^* varies very little even though We varies widely and several breakup regimes are involved. In fact, the correlation developed for shear breakup by Ranger & Nicholls (1969):

$$t_b/t^* = 5.0 \quad [5]$$

provides a good representation of all the measurements illustrated in figure 8 for Oh < 0.1. At larger Oh, however, t_b/t^* increases due to effects of liquid viscosity retarding the rate of deformation as discussed earlier. In this region, an empirical correlation is defined by Hsiang & Faeth (1992) but this expression is only appropriate for Oh < 3.5. Surprisingly, no attempt has been made to apply the characteristic viscous time, τ, to correlate breakup times at large Oh: this should be done in order to both check the development of the large Oh regime transition criteria of [3] and to gain a better understanding of deformation and breakup behavior at large Oh.

Drops undergo significant deformation in the period prior to the onset of breakup. As discussed earlier, drops are initially drawn into flattened (oblate spheroid) shapes due to the relative motion of the gas phase, which affects their motion by influencing drag forces. Hsiang & Faeth (1992) have summarized a relatively large data base of maximum drop deformations for steady disturbances, considering both drop-gas and drop-immiscible liquid environments. Phenomenological analyses lead to a reasonably good correlation of these results in terms of the maximum cross-stream drop diameter, d_{max}, and the minimum streamwise diameter, d_{min}, as follows:

$$d_{max}/d_{min} = (1 + 0.07We^{1/2})^3, \; We < 20 \quad [6]$$

where the second relationship needed to find d_{max} and d_{min} is given by $d_{min}d_{max}^2 = d_0^3$. The correlation of [6] was independent of Oh within experimental uncertainties, which is reasonable because liquid viscous forces mainly act to inhibit the rate of deformation for unsteady conditions after shock wave disturbances. The limitation of We in [6] follows because drops shatter at We ≈ 20 for steady disturbances. Finally, drop deformations for shock wave disturbances are appreciably larger than estimated by [6] due to inertial effects, see Hsiang & Faeth (1992) for initial attempts to quantify this behavior.

Deformation causes the drag force on a drop to increase due to both the increasing cross-sectional area of the drop and an increase of the drag coefficient, C_D. Hsiang & Faeth (1992) have reported measurements of the effect of deformation on the drag coefficients for shock wave disturbances at Oh < 0.1 and Re in the range 1000–2500 where effects of Re on the drag coefficient of drops is expected to be small, see Faeth (1987). It was found that C_D largely was a function of deformations at these conditions and could be correlated in terms of d_c/d_0 as illustrated in figure 9, where d_c is the cross-stream drop diameter. Measurements of C_D for solid spheres and thin disks, obtained from White (1974) for the same range of Re, also are illustrated on the plot. In general, C_D approximates results for solid spheres when d_c/d_0 is near unity, and then increases to approach results for thin disks at $d_c/d_0 \approx 2$ (which is representative of maximum deformations at the point where drop breakup begins). Later work by Hsiang & Faeth (1995) showed that $C_D/C_{D_{sp}}$, where $C_{D_{sp}}$ is the drag coefficient of a solid sphere at the same Reynolds number, were relatively independent of the type of disturbance (shock wave or steady), the drop/surroundings density ratio, We, Oh and Re, and could be correlated in terms of deformation alone along the lines of figure 9. The increase of C_D and cross-sectional area, due to distortion, causes drag forces to increase by factors of roughly 4 and 13 at deformation conditions typical of the onset of breakup for steady and shock wave disturbances, which clearly has an important impact on breakup dynamics, see Hsiang & Faeth (1995).

3.4. Breakup outcomes

Under the assumption that breakup times and distances are small in comparison to characteristic dense spray residence times and distances, secondary breakup can be treated using jump conditions. For this approach to be workable, information about drop size and velocity distributions after secondary breakup is needed. Early measurements along these lines were reported by Gel'fand *et al.* (1963) for the bag breakup regime, but this information was too limited to provide general guidance about the drop sizes produced by secondary breakup. Later work by Hsiang & Faeth (1992, 1993, 1995) using pulsed holography achieved a more complete description of the outcomes of secondary

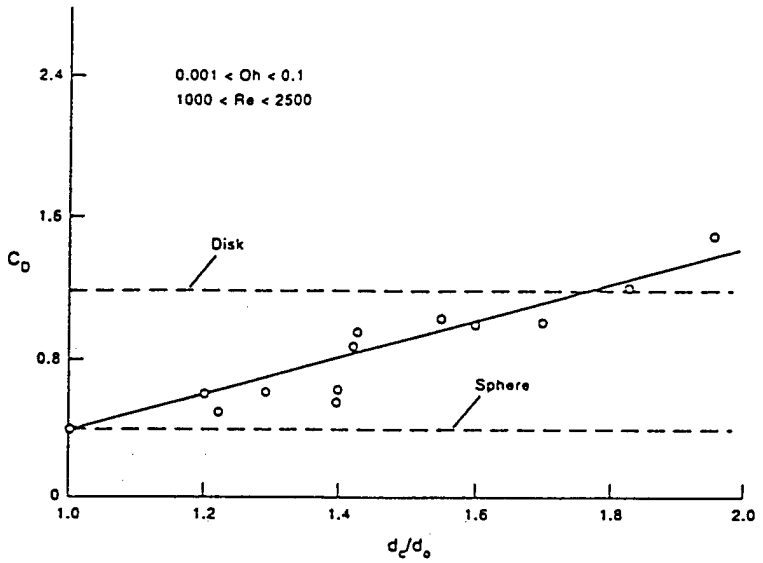

Figure 9. Drop drag coefficient prior to breakup as a function of deformation for shock-wave disturbances with liquid/gas density ratios greater than 500. From Hsiang & Faeth (1992).

breakup for shock wave disturbances at $\rho_L/\rho_G > 500$ and $Oh < 0.1$. Some of the main findings of this work will be discussed in the following.

Similar to observations discussed earlier for the dense spray region, Hsiang & Faeth (1992, 1993, 1995) found that drop size distributions after secondary breakup could be represented by the universal root-normal distribution with MMD/SMD = 1.2, due to Simmons (1977), see Belz (1973) for a discussion of the properties of the root-normal distribution function. This behavior was observed for the bag, multimode and shear breakup regimes, but only if the core or parent drop was removed from the distribution for the shear breakup regime. This behavior is illustrated in figure 10 for shear breakup involving a variety of drop liquids. Thus, given the universal root normal drop size distribution, drop sizes are fully prescribed by the SMD alone, except for shear breakup where the properties of the core drop must be prescribed independently as well.

A correlating expression for the SMD after secondary breakup was developed considering the shear breakup regime. The analysis focuses on the stripping of liquid from the core drop as illustrated in figure 11. It was assumed that the relative velocity at the time of breakup can be represented by the initial relative velocity, that the drop sizes after breakup are comparable to the thickness of the laminar boundary layer that forms in the liquid along the front surface of the drop due to its motion, that the characteristic liquid phase velocities are on the order of $(\rho_G/\rho_L)^{1/2}u_o$, as suggested by Ranger & Nicholls (1969) for shear breakup, and that the SMD is dominated by the largest drop sizes in the distribution so that the length of the liquid phase boundary layer is proportional to the initial drop diameter, d_o. Based on these ideas, the following expression was obtained as the best fit of the available SMD measurements, see Hsiang & Faeth (1992):

$$\rho_G \mathrm{SMD} u_0^2/\sigma = 6.2(\rho_L/\rho_G)^{1/4}[\mu_L/(\rho_L d_o u_o)]^{1/2}\mathrm{We} \qquad [7]$$

Surface tension has been introduced into [7] in order to simplify discussion of the potential for subsequent breakup. Consistent with its derivation, however, surface tension actually does not influence the final SMD. Instead, the main physical properties controlling the SMD are μ_L, ρ_L and ρ_G.

The available measurements of SMD after secondary breakup, along with the correlation of [7], are illustrated in figure 12. Remarkably, a single correlation developed for the shear breakup regime expresses the SMD after bag, multimode and shear breakup. This behavior still needs to be explained, although other properties like breakup time are also relatively independent of the

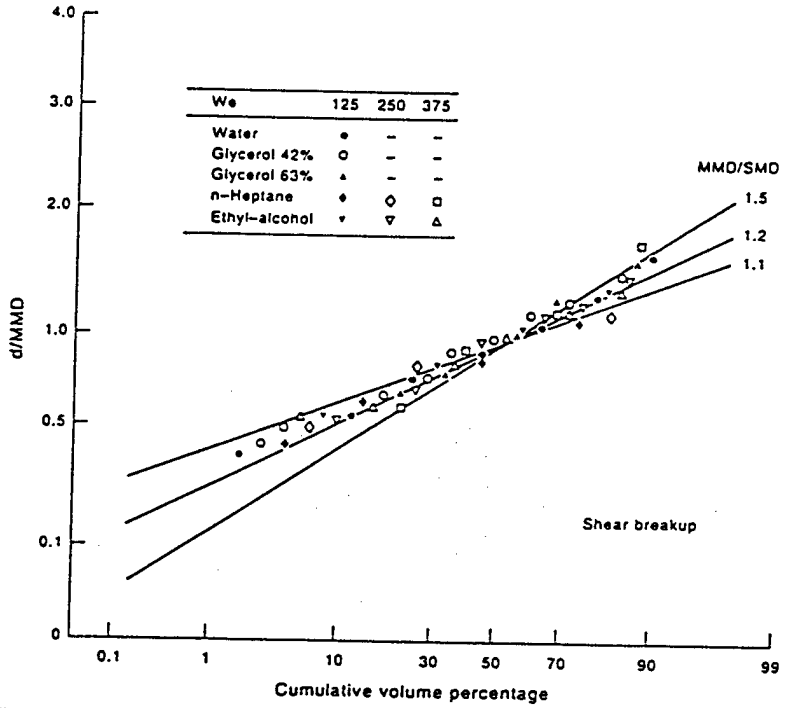

Figure 10. Drop diameter distribution after shear breakup (excluding the parent drops) for shock-wave disturbances with liquid/gas density ratios greater than 500. From Hsiang & Faeth (1993).

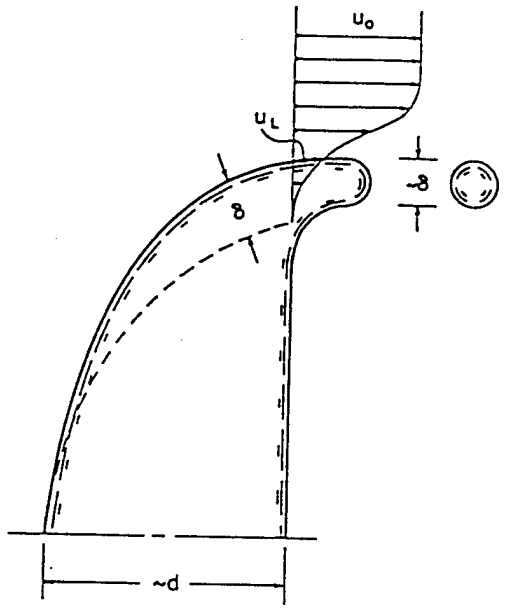

Figure 11. Sketch of the shear breakup process for shock-wave disturbances. From Hsiang & Faeth (1992).

breakup regime, as noted earlier. The results illustrated in figure 12 are in terms of a Weber number based on the SMD after breakup and the initial relative velocity. Superficially, it is evident that this Weber number exceeds criteria for secondary breakup at low Oh, as indicated on the plot which implies that a large fraction of the drops formed by breakup should still be unstable for subsequent breakup (in particular, more than half the mass of the spray formed by breakup has drop diameters greater than the SMD since MMD/SMD = 1.2). Nevertheless, there was no evidence of subsequent breakup of large drops. The reason for this behavior was explored by studying the properties of the parent drop itself as discussed next.

The velocity and size of the parent drop at the end of shear breakup must be known in order to treat it separately from the rest of the drop population. These considerations are described by Hsiang & Faeth (1995), where a simplified analysis was developed to estimate parent drop velocities at the end of breakup. The main assumptions of this analysis were that gas velocities, drop mass and the drag coefficient were constant over the period of breakup, while the time of breakup was taken to be $t_b/t^* = 5.0$. In spite of the simplifications, the resulting correlation proved to be effective for estimating parent drop velocities at the end of breakup. Parent drop velocity-measurements showed that the relative velocities of the parent drop at the end of breakup were 30–40% lower than the initial relative velocity. This still implied that the local Weber numbers of the parent drop at the end of breakup generally were greater than the critical Weber number for shock wave disturbances (We = 13). Thus, the criterion for the end of parent drop stripping is more related to conditions for breakup due to more gradual drop motions, which is plausible because the parent drop has appreciable time to adjust to the flow over the breakup period. Deformation and breakup transitions for gradual disturbances generally are correlated in terms of the Eötvös number, Eo, which is defined as follows:

$$\mathrm{Eo} = a\rho_L d^2/\sigma \qquad [8]$$

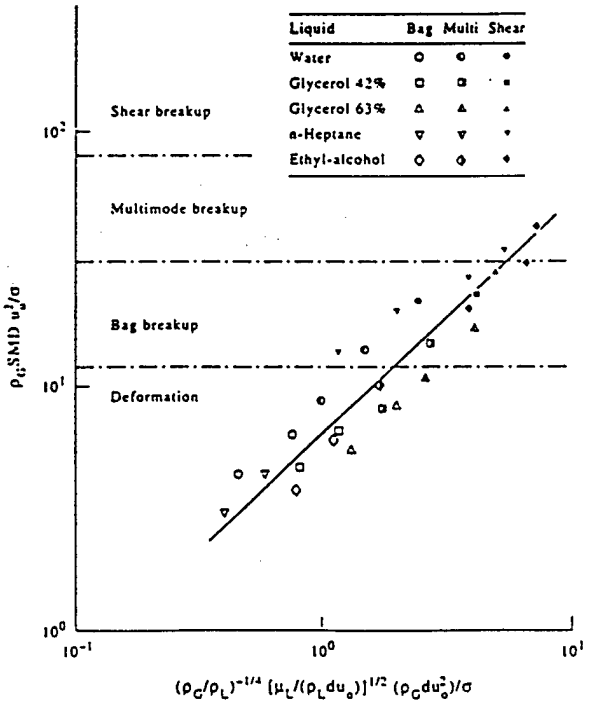

Figure 12. Correlation of SMD after secondary breakup for shock-wave disturbances with liquid/gas density ratios greater than 500. From Hsiang & Faeth (1992).

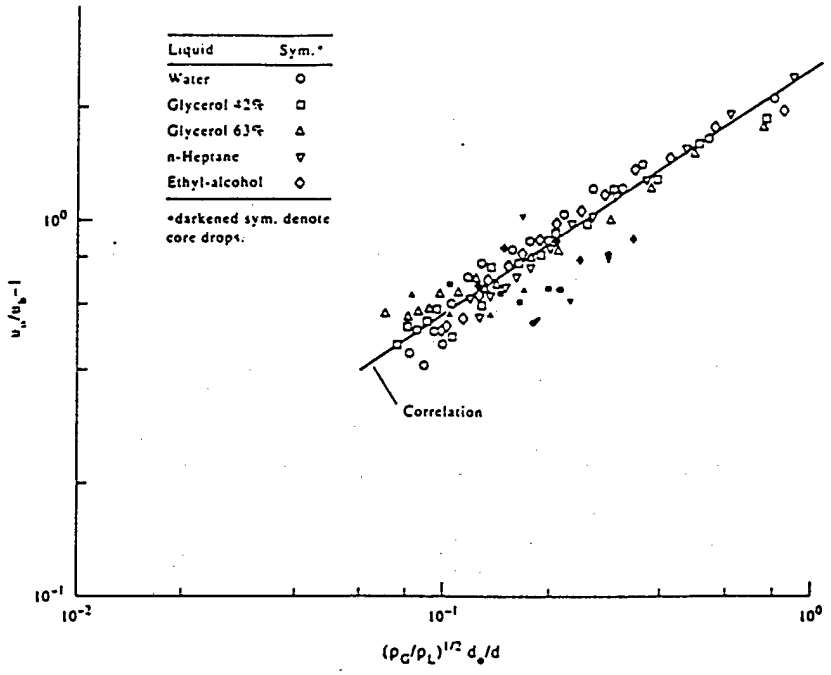

Figure 13. Correlation of drop velocities after secondary breakup for shock-wave disturbances with liquid.gas density ratios greater than 500. From Hsiang & Faeth (1993).

for conditions where $\rho_L/\rho_G \gg 1$, where a is the local acceleration of the drop. It was found that drop stripping for shear breakup ended when Eo = 16 for the parent drop. Finally, this expression yields the parent drop diameter at the end of breakup based on estimates of parent drop acceleration from the simplified analysis for parent drop velocities, see Hsiang & Faeth (1993) for the details of this correlation. With drop diameter distributions defined after secondary breakup, and parent drop diameters and velocities defined after shear breakup, the final problem is to obtain the correlation between drop sizes and velocities (other than for the parent drop) after breakup. This was done using the same approach as the analysis to find parent drop velocities, finally yielding the following drop size and velocity correlation due to Hsiang & Faeth (1993):

$$u_o/u_b - 1 = 2.7((\rho_G/\rho_L)^{1/2} d_o/d)^{2/3} \qquad [9]$$

where u_b is the velocity of drops having diameter d at the end of the breakup period. The drop-size/velocity correlation based on [9] is illustrated in figure 13. The experimental results involve a variety of drop liquids over the bag, multimode and shear breakup regimes. The measurements clearly are independent of the breakup regime and are correlated reasonably well by [9]. Results for the parent drops also are illustrated in figure 13, and exhibit a fair correlation with [9]; nevertheless, the specific parent drop velocity expression is recommended instead because it provides a much better estimate of parent drop velocities.

Finally, the variation of drop velocities with size implies that secondary breakup processes extend over a considerable region of space. For example, parent drops move 30–40 initial drop diameters during the period of breakup while the largest and smallest drops in the size distribution become separated by more than 100 initial drop diameters. In addition, times of breakup extend for $5.5t^*$, at low Ohnesorge numbers, and progressively increase with increasing Ohnesorge number. Thus, in some instances, secondary breakup is more properly treated as a rate process, somewhat like drop vaporization, rather than as an instantaneous process that can be characterized by jump conditions. Such conditions are frequently encountered at high pressures, where the dense spray region becomes relatively short as discussed in connection with [1], see Ruff *et al.* (1992) for a

detailed discussion of this scaling. As a result, the focus of current research on the outcomes of secondary breakup is shifting from outcomes as jump conditions for a rapid breakup process, to outcomes as a rate process, see Hsiang *et al.* (1995) for initial work along these lines limited to shear breakup at low Ohnesorge numbers.

3.5. Conclusions

Secondary breakup of drops has been considered, emphasizing shock-wave disturbances for a variety of liquids in air at normal temperature and pressure. The main conclusions are as follows:

(1) Drop deformation and breakup begin at We ~ 1 and 10, respectively, at low Oh; however, these transitions become proportional to Oh at large Oh, e.g. Oh > 10. This inhibition of deformation and breakup at large Oh is important for high pressure combustion processes where drops reach large Oh as their surface approaches the thermodynamic critical point.
(2) Drop-size distributions after secondary breakup satisfy the universal root-normal distribution with MMD/SMD = 1.2 due to Simmons (1977), similar to other observations within dense sprays (except for the parent drop for shear breakup which must be treated separately). Thus, the drop-size distribution after secondary breakup is completely defined by the SMD alone.
(3) The SMD after secondary breakup could be correlated rather simply in terms of a characteristic liquid boundary layer thickness for all three secondary breakup regimes, see [7].
(4) The relative streamwise velocities of drops after secondary breakup are reduced 30–70%, depending on drop size, from the initial relative velocity. These effects were correlated reasonably well based on a simplified analysis of drop motion, see [9].
(5) The streamwise velocity and size of the parent drop after shear breakup could be correlated successfully based on simplified considerations of drop motion during breakup, and the observation that Eo = 16 for the parent drop at the end of drop stripping, see Hsiang & Faeth (1995).
(6) Secondary breakup in dense sprays is not properly represented by jump conditions at the high pressures of many practical spray combustion devices. Under such circumstances, secondary breakup should be treated as a rate process.

Aside from the deformation and breakup regime map, existing information about secondary breakup is limited to Oh < 0.1 and $\rho_L/\rho_G > 500$. Clearly, effects of both Oh and ρ_L/ρ_G merit additional study in order to better understand the secondary breakup properties of practical combusting sprays. Finally, the rate aspects of secondary breakup are unknown and must be addressed in order to treat high pressure sprays where characterizing the effects of secondary breakup by jump conditions is not appropriate; initial work along these lines for shear breakup at low Ohnesorge numbers has been reported by Hsiang *et al.* (1995).

4. PRIMARY BREAKUP

4.1. Introduction

Primary breakup to form drops near liquid surfaces is a most important process of sprays because it initiates the atomization process, controls the extent of the liquid core and provides the initial conditions of the dispersed flow region. Unfortunately, current understanding of primary breakup is limited due to problems of observing primary breakup in dense spray environments, effects of secondary breakup and interphase transport that modify drop properties prior to drops reaching conditions where their properties can be measured readily, and effects of flow development and liquid disturbances (turbulence) at the jet exit that have an unusually large impact on primary breakup properties. Recently, however, pulsed holography techniques have provided a means of observing the properties of dense sprays so that some progress is being made toward gaining a better understanding of primary breakup processes, see Ruff *et al.* (1991, 1992), Tseng *et al.* (1992b), Wu *et al.* (1991, 1992, 1995) and Wu & Faeth (1993). Thus, the findings of these studies, which are limited to primary breakup along the surface of the liquid core for pressure-atomized sprays

in still gases, will be emphasized in the following. For these conditions, the onset and outcome of primary breakup will be considered, in turn.

4.2. Onset of breakup

Past studies of pressure-atomized sprays have established that all spray properties, including criteria for the onset of breakup, are strongly influenced by the degree of flow development and the presence of turbulence at the jet exit. First of all, early studies of pressure atomization by DeJuhasz *et al.* (1932) and Lee & Spencer (1933) showed that both atomization quality and mixing rates differed for laminar and turbulent flow at the jet exit. Next, Grant & Middleman (1966), Phinney (1973), Hoyt & Taylor (1977a, b), Hiroyasu *et al.* (1982) and Mansour & Chigier (1994) conclude that turbulence generated in the flow passage has a significant effect on jet breakup properties. This behavior is hardly surprising in view of the widely recognized importance of jet exit conditions on the properties of single-phase jets, see Laufer (1950), Tennekes & Lumley (1972), Hinze (1975) and Schlichting (1979), among others. Finally, Arai *et al.* (1988), Hiroyasu *et al.* (1991) and Karasawa *et al.* (1992) showed that breakup could be suppressed entirely for supercavitating flows, where the liquid jet separates from the passage wall near the end of the contraction section (and does not reattach), which have very uniform and non-turbulent velocity distributions at the jet exit. In retrospect, this behavior is not surprising because jet exit conditions of this type are widely used for liquid jet cutting systems, where avoiding breakup is a major design objective, see Yokota *et al.* (1988).

Recent studies using gamma-ray absorption and pulsed holography techniques to penetrate the dense spray region also have helped to quantify effects of flow development and turbulence at the jet exit on primary breakup properties, mixing rates and the structure of the dispersed-flow region, see Ruff *et al.* (1991, 1992), Tseng *et al.* (1992a, b), Wu *et al.* (1991, 1992, 1995) and Wu & Faeth (1993). These studies involved liquid jets in still gases at various pressures with both fully-developed turbulent flow and non-turbulent quasi-slug flow (a non-turbulent flow with a uniform velocity distribution but with wall boundary layers present whose properties were not well defined). Measurements of liquid volume fraction distributions showed much faster mixing rates, and much larger drop sizes after primary breakup, for turbulent than non-turbulent jet exit conditions even though the other properties of these flows were nearly identical. It was also established that aerodynamic effects had no influence on drop properties after primary breakup for conditions typical of pressure-atomized injection into air at normal temperature and pressure. In particular, no effect of liquid/gas density ratio on drop sizes after primary breakup, as anticipated from the classical aerodynamic primary breakup theories of Taylor (1963) and Levich (1962), was observed for liquid/gas density ratios greater than 500. Instead, primary breakup properties were controlled almost entirely by liquid phase flow properties at the exit of the injector passage.

Other studies also have found that liquid phase flow properties have dominated observations of primary breakup in pressure-atomized sprays and that aerodynamic effects are not very important at the liquid/gas density ratios typical of observations of pressure-atomized injection at normal temperature and pressure. For example, Hoyt & Taylor (1977a, b) found that breakup of liquid jets in air at atmospheric pressure was associated with the presence of turbulent boundary layers along the injector passage walls near the exit. They also demonstrated that large changes in the aerodynamic environment, including both coflowing and counterflowing air, had little effect on breakup properties. Unfortunately, similar to most past studies of pressure atomization, the actual properties of the turbulent boundary layers along the passage walls were not quantified by Hoyt & Taylor (1977a, b) for their experimental conditions.

Wu *et al.* (1995) recently have reported a study where the degree of flow development at the jet exit was controlled, so that its effect on primary breakup properties could be examined. This experiment involved pressure-atomized jets provided by a converging passage having a large contraction ratio to yield a non-turbulent flow at its exit. The degree of flow development at the injector exit was then controlled by removing the boundary layer formed along the converging passage, and providing constant-diameter passages of various lengths, L, (or L/d) after boundary layer removal. Test conditions included water, n-heptane and various glycerol mixtures injected into helium, air and Freon 12 at pressures of 1 and 2 atm, to yield ρ_L/ρ_G in the range 104–7240.

The experiments of Wu *et al.* (1995) showed that the onset of breakup along the surface of the liquid core was affected by both the L/d ratio of the constant area section of the injector passage and the Reynolds number of the flow through the injector passage. The effect of L/d is illustrated by the pulsed photographs of the flow appearing in figure 14. Three conditions are shown: boundary layer removal followed by $L/d = 4$ and 10, and a round contraction followed by $L/d = 41$. Passage Reynolds numbers for all three conditions exceed 10^5, which is sufficient to obtain fully-developed turbulent pipe flow for sufficiently long L/d, see Hinze (1975) and Schlichting (1979). In fact, measurements made by Ruff *et al.* (1991) for $L/d = 41$, at similar conditions, showed that flow properties at the jet exit approximated the properties of fully-developed turbulent pipe flow reported by Laufer (1950). Thus, it is not surprising that the liquid surface exhibits the formation of ligaments and drops very near the jet exit, corresponding to what has been termed turbulent primary breakup by Wu *et al.* (1991, 1992, 1995) and Wu & Faeth (1993), for the large L/d condition. In contrast, the flow remains smooth near the jet exit and no breakup is observed for $L/d = 4$, yielding behavior similar to the findings for very short passage lengths ($L/d = 0.15$) suggesting the absence of breakup in the absence of liquid vorticity, i.e. for conditions where the liquid velocity distribution is uniform and no turbulence is present. Increasing the length of the constant area section to $L/d = 10$, however, allows the development of turbulent boundary layers along the walls and the corresponding development of turbulent primary breakup along the liquid surface.

Additional visualization of the breakup of liquid jets for various passage Reynolds numbers and L/d can be found in Wu *et al.* (1995); a breakup regime map summarizing all the test results as a function of L/d and Re_{Ld} is illustrated in figure 15. Observations of turbulent primary breakup are denoted on the figure by cross-hatched, half-darkened and darkened symbols; open symbols denote laminar-like conditions where turbulent primary breakup was not observed although large scale wavy (sinuous) disturbances were seen in some instances. Results shown on the figure include the observations of Ruff *et al.* (1991), Tseng *et al.* (1992b), Wu *et al.* (1991, 1992, 1995), Wu & Faeth (1993) and Grant & Middleman (1966). The results of Grant & Middleman (1966) were of interest because they involved sharp-edged inlets which provided more disturbed flows than the other conditions.

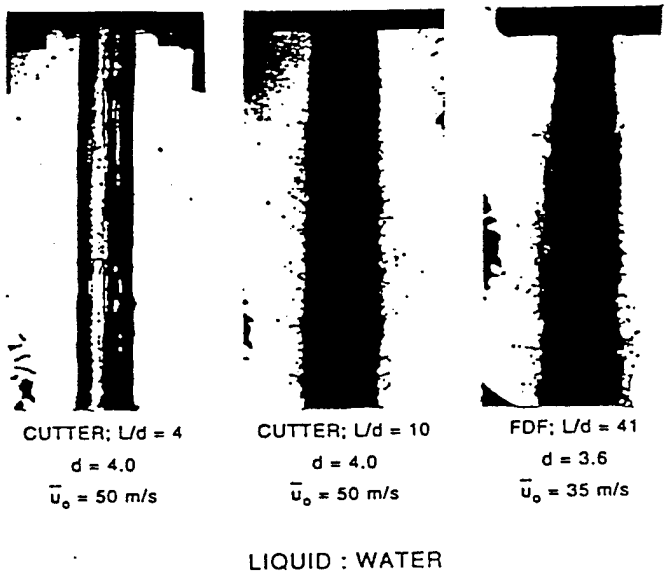

Figure 14. Pulsed-photographs of round liquid jets injected into still air for various L/d. From Wu *et al.* (1991).

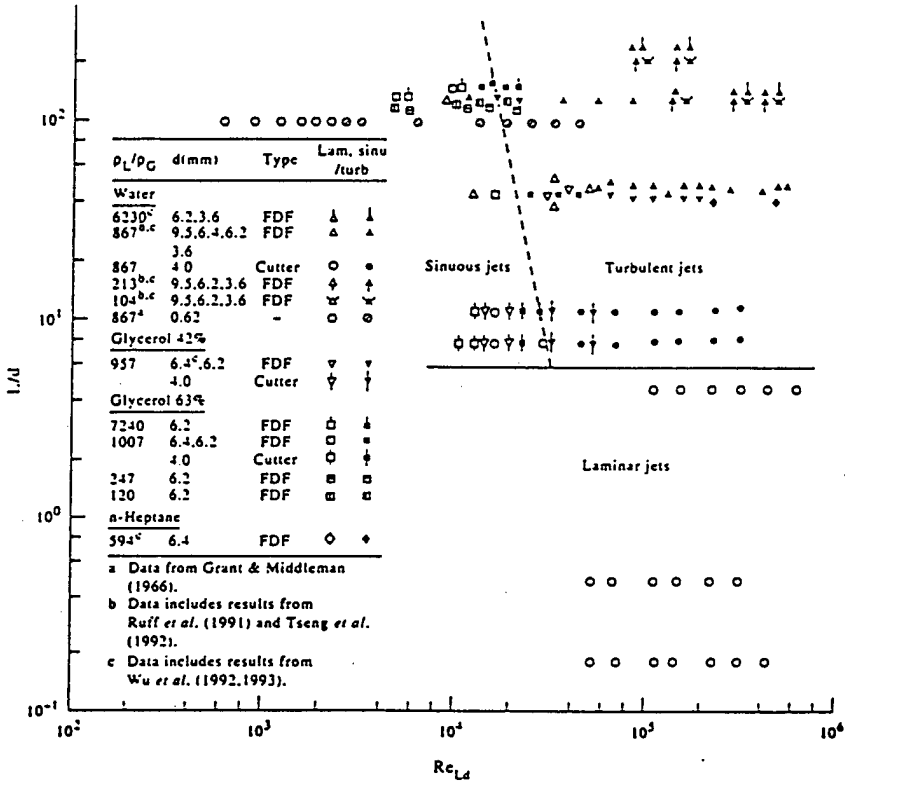

ρ_L/ρ_G	d(mm)	Type	Lam, sinu /turb
Water			
6230[c]	6.2.3.6	FDF	
867[b,c]	9.5.6.4.6.2 3.6	FDF	
867	4.0	Cutter	
213[b,c]	9.5.6.2.3.6	FDF	
104[b,c]	9.5.6.2.3.6	FDF	
867[a]	0.62	-	
Glycerol 42%			
957	6.4[c].6.2	FDF	
	4.0	Cutter	
Glycerol 63%			
7240	6.2	FDF	
1007	6.4.6.2	FDF	
	4.0	Cutter	
247	6.2	FDF	
120	6.2	FDF	
n-Heptane			
594[c]	6.4	FDF	

a Data from Grant & Middleman (1966).
b Data includes results from Ruff *et al.* (1991) and Tseng *et al.* (1992).
c Data includes results from Wu *et al.* (1992,1993).

Figure 15. Primary breakup regime map for round liquid jets injected into still gases. From Wu *et al.* (1995).

Except for the conditions of Grant & Middleman (1966), the results illustrated in figure 15 indicate the presence of turbulent primary breakup for $L/d > 4$–6 and $Re_{Ld} > 1$–4×10^4, with a general tendency for Re_{Ld} at transition to become smaller as L/d increases. This behavior can be anticipated from the well known tendency for large L/d passages to exhibit turbulent flow at the exit at lower Reynolds numbers, and the relatively large values of Re_{Ld} required to achieve turbulent pipe flow for relatively disturbance-free inlet conditions, see Hinze (1975) and Smith (1960). In contrast, the results of Grant & Middleman (1966) highlight potential effects of strong inlet disturbances typical of most practical pressure-atomized injectors, where turbulent primary breakup is observed at Re_{Ld} of roughly 3000, which is comparable to the lowest Reynolds numbers where turbulent pipe flow has been observed, see Hinze (1975) and Schlichting (1960). Finally, observations showed that there was no effect of ambient gas densities on the breakup regime map of figure 15 for ρ_L/ρ_G in the range 104–7240, even though aerodynamic effects begin to influence drop sizes after turbulent primary breakup for $\rho_L/\rho_G > 500$; this behavior is reasonable because the onset of turbulent primary breakup appears to be dominated by effects of transition from laminar to turbulent flow within the injector passage.

Subsequent considerations of primary breakup will be limited to turbulent primary breakup because this condition provides an adequate definition of jet exit conditions. Thus, subsequent data will involve $L/d \geqslant 10$ and $Re_{Ld} \geqslant 20{,}000$. Even for these conditions, however, the onset of turbulent primary breakup along the liquid surface can be delayed, and may not occur before large scale disturbances disrupt the entire liquid core, see Ruff *et al.* (1990). Thus, the properties at the onset of turbulent primary breakup will be considered next.

Wu and coworkers (1991, 1992, 1995) and Wu & Faeth (1993) used phenomenological analysis to develop estimates of the drop sizes and location at the onset of turbulent primary breakup.

Typical of other dense spray conditions, drop sizes after turbulent primary breakup satisfied the universal root normal distribution with MMD/SMD = 1.2 due to Simmons (1977); therefore, the SMD alone is sufficient to define drop size properties, as discussed earlier. See Belz (1973) for a discussion of the properties of this distribution function. Based on time scale considerations, the drops at the onset of turbulent primary breakup are the smallest drops that can be formed. The smallest drops are then either comparable to the Kolmogorov micro-length scale, or to the smallest turbulent eddy that has sufficient kinetic energy relative to its immediate surroundings to provide the surface energy needed to form a drop, whichever is larger. For conditions studied thus far, the energy criterion has controlled, therefore, the analysis has proceeded assuming that the critical eddy size is in the inertial range of the turbulence. The remaining assumptions are as follows: turbulence kinetic energy of the critical eddy size is proportional to the surface energy of the resulting drop, liquid turbulence properties unchanged from jet exit conditions, and turbulent eddy size proportional to the SMD of the drop-size distribution at the onset of breakup. Then relating turbulent eddy size and local relative eddy velocities from well known results for the inertial range of the turbulence spectrum, see Tennekes & Lumley (1972), the following equation is obtained for the SMD at the onset of turbulent primary breakup:

$$\mathrm{SMD}_i/\Lambda = C_{\text{st}}(\bar{u}_o/\bar{v}'_o)^{6/5}\mathrm{We}_{L\Lambda}^{-3/5} \qquad [10]$$

where SMD_i is the Sauter mean diameter at the onset of turbulent primary breakup, Λ is the radial integral length scale of the turbulence, $\bar{u}_o$ and $\bar{v}'_o$ are the mean streamwise and cross-stream rms radial fluctuating velocities, $\mathrm{We}_{L\Lambda} = \rho_L \Lambda \bar{u}_o^2/\sigma$ and C_{st} is an empirical constant involving the various proportionality constants. With fully-developed turbulent pipe flow at the jet exit, $\bar{v}'_o/\bar{u}_o$ also is essentially constant, see Hinze (1975) and Schlichting (1979); therefore, SMD_i/Λ should be only a function of $\mathrm{We}_{L\Lambda}$ for these conditions.

Available measurements of SMD_i are plotted according to [10] in figure 16. The correlation of the available data, which includes several liquids and $L/d > 10$, is seen to be quite good. The power

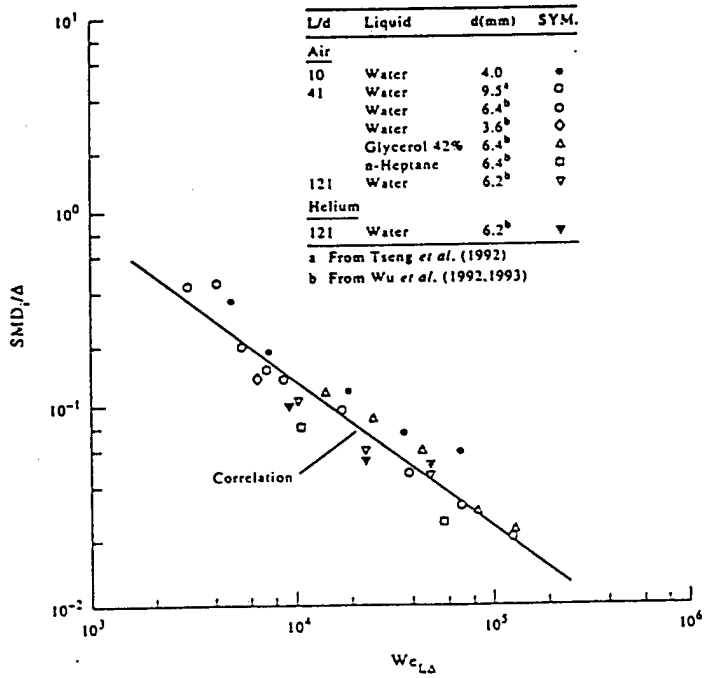

Figure 16. SMD at the onset of turbulent primary breakup for round liquid jets injected into still gases. From Wu *et al.* (1995).

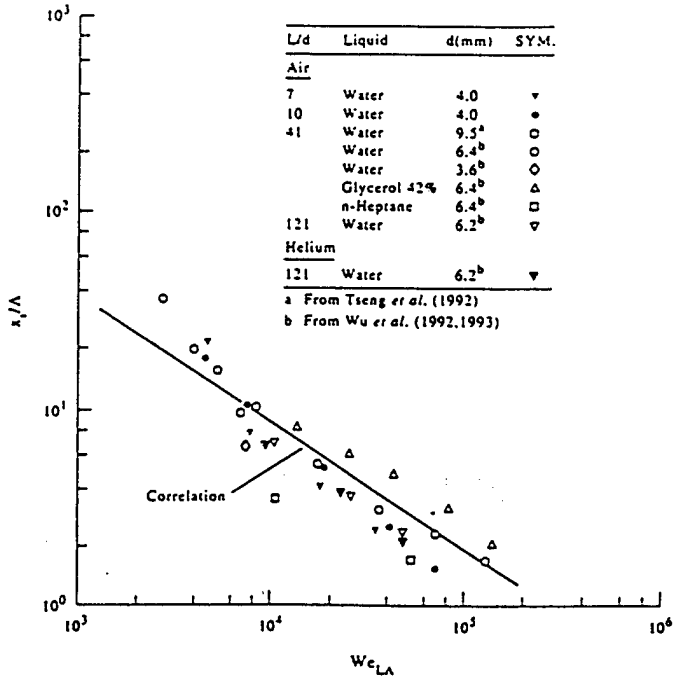

Figure 17. Streamwise location of the onset of turbulent primary breakup for round liquid jets injected into still gases. From Wu *et al.* (1995).

of $We_{L\Lambda}$ for the measurements is not $-3/5$ as suggested by [10], however, but can be represented better by the following empirical fit that is shown on the plot:

$$SMD_i/\Lambda = 133We_{L\Lambda}^{-0.74} \qquad [11]$$

Notably, the powers of $We_{L\Lambda}$ in [10] and [11] agree within experimental uncertainties while the rather large coefficient of [11] is quite plausible because $(\bar{u}_o/\bar{v}_o')^{6/5}$ is large for fully-developed turbulent pipe flow, see Laufer (1950). Thus, the main ideas used to develop [10] appear to be plausible.

The next step involved developing an expression for the distance from the jet exit, x_i, where turbulent primary breakup is initiated. Wu *et al.* (1991, 1992, 1995) and Wu & Faeth (1993) also developed a phenomenological analysis for x_i assuming that the eddy convects along the surface of the liquid core with a velocity $\bar{u}_o$, that the ligament developed by the eddy moves radially outward with the characteristic eddy velocity in the inertial range, and that the critical drop at the onset of breakup separates from the ligament at the characteristic time for Rayleigh breakup, see Wu *et al.* (1992) for discussion of other possible characteristic times. These considerations finally lead to the following expression for the distance from the jet exit where turbulent primary breakup begins:

$$x_i/\Lambda = C_{ut}(\bar{u}_o/\bar{v}_o')^{9/5}We_{L\Lambda}^{-0.4} \qquad [12]$$

where C_{ut} is a constant of proportionality while $(\bar{u}_o/\bar{v}_o')^{9/5}$ also is a constant for fully-developed turbulent pipe flow.

Available measurements of x_i are plotted according to [12] in figure 17. The correlation of available data, for the same range of properties as figure 16, is seen to be quite good. As before, however, the power of $We_{f\Lambda}$ is not -0.4 as suggested by [12] but can be better represented by the following empirical fit, which is shown on the plot:

$$x_i/\Lambda = 3890We_{L\Lambda}^{-0.67} \qquad [13]$$

Similar to the expression for SMD_t, the power of We_{LA} in [13] is not very different from the predicted power in [12], while the large coefficient in [13] can be anticipated because $(\bar{u}/\bar{v}_o')^{9/5}$ in [12] is large for fully-developed turbulent pipe flow.

Subsequent work by Wu & Faeth (1993) showed that aerodynamic effects modified [11] and [13] somewhat for $\rho_L/\rho_G < 500$. In addition, the combined criteria for the presence of turbulent primary breakup along the surface of the liquid core, represented by figure 15 and [13], correspond to a different viewpoint than the classical criteria for the wind-induced and atomization breakup regimes, see Faeth (1990). Thus, more work is needed to establish the relationship between turbulent primary breakup and earlier definitions of atomization breakup regimes. Finally, Wu & Faeth (1995) have identified a range of conditions where turbulent primary breakup ends along the liquid surface before the end of the liquid core was reached, and have successfully correlated conditions for the end of breakup with turbulence properties in the large-eddy subrange of the turbulence spectrum. However, the properties of drops produced by primary breakup in the large eddy subrange, as well as for conditions where Kolmogorov scales are reached that were mentioned earlier, must still be resolved.

4.3. Breakup outcomes

With conditions for the onset of turbulent primary breakup established, the next issues include breakup outcomes, e.g. the variation of drop velocity and size distributions with increasing distance from the jet exit. Similar to the properties of secondary breakup, drop sizes satisfied the universal root normal distribution with MMD/SMD = 1.2 due to Simmons (1977), and drop velocity distributions were uniform, after turbulent primary breakup. Thus, drop size and velocity distributions will be represented by the SMD and mass-averaged velocities in the following.

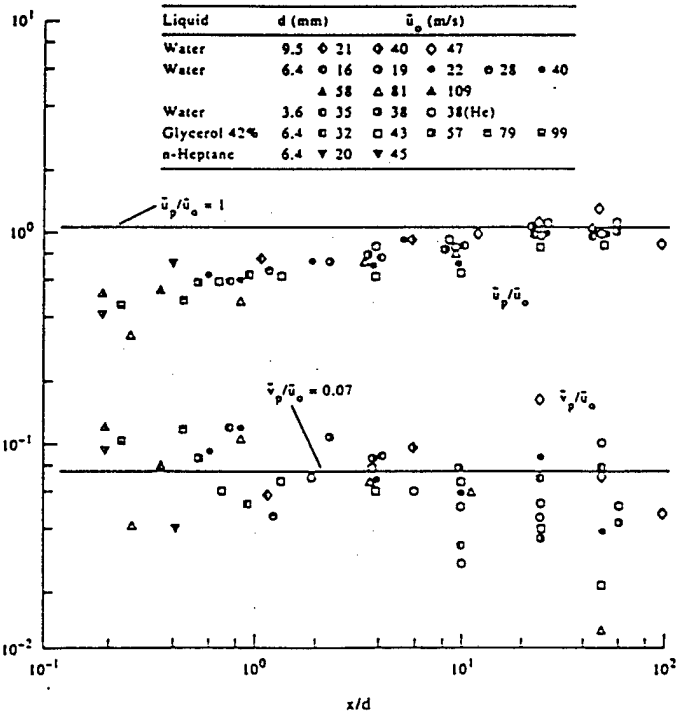

Figure 18. Mass-averaged drop velocities after turbulent primary breakup as a function of distance from the jet exit. From Wu *et al.* (1992).

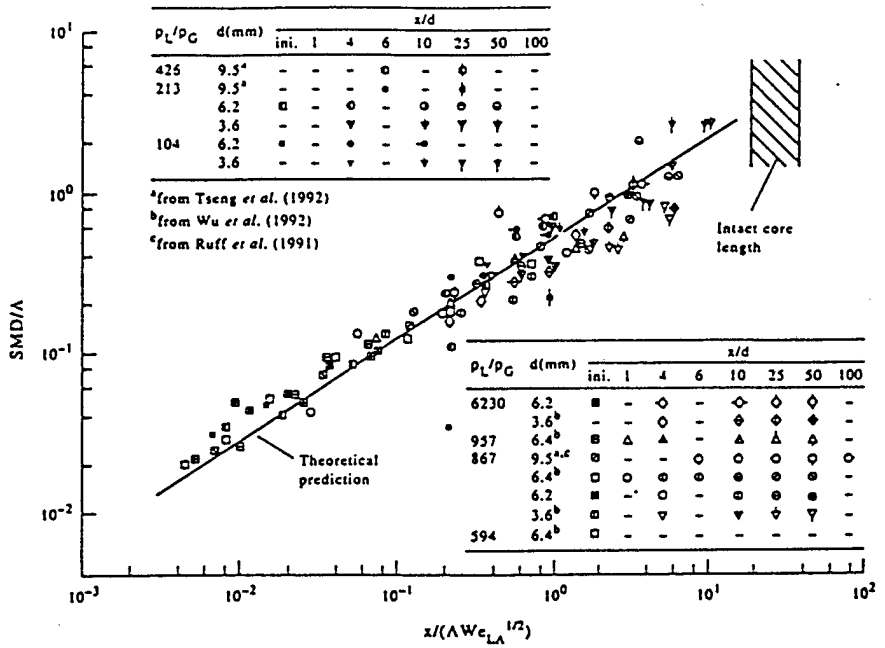

Figure 19. SMD after turbulent primary breakup as a function of distance from the jet exit (for negligible aerodynamic effects) for round liquid jets injected into still gases. From Wu & Faeth (1993).

Mass-averaged streamwise and cross-stream drop velocities, $\tilde{u}_p$ and $\tilde{v}_p$, after turbulent primary breakup are plotted as a function of distance from the jet exit in figure 18. Measurements shown in the plots were obtained from Wu *et al.* (1992), Ruff *et al.* (1991) and Tseng *et al.* (1992b). Results at $\rho_L/\rho_G > 500$ are shown as open symbols while those at $\rho_L/\rho_G < 500$ are shown as filled and half-filled symbols, in order to highlight potential aerodynamic effects. Except for a small region near the jet exit where the effect of the passage walls retards streamwise drop velocities somewhat, $\tilde{u}_p/\tilde{u}_o \approx 0.9$ and $\tilde{v}_p/\tilde{u}_o \approx 0.06$ relatively independent of position. Noting that the maximum value of $\tilde{v}'_o/\tilde{u}_o \approx 0.06$ for fully-developed turbulent pipe flow, see Hinze (1975), it is concluded that mass-averaged streamwise and cross-stream drop velocities after turbulent primary breakup correspond to streamwise velocities and r.m.s. cross-stream velocity fluctuations in the liquid jet, respectively. This behavior is reasonable because the liquid core tends to maintain jet exit properties (it has a large relaxation time due to its large size) while primary breakup occurs reasonably fast so that there is little time for ligament and drop properties to change, as well. Nevertheless, there is a trend for reduced streamwise velocities at small ρ_L/ρ_G so that these approximations for drop velocities should be re-examined prior to application to high pressure sprays.

The variation of SMD along the liquid surface was initially studied for conditions where aerodynamic effects were small, e.g. $\rho_L/\rho_G > 500$, see Wu *et al.* (1992). The approach used to correlate the measurements was an extension of the method used to find x_i. It was assumed that the SMD was proportional to the largest drop that could be formed at a particular position, x, after adopting the Rayleigh breakup mechanism for the ligament. This yielded the following expression for the variation of SMD with distance from the jet exit:

$$\mathrm{SMD}/\Lambda = C_u (x/(\Lambda \mathrm{We}_{L\Lambda}^{1/2})^{2/3} \qquad [14]$$

where C_u is an empirical constant. Available measurements of the variation of SMD with distance from the jet exit are plotted in figure 19 according to the variables of [14]. These results were

obtained from Ruff *et al.* (1992), Tseng *et al.* (1992b) and Wu & Faeth (1993). Some of the results illustrated in figure 19 involve $\rho_L/\rho_G < 500$ and have been corrected for aerodynamic effects; these findings will be discussed subsequently. The correlation is seen to be quite good and can be represented by the following empirical fit:

$$SMD/\Lambda = 0.65(x/(\Lambda We_{L\Lambda}^{1/2}))^{2/3} \quad [15]$$

Notably, the good agreement between the measurements and the somewhat complex power relationships of [14] and [15], coupled with a coefficient of order of magnitude unity in [15], suggests that the physical principles used to derive [14] are reasonable. Another interesting feature of these results is that the SMD approaches the order of magnitude of the liquid core itself near the end of the liquid core based on the correlation measured by Grant & Middleman (1966), for fully turbulent liquid jets in still gases at atmospheric pressure where aerodynamic effects are small, namely

$$L_c/d = 8.51 We_{Ld}^{0.12} \quad [16]$$

Notably, the earlier result of Chehroudi *et al.* (1985), given in [1], yields qualitatively similar results but with a somewhat broader range of L_c/d. In any event, the fact that the SMD is comparable to the diameter of the liquid column near its end clearly is compatible with the liquid column breaking up as a whole in this region.

The final phase of this work was to consider aerodynamic effects on drop sizes after turbulent primary breakup, see Wu & Faeth (1993). For conditions where aerodynamic effects are important, the aerodynamic secondary breakup times for a ligament of characteristic size ℓ_i scale according to $\ell_i(\rho_L/\rho_G)^{1/2}/u_o$ while the Rayleigh breakup times of ligaments are proportional to $(\rho_L\ell_i^3/\sigma)^{1/2}$. As a result Rayleigh breakup times increase more rapidly than secondary breakup times as ℓ_i increases. This implies a tendency for secondary and primary breakup to merge as distance from the jet exit increases. Analysis of these conditions was carried out by using [15] to define initial drop sizes and then applying the secondary breakup results of [7] to obtain the final SMD after merged primary and secondary breakup. The resulting best fit correlation of merged primary and secondary breakup is as follows:

$$\rho_G SMD u_o^2/\sigma = 12.9(x/\Lambda)^{1/3}(\rho_G/\rho_L)^{3/2} We_{L\Lambda}^{3/4}/Re_{L\Lambda}^{1/2} \quad [17]$$

Available measurements of merged primary and secondary breakup are plotted in figure 20 according to the variables of [17]. Measurements shown on the plot were obtained from Tseng *et al.* (1992b) and Wu & Faeth (1993). Equation [17] is plotted on the figure as well and is seen to provide an excellent correlation of the data, tending to support the physical ideas used in its derivation, see Wu & Faeth (1993) for the slightly improved best fit of the data that is also shown on the plot.

The turbulent primary breakup measurements of Wu *et al.* (1991, 1992, 1995) and Wu & Faeth (1993) suggested three regimes of turbulent primary breakup: (1) non-aerodynamic turbulent primary breakup; (2) aerodynamically-enhanced turbulent primary breakup, observed at onset conditions; and (3) aerodynamic turbulent primary breakup, which involves merging of turbulent primary and secondary breakup. The results also indicated that the boundaries of these regimes are fixed by the liquid/gas density ratio and the relative magnitudes of characteristic Rayleigh breakup times of ligaments and the secondary breakup times of liquid fragments. The breakup times used to define these regimes were based on the SMD after primary breakup, or after the primary breakup stage of merged primary and secondary breakup, for conditions beyond the onset of breakup for present data. Thus, the characteristic Rayleigh breakup time was taken to be $\tau_R \sim (\rho_L SMD^3/\sigma)^{1/2}$, while the characteristic secondary breakup time was taken to be $\tau_b \sim (\rho_L/\rho_G)^{1/2} SMD/\bar{u}_o$. Then eliminating SMD from the ratio, the characteristic time ratio was taken to be:

$$\tau_R/\tau_b = (\rho_L/\rho_G)^{1/2}(x We_{f\Lambda}/\Lambda)^{1/3} \quad [18]$$

The resulting turbulent primary breakup regimes based on the available measurements of Ruff *et al.* (1992), Tseng *et al.* (1992b), Wu *et al.* (1991, 1992, 1995) and Wu & Faeth (1993), are illustrated in terms of ρ_L/ρ_G and τ_R/τ_b in figure 21. The total set of measurements yields

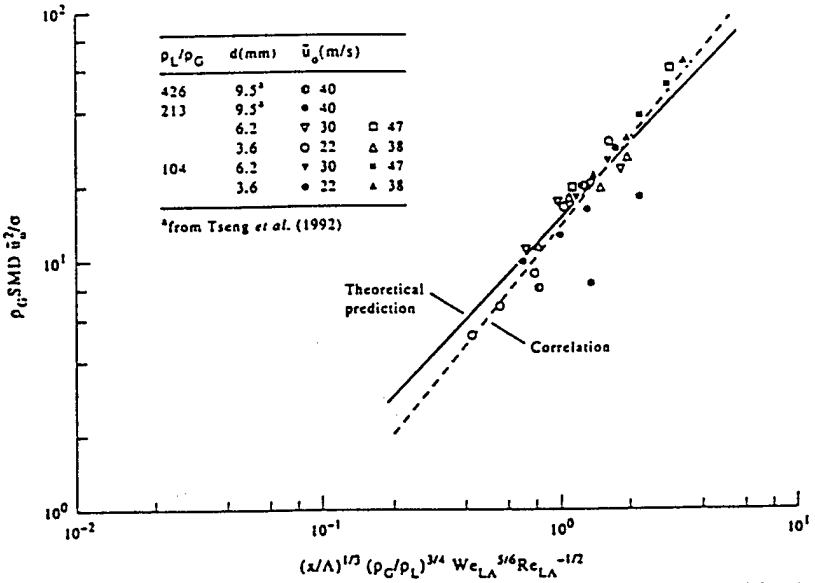

Figure 20. SMD after aerodynamically enhanced turbulent primary breakup for round liquid jets injected into still gases. From Wu & Faeth (1993).

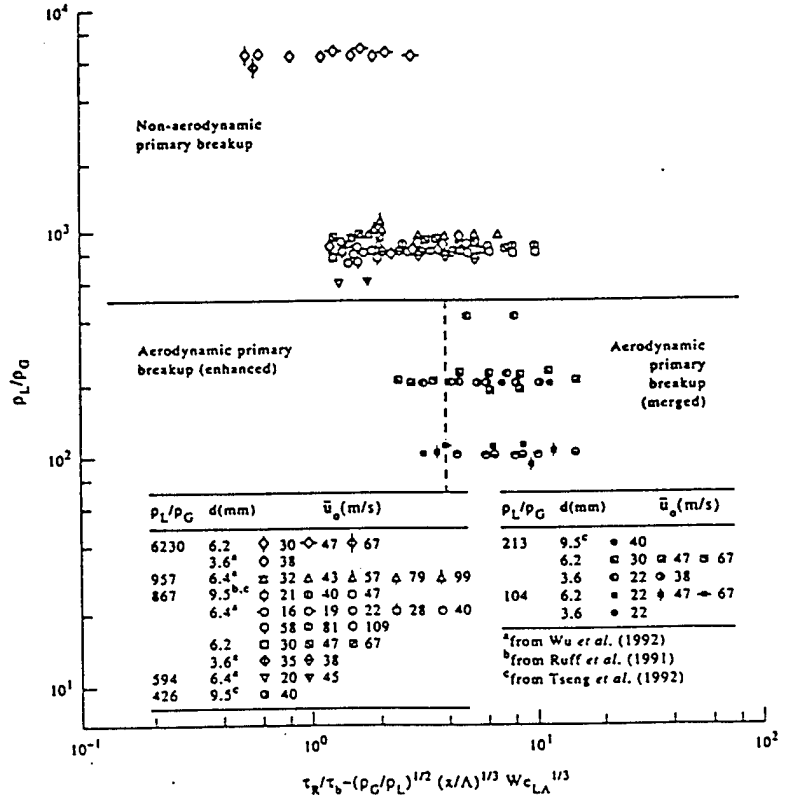

Figure 21. Turbulent primary breakup regime map for round liquid jets injected into still gases. From Wu & Faeth (1993).

$\rho_L/\rho_G = 500$, as the aerodynamic/non-aerodynamic transition, and $\tau_R/\tau_b = 4$, as the enhanced-aerodynamic/merged transition.

5. CONCLUSIONS

Primary breakup along the surface of turbulent liquids was studied, considering liquid jets in still gases with fully-developed turbulent pipe flow at the jet exit (ρ_L/ρ_G of 104–6230, Re_{Ld} of 90,000–780,000, We_{Gd} of 12–3790, We_{Ld} of 60,000–1,090,000 and Oh_d of 0.0011–0.0052). The major conclusions of the study are as follows:

(1) The presence of aerodynamic phenomena for turbulent primary breakup largely is controlled by the liquid/gas density ratio. When this ratio is less than 500, aerodynamic phenomena affect both conditions at the onset of breakup, and drop sizes and velocities (to a lesser extent) after breakup.
(2) Aerodynamic enhancement of the onset of turbulent primary breakup was due to the aerodynamic pressure reduction over the tips of protruding liquid elements. This effect assists the kinetic energy of a corresponding liquid eddy relative to its surroundings to provide the surface tension energy needed to form a drop, thus allowing smaller drops to form. Phenomenological analysis based on these ideas yielded reasonable correlations of onset properties.
(3) For conditions where secondary breakup times become small in comparison to Rayleigh breakup times of turbulence-induced ligaments protruding from the surface, processes of primary and secondary breakup merge, yielding smaller drops than when aerodynamic effects are absent. The reduction of drop sizes at these conditions correlated well with results for the secondary breakup of drops due to shock disturbances.
(4) Drop-size distributions after aerodynamic turbulent primary breakup approximated the universal root normal distribution with MMD/SMD = 1.2 due to Simmons (1977), similar to observations of other drop breakup processes as well as drops in the multiphase mixing layers of pressure-atomized sprays. Additionally, mass-averaged drop velocities after aerodynamic turbulent primary breakup approximate mean and rms velocity fluctuations of the liquid in the streamwise and cross-stream directions, respectively, although there was a tendency for streamwise velocities to be somewhat reduced by aerodynamic effects.

A major issue still open involves primary breakup of non-turbulent liquids and the relevance of the classical primary breakup theories of Taylor (1963) and Levich (1962). Results discussed here indicate that it is difficult to observe the non-turbulent primary breakup mechanism. The main problems are effects of liquid disturbances, the intrusion of secondary breakup and weak aerodynamic effects for most liquids at normal temperature and pressure where measurements are most convenient. Until these experimental difficulties are resolved, understanding of this important primary breakup mechanism will remain limited. The properties of turbulent primary breakup also merit additional study, particularly behavior in the large eddy subrange of the turbulence spectrum, as well as for conditions where drop formation is controlled by the smallest turbulent eddies in the region of the Kolmogorov microscales.

Acknowledgements—The author's research on sprays has been supported by the U.S. Air Force Office of Scientific Research, Grant Nos AFOSR-89-0516, F49620-92-T-0399 and F49620-95-I-0364, under the technical management of J. M. Tishkoff; and by the U.S. Office of Naval Research, Grant Nos N00014-95-1-0234 and N00014-89-J-1199, under the technical management of E. P. Rood and G. D. Roy. The authors would like to acknowledge useful discussions with W.-H. Chou, G. A. Ruff and L.-K. Tseng. The U.S. Government is authorized to reproduce and distribute copies for governmental purposes notwithstanding any copyright notation thereon.

REFERENCES

Annamalai, J. A. & Ryan, W. 1992 Interactive processes in gasification and combustion. Part 1: Liquid drop arrays and clouds. *Prog. Energy Combust. Sci.* 9, 221–295.

Arai, M., Shimizu, M. & Hiroyasu, H. 1985 Break-up length and spray angle of high speed jet. *Proc. 3rd Int. Conf. on Liquid Atomization and Spray Systems*, pp. IB/4/1–IB/4/10.

Arai, M., Shimizu, M. & Hiroyasu, H. 1988 Break-up length and spray formation mechanisms of a high speed liquid jet. *Proc. 4th Int. Conf. on Liquid Atomization and Spray Systems*, pp. 177–184.

Belz, M. H. 1973 *Statistical Methods in the Process Industries*, pp. 103–104. Wiley, New York.

Chehroudi, B., Onuma, Y., Chen, S.-H. & Bracco, F. V. 1985 On the intact core of full-cone sprays. SAE Paper No. 850126.

Clift, R., Grace, J. R. & Weber, M. E. 1978 *Bubbles, Drops and Particles*, p. 346. Academic Press, New York.

De Juhasz, K. J., Zahm, O. F. Jr & Schweitzer, P. H. 1932 On the formation and dispersion of oil sprays. Bulletin No. 40, Engineering Experimental Station, Pennsylvania State University, University Park, PA, pp. 63–68.

Engel, O. G. 1958 Fragmentation of waterdrops in the zone behind an air shock. *J. Res. Nat. Bur. Standards* 60, 245–280.

Faeth, G. M. 1977 Current status of droplet and liquid combustion. *Prog. Energy Combust. Sci.* 3, 191–224.

Faeth, G. M. 1983 Evaporation and combustion in sprays. *Prog. Energy Combust. Sci.* 9, 1–76.

Faeth, G. M. 1987 Mixing, transport and combustion in sprays. *Prog. Energy Combust. Sci.* 13, 293–345.

Faeth, G. M. 1990 Structure and atomization properties of dense turbulent sprays. *Twenty-Third Symp. (Int.) on Combustion*, The Combustion Institute, Pittsburgh, PA, pp. 1345–1352.

Gel'fand, B. E, Gubin, S. A. & Kogarko, S. M. 1974 Various forms of drop fractionation in shock waves and their special characteristics. *Inzh.-Fiz. Zh.* 27, 119–126.

Giffen, E. & Muraszew, A. 1953 *The Atomization of Liquid Fuels*. Chapman & Hall, London.

Hanson, A. R., Domich, E. G. & Adams, H. S. 1963 Shock-tube investigation of the breakup of drops by air blasts. *Phys. Fluids* 6, 1070–1080.

Harrje, D. T. & Reardon, F. H. 1972 Liquid rocket combustion instability. NASA SP-194, pp. 49–55.

Hinze, J. O. 1948 Critical speeds and sizes of liquid globules. *Appl. Sci. Res.* 11, 273–287.

Hinze, J. O. 1955 Fundamentals of the hydrodynamic mechanism of splitting in dispersion processes. *AIChE Jl* 1, 289–295.

Hinze, J. O. 1975 *Turbulence*, 2nd Edn. pp. 427, 724–734. McGraw-Hill, New York.

Hiroyasu, H., Shimizu, M. & Arai, M. 1982 The breakup of a high speed jet in a high pressure gaseous atmosphere. *Proc. 2nd Int. Conf. on Liquid Atomization and Spray Systems*, University of Wisconsin, Madison, WI, p. 69.

Hiroyasu, H., Arai, M. & Shimizu, M. 1991 Break-up length of a liquid jet and internal flow in a nozzle. *Proc. 5th Int. Conf. on Liquid Atomization and Spray Systems*, pp. 275–282.

Hoyt, J. W. & Taylor, J. J. 1977a Turbulence structure in a water jet discharging in air. *Phys. Fluids* 20, Pt II, S253–S257.

Hoyt, J. W. & Taylor, J. J. 1977b Waves on waterjets. *J. Fluid Mech.* 88, 119–127.

Hsiang, L.-P. & Faeth, G. M. 1992 Near-limit drop deformation and secondary breakup. *Int. J. Multiphase Flow* 18, 635–652.

Hsiang, L.-P. & Faeth, G. M. 1993 Drop properties after secondary breakup. *Int. J. Multiphase Flow* 19, 721–735.

Hsiang, L.-P. & Faeth, G. M. 1995 Drop deformation and breakup due to shock wave and steady disturbances. *Int. J. Multiphase Flow* 21, 545–560.

Hsiang, L.-P., Chou, W.-H. & Faeth, G. M. 1995 Temporal variation of drop properties and formation rates during secondary breakup. AIAA Paper 95-2426.

Karasawa, T., Tanaka, M., Abe, K., Shiga, S. & Kurabayashi, T. 1992 Effects of nozzle configuration on the atomization of a steady spray. *Atom. Sprays* 2, 411–426.

Krzeczkowski, S. A. 1980 Measurement of liquid droplet disintegration mechanisms. *Int. J. Multiphase Flow* 6, 227–239.

Lane, W. R. 1951 Shatter of drops in streams of air. *Ind. Engng Chem.* 43, 1312–1317.

Laufer, J. 1954 The structure of turbulence in fully developed pipe flow. NACA Report 1174.

Law, C. K. 1982 Recent advances in droplet vaporization and combustion. *Prog. Energy Combust. Sci.* 8, 169–201.
Lee, D. W. & Spencer, R. C. 1933 Photomicrographic studies of fuel sprays. NACA Report 454.
Lefebvre, A. H. 1980 Airblast atomization. *Prog. Energy Combust. Sci.* 6, 223–246.
Lefebvre, A. H. 1983 *Gas Turbine Combustion*. Hemisphere, New York.
Lefebvre, A. H. 1989 *Atomization and Sprays*, pp. 27–78, 201–272, Hemisphere, New York.
Levich, V. G. 1962 *Physicochemical Hydrodynamics*, pp. 636–546. Prentice-Hall, Englewood Cliffs, NJ.
Loparev, V. P. 1975 Experimental investigation of the atomization of drops of liquid under conditions of a gradual rise of the external forces. *Izv. Akad. Nauk SSSR. Mekh. Zh. Gaza* 3, 174–178.
Mansour, A. & Chigier, N. 1994 Effect of turbulence on the stability of liquid jets and resulting droplet size distributions. *Atom. Sprays* 4, 583–604.
Miesse, C. C. 1955 Correlation of experimental data on the disintegration of liquid jets. *Ind. Engng Chem.* 470, 1690–1697.
Phinney, R. E. 1973 The breakup of a turbulent jet in a gaseous atmosphere. *J. Fluid Mech.* 63, 689–701.
Ranger, A. A. & Nicholls, J. A. 1969 Aerodynamic shattering of liquid drops. *AIAA Jl* 7, 285–290.
Ranz, W. E. 1958 Some experiments on orifice sprays. *Can. J. Chem. Engng* 36, 175–181.
Reinecke, W. G. & McKay, W. L. 1969 Experiments on waterdrop breakup behind Mach 3 to 12 shocks. Sandia Corp. Report SC-CR-70-6063.
Reinecke, W. G. & Waldman, G. D. 1970 A study of drop breakup behind strong shocks with applications to flight. Avco Report AVSD-0110-70-77.
Reitz, R. D. & Bracco, F. V. 1982 Mechanism of atomization of a liquid jet. *Phys. Fluids* 25, 1730–1742.
Ricou, F. P. & Spalding, D. B. 1961 Measurements of entrainment by axisymmetrical turbulent jets. *J. Fluid Mech.* 11, 21–32.
Ruff, G. A. & Faeth, G. M. 1995 Non-intrusive measurements of the structure of dense sprays. *Prog. Astro. Aero.* In press.
Ruff, G. A., Sagar, A. D. & Faeth, G. M. 1989 Structure of the near-injector region of pressure-atomized sprays. *AIAA Jl* 27, 901–908.
Ruff, G. A., Bernal, L. P. & Faeth, G. M. 1991 Structure of the near-injector region of non-evaporating pressure-atomized sprays. *J. Prop. Power* 7, 221–230.
Ruff, G. A., Wu, P.-K., Bernal, L. P. & Faeth, G. M. 1992 Continuous- and dispersed-phase structure of dense non-evaporating pressure-atomized sprays. *J. Prop. Power* 8, 280–289.
Schlichting, H. 1979 *Boundary Layer Theory*, 7th Edn, pp. 234–235, 599. McGraw-Hill, New York.
Simmons, H. C. 1977 The correlation of drop-size distributions in fuel nozzle sprays. *J. Engng Power* 99, 309–319.
Simpkins, P. G. & Bales, E. J. 1972 Water-drop response to sudden accelerations. *J. Fluid Mech.* 55, 629–639.
Sirignano, W. A. 1983 Fuel droplet vaporization and spray combustion theory. *Prog. Energy Combust. Sci.* 9, 291–322.
Smith, A. M. O. 1960 Remarks on transition in a round tube. *J. Fluid Mech.* 7, 565–576.
Taylor, G. I. 1963 Generation of ripples by wind blowing over a viscous liquid. In *The Scientific Papers of Sir Geoffrey Ingram Taylor* (Edited by Batchelor, G. K.), Vol. III, pp. 244–254. Cambridge University Press, Cambridge, England.
Tennekes, H. & Lumley, J. L. 1972 *A First Course in Turbulence*, pp. 226, 248–286. MIT Press, Cambridge, MA.
Tseng, L.-K., Ruff, G. A. & Faeth, G. M. 1992a Effects of gas density on the structure of liquid jets in still gases. *AIAA Jl* 30, 1537–1544.
Tseng, L.-K., Wu, P.-K. & Faeth, G. M. 1992b Dispersed-phase structure of pressure-atomized sprays at various gas densities. *J. Prop. Power* 8, 1157–1166.
Tseng, L.-K., Ruff, G. A., Wu, P.-K. & Faeth, G. M. 1995 Continuous- and dispersed phase structure of pressure atomized sprays. *Prog. Astro. Aero.* In press.
White, F. M. 1974 *Viscous Fluid Flow*. McGraw-Hill, New York.

Wierzba, A. & Takayama, K. 1988 Experimental investigation of the aerodynamic breakup of liquid drops. *AIAA Jl* 26, 1329–1335.

Wu, K.-J., Su, C.-C., Steinberger, R. L., Santavicca, D. A. & Bracco, F. V 1983 Measurements of the spray angle of atomizing jets. *J. Fluid Engng* 105, 406–415.

Wu, K.-J., Coghe, A., Santavicca, D. A. & Bracco, F. V. 1984 LDV measurements of drop velocity in diesel-type sprays. *AIAA Jl* 22, 1263–1270.

Wu, P.-K. & Faeth, G. M. 1993 Aerodynamic effects on primary breakup of turbulent liquids. *Atom. Sprays* 3, 265–289.

Wu, P.-K. & Faeth, G. M. 1995 Onset and end of drop formation along the surface of turbulent liquid jets in still gases. *Phys. Fluids A*. In press.

Wu, P.-K., Ruff, G. A. & Faeth, G. M. 1991 Primary breakup in liquid/gas mixing layers. *Atom. Sprays* 1, 421–440.

Wu, P.-K., Tseng, L.-K. & Faeth, G. M. 1992 Primary breakup in gas/liquid mixing layers for turbulent liquids. *Atom. Sprays* 2, 295–317.

Wu, P.-K., Miranda, R. F. & Faeth, G. M. 1995a Effects of initial flow conditions on primary breakup of nonturbulent and turbulent round liquid jets. *Atom. Sprays* 5, 175–196.

Wu, P.-K., Hsiang, L.-P. & Faeth, G. M. 1995b Aerodynamic effects on primary and secondary breakup. *Prog. Astro. Aero.* In press.

Yokota, M., Ito, Y. & Shinoke, T. 1988 High speed photographic observations of cavitation arising in the high-speed oil-flow through a very small long orifice. *9th International Symposium on Jet Cutting Technology*, Sendai, Japan, pp. 13–21.

Appendix F: Faeth, G.M. (1996) Spray Combustion Phenomena. 26th Symposium (International) on Combustion, The Combustion Institute, Pittsburgh, pp. 1593-1612.

Twenty-Sixth Symposium (International) on Combustion/The Combustion Institute, 1996/pp. 1593–1612

INVITED PLENARY LECTURE

SPRAY COMBUSTION PHENOMENA

G. M. FAETH
Department of Aerospace Engineering
The University of Michigan
Ann Arbor, MI 48109-2118, USA

Aspects of interphase transport and multiphase flow relevant to spray combustion are reviewed, considering the structure of the near-injector (dense-spray) region, drop breakup, drop/turbulence interactions and interphase drop transport. Existing measurements of dense-spray structure show that the dispersed-flow region is surprisingly dilute, that effects of separated flow are important, that atomization involves primary breakup at the liquid surface followed by secondary breakup, and that effects of drop collisions are small (except when sprays impinge on surfaces or on other sprays). Available information about primary breakup is difficult to interpret because of problems controlling effects of disturbances in injector passages and secondary breakup; therefore, although some understanding of turbulent primary breakup has been achieved, more information about aerodynamic primary breakup is needed to address practical spray combustion processes. Studies of secondary breakup have resolved aspects of breakup regimes and outcomes, including the temporal properties of secondary breakup in some instances, for shock-wave disturbances at small gas/liquid density ratios and liquid viscosities; thus, more information is needed about general drop disturbances and the large gas/liquid density ratio and liquid viscosity conditions relevant to spray combustion at high pressures. Several ways to treat the turbulent dispersion of drops within dilute sprays are available. Consequently, the main uncertainties about estimating turbulent dispersion of drops involve long-standing problems of accurately estimating continuous-phase turbulence properties in sprays. Phenomena that complicate estimates of turbulence properties in sprays include turbulence generation and modulation by drops, with turbulence generation being a dominant but rarely studied feature of dense sprays. Understanding of drop evaporation and combustion has increased based on results from numerical simulations allowing for variable properties, multicomponent transport, and detailed chemical kinetic mechanisms; these methods offer promising new ways to study drop ignition, extinction, transport, and behavior near the thermodynamic critical point, among others.

Introduction

The evaporation and combustion of drops and sprays have been studied extensively because of their numerous important applications, including spark-ignition engines, diesel engines, aircraft propulsion systems, liquid rocket engines, liquid-fueled furnaces, and liquid-waste incinerators, among others. As a result, many features of evaporating and combusting sprays are understood reasonably well (see past reviews [1–24] and references cited therein). The present article extends these reviews by briefly discussing recent investigations of the structure, atomization, mixing, drop transport, and drop combustion properties of sprays, while highlighting areas where additional research is needed.

Except for direct discussion of the evaporation and combustion of individual drops, effects of evaporation and combustion will be avoided in the following to simplify interpretation of multiphase flow phenomena in sprays. While avoiding combustion can be justified on physical grounds for premixed combusting sprays, because the fuel is generally premixed and prevaporized before combustion, spray evaporation and multiphase flow phenomena overlap in these applications. Nevertheless, considering nonevaporating sprays still represents a reasonable first step toward understanding premixed combusting sprays because evaporation does not dominate the behavior of other multiphase flow phenomena [20,21].

Separating combustion and multiphase flow phenomena also can be justified for nonpremixed combusting sprays because these processes occur at considerably different levels of mixing. This behavior can be illustrated by analyzing an idealized spray consisting of infinitely small drops so that the locally homogeneous-flow (LHF) approximation can be adopted, where both phases are assumed to have the same velocity and temperature and are in thermodynamic equilibrium at each point in the flow [20]. This provides a reasonable limit of spray behavior, justified by past observations of striking similarities between gas-fueled and well-atomized spray flames [25–31]. Similar to other models of diffusion flames, LHF models yield correlations between scalar properties and the mixture fraction [20]; a typical

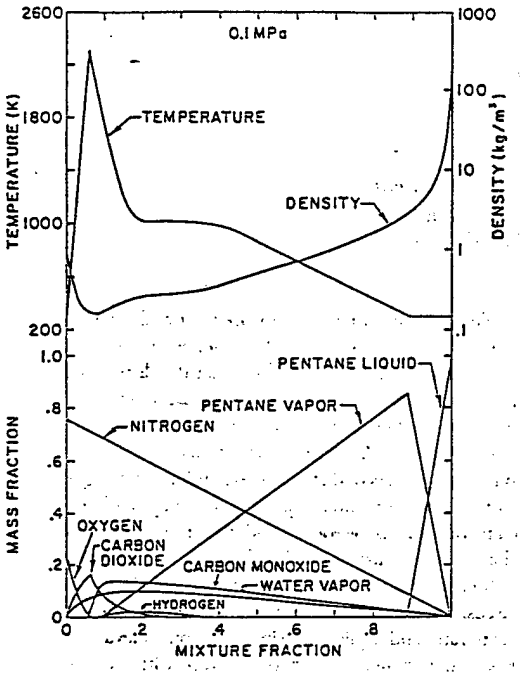

FIG. 1. Predictions based on the LHF approximation of scalar properties as a function of mixture fraction for an *n*-pentane spray burning in air at NTP. From Mao et al. [30].

example for an *n*-pentane spray burning in air at normal temperature and pressure (NTP) is illustrated in Fig. 1, but results at other conditions are similar [30,31]. These results show that the presence of liquid is limited to mixture fractions greater than 0.9, while combustion phenomena associated with the maximum temperature region are limited to mixture fractions less than 0.1. Thus, most spray phenomena occur at relatively cool conditions, remote from combustion phenomena, so that neglecting effects of evaporation and combustion is also a reasonable first step toward understanding non-premixed combusting sprays.

Within the limitations just discussed, the following aspects of spray combustion will be reviewed: the structure of the near-injector (dense-spray) region, primary and secondary drop breakup, drop turbulent dispersion and turbulence modification, and evaporation and combustion of individual drops. The review is designed so that each topic is self-contained, including conclusions, and can be read independently.

Dense-Spray Structure

Flow Regimes and Mixing Properties

Recent observations of the structure of the near-injector (dense-spray) region will be considered first to help define the properties of spray environments and to identify important spray phenomena. The classical configuration of round pressure-atomized sprays in still gases will be used for these purposes because this flow has received considerable attention (see Refs. 20–45 and references cited therein). Early studies of this spray configuration emphasized spray breakup regimes [32–38]; subsequent work concentrated on visualization of the dense-spray region and definition of the properties of the liquid core extending from the jet exit, which is similar to the potential core of single-phase jets [35–40]. The present discussion will be limited to the structure of the dense-spray region for atomization breakup, where drop formation begins right at the jet exit, because of the importance of this regime for practical spray combustion processes. The results to be considered include measurements of liquid volume fractions using gamma-ray absorption and dispersed-phase properties using pulsed holography, as well as predictions using the LHF approximation to illustrate effects of finite interphase transport rates (or separated flow) [41–45].

To define terms, a sketch of the dense-spray region for atomization breakup of a round liquid jet in a still gas is shown in the inset of Fig. 2. The dense-spray region is divided into the liquid core and an adjacent dispersed-flow region. The liquid core is a prominent feature of the flow because of its length (e.g., 200–500 jet exit diameters at NTP [34,39,40]). The dispersed-flow region begins right at the jet exit for atomization breakup; it consists of a developing multiphase mixing layer where the liquid core is present followed by a dispersed flow that eventually becomes a round dilute spray.

Similar to single-phase jets, the degree of flow development and turbulence levels at the jet exit have a significant influence on flow properties within dense-sprays [41–45]. Thus, consideration of dense-spray properties will be limited to fully developed turbulent pipe flow at the jet exit to ensure well-defined jet exit conditions. Measured and predicted time-averaged liquid volume fractions along the axis of pressure-atomized water sprays in air at various pressures are illustrated in Fig. 2 [45]. Mean liquid volume fractions are near unity close to the jet exit and then decrease rapidly. The initial reduction of liquid volume fractions occurs at progressively smaller values of x/d as the pressure increases, implying faster mixing rates at larger ambient gas densities, similar to density ratio effects for single-phase turbulent jets [46]. The LHF predictions reproduce this trend, but this is not definitive because mass mixing levels are small for the conditions shown in the figure and separated flow effects are not important when the flow is mainly liquid [43]. A more important finding is that the large liquid volume fractions seen in Fig. 2 are caused by the presence of the liquid core; in fact, the liquid volume fractions

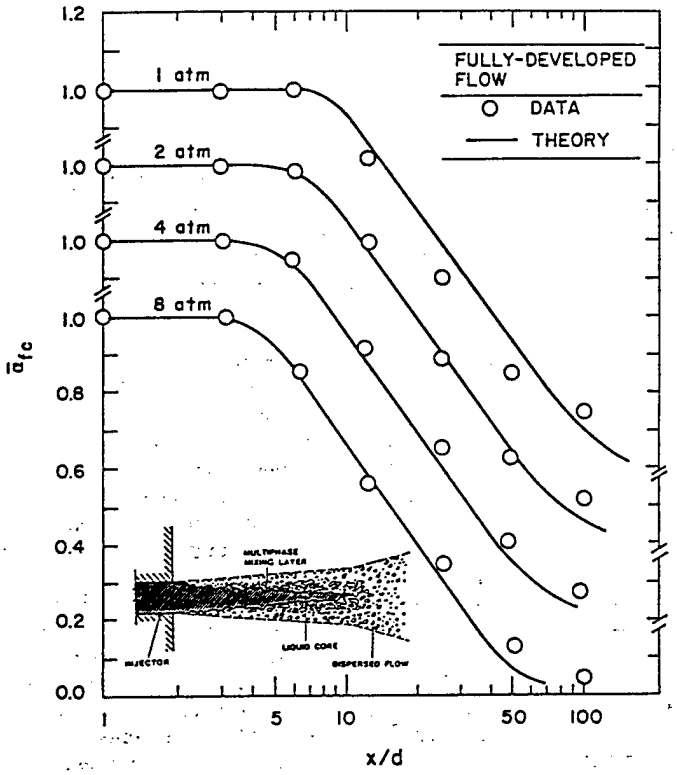

FIG. 2. Time-averaged liquid volume fractions along the axis of round, pressure-atomized water sprays in still air at various pressures for atomization breakup with fully developed turbulent pipe flow at the jet exit. Measurements and LHF predictions from Tseng et al. [44].

of the dispersed-flow region are surprisingly small, generally less than 0.1% [43,45]. Thus, dense sprays are not close-packed arrays of drops; instead, they are relatively dilute dispersed flows with regions of large liquid fractions caused by the presence of the liquid core.

Dispersed-Phase Properties

More insight about dense sprays can be obtained from the radial profiles of dispersed-phase properties plotted in Fig. 3. These results are for $x/d = 25$ in a round pressure-atomized water spray in still air at NTP, but results at other dense-spray conditions are similar. The region near the liquid surface consists of large, irregular, ligament-like elements (large e_p and SMD) resulting from primary breakup, even though this spray was well atomized, while the dilute-spray region near the edge of the flow involves smaller round drops. This provides direct proof of significant effects of secondary breakup near the liquid surface. In contrast, the small liquid volume fractions of the dispersed-flow region imply that drop collisions are improbable [20]. Thus, these findings support the classical picture of atomization within dense sprays [1]: namely, primary breakup into ligaments and large drops at the surface of the liquid core, followed by secondary breakup into smaller round drops, with negligible effects of collisions. It also was observed that drop diameter distributions satisfied Simmons's [47] universal root-normal distribution function, with MMD/SMD = 1.2, at each point within the flow. Consequently, drop size distributions can be represented by the SMD alone because this distribution function only has two parameters and MMD/SMD is a known constant; see Belz [48] for the properties of the root-normal distribution function.

The drop velocities illustrated in Fig. 3 vary considerably with drop diameter, which highlights the significant separated-flow effects observed for most dense sprays [41–45]. Near the liquid core, the largest drops have velocities comparable to mean liquid velocities at the jet exit; however, drop velocities decrease with decreasing drop size and increasing radial distance. A surprising feature of these results is that gas velocities (which approximate the velocities of the smallest drops) are small and nearly constant across the multiphase mixing layer. This behavior emphasizes the relatively ineffective momentum exchange in the multiphase mixing layer because the flow is dilute and large drops that contain most of the momentum respond slowly to drag forces because of their relatively large inertia. Taken together, existing observations of dense sprays [41–45] provide considerable motivation to address the

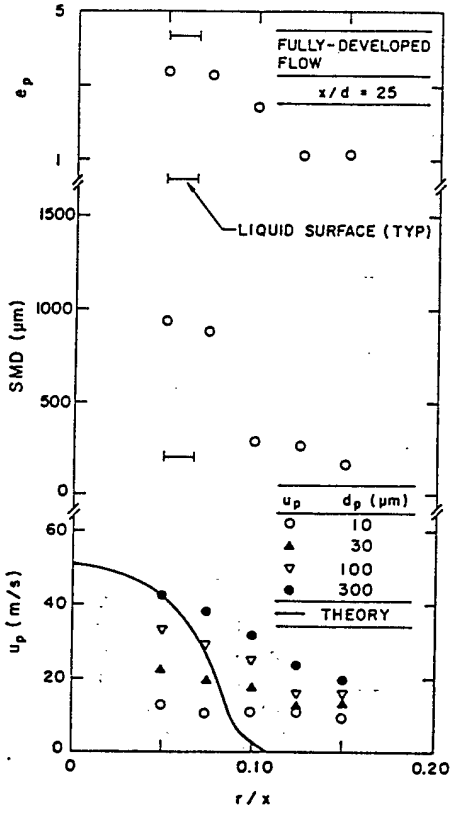

FIG. 3. Radial profiles of dispersed-phase properties for round, pressure-atomized water sprays in still air at NTP for atomization breakup with fully developed turbulent pipe flow at the jet exit. Measurements and LHF predictions from Ruff et al. [43].

multiphase flow properties of sprays discussed in the remainder of this paper.

Drop Breakup

Primary Breakup

Primary breakup to form drops near liquid surfaces is important because it initiates atomization, controls the extent of the liquid core, and defines the initial conditions for the dispersed multiphase flow region. Unfortunately, current understanding of primary breakup is limited because of problems of observations within dense sprays, effects of secondary breakup and interphase transport that modify drop properties before measurements can be made, and incomplete characterization of the degree of flow and turbulence development at the jet exit. Recent work using pulsed holography has addressed some of these deficiencies for primary breakup of round, pressure-atomized sprays in still gases [41–45,49–53]. Thus, the findings of these studies will be discussed in the following, treating the onset and outcome of primary breakup in turn. Consideration of other primary breakup processes can be found in Refs. 1, 4–6, and 12–14 and references cited therein.

Investigations of pressure-atomized sprays have established that primary breakup is affected strongly by the degree of flow and turbulence development at the jet exit. For example, the early studies of DeJuhasz et al. [54] and Lee and Spencer [55] showed that atomization quality differed for laminar and turbulent flow at the jet exit and identified a unique turbulent primary breakup process. Numerous later studies have supported these findings [34–37,41–45,56]. This behavior is not surprising in view of the widely recognized importance of jet exit conditions on the properties of single-phase jets [57–61]. In fact, past studies also show that primary breakup can be suppressed entirely for injection into air at NTP using supercavitating flows where the jet separates from the passage wall near the end of the contraction section and does not reattach, which yields uniform and nonturbulent velocity distributions at the jet exit [62–64]. This behavior also is expected because similar flows are used to prevent liquid breakup for liquid jet-cutting systems [65]. Finally, aerodynamic effects have little effect on drop properties after primary breakup for pressure-atomized sprays in still gases at NTP [36–37,51–53]. In particular, effects of liquid/gas density ratio, expected based on aerodynamic breakup theories [2,66], were not observed for $\rho_f/\rho_g > 500$; instead, primary breakup properties were controlled almost entirely by liquid flow properties at the jet exit [51–53].

Recent measurements of Wu et al. [53] show that primary breakup during pressure atomization is affected by the profile of the injector contraction, the L/d of the constant-area section of the injector, and the Reynolds number of the flow at the jet exit. Some typical pulsed shadowgraphs of the flow near the jet exit are illustrated in Fig. 4 for water injected into still air at NTP with $Re_{fd} > 200{,}000$. Two injector conditions are shown, with and without removal of the boundary layer near the passage walls (boundary layer removal involved a small cutter with $L/d = 0.15$), for a nonturbulent uniform velocity distribution across the inviscid part of the flow. When the cutter is absent, the vortical flow in the boundary layer produces ligaments that break up into drops close to the jet exit; in contrast, when the boundary layer is removed by the cutter, primary breakup is suppressed entirely, yielding a solid liquid stream similar to liquid cutting jets [65]. Additional experiments indicated the appearance of turbulent primary breakup for $L/d > 4$–6 and $Re_{fd} > 1$–4×10^4 for nonturbulent conditions at the contraction exit, with the results of Grant and Middleman [34]

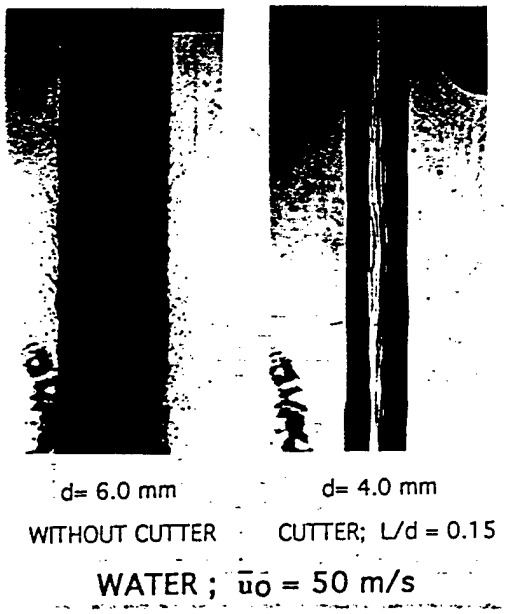

FIG. 4. Pulsed shadowgraphs of water jets injected into still air at NTP for nonturbulent slug flow at the jet exit with and without boundary layer removal. From Wu et al. [53].

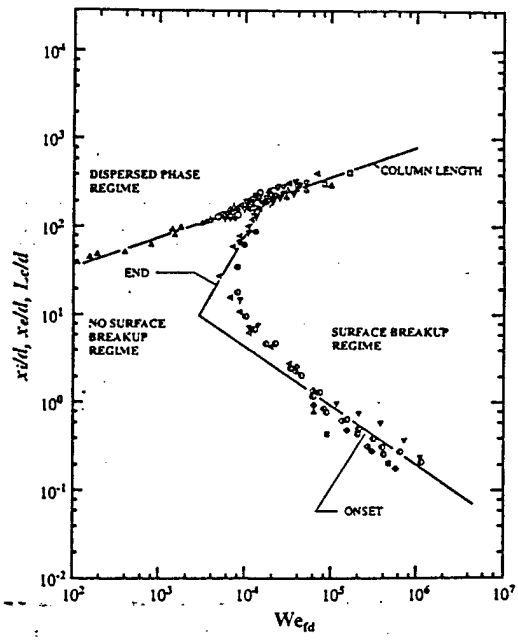

FIG. 5. Liquid-surface and liquid-column breakup regime maps for liquid jets injected into still gases with fully developed turbulent pipe flow at the jet exit and negligible aerodynamic effects. From Wu and Faeth [52], with measurements from Chen and Davis [67], Grant and Middleman [34], Wu and Faeth [52], and Wu et al. [50].

suggesting the presence of turbulent primary breakup for $Re_{fd} > 3000$ in the presence of strong inlet disturbances. More study of the influence of jet exit properties on primary breakup is needed, but these results strongly suggest that measurements of the atomization properties of short L/d injectors at NTP are dominated by effects of inlet and contraction disturbances as well as turbulence generated near the reattachment point of separated (cavitating) flows.

Subsequent considerations of primary breakup will be limited to turbulent primary breakup with fully developed turbulent pipe flow at the jet exit because this process yields repeatable jet exit conditions. The results of Refs. 50–53 will be used to illustrate the following properties of turbulent primary breakup: onset of breakup, length of the liquid core, properties of drops produced by breakup, and effects of aerodynamic forces on breakup.

Phenomenological analyses have been used to define conditions for the onset and end of turbulent primary breakup along the surface of the liquid core and the length of the liquid core [50–53]. These analyses assumed that drops are formed from turbulent eddies when the kinetic energy of the eddy is comparable to the surface energy required to form a drop of comparable size, that the turbulence spectral ranges of interest include the large eddy and inertial subranges (observed drop diameters were much greater than Kolmogorov length scales), that aerodynamic effects were small, that growing disturbances on the liquid surface are convected at the mean streamwise velocity at the jet exit for the Rayleigh breakup time required to form a drop of given size, and that the liquid core ends when drop sizes produced by turbulent primary breakup are comparable to the liquid core diameter. Correlations of available measurements based on these ideas are illustrated in Fig. 5, with best fits of the measurements yielding the following expressions [52]:

$$x_i/d = 2000\, We_{fd}^{-0.67}, \quad x_e/d = 0.000015S\, We_{fd}^{1.68}, \quad L_c/d = 7.40\, W_{fd}^{0.34} \qquad (1)$$

Notably, the predicted powers of We_{fd} for the onset and end of surface breakup, and the liquid core length, are -0.4, 2, and 1/2; thus, while the empirical powers of Eq. (1) differ from these predictions, the differences are not large in view of the approximations of the theories. The magnitudes of the coefficients of Eq. (1) are also reasonable for the processes considered [52]. Thus, results illustrated in Fig. 5 yield the following breakup regimes with increasing We_{fd}: (1) only breakup of the liquid column as a whole, (2) onset and end of surface breakup, followed by breakup of the liquid column as a whole, and (3) onset of surface breakup followed by

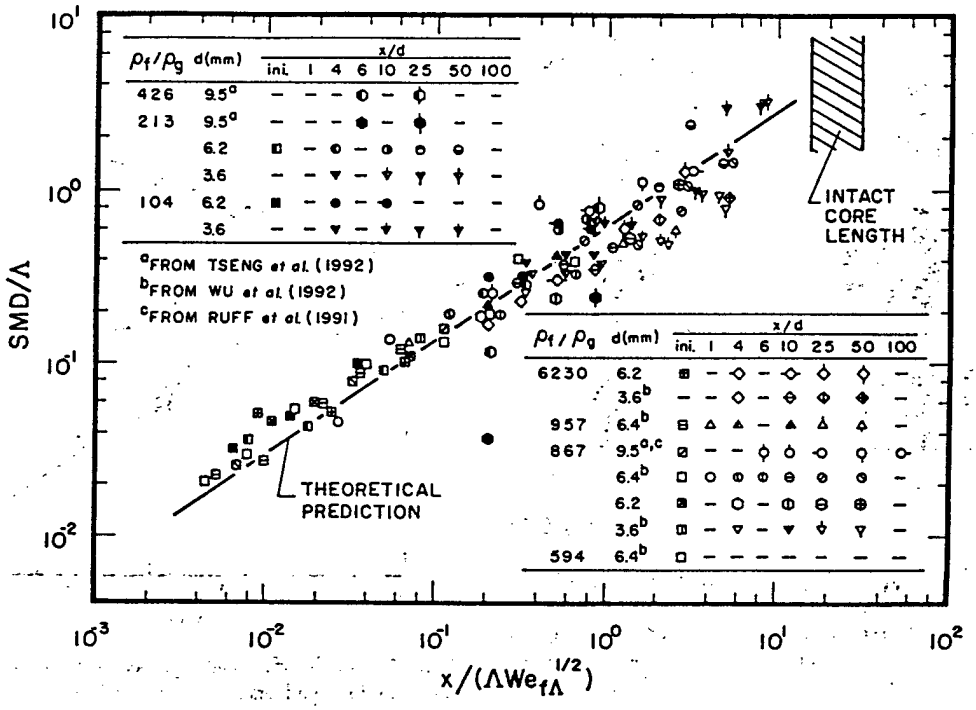

FIG. 6. SMD after turbulent primary breakup as a function of distance from the jet exit for liquid jets injected into still gases with fully developed turbulent pipe flow at the jet exit. Results for $\rho_f/\rho_g < 500$ inverted to account for merged primary and secondary breakup. From Wu and Faeth [51], with measurements from Ruff et al. [42], Tseng et al. [45], Wu and Faeth [51], and Wu et al. [50]; SMD predictions from Wu and Faeth [47], and liquid-column length prediction from Grant and Middleman [34].

breakup of the liquid column as a whole. The first of these is analogous to first wind-induced breakup, while the remaining regimes correspond to second wind-induced and atomization breakup (depending on the distance from the jet exit where the onset of breakup occurs) [20]. Finally, the present correlation of the L_c/d is in good agreement with the measurements of Grant and Middleman [34] and Chen and Davis [67]. Chehroudi et al. [39], however, find a different correlation for atomization at elevated pressures, based on aerodynamic breakup theory, as follows:

$$L_c/d = C_c(\rho_f/\rho_g)^{1/2} \qquad (2)$$

where C_c is in the range 7–16 for atomization breakup of pressure-atomized round jets in still gases. The differences between L_c/d from Eqs. (1) and (2) reflect effects of aerodynamic forces and the degree of flow development at the jet exit that should be quantified in the future.

Wu and co-workers [50–53] also report distributions of drop sizes and velocities produced by turbulent primary breakup. Similar to dense sprays as a whole, drop sizes after turbulent primary breakup satisfy Simmons's [47] universal root-normal distribution with MMD/SMD = 1.2. Mean drop velocities were found to be relatively independent of drop size and position, with mean streamwise and cross-stream values comparable to $\bar{u}_o$ and $\bar{v}_o$, respectively [50]. The variation of SMD along the liquid surface was initially studied for $\rho_f/\rho_g > 500$, where aerodynamic effects are small [50]. Phenomenological analysis was used to interpret these data, similar to the approach used for x_i and x_e. It was assumed that the SMD was proportional to the largest drop that could be formed at a particular position, based on convection and Rayleigh breakup of a similarly sized ligament as earlier. Available measurements for the variation of SMD with distance are plotted as suggested by this theory in Fig. 6. The measurements are in good agreement with the phenomenological theory, yielding the following best-fit correlation:

$$\mathrm{SMD}/\Lambda = 0.65(x/(\Lambda\, We_{f\Lambda}^{1/2}))^{2/3} \qquad (3)$$

The powers of Eq. (3) follow directly from the theory, while the coefficient is of order unity, as expected, which suggests that the physical principles used to derive the equation are reasonable. An interesting feature of Eq. (3) is that the SMD does not depend on liquid viscosity, which is similar to results

based on aerodynamic breakup theories [2,38,66], even though the concepts used to develop the expression for turbulent primary breakup are very different. As noted earlier, the SMD approaches the diameter of the liquid core itself near L_c, as expressed by Eq. (1), which is also plotted in Fig. 6.

The last phase of the turbulent primary breakup studies of Wu and co-workers [49–53] considered effects of aerodynamic forces on the onset and outcomes of turbulent primary breakup. It was found that aerodynamic effects advance the onset of breakup and reduce drop sizes after breakup by merging processes of primary and secondary breakup for $\rho_f/\rho_g < 500$. These properties were also successfully correlated using phenomenological theories [51].

Numerous unknowns concerning primary breakup must still be resolved. Issues about turbulent primary breakup include information about rates of breakup and a more complete treatment of aerodynamic effects, including the relationship between the L_c estimates of Eqs. (1) and (2). Another issue involves primary breakup of nonturbulent liquids and its relationship to the classical aerodynamic theories of primary breakup of Refs. 2 and 66. Finally, effects of flow properties at the exit of practical injectors of various configurations, and interactions between flow development and aerodynamic effects, must be resolved to better understand primary breakup.

Secondary Breakup

Drop deformation and secondary breakup are important: primary breakup yields drops that are intrinsically unstable to deformation and secondary breakup, high-pressure combustion processes involve conditions in which the surface tension becomes small (near the thermodynamic critical point) promoting drop deformation and secondary breakup, deformation affects mixing rates by enhancing interphase transport rates, and secondary breakup affects spray mixing rates by controlling drop sizes [42,43,45,49–53]. Several reviews of early work on drop deformation and secondary breakup have appeared [1,2,4,6,68–71]; therefore, recent studies will be emphasized in the following. Of particular interest are recent findings about secondary breakup regimes and outcomes using pulsed holography [72–75]. Studies of drop deformation and breakup have been limited to either shock-wave disturbances, which provide a step change of the ambient environment of a drop typical of conditions at the end of primary breakup, or steady disturbances, typical of freely falling drops and spray drying processes. Effects of shock-wave disturbances have received the most attention and best approximate drop deformation and secondary breakup in sprays; therefore, these disturbances will be emphasized in the following, considering deformation and breakup regimes, breakup dynamics, and breakup outcomes.

A variety of deformation and breakup regimes have been observed for shock-wave disturbances; see Refs. 68–82 for sketches, descriptions, and photographs of typical deformation and breakup regimes. Existing observations of secondary breakup have been limited mainly to $\rho_f/\rho_g > 500$ and $Re > 100$. For such conditions, Hinze [68] shows that deformation and secondary breakup regime transitions are functions of We and Oh, which are measures of the ratios of drag and liquid viscous forces to surface tension forces, respectively. The resulting deformation and secondary breakup regime map based on available measurements is illustrated in Fig. 7. Various breakup regimes identified by Hinze [68], Krzeczkowski [71], and Hsiang and co-workers [72–75] are in good agreement, which is satisfying in view of the subjective nature of identifying regime transitions.

The regime transitions illustrated in Fig. 7 are relatively independent of liquid viscous forces (or Oh) for $Oh < 0.1$, while drop deformation begins when $We \approx 1$. The first breakup regime, bag breakup, is reached at $We = 13$; this breakup regime involves deformation of the drop into a thin disk normal to the flow direction, followed by deformation of the center of the disk into a thin, balloonlike structure, both of which subsequently divide into drops. The shear breakup regime is observed at larger relative velocities, beginning at $We = 80$; this breakup regime involves deflection of the periphery of the disk-like deformed drop in the downstream direction, rather than the center of the drop, with drops separating from the downstream end of ligaments attached to the drop periphery. The transition between bag and shear breakup is a complex mixture of the two, termed multimode breakup. Finally, a complex breakup regime, called catastrophic or drop-piercing breakup, is observed when $We > 800$ [79–80]. While values of We for particular regime transitions are relatively constant for small Oh, they increase progressively with increasing Oh for $Oh > 0.1$. Some deformation and breakup regimes also disappear at large Oh, for example, oscillating deformation and bag breakup. Another effect of increasing Oh is a progressive increase in the length of the ligaments attached to the periphery of the parent drop during shear breakup, yielding transition to a long-ligament regime for $Oh > 0.1$.

It is important to determine whether the regime boundaries in Fig. 7 eventually become vertical at large values of Oh so that drop deformation and breakup no longer occur; therefore, this issue has been studied using phenomenological analysis [74]. The analysis was based on the observation that the main effect of liquid viscosity was to reduce the rate of drop deformation, tending to reduce relative velocities and the potential for drop deformation and

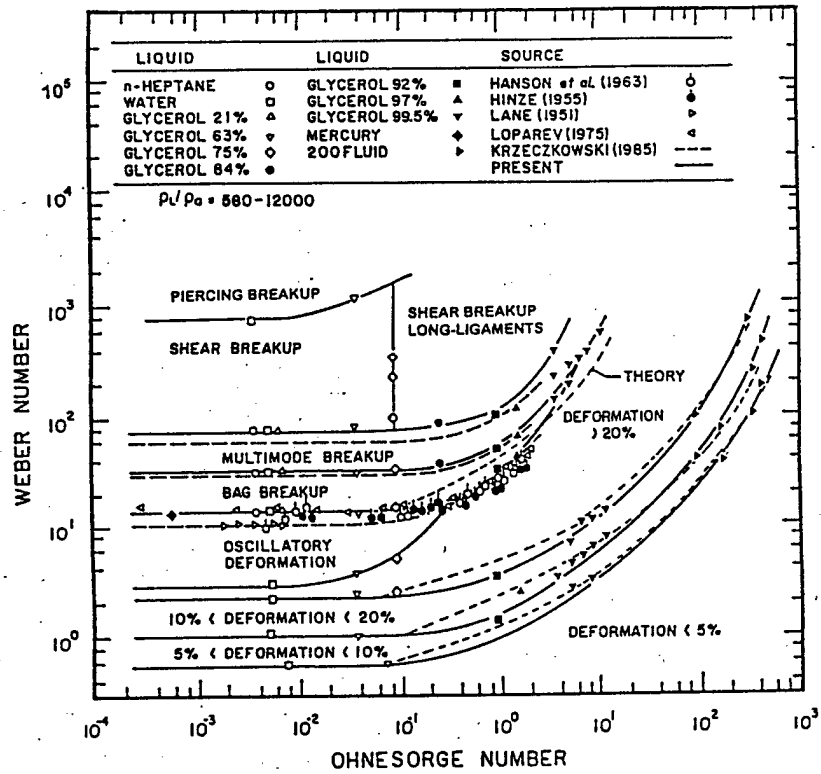

FIG. 7. Drop deformation and secondary breakup regime map for shock-wave disturbances and $\rho_l/\rho_g > 500$. From Chou et al. [75], with measurements from Hansen et al. [76], Hinze [68], Lane [81], Loparev [82], and Hsiang and co-workers [72–74]; correlations from Kreczkowski [71] and Hsiang and co-workers [72–74]; theory from Hsiang and Faeth [74].

breakup at each stage of the deformation process. The drop motion was then analyzed for $Oh \gg 1$, where the maximum deformation occurs at a multiple of the characteristic viscous time of Hinze [83], $\mu_f/(\rho_g u_o^2)$. This analysis yielded the following relationship between We and Oh for particular regime transitions at large Oh:

$$We = (We_{cr}/4)(1 + 4C_{cr}\, We_{cr}^{-1/2} (\rho_g/\rho_f)^{1/2} Oh) \quad (4)$$

where We_{cr} is the local Weber number (based on the maximum deformation condition) that is required for the particular transition to occur and C_{cr} is an empirical factor of order unity. Values of We_{cr} and C_{cr} were fitted to Eq. (4) to yield the best fit of transitions at large Oh (denoted "theory" in Fig. 7); in view of the simplifications of the theory, the agreement between these predictions and measurements is reasonably good. Notably, Eq. (4) implies the $We \sim Oh$ for a given transition at large Oh, instead of yielding an ultimate limit for all We at large Oh, as suggested earlier [2,59]. This difference of behavior is crucial for processes of high-pressure combustion, where both Oh and We become large as drops approach their thermodynamic critical point (because σ approaches zero); then, since We increases more rapidly than Oh as σ becomes small, the fact that $We \sim Oh$ for transitions at large Oh implies that drops at these conditions still undergo deformation and shear breakup. Unfortunately, past considerations have not addressed effects of liquid/gas density ratio on transitions or effects of gradual changes of drop properties (particularly for conditions near the thermodynamic critical point); therefore, the important issues of drop deformation and breakup behavior at high pressures must still be resolved.

Other information about drop deformation and secondary breakup has been limited to $Oh < 0.1$, where liquid viscosity no longer affects regime transitions. At these conditions, the characteristic drop breakup time of Ranger and Nicholls [78], t^*, is a useful normalizing parameter for dynamic processes. For example, times required for initiation and end of secondary breakup are $t_i = 1.5\, t^*$ and $t_b = 5.5\, t^*$ at low Oh for $We < 10^6$ [72,78–80,84–87]. Deformation within a deformation regime, or as part of secondary breakup, increases drag forces on the

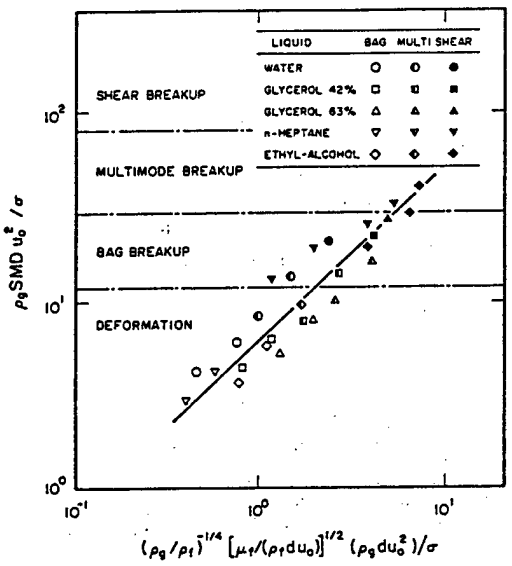

FIC. 8. Correlations of SMD after secondary breakup for shock-wave disturbances, $\rho_f/\rho_g > 500$ and $Oh < 0.1$. From Hsiang and Faeth [72].

parent drop because of increasing drop cross-sectional areas and drag coefficients [72]. Considering behavior over the complete range of parent drop shapes (where the cross-stream/original diameter ratio varies in the range 1–2), drag coefficients vary from values for solid spheres to thin disks (e.g., C_b of 0.4–1.2 for Re of 100–2500 [72]). Combining this result with deformation data then implies that drag forces increase by factors up to 4 and 13 times the initial values for spherical drops for deformation conditions typical of the onset of breakup with steady and shock-wave disturbances. This behavior clearly has an important impact on breakup dynamics and interphase transport rates [72].

Breakup outcomes, or the jump conditions giving drop size and velocity distributions after breakup, have been measured for $\rho_f/\rho_g > 500$ and $Oh < 0.1$ [72–74]. First of all, the size distributions of drops produced by secondary breakup (excluding the parent drop for shear breakup, which must be treated differently) satisfy Simmons's [47] root-normal distribution function with MMD/SMD = 1.2, which is not surprising since this distribution is effective for other drop size properties of sprays. A correlating expression for the SMD after breakup was developed considering the shear breakup regime and focusing on the stripping of liquid from the parent drop. Analogous to ligament growth and drop formation caused by vortical layers during primary breakup (see Fig. 4), it was assumed that ligaments, and drops breaking away from the tips of ligaments, had diameters that were comparable to the thickness of the laminar boundary layer that forms along the liquid surface on the upwind side of the drop. Other major assumptions of the analysis were as follows: liquid velocities in the vortical layer are on the order of $u_{fo} = (\rho_g/\rho_f)^{1/2}\, u_o$, as suggested by Ranger and Nicholls [78] for shear breakup, the length of the vortical region proportional to d_o, the thickness of the vortical region was estimated from the thickness of laminar boundary layer on a flat surface of similar length, and the SMD was also proportional to the thickness of this boundary layer. Based on these ideas, the following expression was obtained as the best fit of available measurements of drop sizes at the end of secondary breakup [72]:

$$\begin{aligned} SMD/d_o &= 6.2(\mu_f/(\rho_f d_o(\rho_g/\rho_f)^{1/2}\, u_o))^{1/2} \\ &= 6.2/Re_{fd}^{1/2} \end{aligned} \tag{5}$$

which can be recognized as a relationship associating the SMD with the thickness of a laminar boundary layer for a flat plate having a length d_o and an ambient velocity u_o [60].

Available measurements of the SMD after secondary breakup for shock-wave disturbances at small Oh and $\rho_f/\rho_g > 500$ are illustrated in Fig. 8 along with the correlation of Eq. (5). (Note that Eq. [5] has been multiplied by $\rho_g u_o^2/\sigma$ and rearranged to provide a plot of ρ_g SMD u_o^2/σ, which is a Weber number based on the SMD, to discuss the potential for subsequent breakup.) Remarkably, the single correlation developed for shear breakup yields the SMD after bag, multimode, and shear breakup. This behavior must still be explained, although other properties, for example, times for the onset and end of breakup, are also independent of the breakup regime. Superficially, it is evident that the Weber number based on the SMD exceeds criteria for secondary breakup at small Oh; nevertheless, subsequent breakup of the large drops in the distribution still does not occur. This comes about because these drops have had time to adjust to the ambient flow so that deformation and breakup criteria for abrupt disturbances are no longer appropriate [72–74]. Another remarkable feature of these results, evident from Eq. (5), is that drop sizes after secondary breakup depend on μ_f but not σ, even though the criteria for deformation and breakup regimes depend on σ but not μ_f at comparable conditions. Naturally, this behavior also contradicts the classical aerodynamic breakup theories proposed for small Oh conditions [2,66]. Thus, for turbulent primary breakup, drop sizes after primary breakup are independent of μ_f (see Fig. 6), while drop sizes after secondary breakup are independent of σ; therefore, general drop size correlations for pressure atomization that involve both properties (see Refs. 1, 4, 6, 12–14 and references cited therein) obtain these effects from separate contributions of primary and secondary breakup.

Jump conditions for the properties of the parent

drop after shear breakup and for the velocity distributions of drops produced by bag, multimode, and shear breakup have also been developed and correlated successfully using phenomenological theories [72–74]. The stabilization of the parent drop provides insight about secondary breakup: it is found that this occurs when the acceleration rates of the drop decline so that the Eötvös number is roughly 16, which is close to the criterion for the onset of drop breakup for steady disturbances. The drop size/velocity correlation predictably shows that the smallest drops produced by breakup have the smallest relative velocities with respect to the gas at the end of breakup because of their small relaxation times.

The findings about jump conditions after secondary breakup show that these processes extend over a considerable region of time and space: total breakup times are 5.5 t^*, and drops extend over a streamwise distance of roughly 100 d_o at the end of shear breakup [72–74]. This behavior implies that secondary breakup should be treated as a rate process rather than by jump conditions, in many instances. Work to provide the needed temporal properties for shear breakup caused by shock-wave disturbances at small Oh and large ρ_f/ρ_g has been initiated [75]; nevertheless, more work along these lines is needed to provide the technology base required for reliable models of practical sprays. Other issues that should be resolved for secondary breakup include consideration of all breakup regimes, behavior at $\rho_f/\rho_g < 500$, and behavior at large Oh.

Drop/Turbulence Interactions

Spray Analysis

Given information about atomization to yield a dilute dispersed flow, subsequent interactions between the phases to produce gaseous reactants for spray combustion must be considered. The approach to these problems, however, depends on the way that sprays are modeled; therefore, typical spray models will be considered briefly in the following (see Refs. 3, 4, 15, 16, and 20 for a more complete discussion).

As shown by the discussion of spray structure, practical spray models must consider separated flow. Continuum formulations provide one approach to treat separated flow, but they will not be considered because they are not widely used for sprays because of problems of computational efficiency for dilute dispersed flows. In contrast, discrete-element formulations provide popular separated-flow treatments for sprays. These methods involve a Eulerian formulation for the continuous phase, a Lagrangian formulation to track representative drop groups through the flow, and terms in both formulations to treat interphase transport [20]. There are two main discrete-element formulations: namely, deterministic separated flow (DSF) where dispersed-phase (drop)/turbulence interactions are ignored and stochastic separated flow (SSF) where drop/turbulence interactions are considered. The DSF approach is not very satisfying, however, because drop motion is limited to deterministic trajectories prescribed by their initial conditions and mean gas properties throughout the dispersed-flow field. As a result, DSF predictions exhibit unphysical, laminar-like behavior where drops collect in low-velocity regions [3,20]; therefore, SSF methods dominate recent spray models to better represent the mixing properties of turbulent sprays.

Motivated by the preceding discussion, present considerations of drop/turbulence interactions will emphasize the SSF model perspective. There are three main drop/turbulence interactions of interest: (1) the dispersion of drops by turbulence, which is an effect of turbulence on drop properties; (2) the modification of turbulence properties by the motion of drops, which is a reverse effect of drops on turbulence properties; and (3) the modification of interphase transport rates by effects of turbulence fluctuations, which is a combination of the two. The modification of interphase transport rates by turbulence will be discussed later; therefore, present considerations are limited to turbulent dispersion and turbulence modification, seeking to extend the earlier reviews of Crowe et al. [88] and Hetsroni [89].

Turbulent Drop Dispersion

The earliest treatments of turbulent drop (particle) dispersion were based on the gradient-diffusion approximation using empirical gas/particle exchange coefficients; unfortunately, implementing a gradient-diffusion process is not convenient for SSF computations, while estimates of needed exchange coefficients are problematic because they are influenced by both particle and turbulence properties [20]. Thus, recent work exploits the SSF method to directly compute particle dispersion by turbulence, based on methods analogous to numerical simulations of turbulence. As a result, these methods tend to compensate for effects of turbulence fluctuations on interphase transport rates—at least for fluctuations at scales larger than particle sizes, which is generally the most important range for combusting sprays [20].

Development of SSF methods to treat turbulent dispersion initially was based on classical measurements of particle dispersion in isotropic turbulence [90,91], although a variety of dispersed turbulent flows were subsequently considered (see Refs. 92–106 and references cited therein). These simulations generally assumed quasi-steady interphase transport while treating effects of particle inertia, drag, virtual mass, Basset history forces, body forces, Magnus forces, and Saffman-lift forces to the extent that

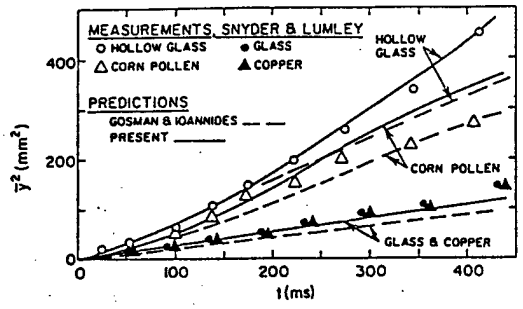

FIG. 9. Turbulent dispersion of particles in a grid-generated turbulent isotropic flow. From Shuen et al. [94]; measurements from Snyder and Lumley [90]; predictions from Gosman and Ioannidis [93] and Shuen et al. [94].

these effects were important (see Clift et al. [6] for review of these effects). Trajectories of a statistically significant number of particles throughout the flow were then computed based on simulation of the flow field along the particle path. Progress with these methods mainly has involved improvements of ways to simulate the flow field, because computing particle motion in a known flow is straightforward.

The earliest SSF simulations of particle dispersion were based on interactions between particles and a succession of uniform-property integral-scale-sized eddies [92–96]. Eddy velocities were found by random selections from the probability density function (PDF) of velocity fluctuations, while interactions between particles and particular eddies extended for either the eddy lifetime or the transit time required for the particle to traverse the eddy. Eddy properties were found mainly from turbulence model predictions, with κ-ε models often used except for fundamental isotropic flows where eddy properties were known from measurements [90,91].

Early turbulent dispersion predictions were surprisingly successful, in view of the crude treatment of flow properties [92–96]. A typical example of the comparison between predictions and measurements is illustrated in Fig. 9. These measurements involve the dispersion of various types of solid particles injected into a turbulent isotropic flow downstream of a grid [90]. SSF predictions from Refs. 93 and 94 involve somewhat different treatments of particle/eddy interactions, yet both are in good agreement with the measurements, which included conditions in which both eddy lifetimes and transit times controlled interaction times.

Subsequent studies of turbulent particle dispersion sought to remove the ad hoc features of the early models. Gouesbet and co-workers [97–99] developed methods to statistically simulate a variety of turbulent flow properties (e.g., moments, correlations) along a particle path, similar to methods used for statistical time series simulations [100], although they developed their procedures independently. Later studies of the dispersion of nearly monodisperse particles in stationary particle-generated turbulence used similar methods to yield good agreement between measured and predicted turbulence properties [101]. Maxey [102] considered alternative simulations based on randomly selected Fourier modes to treat turbulent dispersion in isotropic turbulence. Subsequent work addressed turbulent dispersion in various turbulent isotropic and shear flows, using progressively more detailed simulations of continuous-phase flow properties [103–106].

Taken together, the need to treat turbulent dispersion during analysis of sprays has been established and there has been significant progress toward understanding the main features of the turbulent dispersion of particles (drops). Thus, improved understanding of turbulent dispersion is impeded mainly by long-standing problems of finding accurate, physically based, and computationally tractable ways to simulate the properties of turbulent flows.

Turbulence Modification

Turbulence modification will be defined narrowly in the following to include only direct effects of the dispersed phase on the turbulence properties of the continuous phase. This definition excludes indirect effects in which the motion of the dispersed phase modifies the distribution of mean quantities and thus local distributions of turbulence production and dissipation within the continuous phase. Turbulence modification has been discussed in several earlier articles (see Refs. 20, 88, 89, 101, and 107–114 and references cited therein); thus, present considerations will emphasize recent findings. For convenience, only effects of interphase momentum transport between particles and the continuous phase will be considered because generalization to other dispersed phases and transport processes is not difficult.

Hinze [107] identifies several turbulence modification mechanisms. Two of these mechanisms are of particular interest under the present narrow definition of turbulence modification for dilute dispersed flows typical of sprays [101,105,110–114]: (1) the exchange of kinetic energy between a particle and an eddy as the particle accommodates to the eddy velocity, denoted turbulence modulation in the past [89,105], which generally decreases turbulent fluctuations; and (2) the direct disturbance of the continuous-phase velocity field by particle wakes, denoted turbulence generation in the past [101,105], which generally increases turbulent fluctuations. Evaluating the relative magnitude of these effects to determine whether turbulence modification will increase or decrease turbulence levels has been addressed by a number of investigators [89,110,112]. Based on a review of past measurements, Gore and

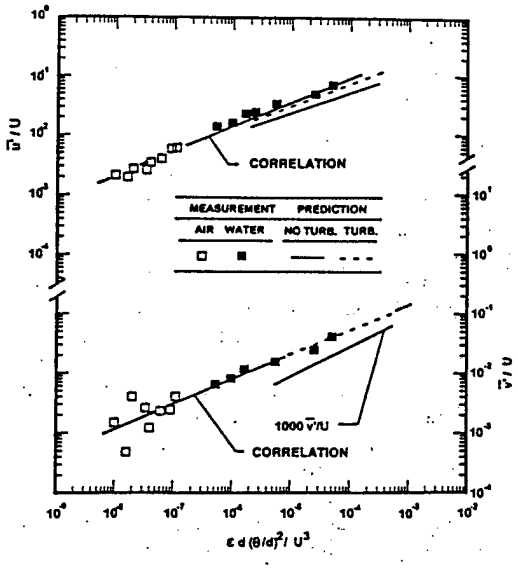

FIG. 10. Streamwise and cross-stream rms velocity fluctuations caused by homogeneous dispersed flows of monodisperse spheres. From Wu and Faeth [114]; measurements from Parthasarathy and Faeth [101] and Mizukami et al. [111]; predictions from Wu and Faeth [114].

Crowe [110] concluded that turbulence modification reduced (increased) turbulence levels for smaller (larger) particles with transition between these regimes at $d_p/l_e \sim 0.1$. This behavior is plausible because small (large) particles accommodate rapidly (slowly) to local eddy velocities, increasing (decreasing) effects of turbulence modulation, and have relatively weak (strong) wake disturbances, decreasing (increasing) effects of turbulence generation. Nevertheless, past observations of effects of turbulence modification are scattered when viewed in terms of d_p/l_e alone, suggesting that other parameters are important as well. Hetsroni [89] observes a similar effect of particle size on turbulence modification and related this behavior to particle Reynolds number, finding a critical particle Reynolds number of 400 (associated with the onset of vortex shedding from the particle) between the turbulence modulation and generation regimes. Finally, Yuen and Michaelides [112] report a more phenomenological treatment of this issue, based on models of both turbulence modulation and generation, that successfully correlates most existing observations of effects of turbulence modification on turbulence levels within dispersed multiphase flows.

Turbulence generation tends to dominate turbulence modification in sprays because they are dilute dispersed flows with large separated-flow effects and thus strong particle wakes [101,111]. In addition, turbulence generation is generally more important than conventional single-phase mechanisms of turbulence production in dense sprays because they usually involve relatively small mean velocity gradients in combination with relatively large velocity differences between the phases (see Fig. 3). Thus, the turbulence properties of dense sprays are dominated by turbulence generation by drops and conventional turbulence dissipation in the continuous phase yielding turbulence fields whose properties differ significantly from conventional single-phase turbulence, as discussed next.

Past measurements carried out to emphasize effects of turbulence modulation have involved uniform fluxes of nearly monodisperse particles moving at terminal velocities through stagnant (in the mean) water and air baths [101,109,111]. The resulting flows are homogeneous and stationary, with turbulence production largely due to turbulence generation by particles. Stochastic analysis has been used to help interpret and correlate laser velocimetry measurements, which involved methods similar to analysis of random noise by considering the flow to result from superposition of randomly arriving particle wakes [101], while basing the structure of the wakes on measurements for spheres at comparable (intermediate) Reynolds numbers in turbulent environments [114]. An interesting feature of these flows is that the local rate of dissipation of turbulence kinetic energy mainly controls continuous-phase properties. This dissipation rate can be found easily because it is equal to the local loss of particle mechanical energy, that is,

$$\varepsilon = \pi\, n'' d_p^2\, C_D \rho_g\, (\bar{u}_p - \bar{u})^2/8 \qquad (6)$$

Measurements of streamwise and cross-stream relative turbulence intensities, $\bar{u}'/U$ and $\bar{v}'/U$, for flows dominated by turbulence generation, are plotted as suggested by the stochastic theory in Fig. 10, along with predictions based on the stochastic theory [114]. Predictions ignoring effects of velocity fluctuations in the particle wakes are not satisfactory because velocity fluctuations are large in intermediate Reynolds number wakes [114]; however, predictions including effects of velocity fluctuations are seen to be reasonably good. The values of relative turbulence intensities are relatively small for particle flows in gases at the conditions of these experiments. Actual turbulence intensities are large, however, because the velocities of the particles are much larger than the gas, which is typical of practical dense sprays. In addition, these particle-generated turbulent flows have properties that are distinctly different from conventional turbulent flows because mean wake properties contribute to the turbulence since the arrival of particle wakes is random. Thus, the degree of anisotropy of these flows is unusually large, length scales correlate with particle wake properties rather than with the mean spacing between particles, and the range of length scales is unusually large because both mean and fluctuating wake properties

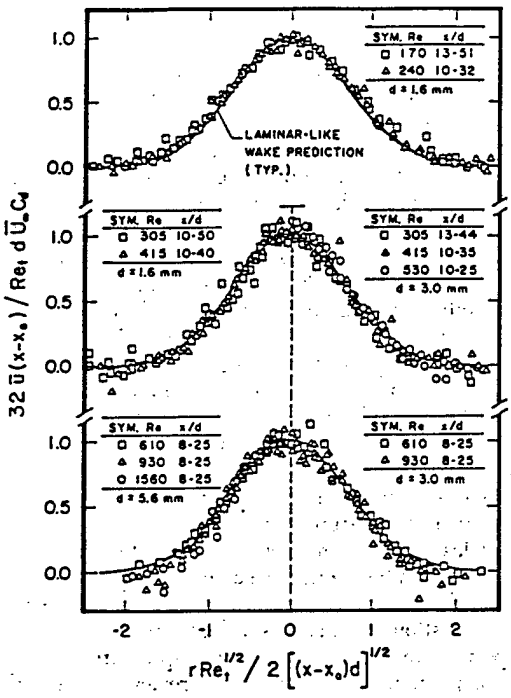

FIG. 11. Measurements of radial profiles of mean streamwise velocities within the laminar-like turbulent sphere wakes at intermediate Reynolds numbers for an ambient turbulence intensity of roughly 4%. From Wu and Faeth [114].

contribute to the turbulence, among others [101,111,114]. Thus, most features of these extraordinary turbulent-like flows, including their behavior when they interact with more conventional mechanisms of turbulence production, are not understood and clearly merit additional study.

The properties of turbulence modification highlight the need for information about the properties of particle wakes at intermediate Reynolds numbers ($Re < 1000$) in turbulent environments typical of dense sprays. This problem has been addressed considering velocities within particle wakes in both nonturbulent and turbulent environments [114]. The latter conditions are most important for processes of turbulence modification and yield rather interesting wake properties; some typical examples of measured mean velocities are illustrated in Fig. 11. A remarkable feature of these results is that the distributions of mean velocities exhibit extended regions in which they scale just like self-preserving laminar wakes having constant viscosities (and thus they have been called laminar-like turbulent wakes) with effects of ambient turbulence manifested by enhanced viscosities compared to molecular viscosities. In addition, the enhanced viscosities correlate with sphere Reynolds numbers and relative turbulence intensities, exhibiting distinct small and large Reynolds number regimes separated by a transition regime for Re of 300–400, where effects of vortex shedding from the spheres are evident. Laminar-like turbulent wakes also have large velocity fluctuations that contribute to the properties of turbulence modification, as discussed in connection with Fig. 10. Thus, improved understanding of the properties of wakes at intermediate Reynolds numbers in turbulent environments is needed to better understand turbulent mixing phenomena within dense sprays, emphasizing a broader range of particle Reynolds numbers and ambient turbulence intensities than past work, ambient turbulence properties typical of conditions in which effects of turbulent modification are dominant, and scalar mixing properties.

Individual Drop Transport

Drop Transport Environment

Drop transport occurs in dilute dispersed flows where effects of nearby drops are small, even in dense sprays [41–45]. In addition, drop evaporation is important even in combusting sprays because reactant gasification and combustion tend to occur in separate stages, as noted earlier. Finally, direct combustion of drops is also important because drops reach the combustion zone of sprays in some instances. As a result, evaporation and combustion of isolated drops have received significant attention (see the earlier reviews [1,8,10,11,20] and references cited therein). The present brief discussion seeks to update this information, emphasizing detailed numerical simulations that are increasingly being used to address complex drop transport processes.

Two aspects of drop transport in dilute dispersed flows will be considered: (1) high-pressure drop evaporation and combustion, where thermodynamic properties are complex because of real-gas effects, and (2) finite-rate chemistry effects during drop combustion, which have been addressed mainly at moderate pressures. Effects of turbulence on drop transport rates also are important but must be omitted because of space limitations; information about these effects can be found in Refs. 1–6 and 20, while recent studies of drop transport in isotropic turbulence (see Birouk et al. [115] and references cited therein) also provide a useful introduction to the field.

High-Pressure Phenomena

Extensive study of drop transport at high pressures has been motivated by applications to diesel engines, liquid rocket engines, and aircraft propulsion systems. The main new issue is the approach of liquids to the thermodynamic critical point during evapo-

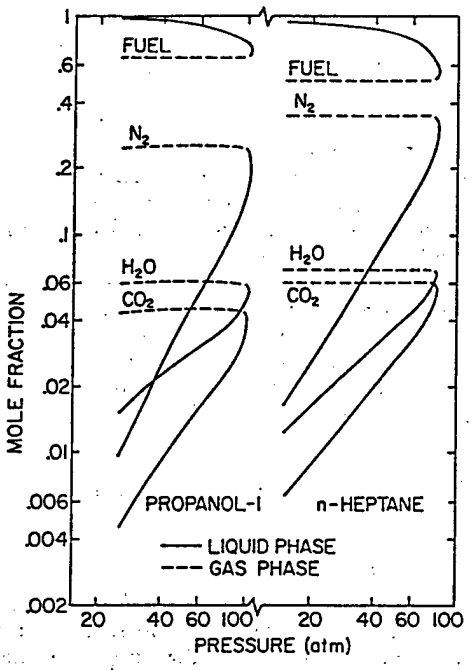

FIG. 12. Phase-equilibrium concentrations at the liquid surface during combustion of motionless propanol-l and *n*-heptane drops in air at high pressures. From Canada and Faeth [118].

ration and combustion at high pressures, where multiphase transport evolves toward mixing of gaseous pockets of the dispersed phase in a gaseous continuous phase. Because of limited available information about high-temperature reaction mechanisms at high pressures, however, past treatments of combustion chemistry have been highly simplified, with thermodynamic issues receiving the greatest emphasis. Past studies of drop combustion at high pressures are reviewed and reported in Refs. 4, 20, and 116–125 and references cited therein.

Real-gas effects and the presence of dissolved gases in the liquid phase are important at high pressures. Effects of solubility are illustrated in Fig. 12, where predicted gas- and liquid-phase compositions at the liquid surface are plotted as a function of pressure for steady drop evaporation at the wet bulb state (where all the heat reaching the liquid surface is used to vaporize the evaporating material). These results are for propanol-1 and *n*-heptane drops evaporating in gas mixtures resulting from adiabatic and stochiometric combustion of these fuels in air, assuming complete combustion, with real-gas effects treated using the Redlich–Kwong equation of state. It should be noted that similar predictions have agreed reasonably well with measured drop surface temperatures and gasification rates at high pressures, in spite of the simplifications [117–119]. The results illustrate the dramatic increase of dissolved gas concentrations, reaching values of 50–60% (molal) as the liquid surface approaches the thermodynamic critical point (where all properties of both phases are the same and liquid surface properties are lost). For the conditions illustrated in Fig. 12, this critical combustion condition is reached at a pressure of roughly 100 atm, which is typical of hydrocarbon drops evaporating in their adiabatic and stoichiometric products of combustion in air. Drops evaporating at conditions other than stoichiometric conditions would reach critical combustion conditions at even higher pressures [30,31]. These critical combustion pressures are significantly higher than the critical pressure of the pure liquid fuel because dissolved combustion product gases tend to have higher critical pressures than the pure fuel, while the critical pressures of mixtures tend to be higher than the critical pressures of the individual pure components of the mixture [116–119].

Clearly, determining conditions at which drop surfaces reach the thermodynamic critical point and establishing reliable ways to treat real-gas effects for combustion gas mixtures at high pressures are important for treating practical high-pressure combustion phenomena. Unfortunately, review of past work treating these problems reveals significant deficiencies, with large error bands and limited evaluation of methods of estimating high-pressure drop combustion properties. Particular limitations involve accurate treatment of the real-gas properties of the light and polar compounds present in combustion gas mixtures (e.g., H_2, H_2O, CH_4) and the lack of convincing experimental evaluations of predictions for combustion gas mixtures of practical interest. Other areas where improvements are needed include ways to treat effects of finite-rate chemistry, fuel decomposition, soot chemistry, and convection for high-pressure drop transport processes.

Effects of convection on high-pressure drop evaporation have been studied recently for liquid oxygen droplets in high-temperature gaseous hydrogen flows, because of liquid rocket engine applications [122–125]. These studies have involved detailed numerical simulations of transient drop convection processes treating real-gas effects using simple corresponding-state principles. Typical results involving oxygen drops at supercritical conditions for various initial relative velocities are illustrated in Fig. 13. Temperatures and compositions are not restrained by phase-equilibrium requirements at supercritical conditions; therefore, two representative mixing states are illustrated by the critical temperature and critical concentration isoclines shown for various times during the process. These results exhibit effects of inhibited deformation and breakup expected for secondary breakup that are discussed in connection with Fig. 7 and clearly resemble drop fluid motion similar to shear breakup. Unfortunately,

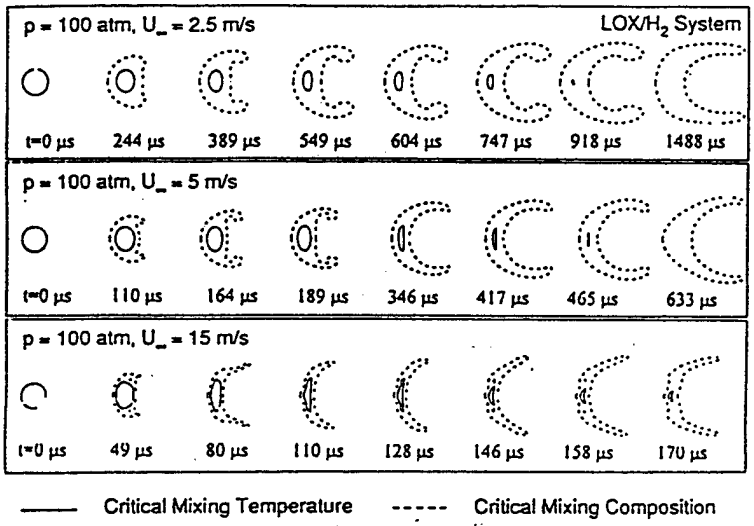

FIG. 13. Evolution of critical mixing temperature and critical mixing concentration profiles for high-pressure vaporization of liquid oxygen drops in a heated hydrogen stream. From Hsiao et al. [125], for an initial drop diameter and temperature of 100 μm and 100 K and the hydrogen stream temperature of 1000 K.

available results of this type are very limited and have not been summarized analogous to experimental investigations of drop deformation, breakup, and transport processes [68–85]. Nevertheless, numerical simulations along these lines offer an attractive alternative to difficult experiments for studies of high-pressure drop breakup and transport that should be exploited in the future.

Combustion Phenomena

The development of detailed numerical simulations of combustion phenomena has been a major new trend in combustion science. These techniques involve consideration of variable thermodynamic and transport properties, realistic treatment of multicomponent transport phenomena, and consideration of detailed reaction mechanisms involving numerous individual reaction steps. Thus far, these methods have been applied mainly to gaseous premixed and diffusion flames; nevertheless, some detailed numerical simulations of liquid-fueled combustion have been reported (see Refs. 126–129 and references cited therein). This methodology provides an attractive way to address drop and spray combustion processes. Consequently, representative work along these lines is discussed briefly in the following, considering studies of drop combustion and related studies of counterflow diffusion flames in turn.

Dryer and co-workers [126–128] have carried out detailed numerical simulations and corresponding experiments for the classical problem of drop combustion in a motionless gas environment. Problems of soot chemistry have been avoided by studying the soot-free flames of methanol/water drops burning in $O_2/N_2/He$ mixtures at NTP, which also addresses issues of water recondensation on drops that are important for high-pressure combustion (see Fig. 12). Such soot-free flames are a useful limiting condition because many practical spray flames involve mixing conditions in which soot formation is avoided while soot-free flames are a logical precursor to the complexities of soot processes in flames. In addition, drop combustion in motionless gases at microgravity conditions is considered to yield a classical flame configuration in which complications caused by forced and natural convection are avoided. The resulting measurements and predictions have provided valuable evaluations of thermodynamic, transport, and chemical models for these flames—demonstrating the potential for future work along these lines. Issues that merit particular attention in the future, including other ways to avoid soot (e.g., diluted ambient gases, reduced pressures), should be considered to address a broader range of liquid fuels; drop processes should be studied for ambient gas conditions representative of practical spray combustion processes rather than just air at NTP (e.g., gas compositions and temperatures for adiabatic combustion at various mixture fractions, as illustrated for the LHF approximation in Fig. 1); the use of advanced diagnostics should be considered to gain more information about flame structure; and effects of various forced-convection conditions should be studied.

Counterflow diffusion flames, involving an oxidizer stream directed vertically downward to impinge on the vaporizing surface of a pool of liquid

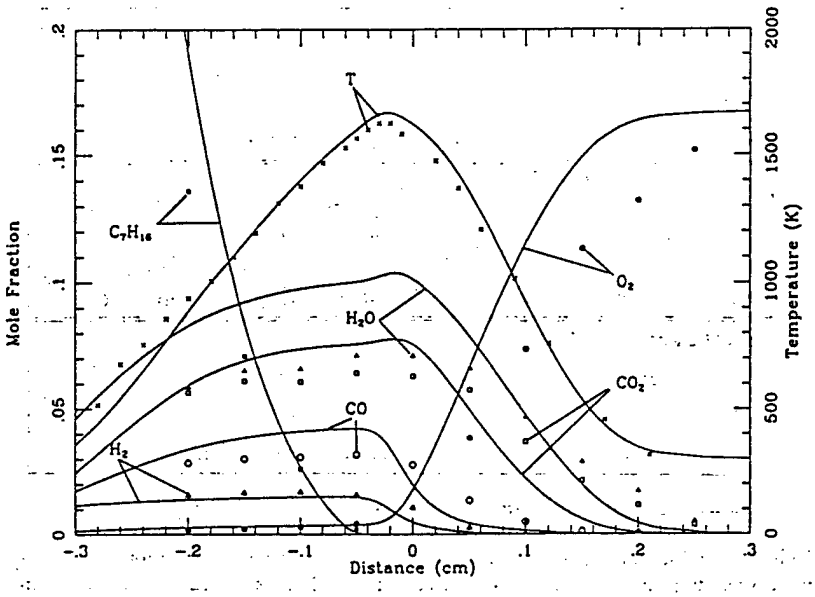

FIG. 14. Measured (points) and predicted (lines) structure of a counterflow n-$C_7H_{16}/O_2/N_2$ diffusion flame at NTP. From Chelliah et al. [129]; measurements of Kent and Williams [130]; predictions of Chellian et al. [129]. Test conditions involved U = 305 mm/s, $Y_{O_2\infty}$ = 0.185, whereas computations used a strain rate of 64 s^{-1}.

fuel, provide an experimental configuration that is useful for studying drop combustion [129–131]. In particular, such flames are steady, allowing detailed measurements of their structure; effects of convection and flame stability can be addressed easily by varying the velocity of the oxidant stream. This configuration yields a one-dimensional steady flow that vastly simplifies numerical computations of the process, allowing consideration of detailed chemical mechanisms.

Chelliah et al. [129] report a representative study of liquid-fueled counterflow diffusion flames. Measurements of n-heptane–fueled flames burning in O_2/N_2 mixtures at various impingement velocities by Kent and Williams [130] and Hamins and Seshadri [131] were considered. The flame structure measurements included temperatures, using thermocouples corrected for effects of radiation, and species concentrations, using gas chromatography. Flame conditions were adjusted to eliminate soot by reducing O_2 concentrations in the oxidant stream and by maintaining reasonably high impingement velocities. The most complex chemical mechanism considered involved 40 reversible elementary reactions, although several reduced mechanisms were studied as well. Typical predictions and measurements for these flames are illustrated in Fig. 14. The agreement between predictions and measurements is quite encouraging, except for discrepancies for H_2O that are attributed to experimental problems. Another area of uncertainty involves the fact that the velocity field was not measured, which allowed some flexibility to match measured and predicted temperature profiles by adjusting the impingement velocity along the axes far from the surface.

Minor deficiencies aside, Refs. 129–131 clearly indicate the potential of studies of counterflow diffusion flames to gain a better understanding of liquid combustion processes. Issues that merit consideration in the future include the following: measurements of velocities and radiative properties should be undertaken along with other structure measurements to reduce uncertainties about evaluations of predictions; similar to the drop experiments discussed earlier, oxidant stream conditions representative of practical spray combustion processes (e.g., Fig. 1) should be addressed in addition to gases at NTP; a broader range of fuels should be considered; evaluation of predictions should extend to flame stability to address the critical issue of transition from envelope to wake flames (see Ref. 20 and references cited therein); advanced diagnostics should be considered to provide more definitive information about chemical mechanisms through the distributions of radicals; and simplified ways of treating drop combustion (e.g., reduced mechanisms) should be considered. A reasonable desire to minimize problems of both measurements and numerical simulations will no doubt encourage consideration of soot-free flames, as in the past; nevertheless, effects of soot on drop combustion processes must be addressed eventually to obtain a reasonably complete technology base for spray combustion phenomena.

Nomenclature

C_d, C_D	drag coefficient
d, d_p	jet exit and drop diameters
e_p	drop ellipticity
l_e	length scale of energy-containing eddies
L	passage length
L_c	liquid core length
MMD	mass median drop diameter
$\dot{n}''$	particle (drop) number flux
Oh	Ohnesorge number, $\mu_f/(\rho_f d_p \sigma)^{1/2}$
r	radial distance
Re, Re_t	drop and turbulence Reynolds number, $u_p d_p/\nu_g$, $u_p d_p/\nu_t$
SMD	Sauter mean diameter
t, t_b, t_i	time, breakup time, time of initiation of breakup
t^*	characteristic time, $d_{po}(\rho_g/\rho_f)^{1/2}/u_{po}$
u	streamwise velocity
u_p, U	drop relative streamwise velocity
v	cross-stream velocity
We, We_{ij}	Weber number, $\rho_g d_o u_g^2/\sigma$, $\rho_i u_o^2 j/\sigma$
x	streamwise distance
x_i, x_e	streamwise distances to onset and end of surface breakup
y	cross-stream distance
Y_i	mass fraction of species i
α_i	volume fraction of phase i
δ	thickness of viscous liquid layer
ε	rate of dissipation of turbulence kinetic energy
Λ	radial integral length scale
μ	molecular viscosity
ν, ν_t	molecular and turbulence kinematic viscosity
ρ	density
σ	surface tension

Subscripts

c	centerline value
f	liquid property
g, G	gas property
L	liquid property
o	initial condition
∞	far from surface

Superscripts

$(\bar{})$	time-averaged mean property
$(\bar{})'$	time-averaged rms fluctuating property

Acknowledgments

The author's research on sprays has been supported by the U.S. Air Force Office of Scientific Research, Grant Nos. 49620-92-J-0399 and 49620-95-I-0364, under the technical management of J. M. Tishkoff, and U.S. Office of Naval Research, Grant Nos. N00014-89-J-1199 and N00014-95-I-0234, under the technical management of E. W. Rood and G. D. Roy. The U.S. Government is authorized to reproduce and distribute copies for governmental purposes notwithstanding any copyright notation thereon.

REFERENCES

1. Giffen, E. and Muraszew, A., *The Atomization of Liquid Fuels*, Wiley, New York, 1953.
2. Levich, V. G., *Physicochemical Hydrodynamics*, Prentice Hall, Englewood Cliffs, NJ, 1962, p. 639.
3. Soo, S. L., *Fluid Dynamics of Multiphase Systems*, Blaisdel, Waltham, MA, 1967.
4. Harrje, D. T. and Reardon, F. H., "Liquid Rocket Combustion Instability," NASA SP-194, 1972, p. 49.
5. Chigier, N. A., *Prog. Energy Combust. Sci.* 2:97 (1976).
6. Clift, R., Grace, J. R., and Weber, M. E., *Bubbles, Drops, and Particles*, Academic Press, New York, 1978.
7. Crowe, C. T., *J. Fluids Engineer.* 104:197 (1982).
8. Law, C. K., *Prog. Energy Combust. Sci.* 8:169 (1982).
9. Elkotb, M. M., *Prog. Energy Combust. Sci.* 8:61 (1982).
10. Sirignano, W. A., *Prog. Energy Combust. Sci.* 9:291 (1983).
11. Sirignano, W. A., *J. Fluids Engineer.* 115:345 (1993).
12. Lefebvre, A. H., *Prog. Energy Combust. Sci.* 9:1 (1983).
13. Lefebvre, A. H., *Gas Turbine Combustion*, Hemisphere Publishing Co., New York, 1983.
14. Lefebvre, A. H., *Atomization and Sprays*, Hemisphere Publishing Co., New York, 1989.
15. Drew, D. A., *Ann. Rev. Fluid Mech.* 15:261 (1983).
16. Bracco, F. V., SAE Paper No. 85-0394, 1985.
17. Annamalai, K. and Ryan, W., *Prog. Energy Combust. Sci.* 8:221 (1992).
18. Bachalo, W. D., *Twenty-Fifth Symposium (International) on Combustion*, The Combustion Institute, Pittsburgh, 1994, p. 333.
19. Maly, R. R., *Twenty-Fifth Symposium (International) on Combustion*, The Combustion Institute, Pittsburgh, 1994, p. 111.
20. Faeth, G .M., *Prog. Energy Combust. Sci.* 3:191 (1977); *Prog. Energy Combust. Sci.* 9:1 (1983); *Prog. Energy Combust. Sci.* 13:254 (1987).
21. Faeth, G. M., *Twenty-Third Symposium (International) on Combustion*, The Combustion Institute, Pittsburgh, 1990, p. 1345.
22. Wu, P.-K., Hsiang, L.-P., and Faeth, G. M., *Prog. Astro. Aero.* 169:247 (1995).
23. Faeth, G. M., Hsiang, L.-P., and Wu, P.-K., *Int. J. Multiphase Flow* 21:99 (1995).
24. Tseng, L.-K., Ruff, G. A., Wu, P.-K., and Faeth, G. M., *Prog. Astro. Aero.* 171:3 (1996).
25. Onuma, Y. and Ogasawara, M., *Fifteenth Symposium*

(International) on Combustion, The Combustion Institute, Pittsburgh, 1974, p. 453.
26. Komiyama, K., Flagan, R. C., and Heywood, J. B., *Sixteenth Symposium (International) on Combustion*, The Combustion Institute, Pittsburgh, 1976, p. 549.
27. Thring, M. W. and Newby, M. F., *Fourth Symposium (International) on Combustion*, The Combustion Institute, Pittsburgh, 1952, p. 789.
28. Newman, J. A. and Brzustowski, T. A., *AIAA J.* 9:1595 (1971).
29. Khalil, E. E. and Whitelaw, J. H., *Sixteenth Symposium (International) on Combustion*, The Combustion Institute, Pittsburgh, 1976, p. 569.
30. Mao, C.-P., Szekely, G. A., Jr., and Faeth, G. M., *J. Energy* 4:78 (1990).
31. Mao, C.-P., Wakamatsu, Y., and Faeth, G. M., *Eighteenth Symposium (International) on Combustion*, The Combustion Institute, Pittsburgh, 1981, p. 337.
32. Miesse, C. C., *Ind. Engineer. Chem.* 47:1690 (1955).
33. Ranz, W. E., *Can. J. Chem. Engineer.* 36:175 (1958).
34. Grant, R. P. and Middleman, S., *AIChE J.* 12:669 (1966).
35. Phinney, R. E., *J. Fluid Mech.* 60:689 (1973).
36. Hoyt, J. W. and Taylor, J. J., *J. Fluid Mech.* 88:119 (1977).
37. Hoyt, J. W. and Taylor, J. J., *Phys. Fluids* 20:S253 (1977).
38. Reitz, R. D. and Bracco, F. V., *Phys. Fluids* 25:1730 (1982).
39. Chehroudi, B., Onuma, Y., Chen, S.-H., and Bracco, F. V., SAE Paper No. 85-0126, 1985.
40. Hiroyasu, H., Shimizu, M., and Arai, M., University of Wisconsin–Madison, ICLASS-82, 1982; Arai, M., Shimizu, M., and Hiroyasu, H., University of Wisconsin–Madison, ICLASS-85, 1985.
41. Ruff, G. A., Sagar, A. D., and Faeth, G. M., *AIAA J.* 27:549 (1989).
42. Ruff, G. A., Bernal, L. P., and Faeth, G. M., *J. Propulsion Power* 7:221 (1991).
43. Ruff, G. A., Wu, P.-K., Bernal, L. P., and Faeth, G. M., *J. Propulsion Power* 8:280 (1992).
44. Tseng, L.-K., Ruff, G. A., and Faeth, G. M., *AIAA J.* 30:1537 (1992).
45. Tseng, L.-K., Wu, P.-K., and Faeth, G. M., *J. Propulsion Power* 8:1157 (1992).
46. Ricou, F. P. and Spalding, D. B., *J. Fluid Mech.* 11:21 (1961).
47. Simmons, H. C., *J. Engineer. Power* 99:309 (1977); *J. Engineer. Power* 99:315 (1977).
48. Belz, M. H., *Statistical Methods in the Process Industries*, Wiley, New York, 1973, p. 103.
49. Wu, P.-K., Ruff, G. A., and Faeth, G. M., *Atomiz. Sprays* 1:421 (1991).
50. Wu, P.-K., Tseng, L.-K., and Faeth, G. M., *Atomiz. Sprays* 2:295 (1992).
51. Wu, P.-K. and Faeth, G. M., *Atomiz. Sprays* 3:265 (1993).
52. Wu, P.-K. and Faeth, G. M., *Phys. Fluids A* 7:2915 (1995).
53. Wu, P.-K., Miranda, R. F., and Faeth, G. M., *Atomiz. Sprays* 5:175 (1995).
54. De Juhasz, K. J., Zahm, O. F. Jr., and Schweitzer, P. H., Bulletin No. 40, Engineering Experimental Station, Pennsylvania State University, University Park, PA, 1932, p. 63.
55. Lee, D. W. and Spencer, R. C., NACA Tech. Note No. 424, 1932; NACA Tech. Note No. 454, 1933.
56. Mansour, A. and Chigier, N., *Atomiz. Sprays* 4:583 (1994).
57. Laufer, J., NACA Tech. Report No. 2123, 1950.
58. Tennekes, H. and Lumley, J. L., *A First Course in Turbulence*, MIT Press, Cambridge, MA, 1972, p. 113.
59. Hinze, J. O., *Turbulence*, 2d ed., McGraw Hill, New York, 1975 pp. 427, 724.
60. Schlichting, H., *Boundary Layer Theory*, 7th ed., McGraw Hill, New York, 1979, p. 599.
61. Smith, A. M. O., *J. Fluid Mech.* 7:565 (1960).
62. Arai, M., Shimizu, M., and Hiroyasu, H., *Proceedings of the 3rd ICLASS*, University of Wisconsin–Madison, 1985; *Proceedings of the 4th ICLASS*, University of Wisconsin–Madison, 1988.
63. Hiroyasu, H., Shimizu, M., and Arai, M., *Proceedings of 5th ICLASS*, University of Wisconsin–Madison, 1991.
64. Karasawa, T., Tanaka, M., Abe, K., Shiga, S., and Kurabayashi, T., *Atomiz. Sprays* 2:411 (1992).
65. Yokota, M., Ito, Y., and Shinoke, T., *Proceedings of the 9th Intl. Symp. on Jet Cutting Tech.*, Sendai, 1988, p. 13.
66. Taylor, G. I., *The Scientific Papers of Sir Geoffrey Ingram Taylor*, Vol. 3, (Batchelor, G. K., Ed.), Cambridge University Press, Cambridge, England, 1963, p. 244.
67. Chen, T.-F. and Davis, J. R., *J. Hydraulic Division, Proc. ASCA* 90HY1:175 (1964).
68. Hinze, J. O., *AIChE J.* 1:289 (1955).
69. Wierzba, A. and Takayama, K., Rept. Inst. High Speed Mechanics 53, Tohoku University, 1987, p. 1.
70. Wierzba, A. and Takayama, K., *AIAA J.* 26:1329 (1988).
71. Krzeczkowski, S. A., *Int. J. Multiphase Flow* 6:227 (1980).
72. Hsiang, L.-P. and Faeth, G. M., *Int. J. Multiphase Flow* 18:635 (1992).
73. Hsiang, L.-P. and Faeth, G. M., *Int. J. Multiphase Flow* 19:721 (1993).
74. Hsiang, L.-P. and Faeth, G. M., *Int. J. Multiphase Flow* 21:545 (1995).
75. Chou, W.-H., Hsiang, L.-P., and Faeth, G. M., *Int. J. Multiphase Flow* (1996), submitted.
76. Hanson, A. R., Domich, E. G., and Adams, H. S., *Phys. Fluids* 6:1070 (1963).
77. Gel'fand, B. E., Gubin, S. A., and Kogarko, S. M., *Inz.-Fiz. Zh.* 27:119 (1974).
78. Ranger, A. A. and Nicholls, J. A., *AIAA J.* 7:285 (1969).

79. Reinecke, W. G. and McKay, W., Sandia Corp. Rept. SC-CR-70-6063, 1969.
80. Reinecke, W. G. and Waldman, G. D., Avco Rept. AVSD-0110-70-77, 1970.
81. Lane, W. R., *Ind. Engineer. Chem.* 43:1312 (1951).
82. Loparev, V. P., *Mek. Zhid. Gaza* 3:174 (1973).
83. Hinze, J. O., *Appl. Sci. Res.* 11:273 (1948).
84. Simpkins, P. G. and Bales, E. J., *J. Fluid Mech.* 55:629 (1972).
85. Engel, O. G., *J. Res. Natl. Bur. Stand.* 6:245 (1958).
86. White, F. M., *Viscous Fluid Flow*, McGraw Hill, New York, 1974.
87. Liang, P. Y., Eastes, T. W., and Gharakhari, A., AIAA Paper No. 88-3142, 1988.
88. Crowe, C. T., Chung, J. N., and Troutt, T. R., *Prog. Energy Combust. Sci.* 14:171 (1988).
89. Hetsroni, G., *Int. J. Multiphase Flow* 15:735 (1989).
90. Snyder, W. H. and Lumley, J. L., *J. Fluid Mech.* 48:41 (1971).
91. Wells, M. R. and Stock, D. E., *J. Fluid Mech.* 136:31 (1983).
92. Brown, D. J. and Hutchinson, F., *J. Fluids Engineer.* 101:265 (1979).
93. Gosman, A. D. and Ioannides, E., AIAA Paper No. 81-0323, 1981.
94. Shuen, J.-S., Chen, L.-D., and Faeth, G. M., *AIChE J.* 29:167 (1983).
95. Shuen, J.-S., Chen, L.-D., and Faeth, G. M., *AIAA J.* 21:1483 (1983).
96. Shuen, J.-S., Solomon, A. S. P., and Faeth, G. M., *AIAA J.* 24:101 (1986).
97. Gouesbet, G., Berlemont, A., and Picart, A., *Phys. Fluids* 27:327 (1984).
98. Desjonqueres, P., Gouesbet, G., Berlemont, A., and Picart, A., *Phys. Fluids* 29:2147 (1986).
99. Picart, A., Berlemont, A., and Gouesbet, G., *Int. J. Multiphase Flow* 12:237 (1986).
100. Box, G. P. and Jenkins, G. M., *Time Series Analysis*, Holden-Day, New York, 1976, p. 47.
101. Parthasarathy, R. N. and Faeth, G. M., *J. Fluid Mech.* 220:485 (1990); *J. Fluid Mech.* 220:515 (1990).
102. Maxey, M. R., *J. Fluid Mech.* 174:441 (1987).
103. Chein, R. and Chung, J. N., *Int. J. Multiphase Flow* 13:785 (1987).
104. Chein, R. and Chung, J. N., *AIChE J.* 34:946 (1988).
105. Squires, K. D. and Eaton, J. K., *Phys. Fluids A* 2:1191 (1991).
106. Call, C. J. and Kennedy, I. M., *Int. J. Multiphase Flow* 18:891 (1992).
107. Hinze, J. A., *Prog. Heat Mass Trans.* 6:433 (1972).
108. Al Taweel, A. M. and Landau, J., *Int. J. Multiphase Flow* 3:341 (1977).
109. Lance, M. and Bataille, J., *Advances in Flow and Heat Transfer*, Vol. 1, Martinus Nijhof, The Hague, 1982, p. 403.
110. Gore, R. A. and Crowe, C. T., *Int. J. Multiphase Flow* 15:279 (1989).
111. Mizukami, M., Parthasarathy, R. N., and Faeth, G. M., *Int. J. Multiphase Flow* 18:397 (1992).
112. Yuan, Z. and Michaelides, E. E., *Int. J. Multiphase Flow* 18:779 (1992).
113. Wang, M. R. and Huang, D. Y., *Atomiz. Sprays* 5:305 (1995).
114. Wu, J.-S. and Faeth, G. M., *AIAA J.* 31:1448 (1993); *AIAA J.* 32:535 (1994); *AIAA J.* 33:171 (1995).
115. Birouk, M., Chauveau, C., Sark, B., Quilgars, A., and Gökalp, I., *Combust. Sci. Technol.* (1996), in press.
116. Faeth, G. M., Dominicis, D. P., Tulpinsky, J. F., and Olson, D. R., *Twelfth Symposium (International) on Combustion*, The Combustion Institute, Pittsburgh, 1968, p. 9.
117. Lazar, R. S. and Faeth, G. M., *Thirteenth Symposium (International) on Combustion*, The Combustion Institute, Pittsburgh, 1970, p. 801.
118. Canada, G. S. and Faeth, G. M., *Fourteenth Symposium (International) on Combustion*, The Combustion Institute, Pittsburgh, 1972, p. 1345.
119. Canada, G. S. and Faeth, G. M., *Fifteenth Symposium (International) on Combustion*, The Combustion Institute, Pittsburgh, 1974, p. 419.
120. Kounalakis, M. E. and Faeth, G. M., *Combust. Flame* 74:179 (1988).
121. Sato, J., Tsue, M., Niwa, M., and Kono, M., *Combust. Flame* 82:142 (1990).
122. Hsieh, K. C., Shuen, J. S., and Yang, V., *Combust. Sci. Technol.* 76:111 (1991).
123. Shuen, J. -S., Yang, V., and Hsiao, G. C., *Combust. Flame* 89:299 (1992).
124. Yang, V., Lin, N. N., and Shuen, J.-S., *Combust. Sci. Technol.* 97:247 (1994).
125. Hsiao, G. C., Yang, V., and Shuen, J. -S., AIAA Paper No. 95-0383, 1995.
126. Held, T. J. and Dryer, F. L., *Twenty-Fifth Symposium (International) on Combustion*, The Combustion Institute, Pittsburgh, 1994, p. 908.
127. Marchese, A. J. and Dryer, F. L., *Combust. Flame* 105:104 (1996).
128. Marchese, A. J., Dryer, F. L., Colantonio, R., and Nayagam, V., *Twenty-Sixth Symposium (International) on Combustion*, The Combustion Institute, Pittsburgh, 1996, pp. 1209–1217.
129. Chelliah, H. K., Bui-Pham, M., Seshardi, K., and Law, C. K., *Twenty-Fourth Symposium (International) on Combustion*, The Combustion Institute, Pittsburgh, 1992, p. 851.
130. Kent, J. H. and Williams, F. A., *Fifteenth Symposium (International) on Combustion*, The Combustion Institute, Pittsburgh, 1974, p. 315.
131. Hamins, A. and Seshadri, K., *Combust. Flame* 68:295 (1987).

COMMENTS

William A. Sirignano, University of California, Irvine, USA. Do you agree that we should distinguish between (1) the fluctuating vorticity advected from upstream in the liquid injector (turbulence) and (2) the vorticity associated with the velocity jump at the edge of the liquid jet? If so, how do you propose to organize the nondimensional groupings to reflect this distinction?

Author's Reply. I agree that it is crucial to distinguish between vorticity originating in the injector passage and vorticity originating at the gas/liquid interface of the liquid jet when primary breakup properties are characterized. One approach for treating this distinction would be to define transitions to corresponding breakup regimes dominated either by jet exit or interface-generated vorticity, somewhat analogous to the use of transition criteria to distinguish whether a particular condition corresponds to laminar or turbulent single-phase flow.

An example of this approach, for a transition similar to the one that you mention, involves transition to the merged turbulent primary breakup regime discussed in Ref. 51, where secondary breakup begins to interfere with turbulent primary breakup. Other examples of the use of breakup regime transitions to define regions where particular phenomena are important are discussed in connection with Figs. 5 and 7.

Derek Dunn-Rankin, University of California, Irvine, USA. The concept of dense sprays representing a dense cluster of wakes rather than a dense cluster of drops is an interesting one. In some of the images you show of secondary breakup, however, there appear to be occurences of locally dense clusters of small droplets that have resulted from the breakup of large primary droplets. Does the dense cluster concept hold under these secondary breakup conditions?

Author's Reply. Existing measurements of Ruff et al. [93] indicate that time-averaged liquid volume fractions near the liquid-core after primary breakup of a liquid jet are less than 0.1 percent, with larger values associated with the intermittent presence of the liquid core itself. I am not aware of similar information, however, concerning distributions of liquid volume fractions for particular realizations of either primary or secondary breakup processes. Informal information, based on observations of hologram reconstructions of dispersed flows resulting from primary and secondary breakup, suggest that these liquid volume fractions are low, but this issue merits more formal study for various breakup regimes and liquid/gas density ratios.